Role of cerebellar LTP at parallel fiber : Purkinje cell synapses in spatial navigation

Julie Lefort

Université Pierre et Marie Curie

Ecole doctorale Cerveau Cognition Comportement

Laboratoire Neuroscience Paris Seine, Equipe Cervelet Navigation et Mémoire

Role of cerebellar LTP at parallel fiber – Purkinje cell synapses in spatial navigation

Par Julie LEFORT

Thèse de doctorat de Neurosciences

Dirigée par Laure RONDI-REIG et Christelle ROCHEFORT

Présentée et soutenue publiquement le 18 juillet 2014, devant un jury composé de:

Dr Laure RONDI-REIG	Directeur de recherche, Paris	Directrice de thèse
Dr Christelle ROCHEFORT	Maître de conférences, Paris	Co-encadrante
Dr Nicole EL MASSIOUI	Directeur de recherche, Paris	Rapporteur
Dr Bruno POUCET	Directeur de recherche, Marseille	Rapporteur
Dr Christiaan DE ZEEUW	*Professor*, Rotterdam	Examinateur
Dr Kathryn JEFFERY	*Professor*, London	Examinateur
Dr Clément LENA	Directeur de recherche, Paris	Examinateur
Dr Jean MARIANI	Professeur des Universités-Praticien Hospitalier, Paris	Président de jury

REMERCIEMENTS

Je tiens tout d'abord à remercier les membres du jury. Merci à Nicole El Massioui et Bruno Poucet d'avoir accepté de consacrer du temps à la lecture et à l'évaluation de ce travail. Merci à Jean Mariani d'avoir accepté de présider ce jury. Je suis également très honorée de la présence Chris De Zeeuw, Kathryn Jeffery et Clément Léna qui ont accepté de faire partie du jury.

Laure, je te remercie de m'avoir accueillie dans ton équipe pour ces quatre années de thèse, riches en découvertes. Merci de m'avoir permis de mener à bien ce projet, avec ses déconvenues et ses joies inattendues. Merci de m'avoir donné l'occasion de créer, d'expérimenter, de me tromper, de développer, de bricoler, de me former, d'apprendre, bien au-delà des connaissances théoriques et compétences techniques liées à ce projet. Je mesure la liberté que j'ai eue pour travailler, et je l'ai appréciée ; merci pour cette confiance que tu m'as donnée. Merci d'avoir toujours fait le maximum pour que je puisse travailler dans les meilleures conditions. Merci pour ces discussions scientifiques, parfois tumultueuses, qui ont fait avancer ce projet. Je te remercie également pour l'ambition que tu places dans chacun des membres de ton équipe : tu permets à chacun de donner le meilleur de lui-même. Je me souviendrai aussi des moments légers loin de la paillasse, et du plaisir que j'ai à te taquiner dès que l'occasion se présente.

Christelle, je te remercie d'avoir encadré ce projet et d'avoir suivi de près l'avancée de mon travail. Merci pour ta bienveillance, ton regard positif, ton optimisme. Merci d'avoir supporté mes humeurs quand les manips ne donnaient pas ce qu'on attendait. Merci d'avoir écouté patiemment mes analyses parfois plus compliquées que nécessaire et de m'avoir aidée à clarifier mon propos. Merci pour ces discussions qui font avancer ma réflexion. Enfin, merci d'avoir relu si minutieusement mon manuscrit, cette relecture attentive a été un vrai soutien.

Merci aux membres de cette équipe qui ont vu grandir ce projet.

Merci à Fred, fidèle compatriote de toutes mes galères, qui m'a trouvé la solution tant de fois. Merci de m'avoir aidée à monter et démonter les set-up au gré des nouvelles idées à tester. Et d'avoir enfilé une blouse pour entrainer ces L7-PP2B ! Merci pour tout ce que tu m'a appris. Un merci spécial pour la programmation ; au labo, elle a changé ma vie!

Merci à Bénédicte… Merci pour tout ce que l'on a partagé au quotidien sur ce long chemin. Merci de m'avoir supportée, de m'avoir soutenue quand je passais par toutes les émotions et toutes les couleurs. Merci de m'avoir initiée aux options magiques de Word, Illustrator et autres... Et surtout, merci pour ces réflexions croisées sur nos projets, c'est là aussi que la science se fait !

Merci à Aurélie, d'avoir assuré la gestion de mes lignées pendant ces quatre années. Merci pour ton travail irréprochable sur lequel on s'appuie en toute sérénité. Merci pour ta disponibilité pour aider, donner un conseil… Merci aussi pour ton écoute compréhensive et ton sourire malicieux.

Merci à Christine pour les discussions philosophiques du déjeuner, pour ton recul sur les choses, ta distance sereine qui interpelle.

Merci à Anne-Lise pour ton humour, ton enthousiasme chaque jour et ta disponibilité pour donner un coup de main.

Merci à Julien d'avoir participé à ce projet, avec un grand souci du travail bien fait. Merci à Tom, Lu, Pauline, Julien et Daphnée pour l'ambiance sympathique de cette équipe. Je vous souhaite le meilleur dans la suite de vos projets !

Merci aux chercheurs qui se sont trouvés sur ma route et qui ont d'une certaine façon ont compté dans ce projet.

Clément, merci d'avoir suivi de près ce travail depuis ses débuts. Merci pour ton enthousiasme, ton avis lucide et bienveillant.

Philippe, merci pour ta présence bienveillante au quotidien. Merci pour les cafés du samedi, pour ces discussions objectives, critiques, constructives.

Karim, le temps où l'on a travaillé ensemble dans cette équipe semble déjà loin, et pourtant je me souviens de ta curiosité, ton enthousiasme, ta rigueur scientifique, que tu transmets autour de toi. Merci pour l'intérêt que tu as porté à nos projets. Merci aussi à Marie et Gaëtan, un duo de choc, parti voler vers de nouveaux horizons. Merci pour ces moments passés ensemble, à bosser, décompresser, dédramatiser.

Merci à Antonin, agent infiltré. Merci pour ton soutien sans faille à toutes les étapes de ce projet. Merci à tous les amis du 5^{e} étage pour l'ambiance sympathique qui règne au labo. Audrey, Carole, Malou, Steeve, Samir, Eléonore, Sébastien, Romain, Alex et tous les autres…

Merci à mes parents de m'avoir toujours soutenue, mais aussi de m'avoir rappelée de temps en temps que l'essentiel n'était pas toujours derrière la porte du labo. Merci à mes amis, Anne Claire, Olivier, Alex, Marie, Aurélie, Laélia, Marine… votre présence quotidienne m'a permis de garder les pieds sur Terre pour mieux avancer.

RESUME

La navigation spatiale peut être subdivisée en deux processus: la construction d'une représentation mentale de l'espace à partir de l'exploration de l'environnement d'une part, et l'utilisation de cette représentation de façon à produire le trajet le plus adapté pour rejoindre le lieu souhaité d'autre part. Lors de l'exploration de l'environnement, des informations externes et des informations de mouvement propre (i.e. vestibulaires et proprioceptives) sont combinées pour former la carte cognitive. Depuis longtemps des études suggèrent que le cervelet participe à la navigation spatiale mais son rôle a souvent été confiné à l'exécution motrice. Notre équipe a étudié des souris mutantes L7-PKCI présentant un déficit de plasticité synaptique de type dépression à long terme (DLT) au niveau des synapses entre fibres parallèles et cellules de Purkinje du cortex cérébelleux. Ces travaux ont montré que les souris présentent à la fois un déficit dans l'optimisation de la trajectoire mais également dans le maintien de la carte cognitive formée dans l'hippocampe. En effet, les propriétés de décharge des cellules de lieu de l'hippocampe sont affectées chez ces souris exclusivement lorsque celles-ci doivent naviguer en se reposant sur les informations provenant de leur mouvement propre, c'est à dire quand elles explorent l'environnement dans le noir.

A ces mêmes synapses, une plasticité de type potentialisation à long terme (PLT) a été observée et permet (avec la DLT) la modulation bidirectionelle de l'efficacité synaptique. La plasticité bidirectionnelle est un processus clé dans les modèles théoriques de type « filtre adaptatif » de traitement de l'information par le cervelet. Selon ces modèles, l'absence de PLT ou DLT devrait affecter de façon similaire la plasticité bidirectionnelle et conduire ainsi à des déficits comparables. Pour tester cette hypothèse, nous avons étudié les conséquences fonctionnelles d'un déficit de type PLT au niveau de la même synapse entre fibre parallèle et cellule de Purkinje. Nous avons utilisé la lignée transgénique L7-PP2B, spécifiquement déficitaire pour cette plasticité.

Malgré un léger déficit moteur révélé exclusivement sur le rotarod, les capacités de navigation des souris L7-PP2B ne sont pas affectées dans une tâche de navigation en labyrinthe aquatique de type piscine de Morris. Les propriétés des cellules de lieu de l'hippocampe des souris L7-PP2B ont ensuite été caractérisées lors de l'exploration d'une arène circulaire dans différentes conditions environnementales. Contrairement à celles des souris L7-PKCI, les propriétés des cellules de lieux des souris L7-PP2B ne sont pas affectées lorsque les souris ne peuvent utiliser que les informations de mouvement propre pour s'orienter, c'est à dire dans le noir.

Par contre, les cellules de lieux des souris L7-PP2B présentent une instabilité en l'absence de toute manipulation d'indice environnemental, dans 23% des sessions d'enregistrement. Cette instabilité, absente chez les souris contrôles, se manifeste de façon imprévisible dans un environnement familier et est caractérisée par une rotation angulaire cohérente de l'ensemble des cellules de lieux enregistrées. Ces données suggèrent qu'en l'absence de PLT cérébelleuse la représentation spatiale de l'hippocampe n'est pas ancrée de façon stable aux indices externes proximaux. Ces résultats, associés à ceux des souris L7-PKCI indiquent que le cervelet contribue de manière complexe à la fois à la représentation spatiale hippocampique et aux capacités de navigation et que DLT et PLT jouent probablement des rôles différents dans ces processus.

SUMMARY

Spatial navigation can be divided into two processes: building a spatial representation from the environment exploration and using this representation to produce an adapted trajectory toward a goal. During the environment exploration, external and self-motion information (i.e. vestibular and proprioceptive) are combined to form the spatial map. It has long been suggested that the cerebellum participates in spatial navigation but its role has often been confined to motor execution. Our team has studied L7-PKCI mice which lack a plasticity mechanism (long term depression (LTD)) at parallel fiber-Purkinje cell synapses in the cerebellar cortex. These works have shown that L7-PKCI mice present a deficit in trajectory optimization as well as in the maintenance of the cognitive map in the hippocampus. Indeed in these mice, the firing properties of hippocampal place cells are affected specifically when mice have to rely on self-motion information, i.e. when exploring the environment in the dark.

A these same synapses, another type of plasticity (long term potentiation (LTP)) has been described, and allows (with LTD) the bidirectional modulation of the synaptic efficiency. Bidirectional plasticity is a key element of the 'adaptive filter' theoretical models of cerebellar information processing. According to these models, a lack of LTP or LTD should similarly affect bidirectional plasticity and result in comparable deficits. To test this prediction, we investigated the functional consequences of a deficit of LTP at parallel fiber-Purkinje cell synapses using the L7-PP2B mice model, specifically impaired for this plasticity.

In spite of a mild motor adaptation deficit, revealed on the rotarod task, spatial learning of L7-PP2B mice was not impaired in the watermaze task. Hippocampal place cell properties of L7-PP2B mice were characterized during exploration of a circular arena, following different experimental manipulations. In contrast to mice lacking cerebellar LTD, place cells properties of L7-PP2B mice were not impaired when mice had to rely on self-motion cues, i.e. in the dark.

Surprisingly, L7-PP2B place cells displayed instability in the absence of any proximal cue manipulation in 23 % of the recording sessions. This instability occurred in an unpredictable way in a familiar environment and was characterized each time by a coherent angular rotation of the whole set of recorded place cells. These data suggest that, in the absence of cerebellar LTP, hippocampal spatial representation cannot be reliably anchored to the proximal cue. These results along with those from L7-PKCI mice, indicate that the cerebellum contributes to both hippocampal representation and subsequent navigation abilities and that LTP and LTD are likely to play different roles in these processes.

TABLE OF CONTENTS

INTRODUCTION

Part I. From spatial navigation to mental representation of space

1 SPATIAL NAVIGATION

Spatial navigation refers to the ability to know where we are and to organize our behavior to reach the desired place. It involves acquiring spatial knowledge (e.g., spatial relations between environmental cues), forming a representation of space, and employing it to adapt its motor response to the specific context (Arleo and Rondi-Reig, 2007). This first chapter does not pretend to give a comprehensive overview of spatial navigation, but rather aims at presenting the bases to understand the role of the cerebellum in navigation.

Locating oneself is only meaningful relative to a reference frame, which can be centered on the subject (egocentric reference frame) or on the external world (allocentric reference frame). It is worth noting that experience of space is fundamentally egocentric, since sensory information is perceived by the subject in an egocentric reference frame (each sensory signal is initially encoded in the respective reference frames of the sensors). Moving across the environment to explore it allows the subject to establish spatial relations between the different elements of the environment without having to refer to its own body. This also allows him to infer its position in an allocentric reference frame, in order to navigate efficiently toward the desired location. Thus, spatial navigation requires a constant interaction between these two reference frames.

1.1 MULTIMODAL INFORMATION IS AVAILABLE FOR SPATIAL NAVIGATION

While exploring an environment, a subject perceives two types of information:

- **external** (or allothetic) **information** which comes from the environment and is transmitted through visual, auditory, tactile and olfactory sensors;
- **self-motion** (or idiothetic) **information** generated by his own movements and conveyed by vestibular, proprioceptive, motoric (through the efference copy of the motor command) and optic flow signals.

This first part exposes experimental evidence showing that these different types of information are indeed used to navigate.

1.1.1 SELF-MOTION INFORMATION

Self-motion information allows the subject to detect changes in position or orientation of its body in the environment. It includes vestibular, proprioceptive and optic flow inputs as well as efference copy of the motor command.

Vestibular information is detected in the inner ear, by the otolith organs which are sensitive to linear acceleration and by the semi-circular which are sensitive to angular acceleration. The integration of this signal by the vestibular system allows to compute the linear and angular speed and then, the position and orientation of the body in space. Proprioceptive information comes from stretch receptors located in the muscles, tendons and joints and allows to perceive the relative position of the different parts of one's body. Optic flow refers to the displacement of images on the retina due to the relative motion between the observer and the scene (Gibson, 1950). The displacement speed can be used to estimate one's proper acceleration (which is the case while sitting on the train for example). Finally, it has been suggested that during an active movement, while the motor cortex sends a command to the periphery, a copy of the motor command (named "efference copy") is also generated and could be used to generate a prediction of the sensory consequences of the intended movement (Von Holst and Mittelstaedt, 1950).

The use of self-motion information to navigate was initially shown using the strong motivation of female gerbils to carry its sucking back home if they are displaced (Mittelstaedt, ML ; Mittelstaedt, 1980). In this paradigm, the gerbil pups were displaced on a circular arena to a shallow cup at various angles and distance from the nest. In complete darkness, the females were able to return on a rather straight course to starting point of the excursion (homing), after varying detours on its way out. This suggests that they integrated self motion information on the way out and used it to compute the return vector. To show the importance of vestibular information, the female was submitted to rotations while it stays at the cup. If the rotation was performed quickly (above the detection threshold of the vestibular system), homing was as good as before. On the opposite, if the cup was rotated with smooth acceleration (below the detection threshold of the vestibular system), the nest was missed by very precisely this amount in the direction of rotation. This shows that during the quick rotations gerbil females did take into account the vestibular signal to adjust their trajectory but that this was no longer the case when the vestibular signal was not perceptible (during smooth rotation). Accordingly, vestibular lesions in rats impaired the homing behavior, a behavior that depends on self-motion information (Wallace et al., 2002).

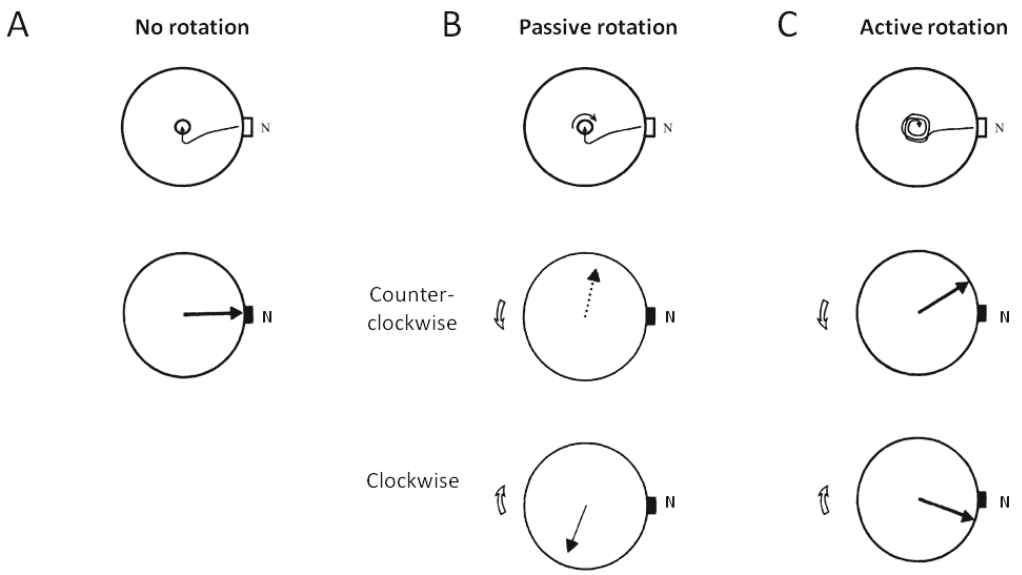

Figure 1. Combination of vestibular and proprioceptive signals for self-motion navigation
Orientation of the return vector after active or passive unidirectional rotations. In darkness, the subject was lured from its nest (N) to a food source located on a small platform at the arena centre. The vector on each circle represents the mean orientation of animals during their return from the centre to the periphery.
A. Control trials. The hamster went directly from its nest box to the food source at the centre of the arena and returns directly to its nest box.
B. Passive rotation trials. The hamster went directly from its nest box to the food source. While it pouched food, the platform was rotated clockwise or counterclockwise (three full turns).
C. Active rotation trials. The hamster followed a bait from the nest to the central region of the arena, and had to perform three full turns before being offered food. The rotations occurred either clockwise or counter-clockwise (see open arrows).
Adapted from Etienne et al. 1988

Similarly, other works examined the homing behavior of golden hamsters, which tend to return directly from a food source at the centre of an experimental arena to their peripheral nest to eat the food. The orientation of their return journey in darkness was analyzed in two experimental conditions (Figure 1.A). In the first situation, the animals walked to a platform at the centre of the arena and were submitted to passive rotations while they were collecting the food items on the platform (Figure 1.B); in the second situation hamsters performed active rotations before being offered the food (Figure 1.C) (Etienne et al., 1988). During passive rotations, the return vector was shifted in the direction of the passively applied rotations whereas during the actively performed rotation this shift was drastically reduced. This reveals that other types of self-motion inputs were taken into account during active trials to estimate the return vector. Etienne et al. suggest that proprioceptive

information is combined with vestibular inputs to correctly estimate the trajectory (Etienne et al., 1988).

1.1.2 EXTERNAL INFORMATION

External information used for navigation can be of different nature: visual, tactile, olfactory or auditory.

Numerous studies have shown the importance of visual cues for spatial localization. Morris developed the watermaze task, in which rats were trained in a pool filled of opaque water, to find a platform at a fixed location but hidden below the water surface. Since rats started from a random departure point in the pool, a sequence of movements (based on self-motion information) could not be use to learn a specific path (Figure 2.A-D) (Morris, 1981). This demonstrated the rats capability to use the configuration of distal visual cues to find the platform. If access to the visual information is disrupted, by masking the environmental cues (Morris, 1984) or by a loss of photoreceptors, animal's performance is altered (O'Steen et al., 1995). Olton and Samuelson developed another spatial paradigm, the radial maze task (Figure 2.E), in which the animals have to retrieve food located at the end of eight equidistantly spaced arms without visiting the same arm twice (Olton and Samuelson, 1976). Similarly, disruption of the visual system (by ocular enucleating, or visual cortex lesion) also triggered behavioral deficits (Figure 2.F) (Zoladek and Roberts, 1978; Goodale and Dale, 1981).

The use of olfactory cues has been investigated by a series of studies by Lavenex and Schenk. Training rats in the radial maze task, they showed that when visual information was sufficient to solve the task, adding olfactory cues did not improve the performances of rats. However, when visual cues were not salient, olfactory cues could enhance animal's behavior (Lavenex and Schenk, 1996). In a hexagonal arena, traces left by the animals allow rats to find a rewarded place in the dark (Lavenex and Schenk, 1998). However, how these traces are established and what kind of information they render available (are they used as an olfactory gradient or as organized trails) remains to be determined. The dispersion of odors with time complicates the understanding of their importance as spatial cues.

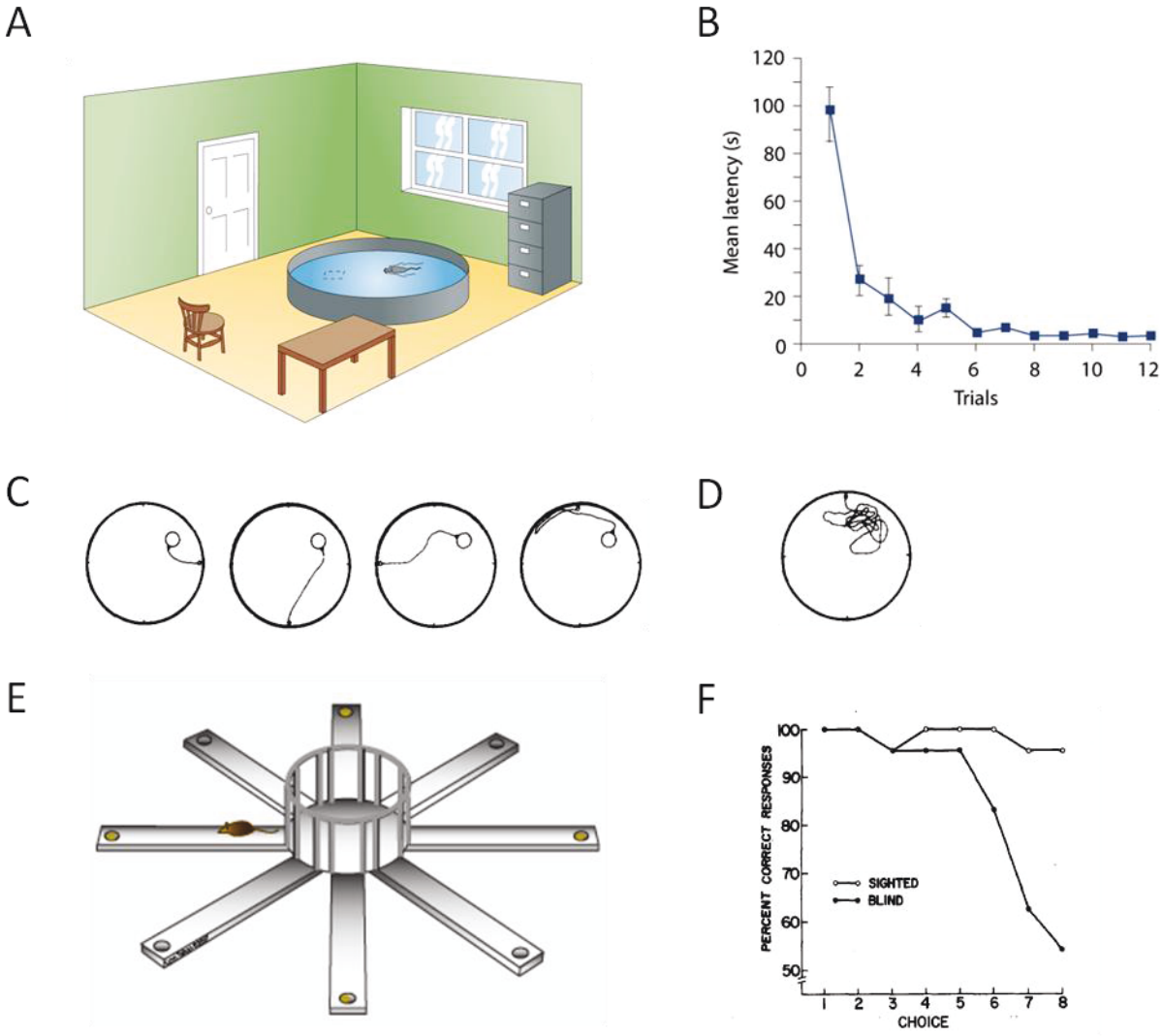

Figure 2. The use of external visual cue for navigation

A. In the water maze task, the animals are trained to use the configuration of distal visual cues to find a platform at a fixed location but hidden below the water surface (Eichenbaum 1999)

B. The decrease in the latency to find the platfom shows that the rats progressively learn to go directly to the correct area.(Eichenbaum 1999).

C. Examples of trajectories at the end of training, from the different departure points. Since rats started from a random departure point in the pool, the sequence of movements (self-motion information) could not be use to learn a specific path (Morris 1981).

D. Examples of trajectories during the probe test (in the absence of platform). The persistent search in the previous platform area evidences that the rats have indeed used the configuration of distal cues to learn the location of the platform.

E. In the radial maze task, the animals have to retrieve food located at the end of eight equidistantly spaced arms without visiting the same arm twice. Similarly, external visual cues around the maze can be used to remember the previously visited arms. (http://btc.psych.ucla.edu/ram.htm)

F. Percentage of correct choices for blind and sighted animals as a function of choice number (Zoladeck and Roberts, 1978)

Auditory cues influence has been investigated in the watermaze task. In darkness, a configuration of auditory cues did not allow rats to learn the position of the platform. However, the combination of the auditory cues with a visual cue potentiates their ability to find the platform (Rossier et al., 2000; Rossier and Schenk, 2003).

The use of tactile information to solve a spatial task has not been explicitly tested up-to-date at the behavioral level. However, tactile cues have been shown to exert a strong influence on the exploratory behavior: in their vicinity, mice form home bases, from which they make excursions toward the rest of the environment (Clark et al., 2006).

Thus, visual cues, when they are available, seem to predominate over the other types of information. Olfactory and auditory cues can potentiate spatial performances when they are combined with another type of information.

1.1.3 INTERACTIONS BETWEEN SELF-MOTION AND EXTERNAL INFORMATION

Interactions between self-motion and external information was shown in tasks that could apparently be solved only based on external information. In the water maze task, once the animals have found the platform they are allowed to stay on it for a few seconds; this procedure is thought to allow them to encode the environment, that-is to say to remember the spatial relationships between the different landmarks and the position of the goal (Vorhees and Williams, 2006). For example, Semenov and colleagues disrupted the vestibular system of rats by submitting them to rotation while they were staying on the platform. This procedure completely disrupted learning of the platform location (Semenov and Bures, 1989). The authors suggested that the vestibular cues are important for the orientation of the animal in order to estimate the angles between the directions corresponding to the different external landmarks. Accordingly, vestibular lesions in rats dramatically impaired their ability to retrieve a food location in the absence of a prominent visual cue (Stackman and Herbert, 2002).

In fact external and self-motion information seem to be involved in two different processes that are likely to work in close relation to shape spatial behavior.

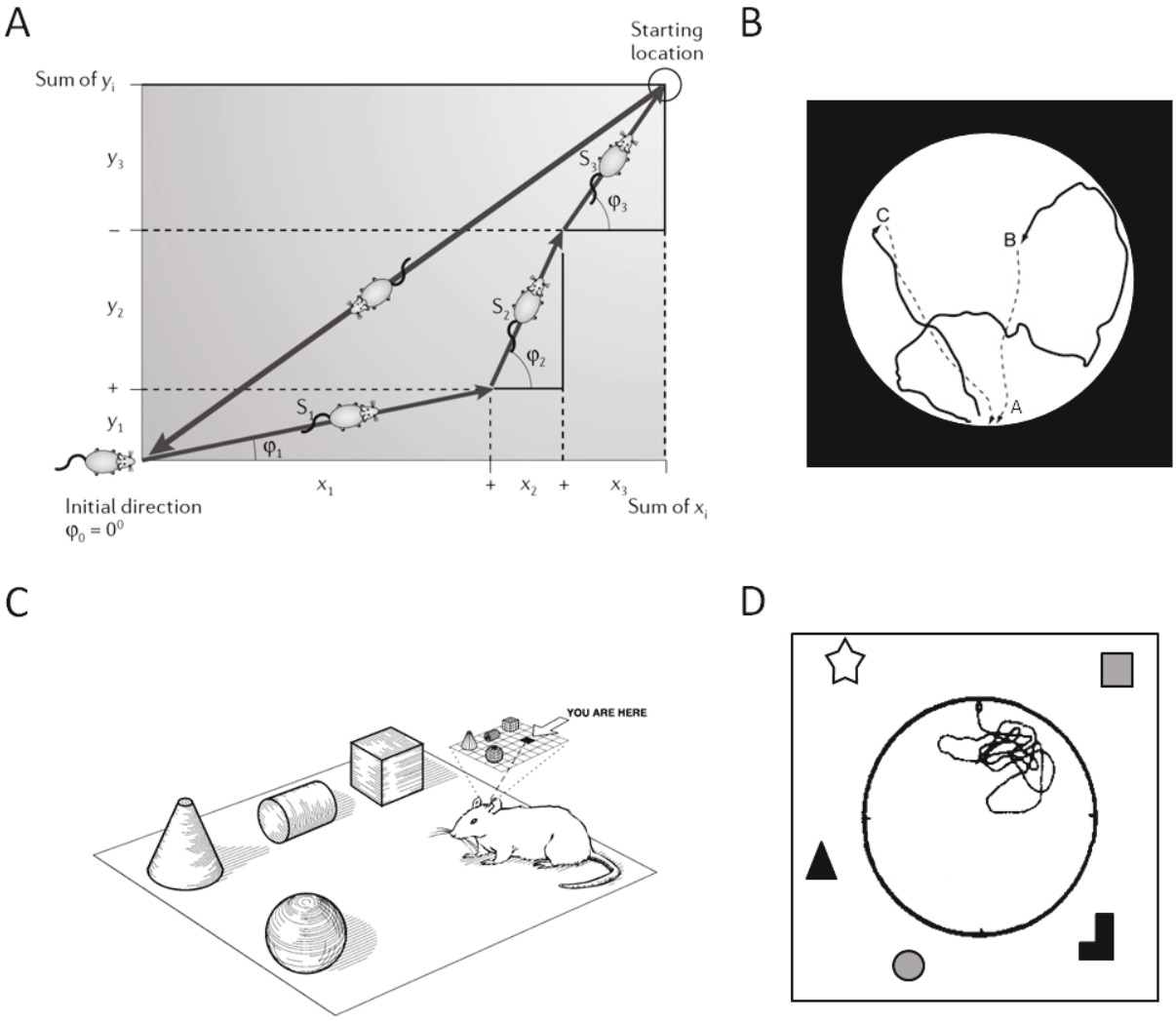

Figure 3. Path integration and map-based navigation

A. Theoretical representation of the path integration process. S1–3 represent vectors lengths of segments of the outbound journey, and φ1–3 are corresponding head directions. Variables x1–3 and y1 –3 are the cartesian components of the segment vectors which, in principle, could be summed to compute the homing vector. (McNaughton et al. 2006).

B. Two examples of homing behavior. After being lured from their nest to a food pellet (solid lines), the animals directly come back to their nest (dotted lines). (Etienne et al. 1998)

C. Theoretical representation of map-based navigation. The cognitive map contains the topographical relationships between the items of the environment as well as the subject's position. (Eichenbaum, 1999)

D. Example of focus search behavior during the probe test following training in the water maze. Based on the configuration of distal cues, the animal localizes the former position of the platform (Morris 1982).

1.2 PATH INTEGRATION AND MAP-BASED NAVIGATION

We have seen than both self-motion and external information that are available to the animal are indeed used to navigate. Based on the use of these different types of information, several navigational strategies have been identified: stimulus-triggered response, target approaching, route based-navigation, path integration, and map-based navigation (Arleo and Rondi-Reig, 2007). However, in the absence of an explicit goal (as it is the case during free exploration), path integration and map-based navigation are the only relevant strategies. I will now present the theoretical processes that have been formalized to explain how sensory information is used to navigate (Figure 3).

Path integration consists in estimating its position in a continuous manner with respect to a reference point, by the addition of successive small increments of movement (Figure 3.A). The estimation of direction and distance relies on signals that derive from its own locomotion. Path integration is manifest by the ability to return to the starting point of a journey without making use of familiar position cues, during homing behavior for example (Figure 3.B). Such a process does not require previous experience of the environment and is usable at the first exploration. However, because position is determined by an incremental process, errors tend to accumulate over time. In the absence of correction, the precision of this system decreases with the length of the path (Etienne and Jeffery, 2004).

Map-based navigation refers to the ability to select stimuli in the environment to form a mental representation of space (a cognitive map), containing the spatial relationships (distance, orientation) of the different points of the environment (Figure 3.C-D). Map-based navigation had first been suggested by Tolman from the observation that rats were able to rapidly adapt their behavior and chose the shortest path to find the reward, a capability which could not be supported by simple sensori-motor association or motor programs (Tolman, 1948). Map-based navigation requires previous exploration of the environment and is thus only usable in known environments. However, once these relationships are established, it allows behavioral flexibility since the subject is able to form new trajectories, by crossing information from the environment and from its mental representation.

Numerous studies showed that these processes are likely to occur simultaneously. For example Fenton et al. (1998) trained rats to avoid footshock that was present in a part of a circular arena. The slow rotation of the arena produced a conflict between spatial information in the room reference frame and spatial information in the arena reference frame (accessed by self-motion signals). The conflict situation led the animals to avoid two distinct areas, one in the room reference frame as well as one in the arena reference frame (Fenton et al., 1998). This suggests that their path integration system and their map-based system had encoded the task simultaneously.

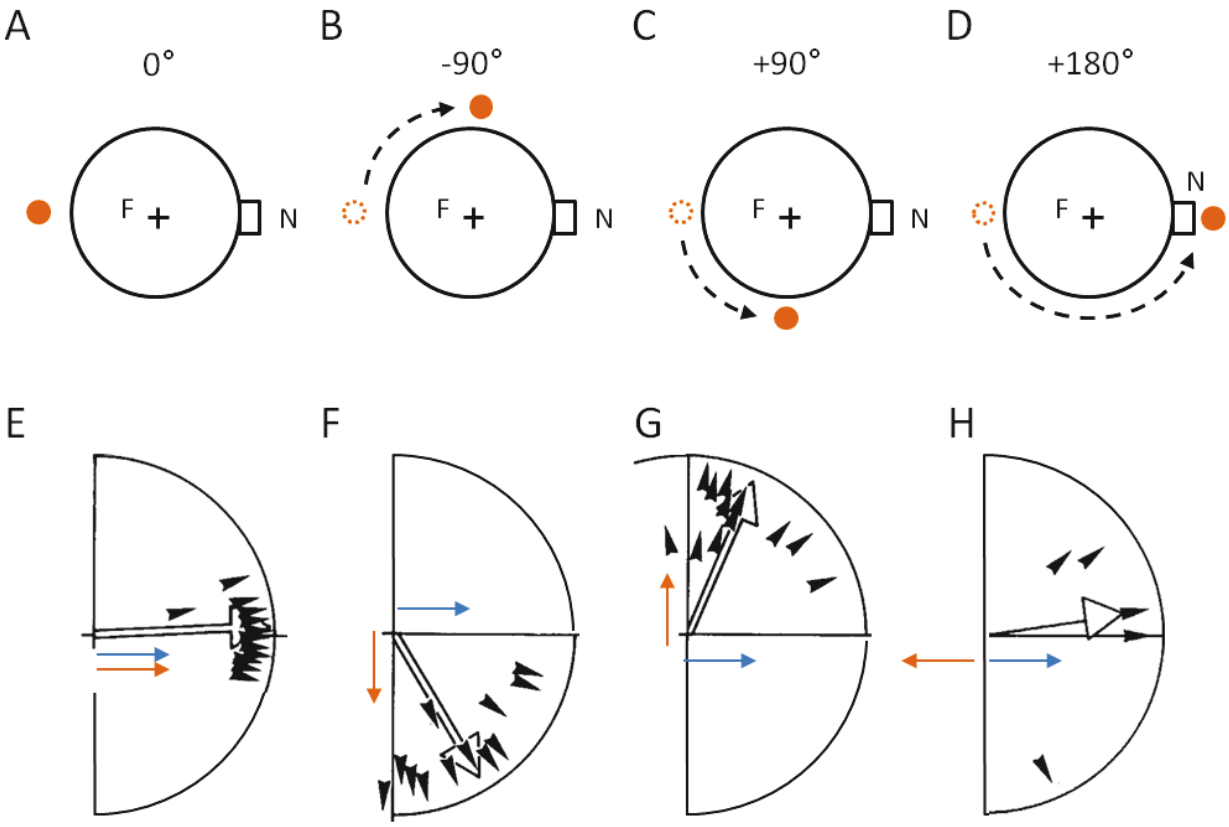

Figure 4. Conflicts between internal route-based information and the spot as a location-based cue.
A-D. Experimental paradigm. During training a light spot was used as the only visual cue. While the animal was taking food, the light spot was lit off, rotated by 90° and switched on again, thus creating a conflict between self-motion information and visual cue information. The numbers on top of the diagrams represent the deviation of the spot from its standard position during the control (0 °) and the experimental (-90°, +90 °, +180°) trials.
E-F. Homing directions. In each quadrant, the small closed arrowheads represent the vectors of 12 subjects when they entered the peripheral annular zone of the arena. The large open vectors represent the mean orientation of the entire experimental group. Colored arrows indicate the theoretical homing directions if the subjects depended either on self-motion (blue arrow) or on visual (orange arrow) information.
Adapted from Etienne et al. 1990

The parallel encoding of multisensory information by both systems allows the animals to clarify ambiguous situations. This was shown by Etienne and collaborators who studied the influence of visual information in a homing task (a task possibly solved with self-motion information only, as seen previously). During training, a light spot was used as the only visual cue (Figure 4.A). While the animal was taking food, the light spot was light off, rotated by 90° and switched on again, thus creating a conflict between self motion information and visual information (Figure 4.B-C). The animals were shown to use a return vector along a compromise direction, which took into account the conflict (Figure 4.F-G) (Etienne et al., 1990). This shows that path integration and map-based navigation processes interacted to determine the animal's behavior. However, for a larger conflict (a 180° rotation of the visual

cue), the return vector was only based on self-motion information (Figure 4.D,H), showing the ability of animals to ignore the direction given by the map-based system if it was judged unreliable (Etienne et al., 1990). Rodents seem to estimate the credibility of each category of cue and give more credit to the more reliable type of information (Etienne and Jeffery, 2004).

1.3 MAIN ANATOMICAL NETWORK CLASSICALLY INVOLVED IN SPATIAL NAVIGATION

The anatomical bases of spatial navigation have been classically investigated by subjecting animals to a spatial navigation task following lesion or inactivation of a specific brain region.

Thus, various studies progressively showed the involvement of a large network of structures. This network primarily involves the hippocampus (O'Keefe and Black, 1977; Morris et al., 1982; Packard and McGaugh, 1996; Whishaw and Gorny, 1999) but also the parietal cortex (Save and Moghaddam, 1996; Save et al., 2001), the retrosplenial cortex (Harker and Whishaw, 2004), the entorhinal cortex (Nagahara et al., 1995; Eijkenboom et al., 2000; Parron and Save, 2004; Van Cauter et al., 2013), the prefrontal cortex (Granon and Poucet, 1995; Floresco et al., 1997; Ragozzino et al., 1998) and the striatum (Moussa et al., 2011; Penner and Mizumori, 2012; Fouquet et al., 2013). Functional imaging in human during virtual reality navigation tasks confirmed the major role of the hippocampus, amongst a larger network of structures (Maguire, 1998; Spiers and Maguire, 2006).

The study of lesions and regional activations in specific tasks allowed to propose distinct functional roles for the different structures of the network. However, since a spatial task can sometimes be resolved by different processes, compensatory mechanisms might prevent us from fully detect the specific role of each structure. To this regard, electrophysiological recordings in freely moving animals performing a spatial task give complementary insights to the way a spatial representation is formed in the brain and used for navigation.

2 BUILDING A SPATIAL REPRESENTATION IN THE BRAIN

Electrophysiological recordings in freely moving animal offered the possibility to correlate the activity of individual neurons with different parameters such as the position of the animal, its orientation or its movement, in order to infer what information these neurons code for. The manipulation of the environmental conditions helped to understand what signals these neurons receive. Finally, simultaneous recordings in several regions (possibly with concomitant disruption of the neighboring region) participate in deciphering the information flow in the spatial network.

2.1 A NETWORK OF STRUCTURES CONTAINING SPATIALLY MODULATED CELLS

2.1.1 HIPPOCAMPAL PLACE CELLS

Place cells are principal cells of the CA1, CA3 and dentate gyrus of the hippocampus. They were initially discovered in CA1 by O'Keefe and Dostrovsky who proposed them to be the neuronal substrate of the cognitive map (O'Keefe and Dostrovsky, 1971). Place cells are characterized by their "place field", a circumscribed region of the environment where cells are active (Figure 5). Typically, a place fires at a very low rate in most of the environment and discharges in bursts (up to 50 Hz) (Muller et al., 1987) whenever the animal crosses the place field.

Since each cell represents a portion on the environment, an ensemble of place cells can represent the whole environment. Consistent with this, it is possible to reconstitute the movement trajectory of a rat by using the activity of its ensemble of place cells (Wilson and McNaughton, 1993; Jensen and Lisman, 2000). The authors estimated that computing the trajectory with a 1-cm accuracy over 1 s would require about 130 cells (Wilson and McNaughton, 1993).

There is no topographical organization between the anatomical position in the pyramidal layer and the location of the place field in the environment (i.e., two neighboring cells are as likely to code for distant regions of an environment as they are to code for nearby regions). However, the size of the place field gradually increases from the dorsal to the ventral pole of the hippocampus (Jung and Wiener, 1994; Kjelstrup et al., 2008).

In experimental arenas commonly used, a place cell displays only one firing field. However, in larger environments, most of the cells display several firing fields (Fenton et al., 2008; Henriksen et al., 2010; Park et al., 2011). The tendency to display multiple place field seems to be graded along the transverse axis of CA1, with distal CA1 cells (far form CA2) showing more dispersed firing and having a larger number of firing fields than proximal cells (near CA2) (Henriksen et al., 2010).

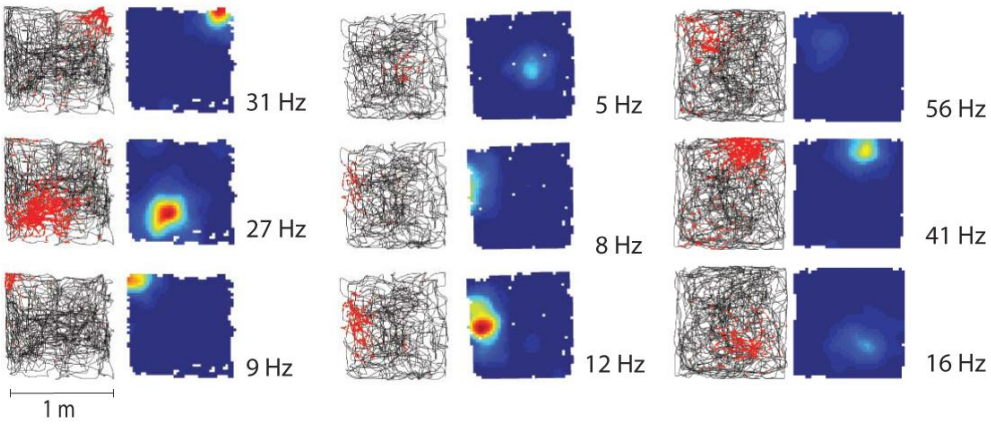

Figure 5. Hippocampal place cells
Examples of 9 different CA3 place cells recorded in a square arena.
The trajectory is in black; firing locations are superimposed in red. Each red dot corresponds to one spike. Rate maps are color-coded, with minimum (in blue) corresponding to zero and maximum values (in red) indicated to the right of each map. (Fyhn et al. 2007)

Remapping

Specific spatial firing can be recorded at the first exposure of an environment (Hill, 1978) and this spatial specificity is preserved over months (Thompson and Best, 1990). However, alterations in the firing pattern can be observed following changes in the environment (Muller and Kubie, 1987). Place fields can appear, disappear or move to unpredictable location, and firing rates can change drastically. Muller and colleagues called this phenomenon “remapping”. Two environments are thus encoded by two independent sets of place cells, and if a place cell has a place field in both environments, there is no relationship between these two place fields. Later, several types of remapping were defined (Figure 6):

- **Global remapping,** corresponding to the initially described “complete remapping” by Muller and Kubie. Following a well-defined change in the environment (changing the shape of the testing enclosure, from circular to rectangular for example), all place cells display changes in spatial discharge and firing rate (Figure 6.A).
- **Rate remapping,** defined as substantial changes in firing rates accompanied by little to no shifts in place field locations (Leutgeb et al., 2005). It occurs following minor changes in the environment, such as changing the color of a wall in the arena or changing the shape of an arena but preserving the environmental cues. It has been proposed that firing rate variations might be a general way for the hippocampus to represent non-spatial aspects of an experience on top of a stable place code (Figure 6.B) (Leutgeb et al., 2005; Ferbinteanu et al., 2011; Allen et al., 2012).
- **Partial remapping** refers to situations where discordance is observed in the place cell population. In partial remapping, different reference frames can be represented by different subsets of cells within the population. When remapping only concerns the place cells located nearby the environmental modification, partial remapping can be

referred as “local remapping” (Paz-Villagrán et al., 2004; Lenck-Santini et al., 2005; Alvernhe et al., 2008, 2011).

-

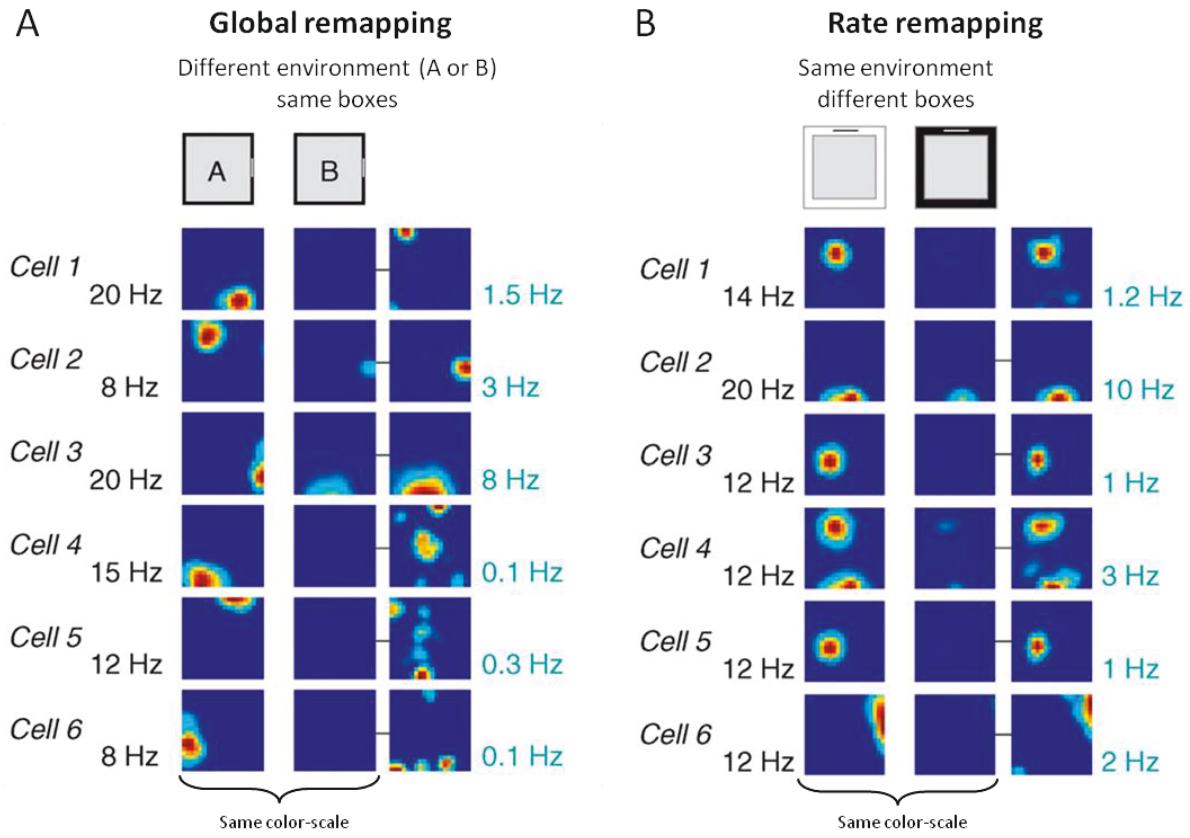

Figure 6. Global and rate remapping of hippocampal place cells
Colour-coded rate maps showing rate remapping and global remapping in 12 CA3 place cells (dark blue = 0 Hz; red = maximum firing rate, as shown on the far left and right of each row). Rats were tested in identical boxes in different locations (A and B) (global remapping) or in boxes with a different colour configuration in a constant location (rate remapping). In each panel, the right column contains the same data as the middle, but the colour maps are now scaled to their own maximum values (indicated to the right of each map). Note that firing locations remained constant in the rate remapping condition, whereas the intensities of firing differed strongly. In the global remapping conditions, both firing locations and firing rates were changed (Colgin et al. 2008).

Some authors also described rotational remapping characterized by the change of place field orientation relative to the only prominent cue, in spite of the preservation of its shape (the contours of the discharge area) (Renaudineau et al., 2009). This rotation coherently affects all the simultaneously recorded place cells and suggests a change in the orientation of the whole spatial representation relative to the prominent cue. However, this phenomenon has only been observed in mutant mice (lacking zif-268), and may not be representative of a normal physiological process.

The role of place cells as the neuronal substrate of the spatial map is suggested by the extensive literature showing coincident alteration of spatial performances and place cell properties, in conditions of cue disruption in control animals, but also in aging animals and genetically modified models, or following pharmacological inactivation (Andersen et al., 2006). More specifically, further arguments from the correlation of place cell firing and the navigational decisions of the animals: the firing fields of place cells stayed in register with their behavioral choices, including during errors (O'Keefe and Speakman, 1987; Lenck-Santini et al., 2002).

2.1.2 HEAD DIRECTION CELLS

Head direction (HD) cell were first described by Taube, from recordings in the post-subiculum, as cells firing in function of the animal's head direction (Taube et al., 1990). A given HD cell discharges whenever the animal points its head toward a particular direction, independently of the animal's behavior, location, or trunk position (Figure 7.A). Each cell is tuned for one allocentric direction, and all directional headings are equally represented within a population of HD cells (Figure 7.B). Its firing rate is maximum at this direction, referred as the cell's preferred direction, decreased linearly on either side of the preferred direction and is at or near zero when the animal's head is not pointing in the cell's preferred direction. The peak firing rate of HD cells varies from 5 to 120 Hz, with a mean of 35 Hz (Taube et al., 1990). The range of HD angles over which discharge is over the baseline is referred as the directional firing range and averages around 90° for most cells (although it can varies from 60° to 150°). For each HD cell, the preferred direction, peak firing rate, and directional firing range remain stable for days (Taube et al., 1990).

Later, HD cells were recorded in several other brain areas including the anterior dorsal thalamic nucleus (ADN, 60% of the recorded cells) (Taube, 1995), lateral mammillary nuclei (LMN, 25%) (Stackman and Taube, 1998), lateral dorsal thalamus (30%) (Mizumori and Williams, 1993), retrosplenial cortex (both granular and agranular regions, 10%) (Chen et al., 1994; Cho and Sharp, 2001), entorhinal cortex (50%) (Sargolini et al., 2006), and the dorsal striatum (6%) (Mizumori and Williams, 1993; Wiener, 1993).

The functional utility of HD cells existing in such a large network is not well understood. Comparison of HD cells properties across structures revealed remarkably similar turning curves but also noticeable differences. LMN HD cells tend to have broader directional firing ranges, and ADN HD cells tend to have higher peak firing rates. In addition, many LMN cells are modulated by turn direction, that is, they exhibit higher peak firing rates for head turns that pass through the preferred direction in one turn direction as opposed to the opposite turn direction (Stackman and Taube, 1998). In addition, HD cells in the ADN and LMN, but not the post-subiculum, generally show a secondary firing correlate with angular head velocity. These findings suggest that HD cells in the different structures might have specific roles, in relation with the integration of the HD signal with other sensory modalities.

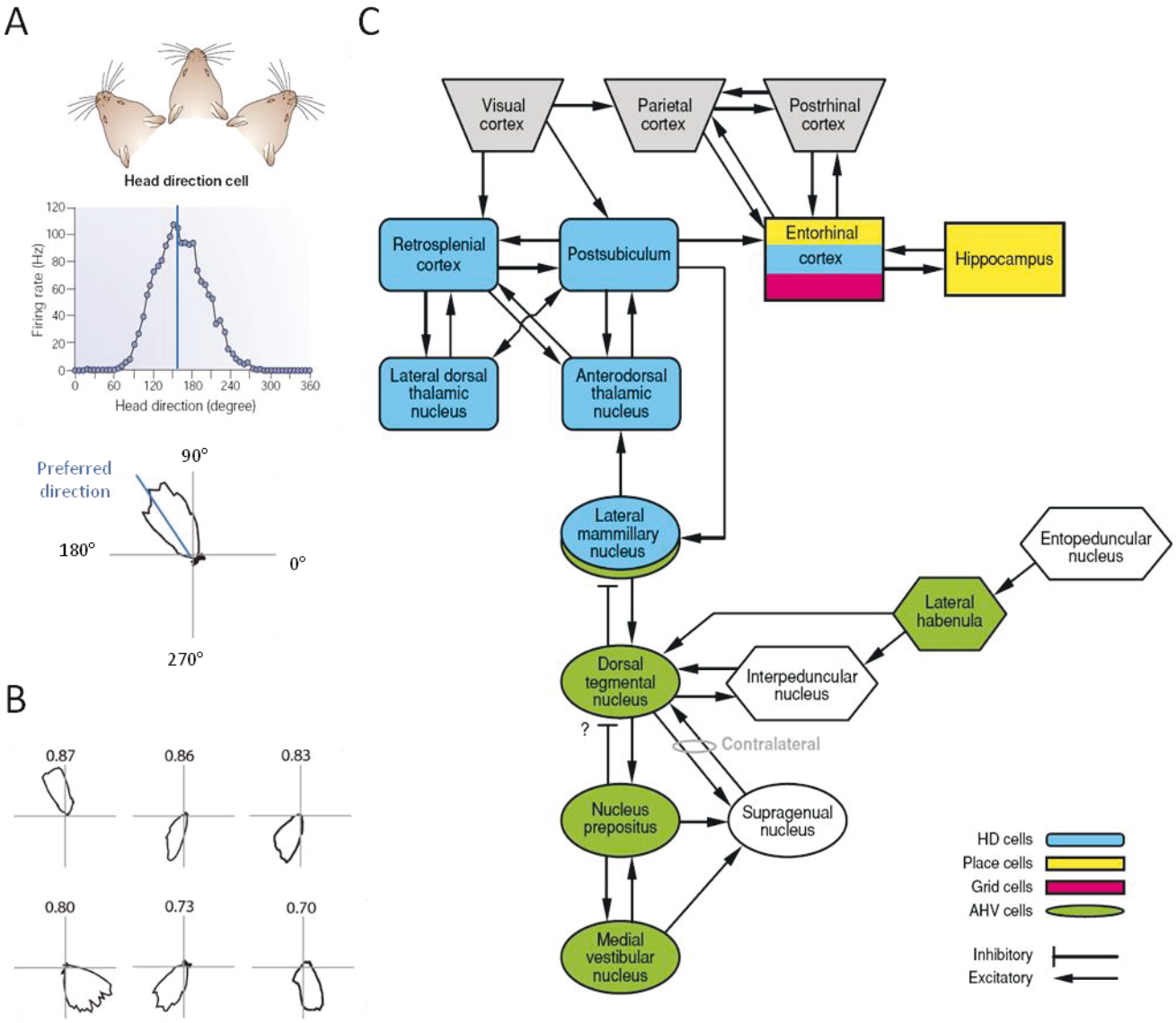

Figure 7. Head direction cells

A. head-direction cell preferentially discharges for a particular orientation of the animal's head. Recording of a head-direction cells. Linear (top) and polar(bottom) representation of its firing rate (Vann and Aggletion, 2004)

B. Polar plots of six head direction cells with various preferred directions (recorded from layers V–VI of medial entorhinal cortex) (Giocomo et al. 2014)

C. Circuit diagram showing principle connections of areas containing HD, place, grid, and angular head velocity (AHV) cells. Color key indicates the types of neuronal correlates identified for cells in that brain area. Note that lateral mammilary nucleus contains both HD and angular head velocity (AHV) cell types, and entorhinal cortex contains HD, place, and grid cell types. (Taube 2007)

To investigate how the HD signal is generated, several labs have recorded HD cells after lesion or inactivation of the neighboring HD cell containing region. It has been shown for example that lesions of the ADN disrupted the presence of HD cells in the post-subiculum, but that lesions of the post-subiculum spared HD cells in the ADN (Goodridge and Taube,

1997). This approach allowed drawing functional connection between areas containing HD cells (Taube, 2007)(See Figure 7.C).

HD cell firing are largely unaffected by inclination of the head (pitch or roll) and are thus comparable to a compass, encoding head direction in the horizontal plane (Stackman et al., 2000; Taube, 2007). Recording of ADN HD cells while the animals were locomoting in other plane than Earth horizontal showed a preserved signal in the vertical plane but a severe degradation when the rats traversed the ceiling inverted (Calton and Taube, 2005). This suggested that the otolith organ input is important for normal HD cell discharge.

HD cells are thought to play an important role in the path integration processes. Indeed, during path integration tasks, HD cell activity is strongly correlated to the rats' heading error in its homing behavior (van der Meer et al., 2010; Valerio and Taube, 2012; Yoder and Taube, 2014).

2.1.3 GRID CELLS

Grid cells were identified in layers II and III of the medial entorhinal cortex (MEC) (Hafting et al., 2005; Sargolini et al., 2006) and have since been also found in pre- and para-subiculum (Boccara et al., 2010).

Grid cells, like place cells, fire in function of the animal position, irrespective of its orientation. However, they display multiple periodic firing fields arranged in a hexagonal lattice, which extends over the whole environment (Figure 8.A). The firing pattern of each grid cell is characterized by several parameters: the size of the fields, the spacing (the distance between the fields) the orientation of the grid (relative to a reference axis) and spatial phase of the grid (the offset of the grid relative to a reference point, i.e. the coordinates of the closest vertex relative to that point) (see Figure 8.B). Neighbouring grid cells have similar spacing and grid orientation but their spatial phase are distributed, so that a limited number of grid cells covers the entire environment.

Grid cells are topographically organized along the dorso-ventral axis, with fields recorded from the dorsal MEC being smaller and closer together whereas fields recorded in ventral MEC are larger and more spread out (Hafting et al., 2005; Fyhn et al., 2008). However, rather than forming a continuum, grid cells seem to form discrete subsets marked by abrupt jumps in scale (Stensola et al., 2012)(Figure 8.C).

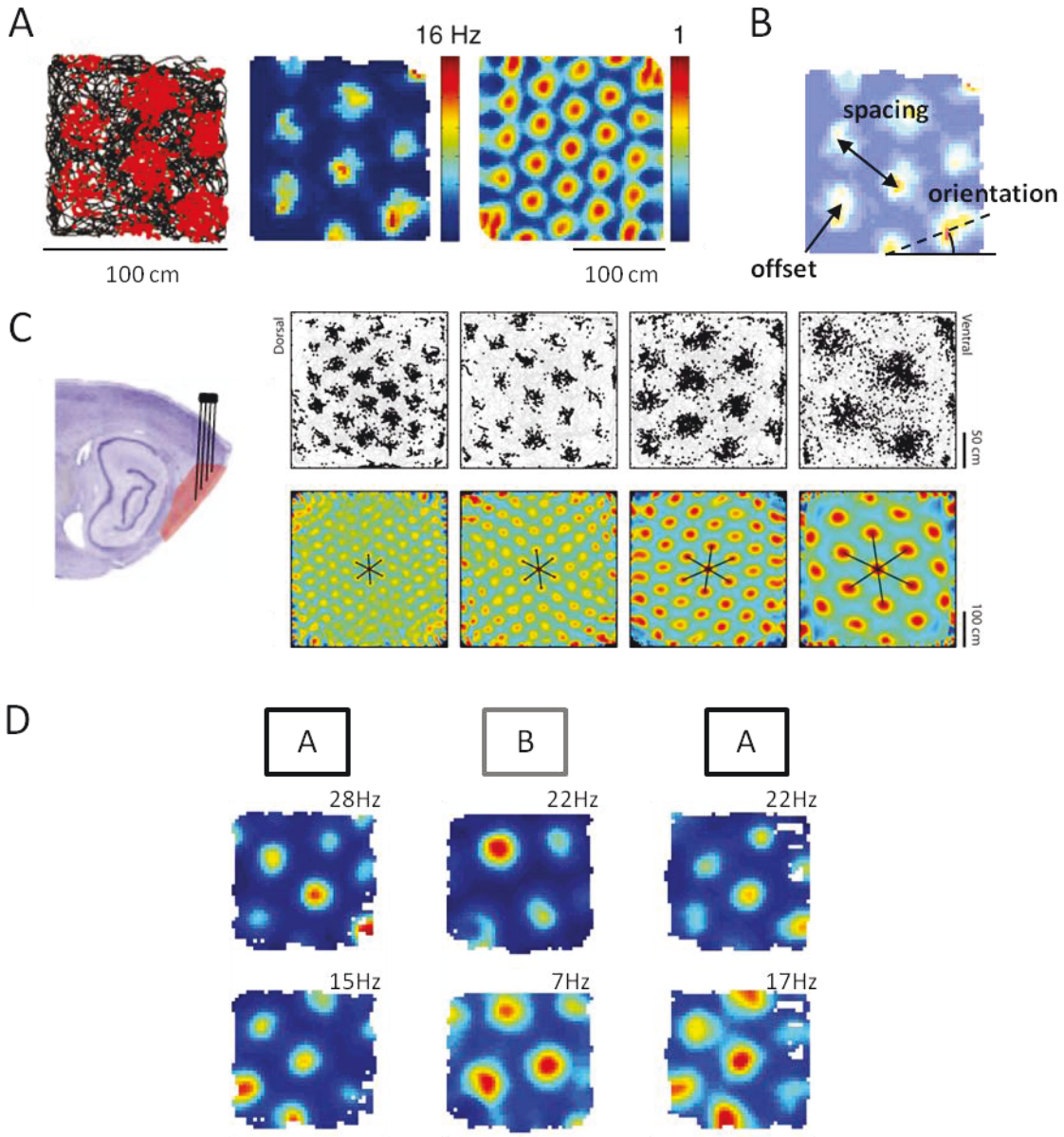

Figure 8. Grid cells

A. Representative example of a presubiculum grid cell recorded during running in an open field. Trajectory with spike positions (left), rate maps (middle left), autocorrelation maps (middle right). Rate maps and autocorrelation maps are color-coded, with color scale bars and minimum and maximum values to the right of each map. The scale of the autocorrelation diagrams is twice the scale of the rate maps. The spatial autocorrelogram reveals repeating activity patterns in the spatial rate map and is generated by correlating the rate map with itself at all spatial offsets. (Boccara et al. 2010)

B. Representation of the parameters characterizing the grid pattern: the spacing (the distance between the fields) the orientation of the grid (relative to a reference axis) and spatial phase of the grid (the offset of the grid relative to a reference point).

C. Step-like increases in grid scale along the entorhinal dorsoventral axis. Left, Schematic representation of tangential and multisite recording approaches (Nissl-stained sagittal sections, MEC highlighted in red). Right, Example grids at successive dorsoventral positions. Dorsoventral location from brain surface is indicated. Top, neuronal spikes (extracellular action potentials) overlaid on trajectory of rat (grey). Bottom, corresponding colour-coded autocorrelograms with colour scale (blue is correlation of-1, red is correlation of 1). Grid spacing was determined from the innermost polygon (black axes). (Stensola et al. 2012)

D. Realignment of entorhinal grid fields during hippocampal global remapping between two rooms (A and B). Rate maps for representative simultaneously recorded MEC cells (Fyhn et al. 2007). Note that the grid cell maintains its spacing and field size but the orientation and spatial phase of grids are modified.

Grid realignment

When grid cells are recorded in different environments, a grid cell maintains its spacing and field size but the orientation and spatial phase of grids are modified (Fyhn et al., 2007)(Figure 8.D). This modification affects all the grid cells in a coherent way, i.e. their spatial phase relationships are preserved. This phenomenon, called "grid realignment", indicates that the map of grid cells in the MEC realigns with changes in the environment without losing its intrinsic spatial phase structure. Interestingly, exposing animals to environmental changes that only induce rate remapping of hippocampal place cells does not result in any change in grid cell fields (Fyhn et al., 2007).

In the MEC, Sargolini and colleagues also described conjunction cells, cells which display a firing pattern resulting from a grid modulation as well as a directional tuning (Sargolini et al., 2006). Conjunction cells have been also recorded from the pre- and para-subiculum (Boccara et al., 2010). These cells are hypothesized to integrate position and direction information as the animal moves around in order to update the representation of spatial location (Sargolini et al., 2006).

The firing properties of grid cells strongly suggest that they are part of the neuronal network underlying path integration (see paragraph 2.2.3). Consistently, mice lacking GluA1-containing AMPA receptors display impaired grid cell spatial periodicity and specific alterations in path integration (without spatial memory deficit) (Reisel et al., 2002; Allen et al., 2014). However, the place cells of these mice are also affected in their spatial selectivity (Resnik et al., 2012), preventing a clear-cut dissociation of the contribution of each cell type.

2.1.4 BORDER CELLS

Border cells are cells whose activity pattern encodes animals distance from the salient geometric border of the environment. They had first been predicted by computational models of hippocampal functioning (Hartley et al., 2000; Lever et al., 2002) and referred as "boundary vector cells". They were subsequently recorded in the entorhinal cortex (Savelli et al., 2008; Solstad et al., 2008), the pre- and para-subiculum (Boccara et al., 2010) the subiculum (Lever et al., 2009), where they are named « boundary vector cell ». As these cells share very close characteristic I will collectively refer them as border cells. In these different areas, border cells are relatively sparse, making less than 10% of the population in the entorhinal cortex, pre- and para subiculum (Solstad et al., 2008; Boccara et al., 2010) and 24% in the subiculum (Lever et al., 2009).

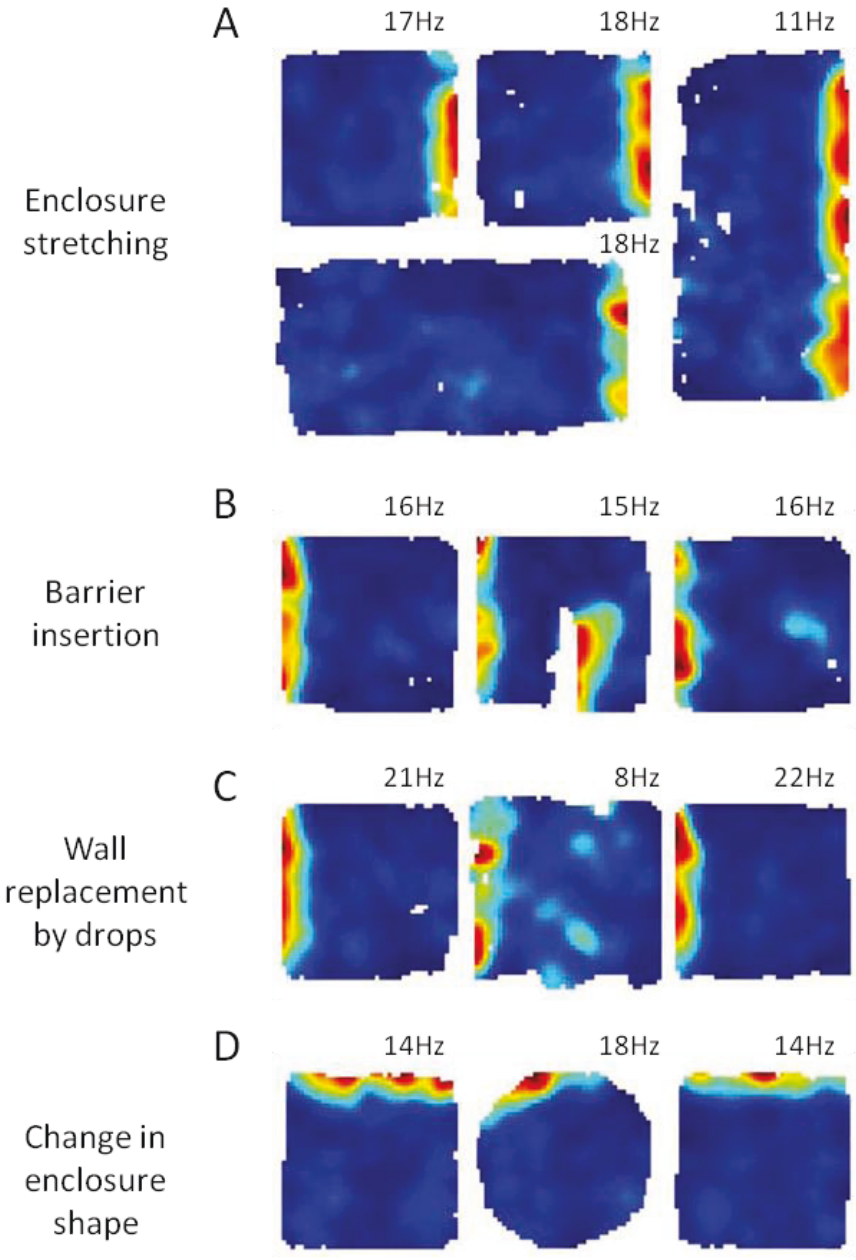

Figure 9. Border cells

Border cells express proximity to boundaries in a number of environmental configurations.

A-D.Color-coded rate maps for a representative border cell in boxes with different geometric configurations. Each panel shows one trial.

A.The border field follows the walls when the square enclosure is stretched to a rectangle.

B. Introducing a discrete wall (white pixels) inside the square causes a new border field to appear (middle panel). The new field has the same orientation relative to distal cues as the original field on the peripheral wall.

C. Border fields persist after removal of the box walls (middle panel). Without walls, the drop along the edges was 60 cm.

D. Preserved firing along borders across rooms and geometrical shapes. All trials in (D) were recorded in a different room than those in (A) to (C).

Solstad et al.,2008

A border cell fires whenever an animal is at a certain distance from the borders of the proximal environment. If the enclosure is stretched (from a square to a rectangle for example), its activity field extends along their preferred wall (Figure 9.A) (Solstad et al., 2008). Inserting a discrete wall into the enclosure triggers the appearance of a new field lined up along the inserted wall (Figure 9.B). Replacing walls of the recording enclosure by drops on the four sides preserves the activity pattern, showing that they also respond to boundaries other than walls (Figure 9.C) (Solstad et al., 2008; Lever et al., 2009). They displayed a similar border-related activity across different recording environments and in enclosures of different shapes (Figure 9.D) (Solstad et al., 2008; Lever et al., 2009), demonstrating that border cells are independent from the context. Interestingly, when they are subjected to environmental manipulation such as 90° cue rotation, simultaneously recorded cells rotated in concert, and in a consistent way with simultaneously recorded grid and HD cells (Solstad et al., 2008). There is a subtle difference between boundary vector cell recorded in the subiculum and the border cells from the other regions (the entorhinal cortex, pre- and para-subiculum). The border cells were defined as cells firing when the animal is closed to the borders of the environment whereas boundary vector cells were described to encode distance from the borders of the proximal environment and thus include cells whose maximum firing rate is far from the border and cells with large firing fields whose firing rate is modulated by the distance from the border. The border cells in the entorhinal cortex, pre- and para-subiculum might be a subclass of boundary vector cells (Lever et al., 2009).

Border cells, by defining the perimeter of the environment are proposed to serve as reference frames to anchor the firing locations of place cells and grid cells to the environment (Solstad et al., 2008).

2.1.5 "MOVEMENT" CELLS

In the posterior parietal cortex, half of the cells are modulated by the displacement of the animal, irrespective of its location or heading (Figure 10.A-C)(McNaughton et al., 1994; Whitlock et al., 2012); I will refer them as "movement cell". A movement cell fires whenever the animal moves to a certain direction (for example, leftward or forward to the right as illustrated by the two examples on Figure 10.D). These cells do not show any preference for a specific location or direction (Figure 10.E-F). These cells are independent from the context since their activity pattern is preserved in different environments (in conditions where grid cells completely realigned). However, when the animals performs a specific sequence of movements (in a hairpin maze), these cells can acquire new movement specificity (from leftward to backward for example). This last finding led the authors to propose that the activity of these cells is determined by the organization of actions (thus playing a role in the execution of spatial behavior rather than the building of spatial representation). However, representation of basic self–motion is likely to play a role in calibrating one's displacement

through space. This could provide an explanation for path integration impairment following parietal lesions (Save and Moghaddam, 1996; Save et al., 2001).

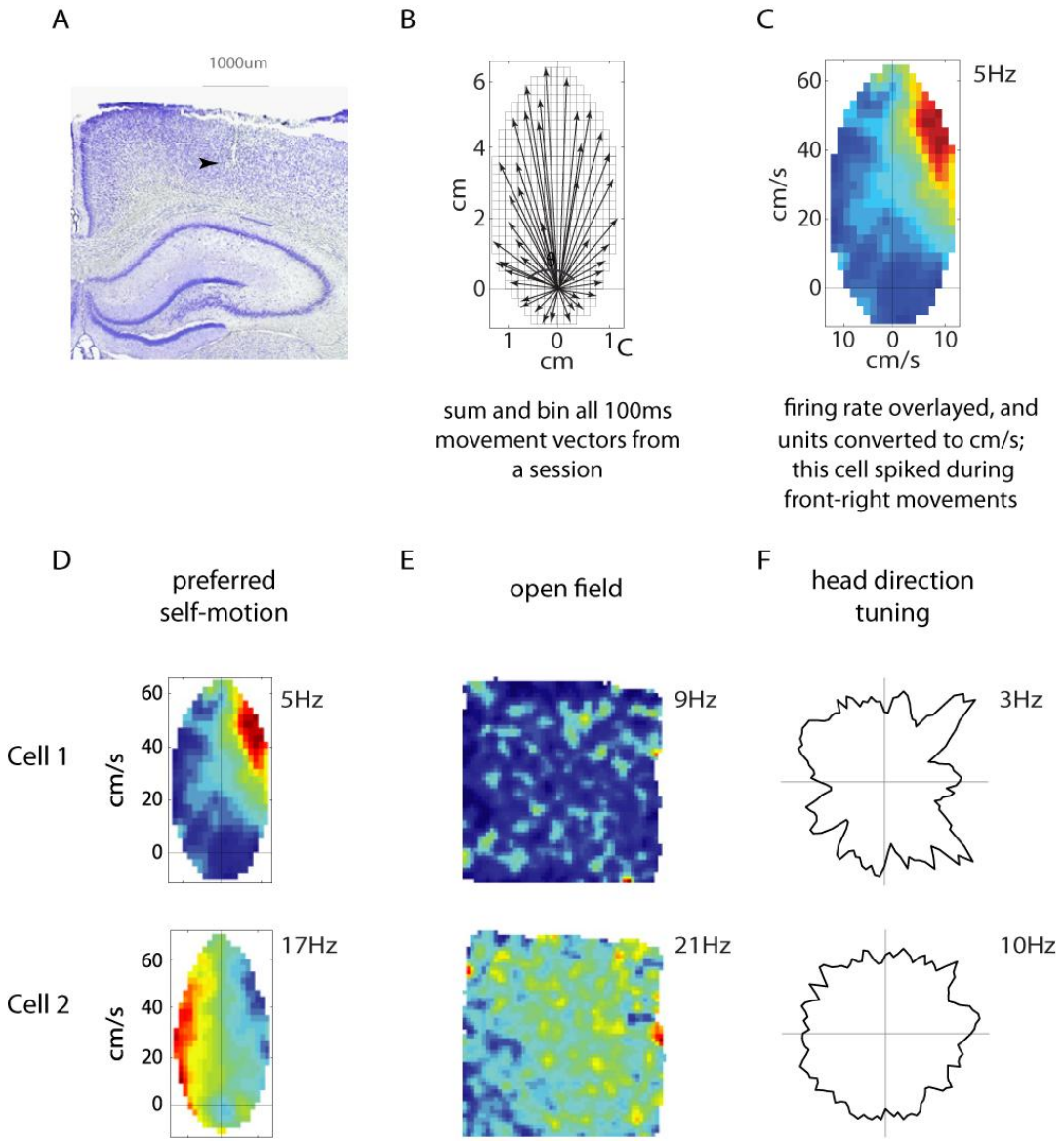

Figure 10. Movement cells

A. Recording site in the posterior parietal cortex (PPC).

B. Every 100ms, the displacement vector is computed from the trajectory and positioned on an egocentric reference frame.

C. The firing rate for the cells recorded is overlayed.

D-F. Rate maps for representative cells recorded in the posterior parietal cortex over 20 min in a squared arena. D. Rate maps in egocentric reference frames. PPC1 is tuned for forward motion to the right and PPC2 for leftward displacement. E-F. Rate maps in an allocentric reference frame. PPC cells do not show any preference for a specific location (E) or direction (F).

(Whitlock et al. 2012)

2.2 SENSORY CONTROL OF SPATIALLY MODULATED CELLS

2.2.1 PLACE CELLS

2.2.1.1 INFLUENCE OF EXTERNAL INFORMATION

Since the discovery of hippocampal place cells, several works have analyzed the influence of sensory information on their properties; I will detail some of the pioneer works that characterized this influence.

Geometry of the environment

To examine the importance of environmental landmark on place cell firing, Kubie and Muller recorded place cells in rats exploring a cylinder containing a white cue card on the wall and applied different types of environmental changes (Figure 11) (Muller and Kubie, 1987). They first observed that the expansion of the recording environment triggered a similar expansion of the place field size (Figure 11.Ai)(Muller and Kubie, 1987). This result has been extended by the works of O'Keefe and Burgess showing that the elongation of the environment in one dimension induced a consistent stretching of the place fields along that dimension (Figure 11.Aii) (O'Keefe and Burgess, 1996). Different cells reacted in different ways, but tended to be most influenced by the closest wall. This strong influence of geometric borders on place field is likely to be representative of inputs from border cells (Barry et al., 2006).

Proximal versus distal landmarks

In the study of Kubie and Muller, the arena was circular and uniformly grey, and the white cue card on the wall was the only visual cue, hence being the sole element polarizing the environment. They observed that if the cue was rotated by 90° in the absence of the animal, the place field correspondingly rotated by 90° such that its relationship with the cue card was preserved (Figure 11.B) (Muller and Kubie, 1987).

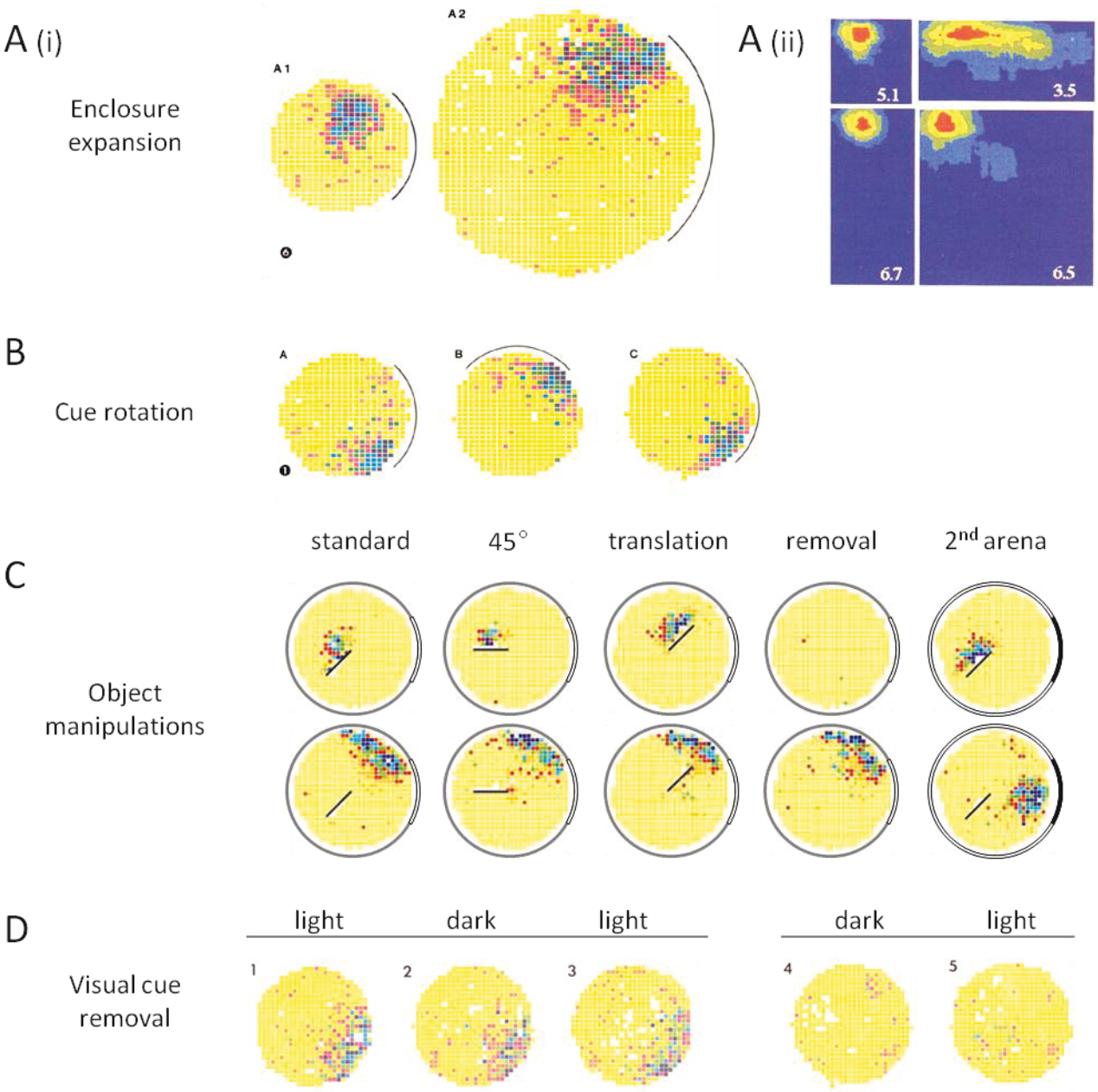

Figure 11. Sensory information controlling place cell firing

A. The response of a place cells to (i) isotropic scaling of the cylinder (Muller and Kubie, 1987) or (ii) anisotropic stretching of the enclosure (O'Keefe and Burgess 1996)

B. Effects of rotating the cue card on the angular position of a firing field. The cue card is in its standard position. When the session was over, the rat was removed from the apparatus the card was rotated 90"counterclockwise. (Muller and Kubie, 1987)

C. Examples of two simultaneously recorded place cells during manipulation of the object inside the arena (the object is represented as a black oblique bar): 45°clockwise rotation, translation, or removal of the object. The arena also contains a stable prominent cue (a white card onto the wall). The last recording session is made in another arena (white, with a black card). These examples illustrate the responses of a cell close to the object (top) and far from the object (bottom). (Rivard et al. 2004)

D. Example of place cell recording during a light-dark-light sequence. If the rat stays in the arena while the light is switch off, the place field persists in the dark condition (1,2,3) but not if the rat is put into the arena directly in the dark (4,5). (Quirck et al.1990)

A series of studies have indeed demonstrated that both proximal and distal cues influence place field location (see for revue Knierim and Hamilton, 2011). The precise role that distal cues play relative to the local cues in controlling place cell firing has been detailed in a nice study from Knierim and Rao (2003). In this work, the recording apparatus was displaced relative to the configuration of environmental cues in the room (Knierim and Rao, 2003). The recording apparatus was a rectangular track, its shape thus constituted proximal cues for the animal. Translations of the apparatus in the room did not affect the place fields: place cells continued to fire at the same location in the apparatus. It has to be noted that apparatus translation produces little change in the perceived configuration of distal cues. On the opposite, rotation of the distal cues in the room triggered an equal rotation of the place fields. This led to the conclusion that distal landmarks orient place fields position relative to the environment whereas proximal information control their precise firing location (Knierim and Rao, 2003). Other studies observed the interaction of proximal and distal cues in the control of place cell firing, with subpopulation of place cells preferentially responding to either type of cues (Shapiro et al., 1997; Renaudineau et al., 2007).

In the absence of distal cues, a single proximal cue efficiently controls place cell location, but what happens when different local visual cues do not give congruent information? Fenton and colleagues recorded place cells in an arena containing a white and a black card and manipulated the spacing between these two cards. Place fields responded differently upon their locations in the arena, with the place fields in the vicinity of a card following the rotation of the card, and the farer place field being less affected (Fenton et al., 2000). This suggests a local distortion of the place cell map to take into account the spatially limited modifications. A similar observation was made by manipulating the position of an object or a barrier inside the recording arena. Muller and Kubie had observed that the insertion of a barrier at the center of a previously recorded place field nearly abolished it (Muller and Kubie, 1987). Displacements of an existing object showed that place fields located near the object followed object translations and rotations, and stopped firing during object removal (Figure 11.C). Contrarily, place fields far from the object showed little if any modification (Rivard et al., 2004; Lenck-Santini et al., 2005). When the object was placed in a second environment, causing remapping of most of the place cells, the cells whose place field was near the object in the first environment continued to fire near the object. This raises the question of information encoded by hippocampal place cell and the possibility for coding local features of the environment, such as objects or barriers.

The modulation of place cells by objects in the environment, which constitutes a source of visual but also tactile and olfactory signals, opens the possibility that such inputs also influence place field characteristics.

Olfactory information

The importance of olfactory cues was shown by Save and colleagues, by applying different combinations of visual and/or olfactory cue manipulation while rats were foraging in a circular arena (Save et al., 2000). After an initial recording session in the light with a cue card on the wall, the rat stayed in the arena and three sessions were run in a row with the cue card removed. The light was either turned off or left on and the floor was either cleaned or left unchanged, thus creating four conditions: dark/cleaning, dark/no cleaning, light/cleaning, and light/no cleaning. Whatever the light conditions, the place fields were unstable when the odors traces were removed (in the dark/cleaning and light/cleaning conditions) whereas they remained stable otherwise (in the dark/no cleaning and light/no cleaning conditions). This evidences the crucial role of olfactory traces in maintaining a stable spatial representation, and suggests that they can be used to compensate the lack of visual information (Save et al., 2000). Additionally, global remapping of place fields was observed when the odor of the familiar recording environment was changed from one trial to another (Anderson and Jeffery, 2003). However, these studies involve two different types of olfactory cues: experimentally controlled odor cues and self-deposited olfactory traces.

The contribution of both types of olfactory information to spatial representation has been further dissected by two recent studies (Zhang and Manahan-Vaughan, 2013; Aikath et al., 2014). Place cells were recorded in a circular arena containing 4 clusters of pinholes diffusing 4 different odors, thus creating a stable configuration of odor cues (Zhang and Manahan-Vaughan, 2013). All the other types of external information were minimized: recordings were performed in darkness, with white noise masking auditory signals, and smooth walls inside the arena. Place fields were shown to be more spatially selective in the presence than in the absence of odor cues. 90° rotation of the odor configuration triggered a consistent rotation of place fields. Finally, odor shuffling induced a remapping or silencing of most of the place cells. This study shows that external odor cues are indeed used to control the location specific firing of place cells (Zhang and Manahan-Vaughan, 2013). On the opposite, Aikath and colleagues showed that self-deposited olfactory traces were not sufficient to stabilize place cell firing (Aikath et al., 2014). Place cells were recorded in different conditions, with preserved or removed olfactory traces, in the presence or absence of prominent visual cues (familiar or novel). When put in conflict with familiar visual cues, olfactory traces were ignored, in favor of visual cues. In the absence of visual cues, olfactory traces did not allow the formation of stable place fields (this condition was not different from the “no odor no visual cue” condition). However, the use of novel visual cues to orient the place fields critically depended on the presence of familiar odor cues, suggesting that olfactory traces are part of the contextual cues (Aikath et al., 2014). The main difference between this study and those of Save et al (2000) is that here the animal was removed from the arena between sessions. This highlights the fact that in the study of Save et al (2000)

olfactory traces needed to be combined with path integration processes to stabilize place cell representation.

Tactile and auditory information

Tactile modulation of place cell properties was demonstrated recently, by recording in rats exploring a square arena covered with sand papers of different grains, in the absence of other external information (in the dark, with the olfactory traces cleaned and the auditory signals masked by white noise) (Gener et al., 2013). Tactile deprivation by lidocaine application on the whisker pad led to place field expansion and decrease in the place cell firing rate. 90° rotation of the tactile cues triggered to the equivalent rotation of place fields (Gener et al., 2013).

Data regarding the auditory cue influence on place cell properties are sparse. To my knowledge, this has been only investigated in a fear conditioning paradigm where rats received electrics shocks paired with a tone. Place cells were shown to respond to the tone when the animal was located in their place field (Moita et al., 2003).

Thus, multiple external sensory information modulates the characteristics of place fields. However, the possibility to record localized firing fields in conditions of very limited external sensory inputs suggests that self-motion cues may also participate in shaping the firing of place cells.

2.2.1.2 INFLUENCE OF SELF-MOTION INFORMATION

The first indications for a role of self motion information in the control of place fields come from the observation that place field could persist in the dark, i.e. in the absence of any visual information (Quirk et al., 1990). However, a place field recorded in the dark resembled the one in the light only if the animal stayed in the arena when the light was switched off (Figure 11.D). Otherwise – if the animal was placed in the arena directly in the dark- the place field could appear at a random location. This suggests that self-motion information was used by the path integration system to maintain the location specific firing of place cell previously recorded in the light. In a experiment where the rat run back and forth in a linear track whose length could be modified, it was observed that on initial part of the journey, the place fields were controlled by the distance run from the departure box whereas on the final parts, they rather depended on the visual cue formed by the destination box (Gothard et al., 1996). This adds further arguments for a role of self motion information in controlling place cell firing.

Among the different self-motion inputs, vestibular information has been shown to be important for hippocampal spatial representation since a temporary inactivation of the vestibular system (by tympanic injection of TTX) dramatically altered the activity pattern of place cells (Stackman et al., 2002). Recently, the possibility to record place cell from mice

placed in a virtual reality environment allowed further dissection of the contribution of the different self-motion signals to place cell firing (Chen et al., 2013a; Ravassard et al., 2013). In such setup, mice are trained to run on an air-cushioned ball with a fixed head-position surrounded by a spherical screen showing a perspective view of a virtual linear track, in which the movement of the viewpoint corresponds to the movement of the ball. In such a paradigm, the mouse receives visual and proprioceptive information but no vestibular signal. Cells with spatially localized activity were effectively recorded on the virtual track. Their firing was dramatically affected by the removal of either visual cues or movement cues (passive unwinding of the visual scene), showing the importance of both visual and proprioceptive information in the control of place fields. Further studies would be required to distinguish the role of visual input in providing environmental information (landmarks) or information relating to self-motion (optic flow). Interestingly, when the relationship between the movement on the ball and the speed of visual input unwinding was modified (producing a conflict between both types of information), the place fields showed a displacement relative to the departure point, revealing a non-linear summation of self-motion and visual inputs for the control of place cell firing (Chen et al., 2013a).

2.2.2 HEAD DIRECTION CELLS

Visual cues were shown to exert a prominent influence on the firing of HD cells. In a circular arena containing a salient cue onto the wall, the rotation of this cue in the absence of the animal leads to the corresponding rotation of the preferred direction of post-subicular and ADN HD cells, thus maintaining their relationship with the cue (see Figure 12.A) (Taube et al., 1990; Goodridge and Taube, 1995; Taube, 1995). Using conflicting situations between distal and proximal cues, distal cues were proven to be more efficient in controlling the preferred direction of ADN HD cells (Zugaro et al., 2001).

However, if the HD system is strongly reliant on landmark cues, removing all the visual cues or turning off the light does not affect much HD cell firing in the post subiculum and ADN (Taube et al., 1990; Goodridge et al., 1998), although the preferred direction drifts over time (Figure 12.B, the peak firing rate and directional range are preserved for both cells but their preferred directions are shifted by 180°). This suggests that self-motion information can maintain HD signals to some extend in the absence of visual information. In fact, vestibular lesions abolished the directional firing properties of HD cells, demonstrating that the HD signal critically depends on vestibular information (Stackman and Taube, 1997; Stackman et al., 2002). The importance of proprioceptive (and motor command) information was shown by recording ADN HD cells in two environments (in two different rooms) connected by a passageway (Figure 12.D). In the dark, if the animal actively walked from one environment to the other, HD cells could partly retain their preferred direction between the two environments. Indeed the directional firing is similar when going from room 1 (familiar)

to room 2 (novel) and back to room 1 (return) (Figure 12.D). However, this was no longer the case if animals were passively transported in the dark from room 1 to room 2, conditions in which the vestibular signal is the only available information (Figure 12. D) (Yoder et al., 2011). This showed the requirement to combine different types of self-motion information (vestibular and proprioceptive) to maintain HD signals in the absence of visual information. HD cell were recently been shown to be also sensitive to optic flow information. Rats were freely moving in an arena where the repetitive background (not usable as landmark) of the cylinder wall slowly rotated, thus providing a continuously drifting optic flow. Recordings in the ADN showed that HD cells exhibit a significant drift in the same direction as the rotating background (Arleo et al., 2013).

Interestingly, when multiple HD cells are recorded simultaneously in the ADN, the angular shift in the preferred direction following landmark removal and rotation is similar between the different HD cells (Figure 12.B), such that their preferred direction always remain at a fix angle apart from one other (Goodridge et al., 1998; Yoganarasimha et al., 2006). This suggests that the HD cell population functions as a coherent ensemble producing unified responses to environmental modifications.

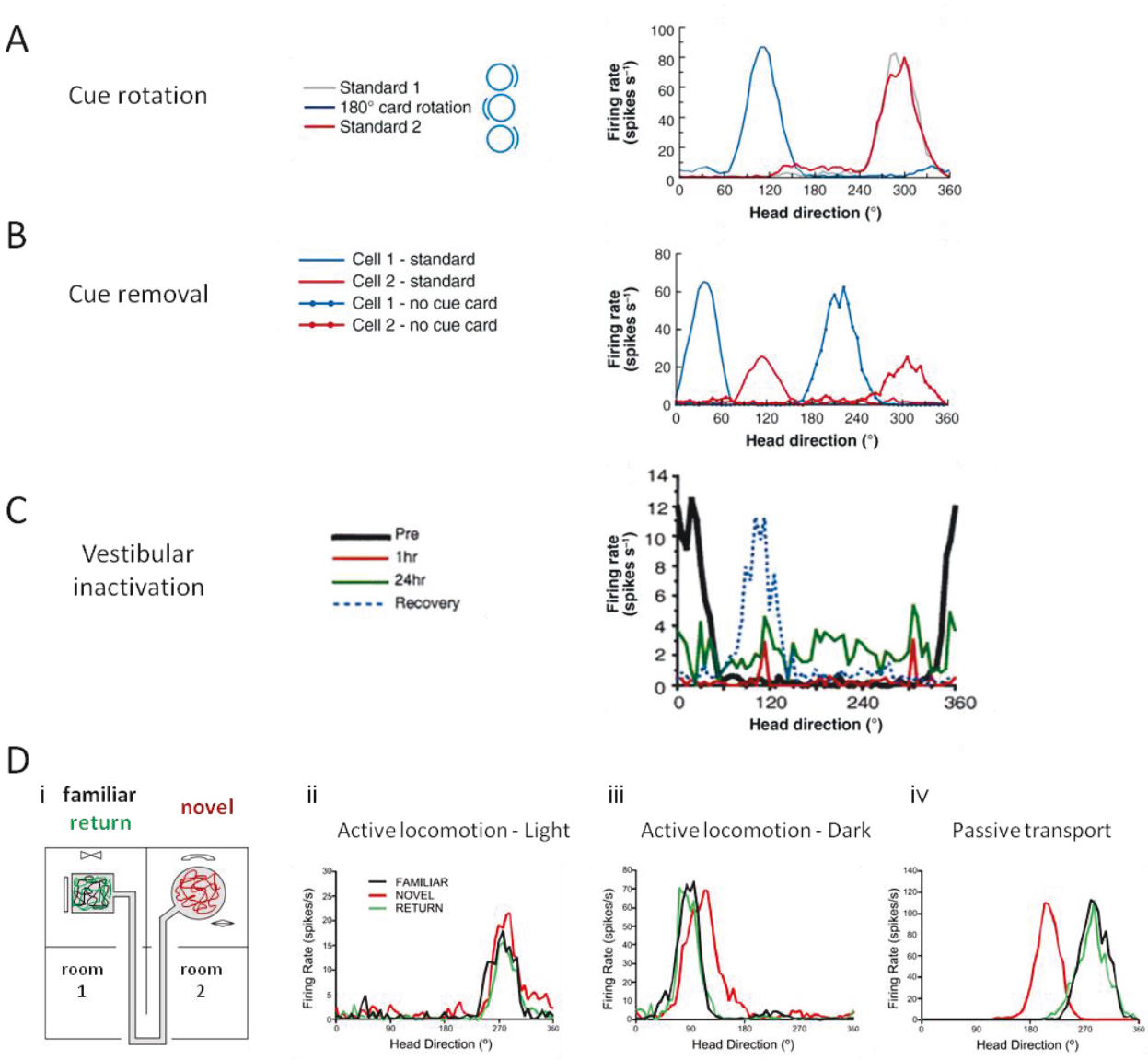

Figure 12. Sensory information controlling head-direction cell firing

A. Responses of an ADN HD cell following an 180◦ rotation of the visual cue card. The preferred firing direction of the cell shifted a similar amount as the cue rotation (blue line) and returned to its original orientation when the cue card was returned to its initial position (red line). Initial recording session is shown as gray line. (Taube 2007)

B. Responses of two post-subicular HD cells recorded simultaneously following removal of the visual cue card. Both cells retained direction-specific firing in the absence of the visual cue, but their preferred firing directions shifted equal amounts and remained in register with one another. (Taube 2007)

C. Response of postsubicular HD cell recorded before and after inactivation of the vestibular apparatus. Directional discharge was abolished by 1 h postinjection. Upon recovery of vestibular function, the HD cells exhibits a marked shift in preferred firing direction as compared to the baseline session. (Stackman and Taube, 2002)

D. Responses of 3 representative HD cells recorded during performance of the multiroom maze. Ischematic representation of the recording apparatus. (ii) During active locomotion in light, this cell's preferred direction remained relatively stable between the familiar and novel arenas, as well as on return to the familiar arena. (iii) During active locomotion in darkness, the preferred direction showed slightly less stability, with a shift of 30°. On return to the familiar arena, the preferred direction returned to its original alignment. (iv) During passive transport, the preferred direction shifted 78°, only to become precisely realigned on return to the familiar arena (Yoder et al. 2011)

2.2.3 GRID CELLS

Several observations initially indicated that grid cell firing primarily depends on self-motion information (Hafting et al., 2005). First, a grid cell fires in all environments (in contrast to the hippocampus where an environment is encoded by a subset of active cells), and the spacing of a grid cell is independent of the environment identity. Second, grid fields appears relatively independent of specific landmarks since they can be observed immediately as an animal starts to explore an environment, and the grid pattern does not change drastically in the dark (Figure 13.A). Third, recording in larger environments allows to see additional fields (with similar spacing) such as the grid covers the entire environment, suggesting that the grids may potentially have infinite size (Figure 13. B) (Hafting et al., 2005). Grid cells were thus proposed to encode a metric system for spatial navigation, whereby the animal can update its own location using self-motion information (path integration) (Jeffery and Burgess, 2006; Moser and Moser, 2008). This was also consistent with the fact that entorhinal cortex lesions altered self-motion based navigation (Parron and Save, 2004).

However, a panel of evidence also shows that grid cells do not encode a pure metric. Indeed, the grid vertices are stable across trials in a familiar environment, suggesting that the external landmarks exert a significant influence. Rotating the prominent cue in a circular arena in the absence of the animal induces an equal rotation of the grid, showing that the grid is indeed anchored to external cues (Figure 13.C) (Hafting et al., 2005). Finally, this sensitivity to external cues was shown to be experience-dependent. Deformation of a familiar enclosure triggers a rescaling of the grids along that dimension (expansion or compression, accordingly) (Figure 13.D) but repeated exposure to such a transformation decreased the amount by which the grid rescaled (Barry et al., 2007). These data suggest that, grids can be associated with environmental features such as boundaries but also that the grid system can revert to an intrinsic grid scale with repeated experience.

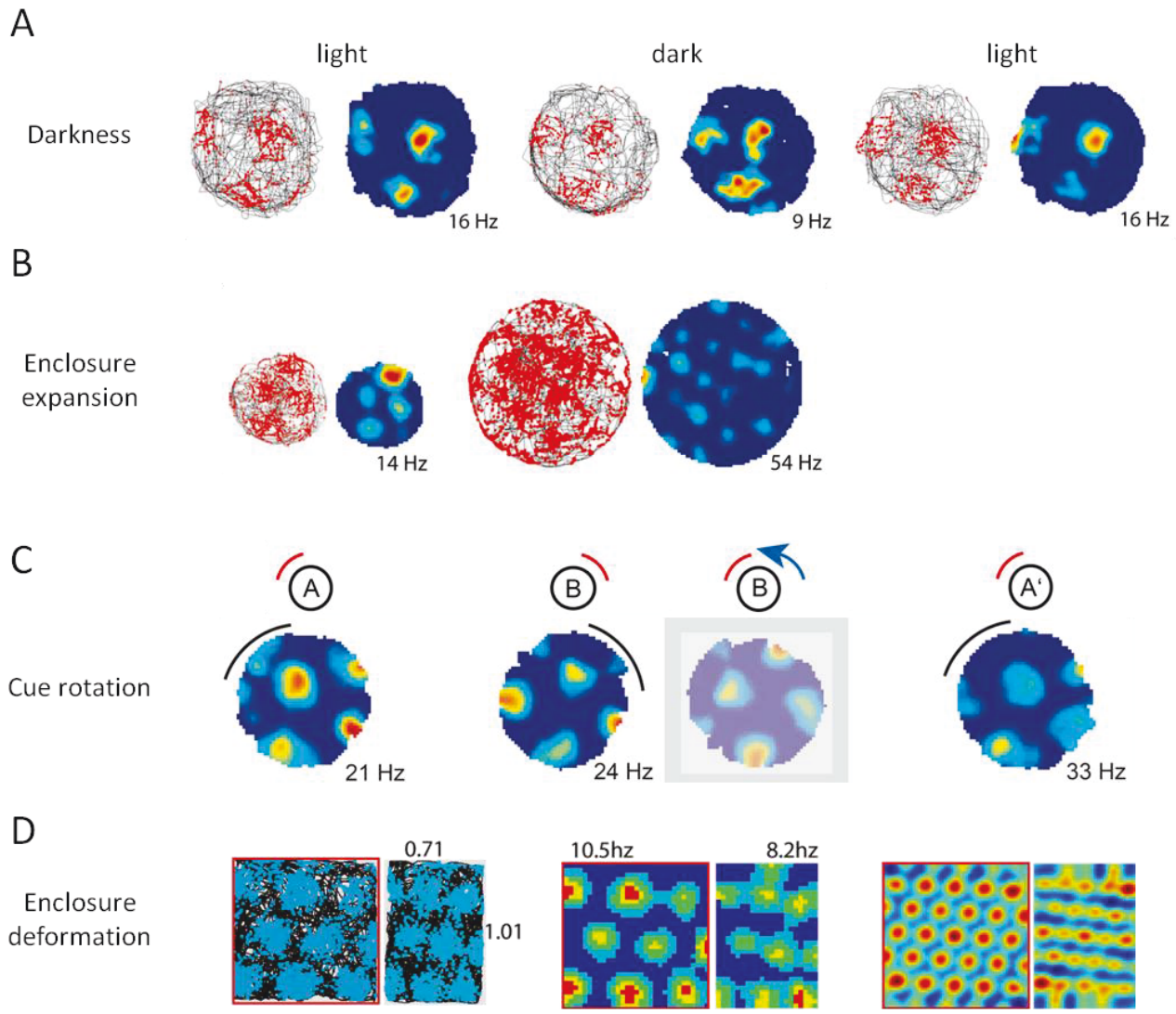

Figure 13. Sensory information controlling grid cell firing

A. Grids persist in darkness. Trajectory and rate maps for a representative dMEC cell after onset of darkness. Room lights were on for 10 min (L), off for 10 min (D), and on for another 10 min (L'). (Hafting et al. 2005)

B. Grid cell maintain their spacing in environment of different size. (Hafting et al. 2005)

C. Grids are aligned to environment-specific landmarks. a, Rate maps for a representative cell after rotation of the cue card (arc) on the small cylinder. Left and right, cue card in original position (A and A'). Middle pair, cue card rotated 90° (B). Shaded map, rate map counter-rotated 90°. (Hafting et al. 2005)

D. Grid cell rescale in response to environmental deformation. (Left) Action potentials (colored dots) superimposed on the animal's path (black) reveal the spatial periodicity characteristic of grid cells. The red outline indicates the familiar configuration (large square). Numeric labels show, for each dimension, the transformation of the rate map relative to baseline (>1 = expansion, <1 = contraction). (Middle) Corresponding firing rate maps.. Peak firing rate is indicated against each map. (Right) Spatial autocorrelograms were constructed from rate maps. (Barry et al. 2007)

Concerning the contribution of the different types of self motion information, the ability to record grid cells in virtual linear paradigm shows that the formation of a multi-peak periodic firing pattern can occur in the absence of vestibular signal (with proprioceptive and

optic flow information only) (Domnisoru et al., 2013; Schmidt-Hieber and Häusser, 2013). However, further studies would be required to understand the relative contribution of each signal to the formation of grid firing patterns.

We have seen that the different kinds of spatially modulated cells display modifications of firing in response to the manipulation or suppression of the different types of self-motion or external cues. Manipulations of individual sensory signals reveal the diversity of information types that are taken into account, and illustrate the necessity to combine them to correctly shape the firing characteristics of the spatially modulated cells. The differences in responses between the different cell types indicate that the relative contribution of each signal may differ from one structure to the other. However, their similar responses to certain manipulations suggest that cells might interact with each other. Specific examination is required to understand how the way information is transmitted to the different cell types and how they interact to form a coherent spatial representation.

2.3 INTERACTIONS BETWEEN SPATIALLY MODULATED CELLS AND INFORMATION FLOW IN THE SPATIAL NETWORK

Interactions between different types of spatially modulated cells can be assessed by several means: (i) simultaneous recording to observe the cohesiveness of their responses during environment modifications or conflicting situations (ii) recording of one cell type while inactivating the regions containing another cell type or disrupting the signal they encode, (iii) investigating the temporal course of tuning of each cell type during development.

2.3.1 PLACE CELLS AND HEAD DIRECTION CELLS

Several studies initially showed that place and HD cell systems function in a coordinated manner. Indeed, Knierim and colleagues simultaneously recorded CA1 place cells and HD cells from the antero-dorsal thalamic nucleus (ADN) while rats explored a circular arena containing a single salient cue (a card onto the wall). Rotation of the cue in the absence of the animal produced a consistent rotation of both place and HD cells. To further examine the relationships between place and HD cells, rats were divided in two groups: one group of rats were systematically disoriented before the recording sessions (in standard conditions, with a stable cue card), thus reducing their perception of the cue stability; the other group of rats were not disoriented before being placed in the cylinder. For the disoriented group, the rotation of the cue had weaker control over the place and HD cells, leading to random rotation angles; but in all cases place and HD cells responses were strongly coupled (Knierim et al., 1995).

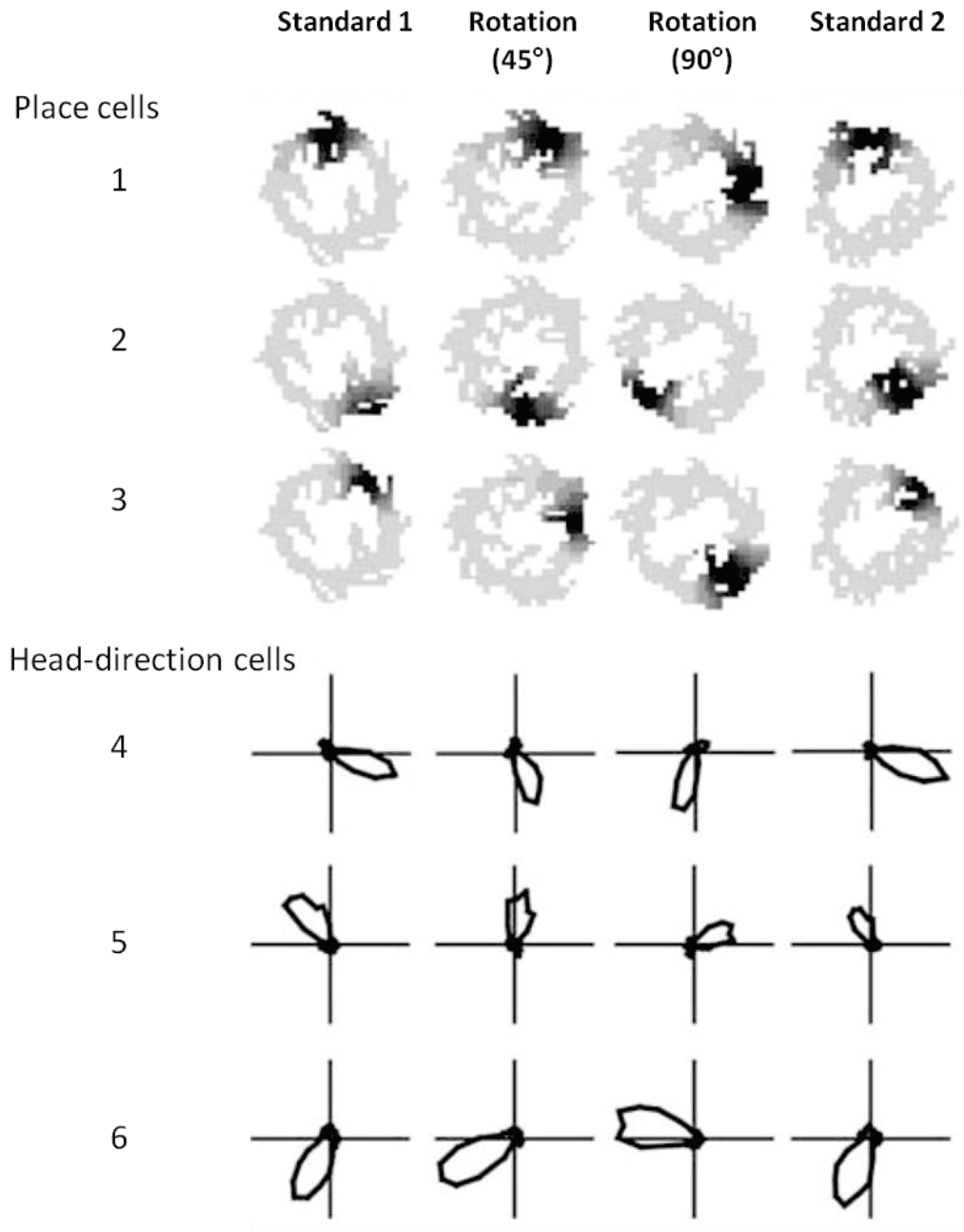

Figure 14. Place cells and head direction cells
Representative examples of effect of distal cue rotation: simultaneously recorded ensembles of CA1 place fields (cells 1–3) and head direction (HD) tuning curves of ADN cells (cells 4–6) in a circular track. Their place fields or preferred directions rotated along with the 45° rotations of the distal landmarks.
The place cell firing rate maps are plotted with a gray scale (the lightest gray: no firing; black: maximum firing rate; white: unvisited pixels)
(Yoganarasimha et al. 2005)

In other works, both types of cells were simultaneously recorded during a conflict between proximal and distal cues, produced by displacing the circular track in which rats were navigating relative to the distal cues of the recording room. Apparatus translation had

little influence on place and HD cells whereas rotation of the distal cues around the apparatus induced a consistent rotation of place fields and preferred direction of HD cells, which followed distal cues (Figure 14) (Yoganarasimha and Knierim, 2005). Given the strong control of distal cue over HD firing, these findings suggest that the orientation of the CA1 ensemble representation relative to the distal landmarks may be controlled indirectly by the distal landmarks' influence over the bearing of the HD cell system. Developmental studies using recordings in rats pups indicated that HD cells tuning preceded those of place cells (Figure 14), which would be compatible with a directional control of place cells by HD cell signals (Langston et al., 2010; Wills et al., 2010). Such a hypothesis predicts that the disruption of the HD system should affect the directional control of place field by distal cues. Calton et al. 2003 showed indeed that in a circular arena containing a single salient cue, a post-subicular lesion led to place field instability and abolishes the landmark control of place fields (Calton et al., 2003).

Conversely, hippocampal lesions do not affect the HD signal in the post subiculum in a circular arena (neither their stability nor their control by salient cues) (Golob and Taube, 1997). However, when the rats locomoted from a familiar to a novel environment in the dark, a process thought to require path integration (since only self-motion information is available, see protocol Figure 14.Di), hippocampal lesions disrupted directional tuning of subicular HD cells (Golob and Taube, 1999). This suggests that hippocampus is involved in path integration mechanisms, which enable an animal to maintain an accurate representation of its directional heading when exploring a novel environment.

However, this initial view of place and HD cells as two coupled system was revised by a more detailed analysis of the responses of place cell population. In a set of experiments in which a conflict between proximal and distal cues has been created, HD cells systematically rotated as a coherent ensemble mostly controlled by distal cues. On the opposite, in most of the experiments, CA1 place cells split into different subpopulations: although the majority of place cells follow the rotation of the HD cell population, a significant proportion of place cells followed the proximal cues, or acquired a new place field (Yoganarasimha et al., 2006). These discrepancies between place and head direction responses are likely to be representative of the parallel input streams reaching the hippocampus. The authors propose that distal cues influence would be mediated by the HD system while local cues would be processed by the perirhinal and lateral entorhinal cortices thus directly influencing the place cell system (Yoganarasimha et al., 2006). Accordingly, in other works, place and HD cells were recorded during rotation of the only visual cue in the view of the animal, thus producing a conflict between self-motion and external cue information. Although in all sessions the dominant responses of place and HD cells were consistent, CA1 ensembles exhibited a greater degree of response heterogeneity, with a few cells remapping or rotating in the opposite direction (Hargreaves et al., 2007). These data are in accordance with the

view that hippocampal place cell responses reflect the integration of conflicting streams of input (i.e., different place cells are affected by different subsets of contextual stimuli).

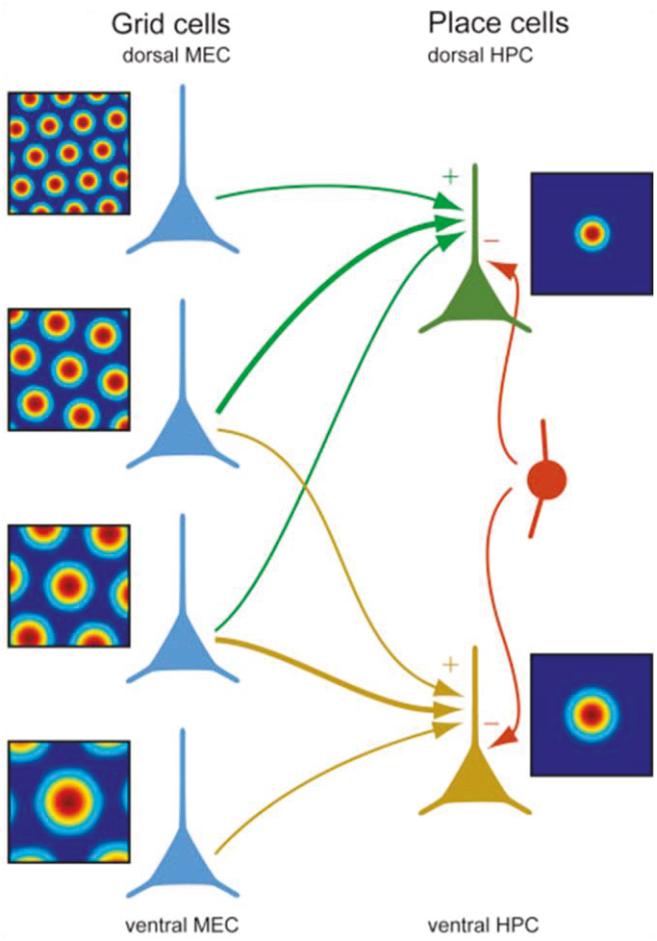

Figure 15. Model for place-field formation.
Assumed anatomical connectivity between grid cells in the medial EC (MEC) and place cells in the hippocampus. Grid cells (blue) are illustrated with small grid spacings in the dorsal pole of MEC and with larger grid spacings at more ventral levels. All place cells with a place field receive input from grid cells of similar spatial phase (a common central peak) but a diversity of spacings and orientations. Hippocampal place cells with a small firing field (green) are innervated by grid cells from more dorsal parts of the EC than place cells with a larger field (yellow). Connection weights are indicated by the thickness of the arrows. Interneurons (red) provide nonspecific inhibition to keep overall firing rates at physiological levels. The color code for the rate maps ranges from blue (0 Hz) to red (peak rate).
Solstad et al. 2006

2.3.2 PLACE CELL AND GRID CELLS

Grid cells, a basis for generating localized place fields?

From their discovery in 2005, grid cells have been rapidly proposed to be the origin of the spatial signals conveyed to the hippocampus. Indeed, grid cells are one synapse

upstream to the hippocampus, and the dorsal medial entorhinal cortex send strong connections to the hippocampus (Zhang et al., 2013). Moreover, several models demonstrated that the triangular array of grid cells could be used to generate individual place fields. For example, Solstad et al. showed that the linear summation of grid cell patterns with different spacing would result in a pattern containing periodic peaks at the locations where most of the grid cells are in phase (Solstad et al., 2006). But these peaks would be spaced of a large distance (equal to the least common multiple of grid spacing) and given the relatively small surface of the standard experimental apparatus, only one field would be observed (Figure 15). This model takes into account the fact that grid cells with more densely arranged fields in the dorsal part of the MEC preferentially project to the dorsal hippocampus and those with more widely spaced fields to project to the ventral hippocampus. It correctly predicts that temporal place cells have larger firing fields (Jung and Wiener, 1994; Kjelstrup et al., 2008).

The observation that global remapping of place cell is associated with grid cell realignment whereas rate remapping coincides with stable grid patterns is consistent with the idea that the place cell map arises from the grid cell map (Fyhn et al., 2007) (even if the opposite would also be consistent with this observation). Moreover, recordings in multi-compartment environments revealed a markedly similar modification of place and grid cell representations. Indeed, in a hair-pin maze, both place and grid cells were shown to remap into fragmented firing fields of activity, associated with a dependence on the running direction of the rat in the corridor (Derdikman et al., 2009). Besides, in recent models in which grid cells are organized in modules (according to recent data (Stensola et al., 2012)), slight rotations or translations of the grid modules with respect to each other were shown to result in global remapping in the hippocampus (Monaco et al., 2011).

Place field and grid pattern dissociation

However, several observations challenge this model. First, developmental studies indicate that firing properties of place cells may mature prior to those of grid cells. When rats pups leave the nest for the first time, at 2.5 post natal weeks, place cell have adult-like firing pattern whereas grid cell show irregular and variable fields until the fourth week (Langston et al., 2010; Wills et al., 2010)(Figure 16, A,B,D,E). Moreover, it is possible to record place cells in the absence of grid cells. Indeed, the reduction of theta oscillations by pharmacological inactivation of the medial septum abolished the characteristic hexagonal firing of grid cells and conjunction cells while sparing the location specific firing of hippocampal place cells (Figure 16) (Brandon et al., 2011; Koenig et al., 2011). These findings suggest that place cells firing does not depend on the convergence of grid cell firing pattern onto place cells.

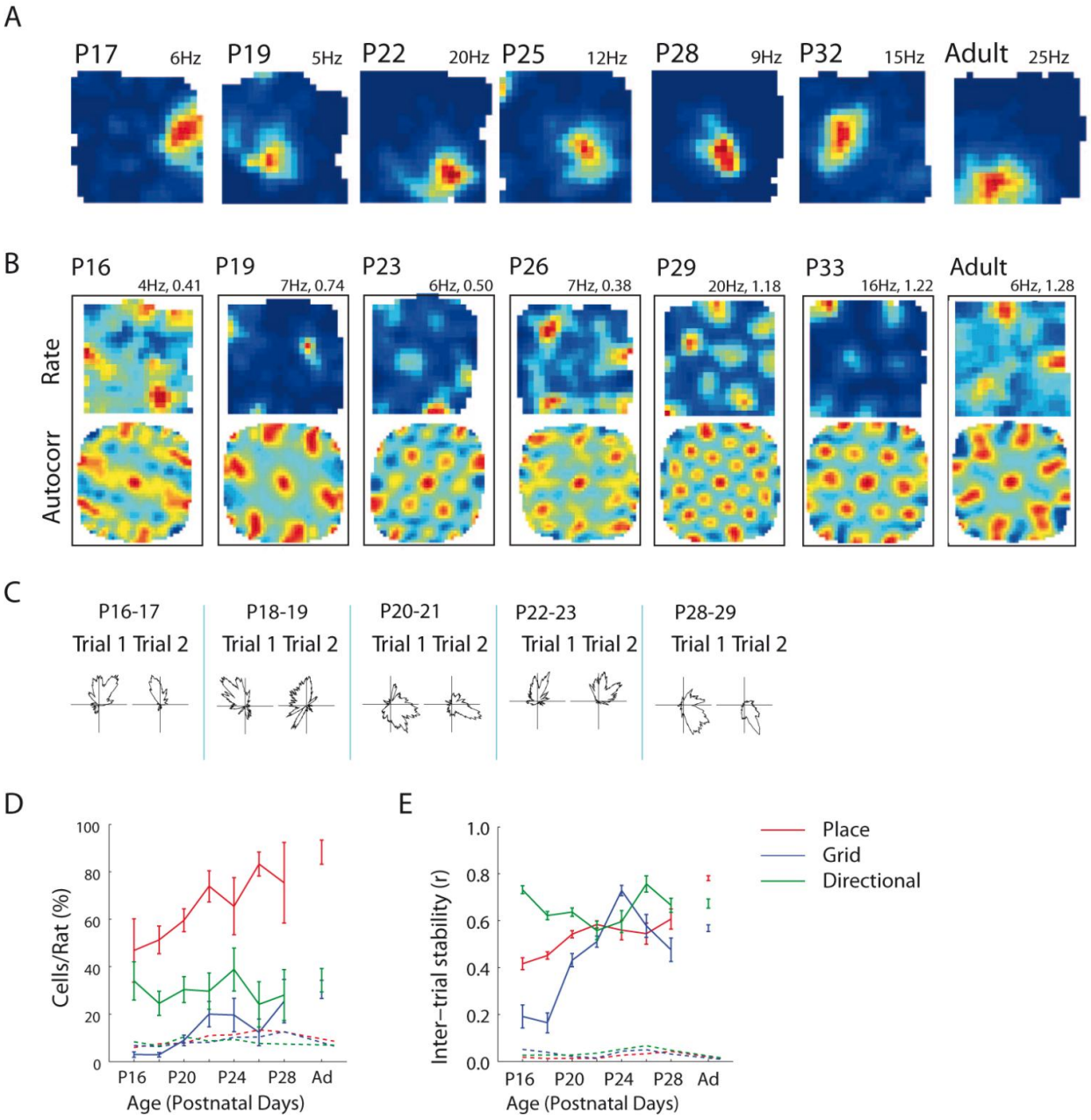

Figure 16. Development of directional, place, and grid cell firing with age.

A-C.Representative examples of each type of firing are shown across a range of ages

A. Place cells firing rate maps

B. Grid cell firing rate maps (above) and spatial autocorrelograms (below) (color scale from blue (r = – 1) to red (r = + 1). Grid scores are indicated.

C. Polar plots for directional firing

D. The proportions of cells per rat fulfilling the criteria for directional (green), place (red), and grid (blue) cells as a function of age. Solid lines represent the mean percentage of cells per rat that fulfilled the spatial firing criteria. Dotted lines represent the P = 0.05 significance level for the mean percentage of cells for each cell type, based on spike-shuffled data.

E. Spatial firing properties of the directional (green), place (red), and grid cells (blue) as a function of age. Adapted from Langston et al., 2010 and Wills et al., 2010

Conversely, recent studies even demonstrated that hippocampal backprojections to the MEC are necessary for grids cells structure. Indeed, transient muscimol inactivation of the hippocampus dramatically disrupted the spatial periodicity of grid cell in the medial entorhinal cortex and parasubiculum (Figure 17) (Bonnevie et al., 2013). One possibility is that the hippocampus, storing associations between features of the environment and path integrator coordinates, would prevent the accumulation of errors in the entorhinal representation of self-position. However, short-period analyses show that the disappearance of the hexagonal pattern is not due to a drifting grid that would be averaged over time. Thus, without ruling out the possibility of a hippocampal error correction process, the excitatory drive from the hippocampus is primarily required for the generation of the grid pattern itself.

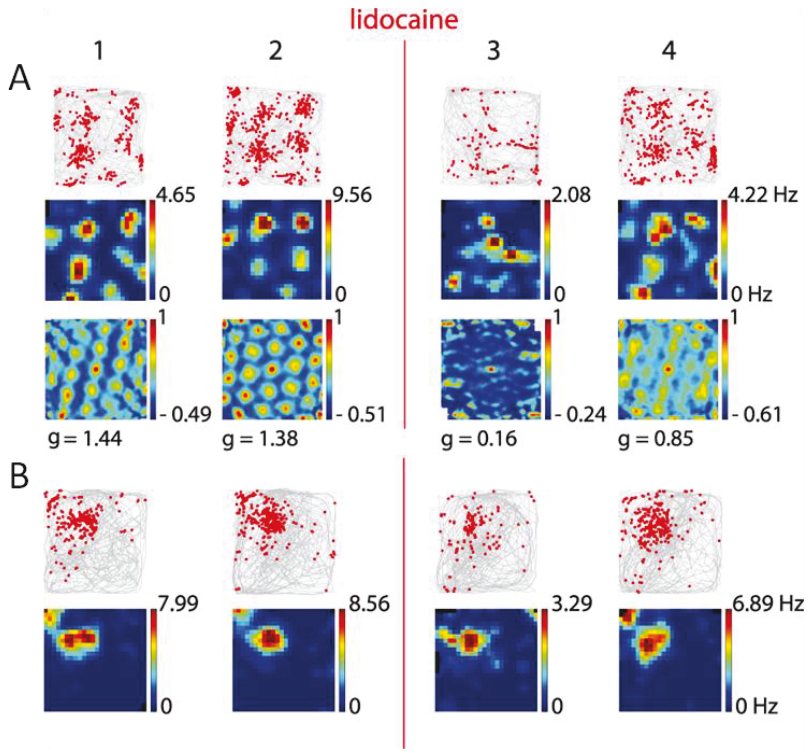

Figure 17. Place cells in the absence of grid pattern
A. The spatial periodicity of grid cells in the MEC vanished during periods of reduced theta activity.
Firing correlates for A representative MEC grid cell. Trajectories (gray) with superimposed spike locations (red dots) are shown in the top row of each cell's panel. The corresponding color-coded rate maps and spatial autocorrelation matrices compose the middle and bottom rows, respectively. The color scale for rate maps (shown for each 10-min recording interval) is from 0 Hz to the peak rate, and for the spatial autocorrelation matrices is from the minimum correlation coefficient to 1.
B. Location specificity of place cells is retained during reduced theta oscillations.
Firing correlates for a CA1 hippocampal place cells .Trajectories with spike locations (at the top of each cell's panel) and corresponding color-coded rate maps (bottom).
(Koenig et al. 2011)

Interestingly, the loss of the hexagonal firing following the reduction of theta oscillation was also observed in conjunctive cells (grid x HD) but their directional tuning was preserved,

suggesting a dissociation between the head directional signal and the expression of the grid pattern (Brandon et al., 2011; Koenig et al., 2011). Moreover, the grid vanishing induced by hippocampal inactivation coincided with the acquisition of a directional tuning (Figure 18) (Bonnevie et al., 2013). The authors suggest that in the absence of hippocampal input, the activity pattern of grid cells might be in part controlled by external inputs including head direction signal from adjacent structures or broadly tuned non periodic signal from other regions such as the postrhinal cortex (Burwell and Hafeman, 2003).

These findings emphasize that the localized firing properties of place cells do not derive from a unique source of spatial information in the brain. Rather, growing evidence converges to show the probable involvement of many functional classes of cells to shape place cells properties.

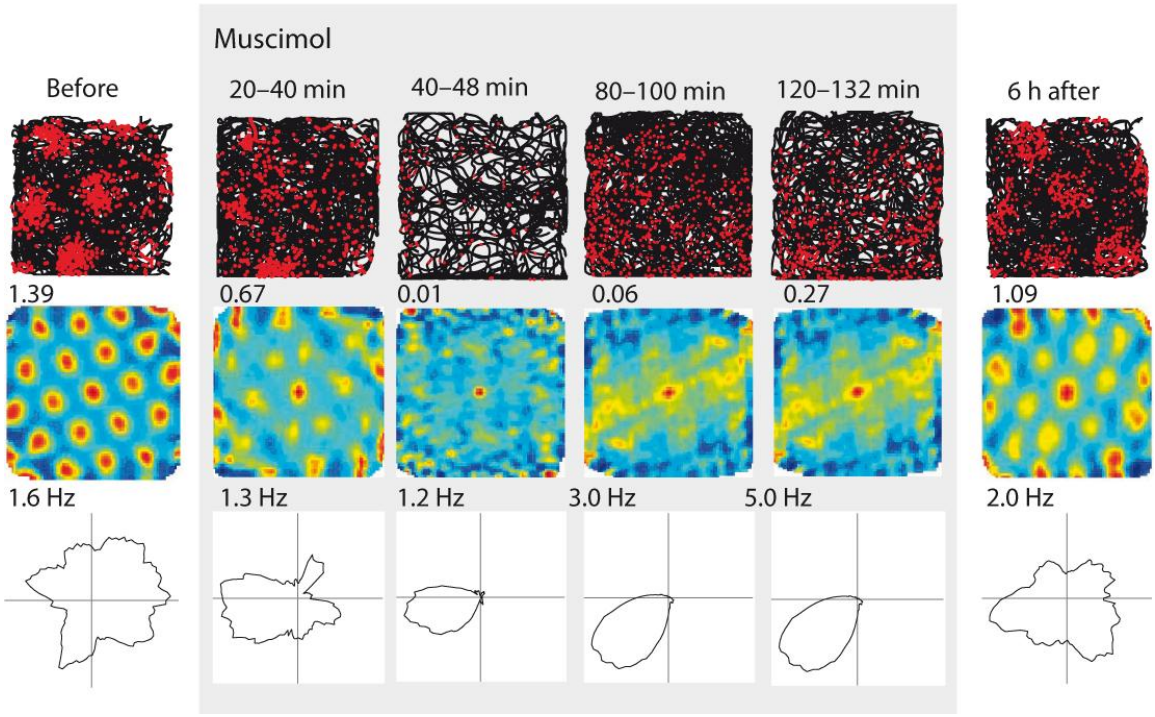

Figure 19. Disruption of entorhinal grid structure and acquisition of directional tuning after inactivation of the hippocampus

The top two rows show the trajectory with spike locations and the spatial autocorrelation maps, respectively. The grid scores are indicated above the autocorrelation maps. The bottom row for each cell shows polar plots of firing rate as a function of head direction. The peak firing rate is indicated over each plot.

(Bonnevie et al. 2013)

2.3.3 THE ROLE OF BORDER CELLS

Several modeling studies showed that spatially localized firing in place cells could be generated based on inputs from cells whose firing depended on the proximity of the rat to

geometric boundaries (border cells) (Hartley et al., 2000; Barry et al., 2006). These computational models produced a good fit to the firing of individual place cells, and populations of place cells across environments of differing shape. Importantly, border cells were identified in juvenile rats from the first days of exposure to an open environment, at a time when place and head direction cells display adult-like properties whereas grid cells only show minimal periodicity (Bjerknes et al., 2014). Thus, they constitute an interesting candidate for providing spatial information to the hippocampus of young animals (Bjerknes et al., 2014). Besides, retrograde labeling showed that all types of spatially modulated cells of the MEC, including the border cells, project to the hippocampus (Zhang et al., 2013). These findings also shed another light on the possible importance of border cells in building a spatial representation in the adult brain.

2.3.4 THE PARALLEL INPUT MODEL

We have seen that HD cell and place cell responses were frequently consistent, but not always or not completely, since the place cells population could split into groups responding preferentially to different types of information whereas HD cells are very cohesive. This is representative of the strong influence of the HD signal onto place cell firing but also of the existence of other inputs influencing place field formation. On the opposite, grid and place maps display a high degree of coordination, as observed in the similarity of their responses to environment deformation, or larger modifications leading to remapping (in new or fragmented environment). Besides, in multi-compartment environments, HD cells maintained a stable directional tuning whereas place and grid cells remap into fragmented firing fields of activity (Whitlock and Derdikman, 2012), confirming the relative independence of grid and HD tuning of MEC cells (Brandon et al., 2011; Koenig et al., 2011).

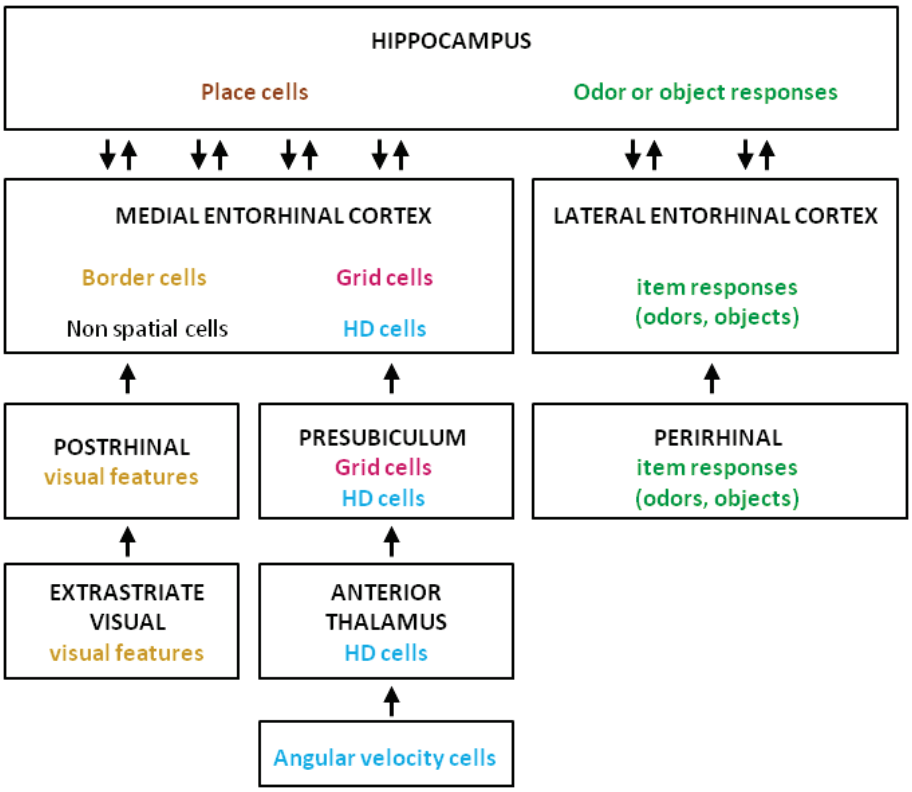

Figure 20. Possible parallel networks contributing to spatial processing.
Place cells in the hippocampus may arise from the inputs of boundary cells in the medial entorhinal cortex, as proposed by the model of boundary vector cells.(Hartley et al 2000, Barry et al 2006). These boundary vector cells may arise from visual features coding the distance and angle to boundaries in the environment. Head-direction cells could arise from input from angular velocity cells. Models of grid cells have shown how grid cell firing fields could arise from integrating head-direction inputs in combination with either oscillatory interference or attractor dynamics within entorhinal cortex (McNaughton 2006). Feedback connections from the hippocampus to the entorhinal cortex may play an important role in updating and aligning the representations of locations by grid cells and boundary vector cells.
On the right, odor and object responses found in the hippocampus may arise from representations of odors and objects coded in the lateral entorhinal cortex
Adapted from Brandon et al. 2014

These findings led to the emergence of a parallel input model (Figure 20), where several streams of information converge onto the hippocampus. The visual features are possibly transmitted from the extra striate to the postrhinal cortex then to the MEC border cells, coding the distance and angle to boundaries in the environment. Vestibular information is integrated into angular velocity and head direction information subcortically, and the antero-dorsal thalamic nucleus provides head direction information to the HD cell network (including MEC HD cells). The grid pattern of MEC grid cells is likely to result from the

combination of either oscillatory interference or attractor dynamics[1] within entorhinal cortex and strong interconnection with the hippocampus. Association of different types of inputs may occur in the MEC, where border, HD, grid as well as conjunctive cells are intermingled. The lateral enthorinal cortex (LEC) may supply the hippocampus with item or object information. Indeed LEC cells do not carry a strong spatial signal (Hargreaves et al., 2005) and the LEC receive strong inputs from the perirhinal cortex which had been implicated in the representation of single items (Brown and Aggleton, 2001; Norman and Eacott, 2005).

This model is also supported by anatomical data, with afferent connections organized in parallel loops. Indeed, two parallel pathways emerge from the perirhinal and postrhinal cortex. Inputs from postrhinal cortex contact medial entorhinal cortex, which then projects to the regions of proximal CA1 and regions of the distal subiculum (Witter et al., 2000). These areas project back to the medial entorhinal cortex either directly or via the pre- and parasubiculum. In the parallel pathway, input from perirhinal cortex primarily enters the lateral entorhinal cortex, which projects to the regions of distal CA1 and proximal regions of subiculum, which then project back to lateral entorhinal cortex. In the rodent, the two pathways are further distinguished by highly selective inputs from presubiculum to the medial but not lateral entorhinal cortex (Witter and Moser, 2006). Additional division comes from the dorso-ventral organization of the entorhino-hippocampal projection since the dorsal entorhinal cortex projects to dorsal regions of the hippocampus, whereas the ventral entorhinal cortex projects to more ventral regions of the hippocampus.

Importantly a recent study showed that all functional classes of MEC cells project onto the hippocampus (border, grid, HD and conjunctive cells but also non-spatial cells) (Zhang et al., 2013). This is consistent with the idea that signals of different nature converge onto the hippocampus to shape the firing fields of place cells.

[1] *Oscillatory interference or attractor dynamics are two models which propose an explanation for the generation the grid pattern. The oscillatory interference model relies on intracellular processes and hypothesizes that the grid arise from the interference between membrane potential oscillations at two frequencies in the theta range differing by an amount that is proportional to the running speed of the rat (Burgess et al., 2007). The attractor dynamic model relies on the properties of the neural network. This model proposes that in a network containing dense interconnections between neighboring cells, the bump of activity is centered on mutually connected cells, and moves between grid cells with different vertices, as the animal runs from one place to the other in its environment (Mcnaughton et al., 2006).*

This first chapter presented how the different types of information available to the subject – self-motion and external cue - are indeed used for spatial navigation. Path integration and map-based navigation, two processes respectively relying on either types of information, are likely to occur simultaneously and to interact to shape spatial behavior.

The research of the neural correlates of spatial navigation confirmed the participation of large network of structures. The spatial representation in the brain consists in several ensembles of spatially modulated cell, with different characteristics. They include hippocampal place cells, head direction cells, grid cells, border cells, movement cells, non periodic spatial cells. The characterization of their responses to experimental manipulations revealed the different signals controlling their firing properties. These works also evidenced that these ensembles of spatially modulated cells mostly responded in a coordinated manner, thus encoding a coherent spatial representation. These findings, along with anatomical and functional projections data, led to a picture in which parallel streams of information converge onto the hippocampus to shape the localized firing of place cells: features of the environment are transmitted from the postrhinal cortex via the border cells, self-motion information comes from the head direction and grid cells, local item information is conveyed by cells of the lateral entorhinal cortex.

Electrophysiological recordings are thus a powerful technique to decipher the contribution of each region to spatial navigation. However, this approach is limited to the regions containing cells whose activity correlates with a feature of navigation. Importantly, lesions and functional imaging studies had suggested an even larger navigation network in the brain. During my PhD I have been interested in the participation of the cerebellum in spatial navigation. Before exposing the current data on its potential contribution, the second chapter presents the cerebellum –its functional organization as well as its particular way to process information.

Part II. Cerebellum, information processing and plasticities

1 FUNCTIONAL ORGANIZATION OF THE CEREBELLUM

The cerebellum is a structure of the nervous system located beneath the telencephalon, behind the brainstem. In spite of it Latin name meaning “little brain”, it contains more neurons than the rest of the brain, for only 10% of its volume (Kandel et al., 2000). Like the forebrain it has its own cortex, whose principal neurons project onto three subcortical nuclei, located inside the white matter (Figure 21, A). The cerebellum is present in all Vertebrates. As its morphology varies widely across species, we will focus on the rodent cerebellum to present its organization.

1.1 STRUCTURE OF THE CEREBELLUM

1.1.1 ANATOMICAL STRUCTURE

In Mammals, two deep fissures separate 3 lobes along the rostro-caudal axis: the anterior lobe, the posterior lobe and the flocculo-nodular lobe. Minor fissures divide these lobes in ten lobules (or folia), numbered from I to X (Figure 21, B) (Larsell, 1952, 1953).

On each side of the midline, the cerebellum is portioned in three longitudinal regions (Figure 21.C): the vermis (medial cerebellum), the paravermis (intermediate cerebellum or pars intermedia) and the hemisphere (lateral cerebellum). In all regions, the cortex is a simple structure consisting in three layers: the innermost or granule cell layer, the Purkinje cell layer and the outermost or molecular layer (their cyto-architecture is detailed in paragraph 1.4 and Figure 21).

In the subcortical white matter are located three pairs of deep cerebellar nuclei: the fastigial (or medial) nuclei, the interposed (or intermediate) nuclei and the dentate (or lateral) nuclei (Ghez, 1991). The interposed nuclei are further divided into anterior and posterior nuclei (also named emboliform and globase nuclei in Primates) (Ramnani, 2006). The deep cerebellar nuclei, along with the vestibular nuclei form the output of the cerebellum to other brain areas (Figure 21, A).

1.1.2 FUNCTIONAL STRUCTURE

The cerebellum is traditionally divided in three functional regions, which correspond roughly to anatomical divisions, and have evolved successively in phylogeny (Figure 21, C) (Ghez, 1991). This initial compartmentalization was based on the main projections of the cerebellar cortex onto the deep nuclei, and the roles of the different regions inferred from the consequences of their lesions.

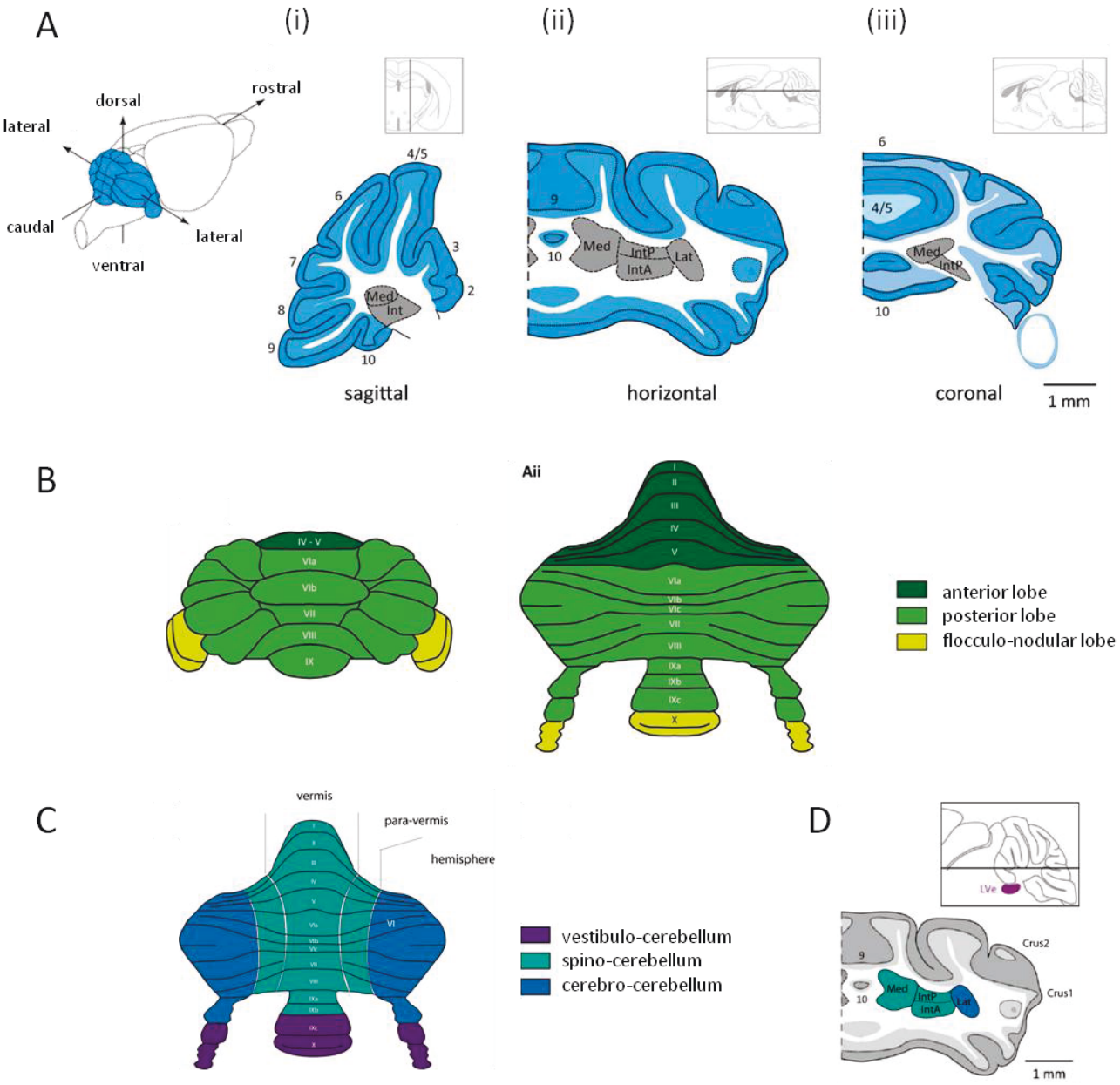

Figure 21. Anatomical organization of the cerebellum

A. Anatomical structure of the cerebellum. Left. Representation of the mouse cerebellum. A(i)-(iii): Cerebellar sections in the 3 orientations : the cerebellar nuclei are in grey, the granular layer in light blue, the molecular layer in blue.

B. Anatomical divisions of the cerebellar cortex along the anterio-posterior axis. Left, Dorsal view. Right, Unfolded view of the cerebellar cortex showing the 10 lobules.

C. Functional division of the cerebellar cortex.

D. Projections zones of the cerebellar in the deep cerebellar (blue and green) and vestibular (purple) nuclei.

Abbreviations: IntA: anterior interposed nucleus; IntP: posterior interposed nucleus; Lat: lateral cerebellar nucleus; Med: medial cerebellar nucleus; Lve: lateral vestibular nucleus.

Adapted from Chaumont, 2013

The vestibulo-cerebellum (or archeo-cerebellum) is the most ancestral part of the cerebellum and corresponds to the flocculo-nodular lobes. It receives vestibular input from the vestibular labyrinth and nuclei as well as visual information from the pontine nuclei. Through its afferent and efferent connections with the vestibular nuclei in the brainstem, the vestibulo-cerebellum is involved in the control of eye movements and body equilibrium during stance and gait.

The spino-cerebellum (or paleo-cerebellum) appears in Reptiles and corresponds to the vermal and paravermal part of both the anterior and posterior lobes. It receives sensory information from the periphery. Its principal input is somatosensory information from the spinal cord, hence its name, but it also receives information from the auditory, visual and vestibular systems. It projects onto the medial and intermediate nuclei. Through these two nuclei, the spino cerebellum plays a major role in controlling the ongoing execution of limb movement.

The cerebro-cerebellum (or neo-cerebellum) appears in Mammals and corresponds to the hemispheres. It receives inputs exclusively from the pontine nuclei that relay information from the cerebral cortex. It projects onto the dentate nuclei which convey information to the thalamus and from there to the motor and premotor regions of the cerebral cortices. In conjunction with the motor and pre-motor cortices, the cerebro-cerebellum plays a role in the planning and initiating of movement.

However, more detailed descriptions of the cerebellar connectivity as well the discovery of new cerebellar projections led to re-evaluate such a strict distinction (Apps and Hawkes, 2009; Strick et al., 2009).

1.2 CONNECTIVITY OF THE CEREBELLUM

The input and output connections of the cerebellum run through three symmetrical pairs of tracts called the cerebellar peduncles. These three peduncles – inferior, middle and superior cerebellar peduncles – contain efferent and afferent fibers.

1.2.1 AFFERENT CONNECTIONS

Mossy fibers and climbing fibers are the principal afferent inputs that connect the cerebellum. These two glutamatergic inputs arise from different sources and project onto different layers of the cerebellar cortex.

1.2.1.1 THE MOSSY FIBER PATHWAY

Mossy fibers provide the bulk of the afferent input. They originate from a variety of pre-cerebellar nuclei in the brainstem and from neurons in the spinal cord (Figure 22). A single mossy fiber can divide across different folia into multiple branches, staying ipsilateral or

crossing the midline and distributing bilaterally in the cerebellar cortex (Palay and Chan-Palay, 1974). Each mossy fiber gives rise to a hundred of terminations, called “rosette” (Quy et al., 2011). Some of them also send a collateral to the deep cerebellar nuclei (Gerrits and Voogd, 1987; Mihailoff, 1993; Matsushita and Yaginuma, 1995).

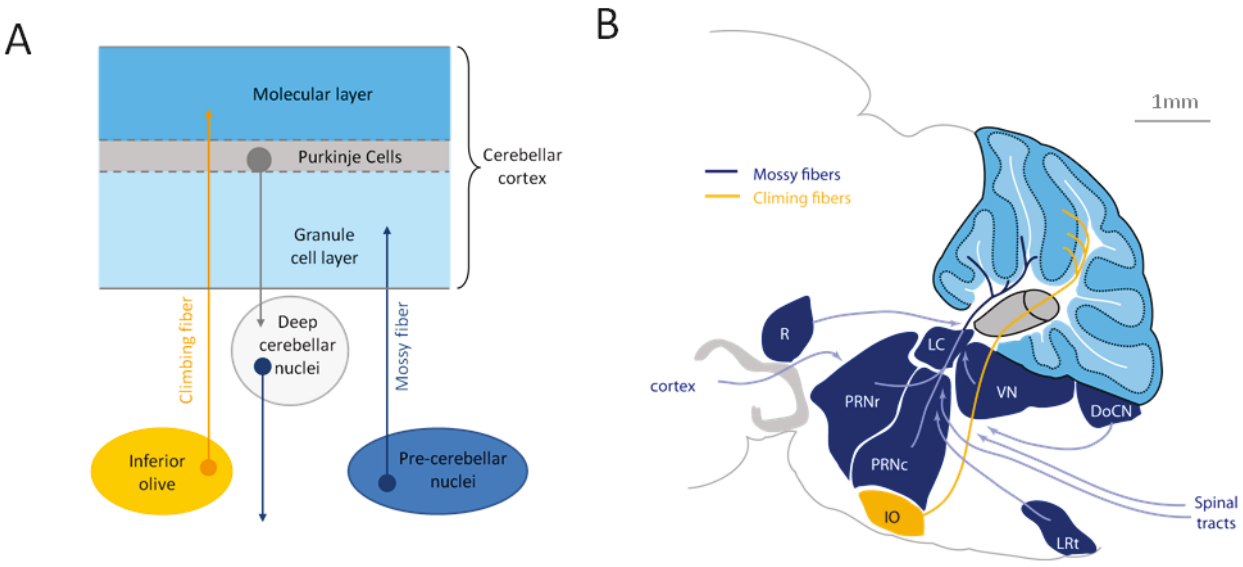

Figure 22. Afferent connections to the cerebellum
A. Schematic diagram of cerebellar organization.
B. Representation of the pre-cerebellar nuclei and spinal cord sending mossy fiber projections (blue) and of the inferior olive sending climbing fibers (yellow) to the cerebellar cortex.
Abbreviations: DoCN: Dorsal Column Nucleus; IO: Inferior Olive; LRt: Lateral Reticular Nucleus; LC: Locus Ceruleus; PRNr, PRNc: Pontine Reticular Nuclei (rostral and caudal parts); R: Red nucleus; VN: Vestibular nucleus. Note that the Trigeminal nuclei and the Reticular tegmental nucleus are not visible on this scheme.

Sensory information conveyed by mossy fibers can follow two pathways. First, the direct pathway relays information from the face or the periphery (trigemino-cerebellar and spino-cerebellar pathways respectively), informing about limb position, cutaneous pressure, head inclination or eye orientation. The indirect pathway (or cerebro-cerebellar pathway) transmits already processed information, essentially from the sensory cerebral cortices (Morissette and Bower, 1996)

Pre-cerebellar nuclei

Most of the mossy fibers come from a wide range of nuclei in the brainstem, conveying information from cerebral cortices, body and face (Figure 22.B) (see for review Ruigrok, 2004):

- The pontine nuclei are an important source of mossy fibers (Serapide et al., 2001). They receive mainly input from the sensori-motor and visual cerebral areas, and to a minor extent, inputs from the auditory and associative areas.

- The lateral reticular nuclei receive information from the spinal cord and some supra-spinal structures (Bruckmoser et al., 1970). They contact all cerebellar regions except the flocculo-nodular lobe (Wu et al., 1999).
- The trigeminal nuclei convey somato-sensory information from the face (Van Ham and Yeo, 1992).
- The vestibular nuclei bring vestibular information from the sensory receptors in the inner ear and project onto the flocculo-nodular lobe principally.
- The dorsal column nuclei, which are composed of the cuneiform nuclei and the gracile nuclei, relay information from the spinal cord, mainly somato-sensory information from the body.

Different bundles from the spinal cord also send mossy fibers to the cerebellar cortex. The dorsal and ventral spino-cerebellar pathway are dedicated to information from the inferior limbs, the rostral pathway, with a relay in the dorsal column nuclei, to the superior limbs (Yaginuma and Matsushita, 1986).

1.2.1.2 THE CLIMBING FIBER PATHWAY

The climbing fibers constitute the other main class of cerebellar afferents. They arise exclusively from the inferior olive, a well defined nucleus in the ventral part of the brainstem (Figure 22.B). The axon of an olivary neuron divides into several branches along a parasagittal plane which terminate in the molecular layer where their wrap around the dendritic tree of a Purkinje cell and make numerous synaptic contacts. Remarkably, in adult each Purkinje cell is contacted by only one climbing fiber but each climbing fiber contacts seven Purkinje cell on average in rats (Armstrong and Schild, 1970). Olivary neurons also send collaterals to the granular layer and to the cerebellar nuclei (Sugihara et al., 1999).

The inferior olive can be divided in three subregions: the principal olive, the dorsal accessory olive and the medial accessory olive. The inferior olive receives information from many sources, including the spinal cord, the vestibular nuclei, the deep cerebellar nuclei, the trigeminal nuclei, the superior colliculus as well as the sensori-motor and parietal cortices (see for review Ruigrok, 2004).

1.2.1.3 AMINERGIC FIBERS

The cerebellar cortex also receives diffuse afferents from aminergic fibers, playing a modulatory role on synaptic transmission between cortical interneurons and Purkinje cells (Oertel, 1993). Noradrenergic fibers, coming from the locus coeruleus terminate as a plexus in all three layers of the cerebellar cortex. Serotoninergic fibers come from the raphe nuclei terminate in both the granular and molecular layers. Additionally, cholinergic fibers from the vestibular nuclei sparsely project onto the flocculo-nodular lobe where they could modulate Purkinje cell activity (Altman and Bayer, 1977).

1.2.2 EFFERENT CONNECTIONS

The deep cerebellar and vestibular nuclei are the final step of integration of the cerebellar circuitry, and constitute the only output of the cerebellum. Given their position and connectivity, they play a central role in all of the cerebellar functions.

1.2.2.1 DEEP CEREBELLAR AND VESTIBULAR NUCLEI

The deep cerebellar nuclei receive constant inhibitory input from the Purkinje cells. The ratio between Purkinje cells and cerebellar nuclei neurons is about 11:1 in the mouse (Caddy and Biscoe, 1979; Harvey and Napper, 1991; Heckroth, 1994). At the synaptic level, a Purkinje cell contact about 30 nuclear neurons but may have 3-6 primary targets (Palkovits et al., 1977). Conversely, a neuron of the cerebellar nuclei is contacted by ten to several hundreds of Purkinje cells. Thus, the transfer of information from Purkinje cell to nuclear neurons allows both convergence and divergence of information (Person and Raman, 2012). The deep cerebellar nuclei are composed of three populations of neurons: large glutamatergic projection neurons, small glycinergic interneurons and small GABAergic neurons. This last population exerts an inhibitory feedback control onto the inferior olive (Uusisaari et al., 2007).

The vestibular nuclei receive projections from Purkinje cells in the flocculus and nodulus. Vestibular nuclei are composed of four nuclei: the lateral, medial, superior and inferior vestibular nuclei. They are distinguished on the basis of the architecture and their sets of connections with the periphery and central nervous system (Kelly, 1991).

1.2.2.2 ORGANIZATION OF CEREBELLAR PROJECTIONS

The deep cerebellar nuclei send projections to a wide range of structures in brain and the spinal cord (Figure 23)(see for review Voogd, 2004). In the pons and medulla oblongata, they connect the inferior olive, the vestibular nuclei, the pontine nuclei, the reticular formation, the para-brachial nuclei, and the reticular tegmental nuclei. In the midbrain, cerebellar targets include the red nucleus, superior colliculus, the periaqueductal gray, the occulo-motor complex, the nucleus of Darkschewitsch and the deep mesencephalic nucleus. The deep cerebellar nuclei also target the zona incerta in the hypothalamus (Voogd, 2004). In the thalamus, they send strong projections to the ventro-medial and ventro-lateral nuclei (Asanuma et al., 1983; Angaut et al., 1985), as well as to centro-lateral, ventro-posterior, parafascicular and subparafascicular nuclei (Haroian et al., 1981; Aumann et al., 1994).

Importantly, the thalamic connections constitute a relay toward the cerebral cortex. Thus, the cerebellar projection to the parietal cortex via the thalamus has been demonstrated in rats (Giannetti and Molinari, 2002) and in monkeys (Amino et al., 2001; Clower et al., 2001, 2005; Prevosto et al., 2010). In primates, viral tracing studies showed

that the cerebellum projects, with a thalamic relay, to various cerebral cortices, including the motor and supplementary motor areas (Hoover and Strick, 1999; Akkal et al., 2007) but also the prefrontal cortex (Middleton and Strick, 2001; Kelly and Strick, 2003). In fact the cortical areas that are target of the cerebellar output also have prominent projections to the cerebellum, via the pontine nuclei (Strick et al., 2009), opening the possibility that the cerebro-cerebellar connections are organized in closed loops. This has been demonstrated for the motor cortical areas M1, and area 46 in the dorsolateral prefrontal cortex (Kelly and Strick, 2003). It is thus conceivable that a similar organization also exists in the cerebellar connections to the other cortices, and in other species (the rodents for example).

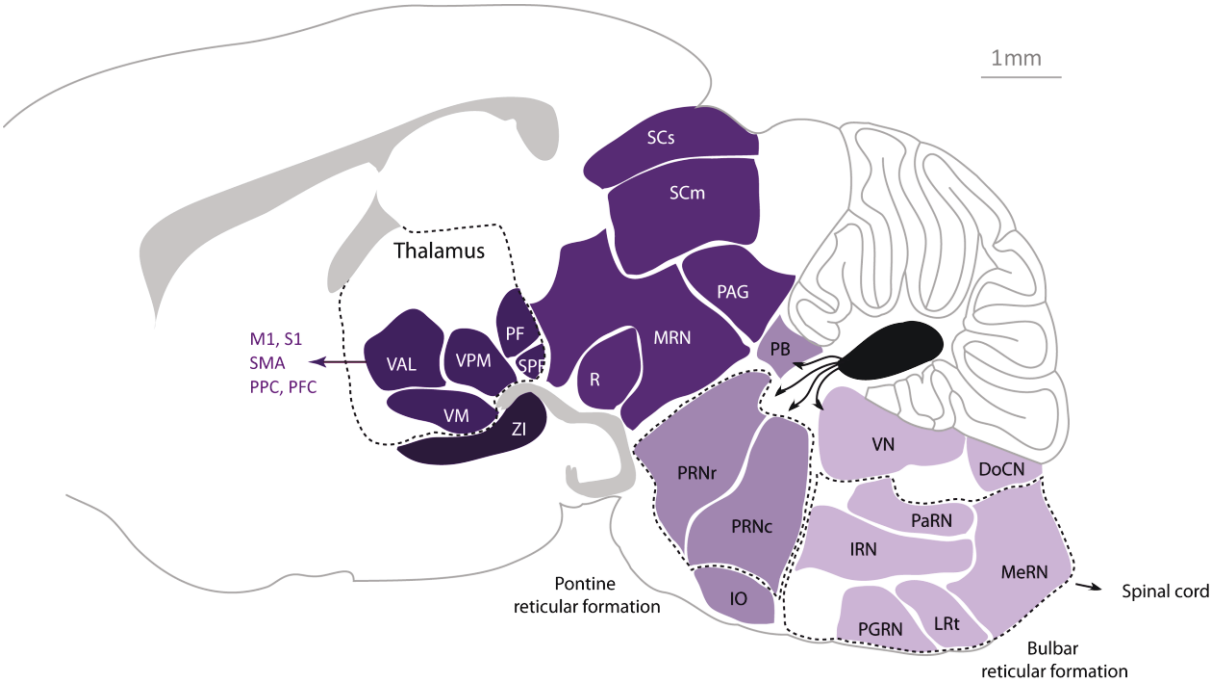

Figure 23. Efferent connections from the cerebellum
Representation of the different regions receiving projections from the deep cerebellar nuclei
Abbreviations: VAL: Ventral anterior lateral thalamic nucleus; VM: Ventro-medial thalamic nucleus; VPL: Ventral posterior lateral thalamic nucleus; PF Parafascicular thalamic nucleus; SPF Subparafascicular thalamic nucleus ; M1: Primary motor cortex; S1: Primary sensory cortex; PFC: Prefrontal cortex; PPC: Posterior parietal cortex; SMA: Supplementary Motor Area; ZI: Zona incerta; R: Red nucleus; SCs, SCm: Superior colliculus (sensory and motor parts); PAG Periaqueductal gray; IO: Inferior olive; PRNr, PRNc: Pontine reticular nuclei (rostral and caudal parts); PB: Parabrachial nucleus; VN: Vestibular nuclei; DoCN Dorsal column nuclei; IRN: Intermediate reticular nucleus; MeRN Medullary reticular nucleus; PaRN Parvicellular reticular nucleus; LRt Lateral reticular nucleus; GRN Paragigantocellular reticular nucleus. Note that the Oculo-motor complex and the Reticular tegmental nucleus are not visible on this scheme.

1.3 MODULAR ORGANIZATION OF THE CEREBELLUM

As mentioned before, the initial large-scale division of the cerebellum in vestibulo, spino and cerebro-cerebellum has been revised, notably by a better description of its connectivity. Here are the anatomical, molecular, and electrophysiological data that contributed to understand its fine-scale functional organization.

1.3.1 OLIVO-CORTICO-NUCLEAR CONNECTIVITY: LONGITUDINAL ZONES AND MICROZONES

The projections of the cerebellar cortex to the deep cerebellar and vestibular nuclei have been used to define parallel longitudinal zones, narrow rostro-caudally elongated regions that run perpendicular to the long axis of the lobules (Figure 24.A). Voogd initially defined 6 longitudinal zones (A,B,C1,C2,C3,C,D1,D2) and additional zones have subsequently been added (X, CX, D0 for example, see Figure 24). The same zonal arrangement was observed for olivo-cerebellar climbing fiber projections (Groenewegen and Voogd, 1977). Electrophysiological studies of olivary inputs confirmed this zonal organization (Oscarsson, 1979). Then anatomical tract tracing revealed that each longitudinal zone receives climbing fibers from a discrete area of the inferior olive and projects to a particular area of the cerebellar or vestibular nuclei. This organization was designed as a ‘module’ (Buisseret-Delmas and Angaut, 1993). The notion of module also includes the nucleo-olivary connection and reciprocal olivary-nuclear projection (Ruigrok, 1997).

Then high resolution electrophysiological studies allowed subdividing longitudinal zones into microzones, groups of Purkinje cell with a similar somatotopic receptive field. Each microzone contains approximately 1000 Purkinje cells and occupies a rostro-caudally oriented strip (100-300µm in width, within a longitudinal zone of 1mm). However, this organization may vary across regions. The length of a microzone differs importantly between the studied longitudinal zones. In addition, the microzones located in different parts of the paravermal cortex can have the same climbing fiber receptive field characteristics (for example, there are at least four separate ‘eyeblink’ microzones in each paravermis (Hesslow, 1994)). This has led to the concept of ‘multizonal microcomplexes’, a set of spatially separated microzones with common climbing fiber input. Such an organization might be important for the parallel processing and integration of information from mossy fiber inputs derived from multiple sources (Garwicz et al., 1998; Apps and Garwicz, 2005).

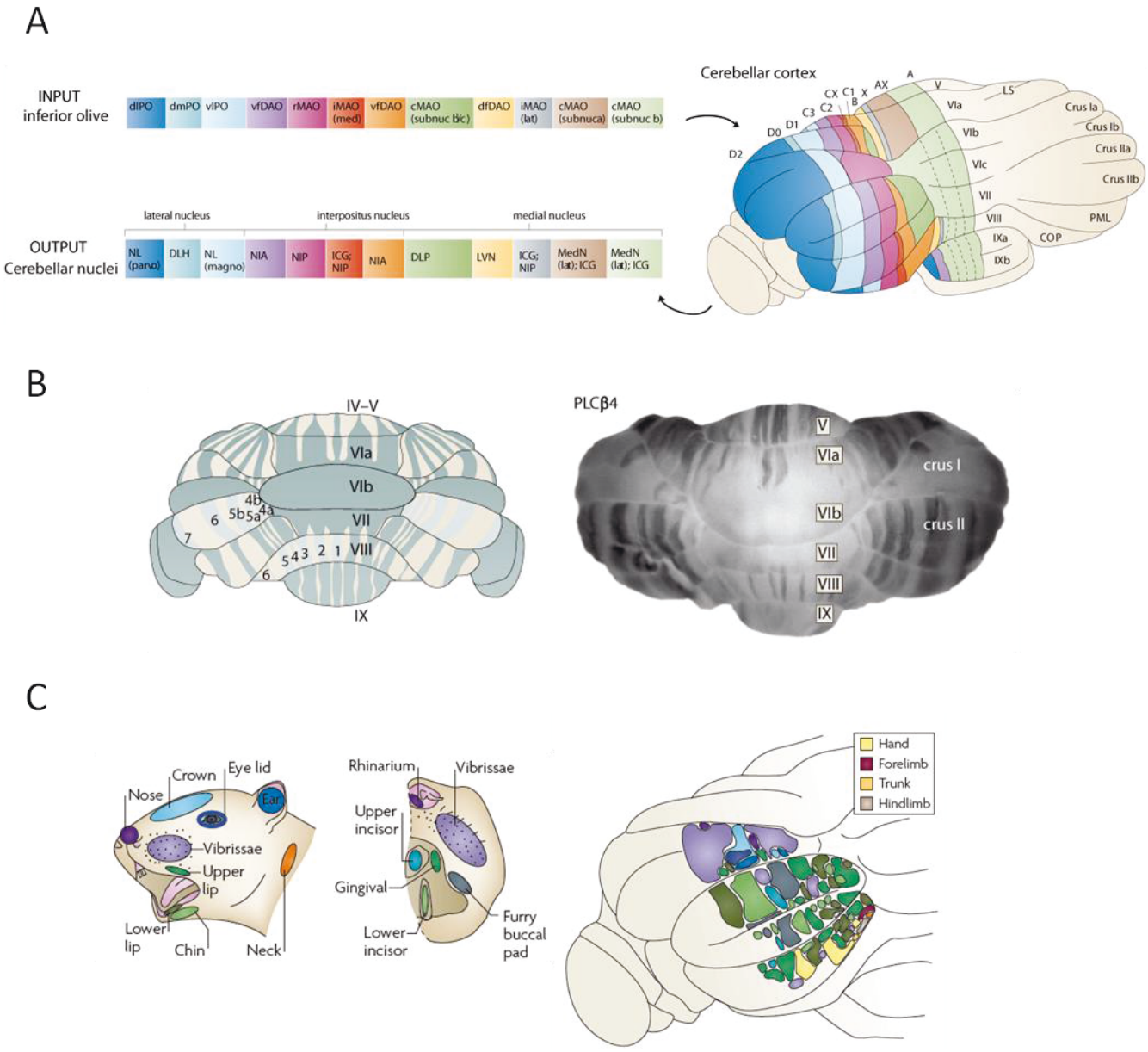

Figure 24. Modular organization of the cerebellum

A. Olivo-cortico-nucleo connectivity pattern: Longitudinales zones. Dorso-posterior view of the rat cerebellum, indicating the approximate location of different longitudinal zones on the cerebellar surface on the left hand side. Each longitudinal zone is defined by its inferior olive climbing fibre input and Purkinje corticonuclear output. Longitudinal zones in the paraflocculus and flocculus are not shown. In the simplified block diagrams, matching colours show, for individual cerebellar cortical zones, the sites of origin of climbing fibres in the contralateral inferior olive, and the corresponding Purkinje cell corticonuclear output targets in the ipsilateral cerebellar and vestibular nuclei.

B. Histochimic compartimentation: zebrin stripes. Representation of the distribution of Purkinje cells that are immunoreactive to zebrin II in the cerebellum of the adult mouse (dorsal view). Zebrin II+ stripes of Purkinje cells are referred to as P1+ to P7+ (numbered in the figure as 1–7 for clarity) from the midline laterally. Lobules in the vermis are indicated by Roman numerals. Left: One examples of stripes. Immunocytochemical staining for PLCβ4.

C. Mossy fibers afferent: patches. Dorso-posterior view of the left hand side of the rat cerebellum showing the spatial distribution of receptive fields recorded in the granular layer in response to mechanical stimulation of different body parts as detailed in the panels on the left. Note the multiple representations of the same body parts to produce a 'fractured somatotopical' mosaic pattern of variable sized patches.
cMAO (subnuc a), subnucleus a of caudal medial accessory olive; cMAO (subnuc b), subnucleus b of caudal medial accessory olive; cMAO (subnuc b1/c), subnucleus b1 and c of caudal medial accessory olive; COP, copula pyramidis; dfDAO, dorsal fold of dorsal accessory olive; DLH, dorsolateral hump; DLP, dorsolateral protuberance of medial nucleus; dlPO, dorsal lamella of the principal olive; dmPO, dorsomedial subnucleus of the principal olive; ICG, interstitial cell group; iMAO (lat), lateral part of intermediate medial accessory olive; iMAO (med), medial part of intermediate medial accessory olive; LVN, lateral vestibular nucleus; LS, lobulus simplex; MedN (lat), lateral part of medial nucleus; MedN (med), medial part of medial nucleus; NIA, nucleus interpositus anterior; NIP, nucleus interpositus posterior; NL (magno), magnocellular part of lateral nucleus. NL (parvo), parvocellular part of lateral nucleus; PML, paramedian lobule; rMAO, rostral medial accessory olive; vfDAO, ventral fold of dorsal accessory olive; vlPO, ventral lamella of the principal olive.
Adapted from Apps & Hawkes 2009

1.3.2 HISTOCHIMIC COMPARTIMENTATION: ZEBRIN STRIPES

Immuno-histochimic studies revealed a heterogeneous expression of several molecular markers in the cerebellar cortex. The expression profiles were characterized by positive and negative parasagittal bands, hence their name, zebrin (Hawkes et al., 1985). These bands are symmetrically distributed across the midline and highly conserved between species (Sillitoe et al., 2005). The most famous is zebrin II which divides the cortex into seven positive bands from P1 to P7 from the midline to the hemisphere and proved to be Aldolaze C (Figure 24.B) (Brochu et al., 1990; Ahn et al., 1994). Numerous other markers have been identified and correspond to various functions such as the phospholipase Cβ3 (Sarna et al., 2006), the excitatory amino-acid transporter 4 (EAAT4) (Dehnes et al., 1998), metabotropic glutamate receptor 1a (Mateos et al., 2001) or the integrin β1 (Murase and Hayashi, 1996).

However, zebrin expression profiles do not give a unified pattern to understand cerebellar longitudinal organization. Indeed, some markers follow the same expression profile as zebrin II – being co-expressed or following a complementary pattern (the phospholipase Cβ3 and the phospholipase Cβ4 respectively (Sarna et al., 2006)). But other markers reveal strips in zones where zebrin is uniformly expressed such as HSP 25 or HNK1 (Armstrong et al., 2000). So far no single molecule has been found to that visualizes all stripes. Similarly, even if co-localization of zebrin stripes and longitudinal zones has been observed in numerous studies (Gravel et al., 1987; Voogd et al., 2003; Sugihara and Quy, 2007), the exact relationships are more complex.

1.3.3 MOSSY FIBERS AFFERENTS: PATCHES

Recording of activity in the granular layer evoked by mechanical stimulation of different body parts allowed to identify tactile receptive fields associated to mossy fiber inputs (Figure 24.C). A given cutaneous stimulus triggers activation in one or several surfaces of variable size (up to $1mm^2$) (Stein and Glickstein, 1992), called "patches". The multiplicity of receptive

fields with the same tactile specificity produces a 'fractured somatotopy' (Shambes et al., 1978) and is interpreted as the effect of collaterals of a single mossy fiber, which can be parasagittal or medio-lateral (Woolston et al., 1982). This topographical organization seems to be conserved between individuals of the same species (Gonzalez et al., 1993). A study examining the spatial relationship between the mossy fiber and climbing fiber projections analyzed the Purkinje cell's complex spikes (characteristic Purkinje cell discharge in response to climbing fiber stimulation). This study showed that the receptive field for a single Purkinje cell's complex spike is similar to the primary receptive field of the granule cells immediately subjacent to that Purkinje cell (Brown and Bower, 2001). This suggested that small patches defined by the mossy fiber input might correspond to individual microzones defined by their climbing fiber input (Apps and Hawkes, 2009).

Anatomical tracing studies have showed that the olivo cerebellar system was organized in modules, receiving climbing fiber from a particular subnucleus of the inferior olive and in turn inhibiting neurons in particular vestibular or cerebellar nuclei that project back to the same olivary subnucleus. In some cases the resolution of the anatomical mapping has been sufficient to reveal this connectivity at a level that might correspond to microzones (Apps and Garwicz, 2000; Sugihara and Shinoda, 2004). The basic operational unit of the cerebellar cortex may be an individual microzone with its olivary and nuclear projections, an entity referred as a micro-complex.

1.4 CELLULAR ARCHITECTURE OF THE CEREBELLAR CORTEX

The cerebellar cortex is a highly repetitive structure organized in three parallel layers that follow the circumvolutions of the cortex. The different units of each layer were initially revealed by Ramon y Cajal (Ramon Y Cajal, 1911).

From the surface to the innermost, the three successive layers are characterized by different cell types and fibers (Figure 25):

- **The molecular layer** contains two types of interneurons, the stellate cells and the basket cells, the dendritic trees of the Purkinje cells as well as the axonal terminations of the granule cells (the parallel fiber) and of the olivary cells (the climbing fibers).
- **The Purkinje cell layer** contains the somas of Purkinje cells arranged in a mono-layer.
- **The granule cell layer** contains the granule cells, the Golgi cells, the Lugaro cells, the unipolar brush cells (UBC) as well as the terminations of the mossy fibers.

The cerebellum also contains an important amount of glial cells, which are in both the white and the grey matter (Sotelo, 1967). All glial cell types are represented (astrocytes, oligodendrocytes and microglial cells).

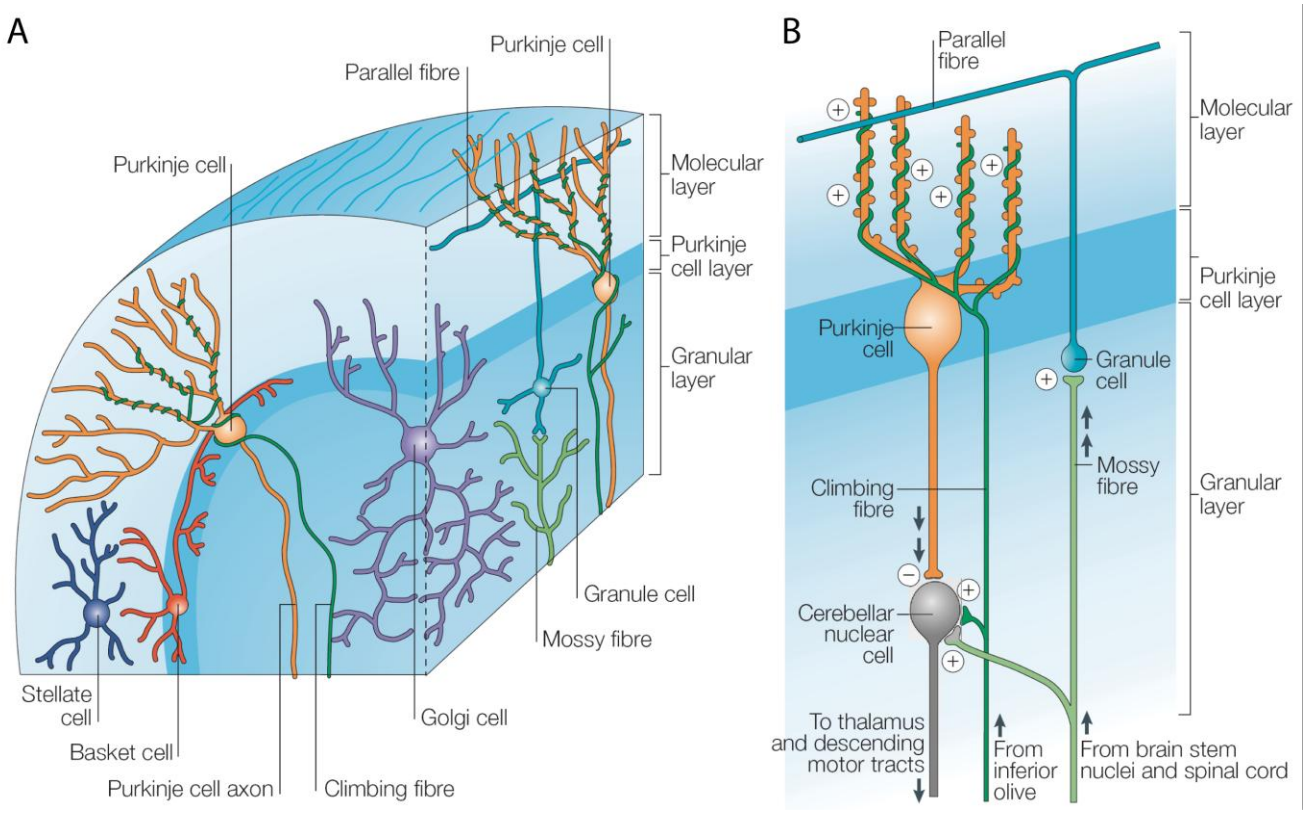

Figure 25. Basic structure of the cerebellar cortex.

A. Three dimensional view of the cerebellar cortex showing the different cell types in each layer.

There are two main afferents to the cerebellar cortex: climbing fibers, which make direct excitatory contact with the Purkinje cells, and mossy fibers, which terminate in the granular layer and make excitatory synaptic contacts mainly with granule cells, but also with Golgi cells. The ascending axons of the granule cells branch in a T-shaped manner to form the parallel fibers, which, in turn, make excitatory synaptic contacts with Purkinje cells and molecular layer interneurons — that is, stellate cells and basket cells. Note that this representation does not include the unipolar brushed cells and the Lugaro cells.

B. Enlarged view of the Purkinje cell showing the two main afferents to the cerebellar cortex as well as its efferent projection onto the cerebellar nuclear neurons.

From Apps and Garwicz 2005.

1.4.1 THE PURKINJE CELLS

1.4.1.1 MORPHOLOGY

The Purkinje cell, first described by the physiologist Johannes Purkinje in 1837, is the central core of the cortical cerebellar network since it constitutes the convergence site of all cortical inputs and its axon is the sole output of the cerebellar cortex. Purkinje cells are the first neurons of the cerebellar cortex to be born; in the mouse they develop on embryonic day 10 (E10-E13) (Miale and Sidman, 1961). Purkinje cells are large GABAergic neurons. Theirs cellular bodies, which measure around 20µm in mice, are among the largest in the brain (Caddy and Biscoe, 1979). They have large dendritic trees which extend up into the molecular layer, perpendicular to the folium axis (Figure 25, Figure 26). They spread out 300-400µm in the sagittal plane but their depth in the transversal plane is only of 15 to 20 µm. A principal dendrite emerges from the apical pole of the cell and branches into secondary dendrites, which in turn, branch into a fine tertiary arborization, covered by thousands of dendritic spines receiving parallel fiber inputs (Palay and Chan-Palay, 1974).

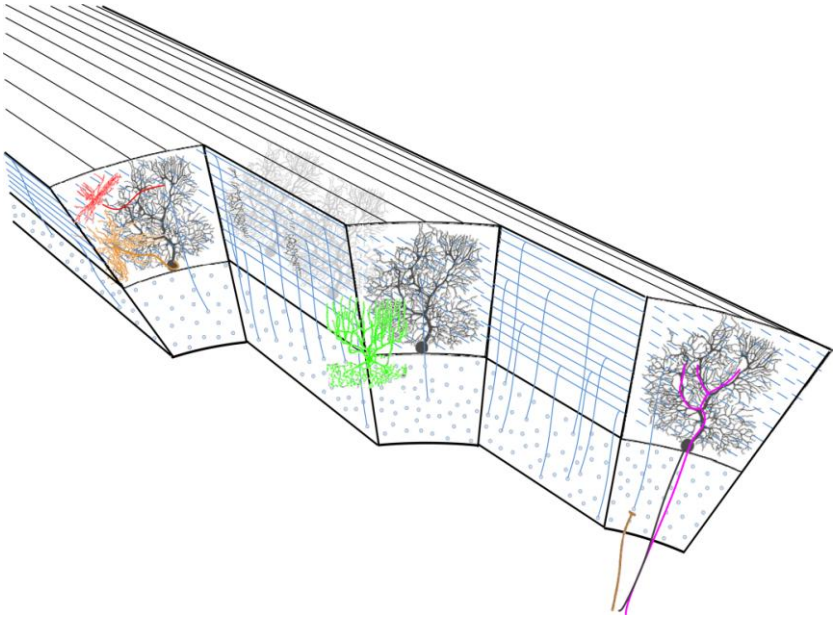

Figure 26. The cytoarchitecture of the cerebellar cortex. A parasagittal cut through the cerebellar cortex shows the arrangement of the cell types. Black – Purkinje cells. Blue – granule cells. Green – Golgi cell. Red – stellate cell. Orange – basket cell. Mossy and climbing fibers are shown in brown and magenta, respectively. (Rokni et al., 2008).

This particular disposition of the dendritic tree is oriented perpendicularly to the transverse bundle parallel fiber, the axons of granular cells. Thus, each Purkinje cell is crossed by several hundred of thousands of parallel fibers (Figure 26) (Harvey and Napper, 1991), potentially producing 170 000 synaptic inputs from the granular cells (Harvey and

Napper, 1988). On the opposite, each Purkinje cell is innervated by only one climbing fiber (Palay and Chan-Palay, 1974), which wraps around the primary and secondary dendrites, forming up to 26 000 synaptic contacts (Nieto-Bona et al., 1997). It is worth noting that this mono-innervation by climbing fibers is preceded by a multi-innervation phase, which regressed during the three first weeks post-natally (Crepel and Mariani, 1976; Crepel et al., 1976, 1981; Watanabe and Kano, 2011). Inhibitory interneurons of the molecular layer synapse onto the dendritic tree and the soma of Purkinje cells.

The myelinated axon emerges from the basal region of the soma, crosses the granular layer and terminates onto the neurons of the deep cerebellar or vestibular nuclei. This axon also emits collaterals in the cerebellar cortex, which can contact other Purkinje cell (hence their name (recurrent collateral) (Ramon Y Cajal, 1911; Palay and Chan-Palay, 1974; Orduz and Llano, 2007), Golgi cells and Lugaro cells (Palay and Chan-Palay, 1974; Hawkes and Leclerc, 1989) and potentially stellate and basket cells from the molecular layer (Palay and Chan-Palay, 1974; O'Donoghue et al., 1989).

1.4.1.2 PHYSIOLOGY

Purkinje cells generate two types of action potentials, the simple spikes and complex spikes, named after the distinct shapes of their waveforms (Figure 27.A).

Simple spikes occur at a very high and regular frequency (30-150Hz). Purkinje cells discharge in the absence of any synaptic entry (Häusser and Clark, 1997; Raman and Bean, 1999) but the simple spike frequency is modulated by excitatory and inhibitory inputs (from the parallel fibers and molecular layer interneurons respectively) (Llinás and Sugimori, 1980; Miyashita and Nagao, 1984; Wada et al., 2007) and by the occurrence of complexe spikes. These inputs do not only modulate the average firing rate of simple spikes but contribute to create temporal pattern of simples spikes, which are thought to play an important role in Purkinje cell coding of information (De Zeeuw et al., 2011).

Complex spikes are generated following the activation of a climbing fiber (at a rate of 2-9Hz (De Zeeuw et al., 2011)). Indeed, each Purkinje cell being innervated by a single climbing fiber with around 1000 release sites, the activation of a climbing fiber depolarizes the bulk of dendritic tree (Simpson et al., 1996; Schmolesky et al., 2002) and systematically triggers a complex spike. Consequently, both action potentials and high frequency bursts in the climbing fiber are reliably transmitted to the Purkinje cell. A complex spike is composed by an initial action potential followed by a plateau potential with superimposed calcium (Ca^{2+}) spikelet's and a subsesquent long lasting hyperpolarization (Figure 27.A).

The patterns of complex spikes and simple spikes can influence one another. Simple-spike activity can modify climbing-fiber activity patterns through GABAergic feedback from the cerebellar nuclei to the inferior olive (Lang et al., 1996; De Zeeuw et al., 1998b).

Climbing-fiber activity in turn can influence the generation of simple spike activity in the cerebellar cortex. First, immediately after the complex spike generation several modulations succeed (Figure 27.B): simple spike pause (absence of simple spikes during ten milliseconds or more), simple-spike facilitation (immediately after, during 20-40ms) and simple spike suppression (30% reduction of simple spike rate during tens of ms) (Simpson et al., 1996). Secondly, climbing fiber activity triggers heterosynaptic plasticity at the parallel fiber–Purkinje cell synapse, at the molecular layer interneuron–Purkinje cell synapse and, through spillover, at the parallel fiber–molecular layer interneuron synapse (Jörntell and Ekerot, 2002). Finally, climbing fiber activation exerts global short-term and long-term inhibitory effects that profoundly affect the basic firing frequency of simple spikes during rest and during modulation, probably by the intrinsic pacemaker activity of Purkinje cells (Cerminara and Rawson, 2004).

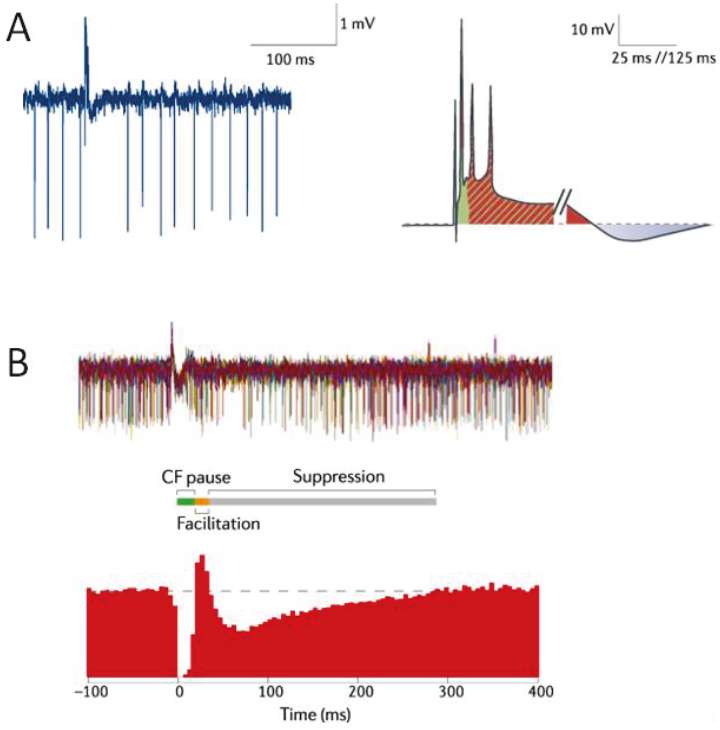

Figure 27. Purkinje cell firing

A. Simple spikes and complex spikes. Purkinje cell activity in an alert mouse shows simple spikes (left panel, negative events) and a complex spike (left panel, positive event). Complex spikes are mediated by voltage-gated sodium channels (right panel, shown in green) and calcium channels (right panel, shown in red), whereas the subsequent afterhyperpolarization is mediated by calcium-dependent potassium channels (right panel, shown in blue). Note the extended timescale for the afterhyperpolarization.

B. Complex spikes – simple spike interaction. The complex spike is followed by a pause in simple-spike activity, followed by a facilitation period (increase in simple spike rate) and then a simple-spike suppression (reduction of simple spike rate).

From De Zeeuw et al. 2011.

1.4.2 THE GRANULE CELLS

Granule cells are by far the most numerous elements in the cerebellar cortex and in the brain as a whole (Voogd et al., 1996). They are small glutamatergic neurons densely packed in the granule cell layer: their soma measures 5 µm and their density is around 2. 10^6 cell per mm^3 in rats (Harvey and Napper, 1988), which gives the granular aspect to this layer. Their dendritic trees are composed of 3 to 5 short dendrites which terminate in glomerules, where they receive excitatory input from the mossy fibers and inhibitory input from the Golgi cells. Each granule cell gives rise to an axon, which ascends vertically into the molecular layer, where it bifurcates in a T-fashion to form the parallel fibers, which then run horizontally from each side of the bifurcation point along the medio-lateral axis. These branches extend over long distance, between 4.2 to 4.7 mm in rats (Pichitpornchai et al., 1994). Their perpendicular orientation relative to the planes of the Purkinje cell dendritic trees allows a single granule cell to establish around 675 synaptic contact with Purkinje cells (Harvey and Napper, 1988) but a single parallel fiber establishes only one or two contacts with the dendrites of one Purkinje cell (Pichitpornchai et al., 1994). The ascending axon also makes synaptic contacts before branching but the functional importance is debated (Napper and Harvey, 1988; Pichitpornchai et al., 1994). A small proportion of synaptic contacts (fewer than 10 %) are made by parallel fibers onto molecular layer interneurons and apical dendrites of Golgi cells. This last connection constitutes a feedback inhibition on granule cell via the Golgi cell-granule cell synapses in the glomerule (see Appendix)(Pichitpornchai et al., 1994).

Since a single mossy fiber rosette provides excitatory input to tens of granule cells within a glomerules (Palay and Chan-Palay, 1974), granule cells are thought to be involved in the amplification and expansion of the mossy fiber signals in the cerebellar cortex.

As parallel fibers run transversely whereas Purkinje cell dendritic trees are sagittaly oriented, different Purkinje cells along the parallel fiber beam can be in principle activated consecutively by a spreading wave of excitation(Figure 28) (Braitenberg and Atwood, 1958). However, such transverse excitatory waves are rarely observed in physiological conditions; tactile stimulations rather trigger activation of Purkinje cells in local ‘patches’ (Shambes et al., 1978). This might be explained by the non-homogeneity of the synaptic connections along the parallel fiber, with stronger connections proximally than distally. Indeed varicosities are larger and denser in the proximal region of the parallel fiber beam than at the distal end (Pichitpornchai et al., 1994).

1.4.3 MOLECULAR LAYER INTERNEURONS

Molecular layer interneurons are the only neurons having their somas located in this layer. Two kinds of interneurons are classically distinguished, the basket and stellate cells, based on the position of the soma. Stellate cells are located in the upper two thirds of the

molecular layer. Their dendrites ramify between Purkinje cells in a parasagittal plane and their axon makes inhibitory synapses onto the dendrites of Purkinje cells. Basket cells are located in the inner third of the molecular layer (Palkovits et al., 1971). They emit dendrites in every direction in the sagittal plane from their somas and an axon parallel to the Purkinje cell layer. Axon terminals from multiple basket cells enlace Purkinje cell somata, forming 'baskets' that contain synapses and then extend to wrap around the initial segment of the Purkinje cell axon in a structure called the pinceau (Ramon Y Cajal, 1911). This structure is thought to inhibit Purkinje cell firing by directly controlling the extracellular voltage at the site of spike initiation (ephaptic inhibition), a inhibition process faster than any other described in the nervous system (Blot and Barbour, 2014). However, this dichotomy is often opposed to the possibility of a morphological continuum between basket cells and stellate cells (Ramon Y Cajal, 1911; Sultan and Bower, 1998).

Molecular layer interneurons are GABAergic. They receive several hundred of synaptic inputs from the parallel fibers (Palay and Chan-Palay, 1974) and are thus involved in feed forward inhibition (see Appendix). Given the organization of the axon, this process produces an inhibition of Purkinje cells on both sides of the excited parallel fiber bundle (Figure 28) (Braitenberg and Atwood, 1958; Eccles et al., 1967; Cohen and Yarom, 2000). They can also be activated by diffusion of glutamate from the climbing fibers (spillover (Szapiro and Barbour, 2007). Besides, an interneuron receives inhibitory connections from other molecular layer interneurons (Lemkey-Johnston and Larramendi, 1968; Llano and Gerschenfeld, 1993). Additionally, electric synapses couple interneurons and participate in the synchronization of their activity (Mann-Metzer and Yarom, 2000; Alcami and Marty, 2013).

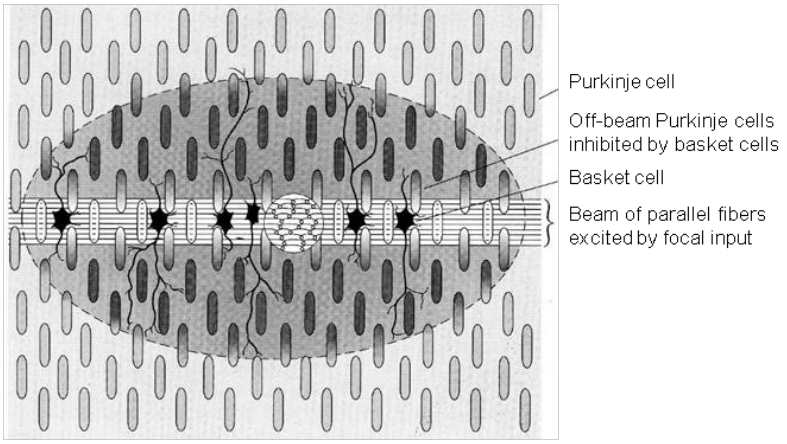

Figure 28. Representation of a spreading wave of excitation as proposed by Braintenberg and Atwood (1958). Excitation of a beam of parallel fibers by a focal mossy fiber input leads to excitation of central (on-beam) region of Purkinje cells and inhibition of surrounding (off-beam) Purkinje cells (via excitation of the inhibitory basket cells). In this schematic view of the surface of the cerebellar folium, the dark area surrounding the excited beam of parallel fibers indicates inhibitory effects
(Ghez 2000)

1.4.4 GRANULAR LAYER INTERNEURONS

1.4.4.1 GOLGI CELLS

Golgi cells are the main population of inhibitory interneurons in the granular layer. Their dendrites arborize in both the granular and molecular layers preferentially following the parasagittal plane (Sillitoe et al., 2008). Golgi cells receive most of their inputs from parallel fibers (Palay and Chan-Palay, 1974). Single axons of Golgi cells innervate hundreds of granule cells and, in the vestibulo-cerebellum, also tens of unipolar brush cells (UBCs) (Dugué et al., 2005). The terminals of their axonal tree end predominantly in the periphery of glomeruli in the granular layer (Palay and Chan-Palay, 1974). Two-thirds of Golgi cell axons use both GABA and glycine as their neurotransmitter and the rest use either GABA or glycine (Simat et al., 2007). Golgi cell inhibition of granule cells is mediated by GABA receptors, whereas that of UBCs is dominated by glycinergic currents (Rousseau et al., 2012), suggesting that postsynaptic selection of co-released transmitters is used to achieve target-specific signaling (Dugué et al., 2005). In glomerule, mossy fibers also produce a axo-axonic excitation on Golgi cells, triggering a modulation of synaptic activity of granule cell. Thus Golgi cell are also involved in limiting the propagation of incoming information.

1.4.4.2 LUGARO CELLS

The presence of Lugaro cells has long been known, but they have been characterized relatively recently. Their fusiform somas are located beneath the Purkinje cell layer (Aoki et al., 1986; Sahin and Hockfield, 1990). Their axons form a parasagittal plexus but they also extend transversely for 2 mm, making contact with the apical dendrites of Golgi cells. Also the axons of more than 10 Lugaro cells converge onto only one Golgi cell, while the axon of one Lugaro cell diverges onto 150 Golgi cells (Dieudonné and Dumoulin, 2000). Normally silent in slice preparation, they are highly sensitive to serotonine and discharge regularly at 5-15 Hz. Because of the large divergence of Lugaro cells onto Purkinje cells (1:150), an interesting possibility is that Lugaro cells play a role in synchronizing activity among Golgi cells situated along the parallel fiber beam (Vos et al., 1999; Ito, 2006).

1.4.4.3 UNIPOLAR BRUSH CELLS

Unipolar brush cells (UBC)are excitatory interneurons that are prominently distributed in the vermis and the flocculo-nodular lobe (Mugnaini et al., 2011). They have a single brush-like dendrite, which receives input from, in most cases, a single mossy fiber terminal. In turn, UBCs give rise to intrinsic mossy fibers that contact both granule cells and other UBCs (Nunzi and Mugnaini, 2000). This feed-forward excitation is thought to be involved in the amplification of single mossy fiber afferent signals (Mugnaini et al., 2011).

We have seen that the cerebellar cortex is organized in microcomplexes, with specific projection from the inferior olive and to the cerebellar or vestibular nuclei. In the cerebellar cortex, the dendrites and axons of the molecular layer interneurons (MLIs) and Golgi cells stay within the boundaries of the sagittal Purkinje cell (PC) zones (Palay and Chan-Palay, 1974; Sillitoe et al., 2008). Thus, these cells involved in feedforward and feedback inhibition, operate within the same sagittal PC zone as the climbing fibers that provide the dominant drive of that particular PC zone. This reinforces the possibility that the microcomplexes represent functional units able to work in parallel. Moreover, these units display plasticity at different sites of the micro circuit, which are likely to be determining for their processing capacities.

1.5 PLASTICITIES OF THE CEREBELLAR CORTEX

Plasticity can be defined as the brain ability to modify in response to environmental changes (it can relate to an area, a neuron, a synapse...). At the level of a neuron, it corresponds to the capacity of a particular region of the neuron to change its response to a given input (excitatory or inhibitory). It comprises synaptic plasticity and intrinsic plasticity. Synaptic plasticity deals directly with the strength of the connection between two neurons, whereas intrinsic plasticity involves modification of neuronal excitability of an individual neuron (in the axon, dendrites, and soma independently of changes in synaptic transmission). Plasticity can be expressed on different time scales; short term plasticity (reverting after several hours) is distinguished from long term plasticity (persisting after several hours). Synaptic plasticity can correspond to an increase or decrease in the synaptic strength, respectively named potentiation or depression of the synapse. It can result from alterations in the quantity of released neurotransmitters, or of the number of neurotransmitter receptors located on a synapse. The location of the mechanisms underlying synaptic plasticity categorizes it as pre- or post- synaptic. Homo-synaptic plasticity is a change that results from the history of activity at a particular synapse whereas heterosynaptic plasticity is a change in synaptic strength that results from the activity of other neurons. I will here review the various types of plasticity that have been reported in the cerebellar cortex, their implication in cerebellar processing of information will be described in the next chapter. As many forms of synaptic and intrinsic plasticity were progressively described at different sites of the cerebellar network, I will present them as following: plasticities in the Purkinje cell network, in the granule cell network and in the deep cerebellar nuclei (Figure 29).

1.5.1 PLASTICITIES IN THE PURKINJE CELL NETWORK

1.5.1.1 AT THE PARALLEL FIBER-PURKINJE CELL SYNAPSE

Historically, **long-term depression (LTD) at the parallel fiber–Purkinje cell (PF-PC)** synapse has been proposed to be the cellular mechanism underlying motor learning in the cerebellum (Marr, 1969; Albus, 1971). The first experimental evidence comes from studies in decerebrated rabbits and in slices, which showed that co-activation of climbing fiber (CF) and parallel fiber (PF) induced a long-lasting depression of PC responses to subsequent PF inputs (Ito and Kano, 1982; Ito et al., 1982). Further characterization in vitro (in slices) indicated a **post-synaptic process** and allowed a detailed description of the molecular mechanisms. The combined stimulation of PF and CF activates both AMPA and mGluR1 receptors and induces a large Ca2+ influx, which activates kinases (PKCα and CamKII)(Linden and Connor, 1991; Hartell, 1994; Leitges et al., 2004; Hansel et al., 2006). The PKCα kinase phosphorylates the GluR2 subunit of AMPA receptor, which triggers its internalization (Chung et al., 2003). The reduction of AMPA receptor number at the Purkinje cell membrane is responsible of the decrease of synapse efficacy (Wang and Linden, 2000).

Interestingly, Jorntell and Ekerot examined the receptive field of Purkinje cells by tactile cutaneous stimulation of the forelimb in anaesthetized cats (Jörntell and Ekerot, 2002). They showed that pairing a PF burst stimulation with CF activity led to a decrease in the receptive field size of Purkinje cells. This modification was suggested to be underlain by post-synaptic mechanisms at the PF-PC synapses. On the opposite, they observed that a PF burst alone increased the size of Purkinje cell receptive field, and that these receptive field changes were reciprocal (i.e. the induction protocols could reverse each other). This suggested the existence of another form of plasticity, in the opposite direction, able to reverse the long lasting depression of PF input in Purkinje cells (Jörntell and Ekerot, 2002).

Confirmation of such plasticity was brought by in vitro studies, which also allowed to disentangle the pre- and post-synaptic contributions of the observed depression and potentiation. At the PF–PC synapse, all forms of long-term synaptic plasticity have been described (postsynaptic LTP and LTD, as well as presynaptic LTP and LTD).

Postsynaptic LTP can be reliably induced by low-frequency PF stimulation without CF stimulation (Lev-Ram et al., 2002). The relatively small postsynaptic Ca2+ transient activates protein phosphatase 2B (PP2B) which in turn activates protein phosphatase 1 (PP1). Phosphatases dephosphorylate AMPA receptors, which leads to their externalization (Belmeguenai and Hansel, 2005). This mechanism is able to reverse long term depression at the PF-PC synapse, providing the basis for bidirectional plasticity, whose orientation is controlled by CF inputs (Lev-Ram et al., 2003; Coesmans et al., 2004).

The PF-PC synapse also displays plasticity at the presynaptic site. **Presynaptic LTP** is elicited by a relatively short period of activity in parallel fibers and depends on cAMP signaling (Salin et al., 1996). **Presynaptic LTD** was also reported, with a similar induction protocol but was only observed when presynaptic LTP was pharmacologically blocked (Qiu and Knöpfel, 2009).

The description of a plasticity mechanism in vitro does not imply that such plasticity does occurs in vivo, but indicates that the pathway exists and might be recruited under some circumstances in vivo. The link between plasticities described in vivo and in vitro is not straightforward, since the induction protocols are quite different. Indeed in vivo plasticities requires PF burst stimulation (100 Hz) whereas LTP and LTD in slices are induced by 1Hz PF stimulation or co-activation of PF and CF. Shared molecular mechanisms argue for a common process: for example in vivo depression also requires PKC activation and mGluR1 receptors (Gao et al., 2003). However, this is not always the case, since mGluR1 receptors are required for in vivo potentiation (Wang et al., 2009) but not in vitro LTP (Belmeguenai et al., 2008).

Plasticity has also been described in the parallel pathway Parallel fiber -> Molecular layer interneuron -> Purkinje cell, mediating feed forward inhibition (feed forward inhibition, see Appendix).

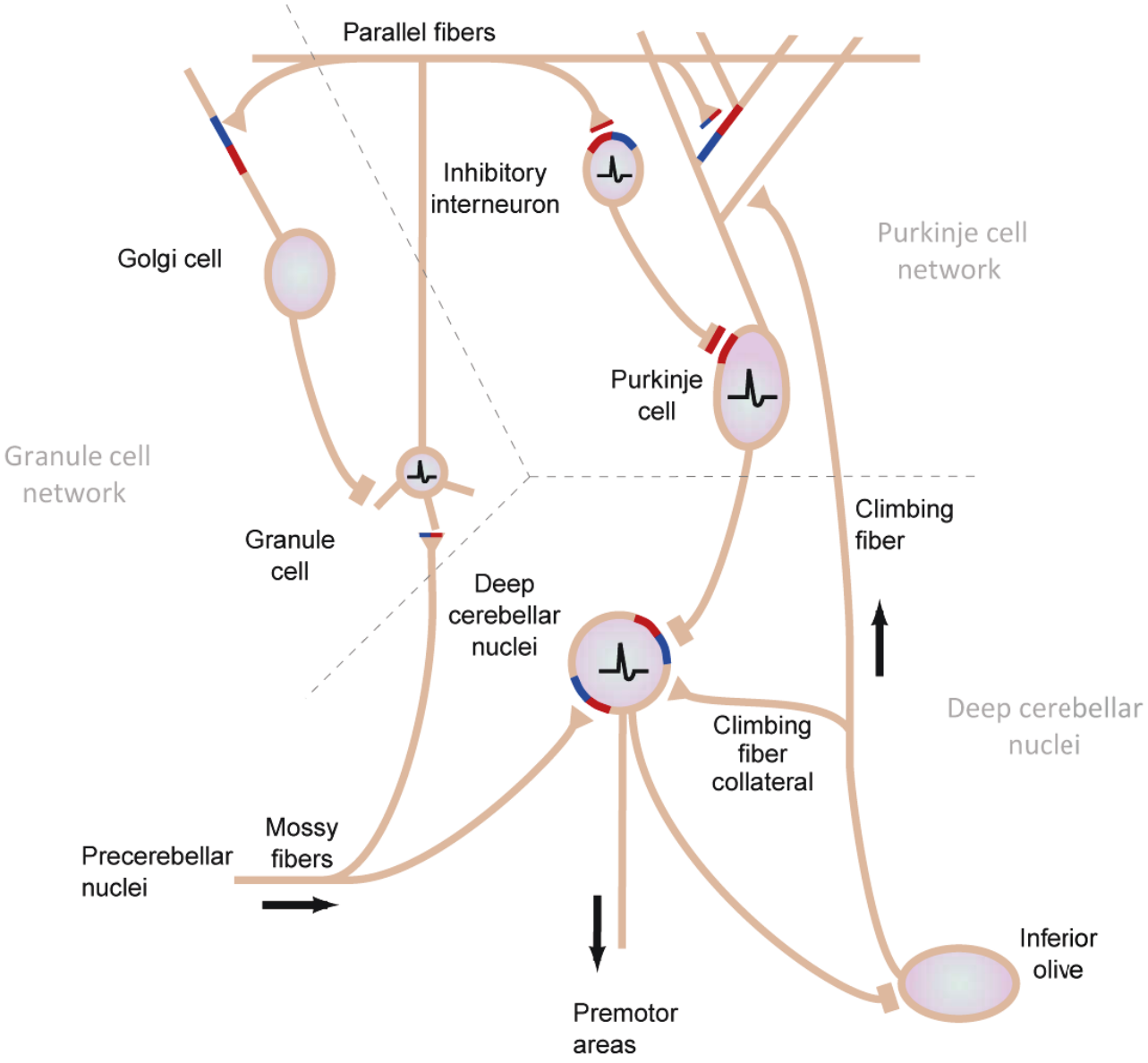

Figure 29. Synaptic and non-synaptic plasticities in the cerebellar circuit.
In this drawing, the occurrence of long-term use-dependent plasticity has been coded with color: red indicating potentiation (LTP) and blue indicating depression (LTD). Black action potentials in neuronal somas indicate persistent increases in intrinsic excitability, whereas bars of color at synapses indicate conventional synaptic LTP or LTD. The location of the color bar in the presynaptic or postsynaptic membrane represents the best current understanding of the locus of expression of these forms of LTD.
Adapted from Hansel et al. 2001

1.5.1.2 AT THE PARALLEL FIBER-INTERNEURON SYNAPSE

Plasticities onto inhibitory interneurons were first suggested by the study of Jorntell and Ekerot (2002) who observed opposed changes in the receptive field size of interneurons: PF burst stimulation alone induced an enlargement of Purkinje cell receptive field and a shrinkage interneuron receptive field, and the reverse effect was observed when PF bursts were combined with CF activation (i.e. a shrinkage of Purkinje cell receptive field and an enlargement interneuron receptive field). Like for the Purkinje cells, the changes in size of the interneuron receptive fields were reciprocal, and were suggested to occur post-synaptically. Potentiation of PF synaptic inputs to interneurons was then confirmed by patch clamp recording of interneurons in vivo (Jörntell and Ekerot, 2003).

In vitro, **parallel fiber - molecular layer interneuron** synapses can undergo postsynaptic LTD, postsynaptic LTP and presynaptic LTP. Post synaptic LTD is induced by low frequency stimulation of PF (Piochon et al., 2010). Being restricted to activated synapse, this LTD is a form of self limiting plasticity. Postsynaptic LTP can be induced by PF stimulation combined with stellate cell depolarization, which in turn may be mediated, through spillover, by CF activation (Rancillac and Crépel, 2004; Szapiro and Barbour, 2007). Presynaptic LTP can be induced by parallel fiber stimulation alone (Bender et al., 2009) and constitutes a positive feedback mechanism.

1.5.1.3 AT THE INTERNEURON –PURKINJE CELL SYNAPSE

In vitro, **molecular layer interneuron-Purkinje cell** synapse expresses post-synaptic potentiation, also called rebound potentiation, following the activation of Purkinje cell by CFs (Kano et al., 1992). Pre-synaptically, CF activation of Purkinje cells also triggers an increase of GABA release from the interneuron by retrograde signaling, this processed is called depolarization-induced potentiation of inhibition (Duguid and Smart, 2004). The plasticity of this synapse could not be specifically studied in vivo but was suggested to play a major role in the changes of Purkinje cell receptor field size during peripheral stimulation (Jörntell and Ekerot, 2002).

1.5.1.4 AT THE CLIMBING FIBER –PURKINJE CELL SYNAPSE

In cerebellar slices, **climbing fiber–Purkinje cell** synapses were shown to display post synaptic LTD (Hansel and Linden, 2000) and LTP (Bosman et al., 2008) as well as pre-synaptic LTP and LTD (Ohtsuki and Hirano, 2008) but these plasticities are likely to be confined to the immature cerebellum and be involved in climbing fiber elimination.

1.5.1.5 PURKINJE CELL INTRINSIC PLASTICITY

Finally, Purkinje cells are also characterized by **intrinsic plasticity**. Purkinje cell excitability can be enhanced by somatic current injections or by PF stimulation (Belmeguenai et al., 2010; Schonewille et al., 2010). Intrinsic plasticity can be triggered by PF-LTP protocols, but lowers the probability for subsequent LTP induction. Thus, LTP at activated PF could inhibit the induction of PF-LTP at neighboring non-potentiated dendrites through intrinsic plasticity of Purkinje cells. Ultimately, enhanced excitability of a Purkinje cell could lead to an increase in firing frequency *in vivo* during spontaneous activity and/or during particular patterns of activation by parallel fibers and/or molecular layer interneurons.

Numerous forms of plasticity have been progressively unraveled in the granule cell network and the deep cerebellar nuclei, however to my knowledge, they were only studied in vitro.

1.5.2 PLASTICITIES IN THE GRANULE CELL NETWORK

In the granule cell network, the **mossy fiber–granule cell** synapse undergoes both presynaptic LTP and LTD, which can reverse each other (D'Angelo et al., 1999; Gall et al., 2005) . This bidirectional plasticity is determined by the concentration of intracellular calcium, linked to the length of mossy fiber bursts (a long burst >250 ms inducing LTP whereas a short burst induces LTD). It thus provides a mechanism for learning of burst patterns at the input stage of the cerebellum (Gall et al., 2005).

Theta bursts of mossy fiber stimulation enhanced **intrinsic excitability of the granule cell** (Armano et al., 2000). Thus, although granule cells have low background firing rates owing to tonic inhibition by Golgi cells, sensory activation can cause bursting in granule cells, such that mossy fiber input is transmitted with high reliability to Purkinje cells (Chadderton et al., 2004).

Golgi cell - Granule cell synapses exhibit post-synaptic LTD following high PF stimulation but its relevancy is unclear given the already weak efficacy of this transmission at its baseline level. However, CF inputs may induce LTP of this synapse during peripherical activation (Xu and Edgley, 2008).

1.5.3 PLASTICITIES IN THE DEEP CEREBELLAR NUCLEI

Mossy fiber – nuclear neurons synapse has been shown to exhibit LTP after high frequency stimulation of mossy fibers (Racine et al., 1986). Zang and Linden reported post synaptic LTD evoked by high-frequency burst stimulation of mossy fibers, either alone or paired with postsynaptic depolarization.

Purkinje cell - nuclear neurons synapse has been shown to exhibit LTP and LTD. Nuclear neurons exhibit a prominent rebound depolarization upon release from hyperpolarization. The polarity of the induced plasticity depends on the level of post synaptic excitation of nuclear neurons (Aizenman et al., 1998): LTP can be elicited by short, high-frequency trains of inhibitory postsynaptic potentials (IPSPs), whereas LTD is induced by the same protocol but in conditions of lower post-synaptic excitation. The pre or post synaptic locus remains to be determined (Hansel et al., 2001).

Neurons of the deep cerebellar nuclei showed persistent increases in their intrinsic excitability following titanic stimulation of mossy fibers (Aizenman and Linden, 2000) but it is likely that any stimulus resulting in the appropriate post synaptic transient will produce this effect (Hansel et al., 2001).

This chapter gave an overview of the organization of the cerebellum, presenting the different functional units and their properties. To understand how these modules could process information in a behaviorally relevant context, different paradigms were developed. I will now present them with a focus on the works which contributed to decipher the role of plasticity in cerebellar processing of information.

2 CEREBELLAR INFORMATION PROCESSING UNDERSTOOD IN SIMPLE MOTOR LEARNING

From the XIX century it has been noticed that cerebellum ablation resulted in troubles in gait and voluntary movement control (Flourens, 1824). Subsequent theories proposed a role in spontaneous movement coordination as well as gait and balance regulation (Dow and Moruzzi, 1958). Following experimental works showed a more precise role on motor execution adaption in function of environmental constrains (Ito, 1984; Lisberger, 1988). These studies were based on the development on simple motor paradigms, allowing a fine characterization of the underlying cerebellar processes. The most famous are the eyeblink conditioning and the adaptation of the vestibulo ocular reflex (VOR).

2.1 VOR ADAPTATION AND EYEBLINK CONDITIONING PARADIGMS

The VOR is responsible for the stabilization of image on the retina during head movements. For this it induces compensatory eye movement, of the same amplitude, in the opposite direction. The ratio head /eye rotation speed is called the VOR gain and is normally equal to 1. Experimental combination of head turns with image motions in the same direction induces retinal slip of the image of the retina (Figure 30.A). Repetitive exposure to the same discrepancy triggers a reduction of the compensatory eye movement to stabilize images during head movement (the VOR gain becomes lower than 1). On the opposite, combining head turns with image motions in the opposite direction increases the amplitude of eye movements (the VOR gain becomes higher than 1).

The eyeblink reflex consists in the eyelid closure in response to an aversive stimulus, like a corneal air puff for example. Eyeblink conditioning is the repeated exposure to a behaviorally neutral stimulus such as an auditory tone, paired with the aversive stimulus a few hundred of milliseconds later (Figure 30.B). In this paradigm, learning the tone-air puff association allows the animal to anticipate the delivery of the aversive stimulus. Indeed this protocol leads to a gradual development of eyeblink responses to the auditory tone, and the responses are accurately timed so that their peak coincides with the impact of the aversive stimulus.

Lesions and inactivations of the cerebellar cortex, the cerebellar nuclei and the inferior olive showed that the whole cerebellar circuitry was involved in both VOR adaptation (Ito et al., 1974; Nagao and Ito, 1991; Attwell et al., 2002; Nagao and Kitazawa, 2003) and eyeblink conditioning (Krupa et al., 1993; Chen et al., 1996; Welsh and Harvey, 1998; Attwell et al., 2001). However at that time, the cellular mechanism of motor learning remained to be determined.

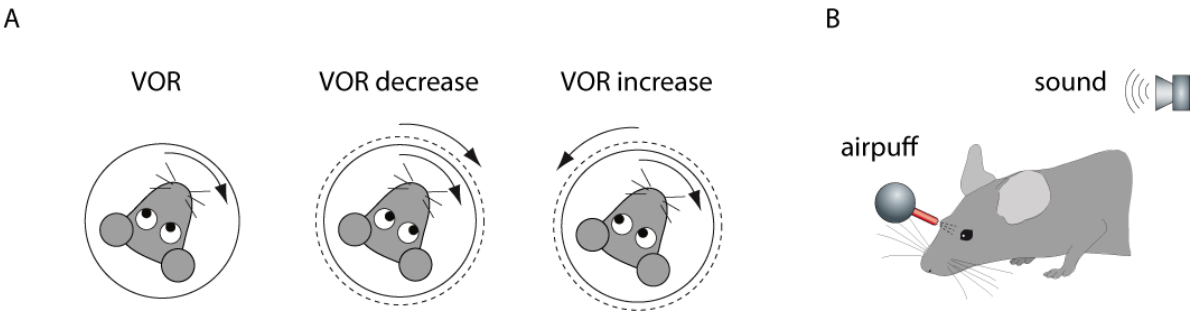

Figure 30. Two paradigms to study cerebellar mechanisms of motor learning.
A. The VOR adaptation task. The mouse is placed in a restrainer, fixed onto the center of a turntable that is surrounded by a cylindrical screen. Vestibulo-ocular reflex is evoked by rotation the turntable. Three paradigms are represented: VOR (no change in the cylindrical screen), VOR decrease (rotation of the screen in the same direction as the turntable), and VOR increase (rotation of the screen in the opposite direction to the turntable). Gain value (eye velocity/stimulus velocity) is calculated. Adapted from Schonewille et al. 2011
B. The eyeblink conditioning task. An auditory tone (350 ms) is paired with a mild corneal airpuff (30 ms), and both stimuli co-terminate. Eyelid responses are measured.

2.2 CEREBELLAR LTD AS A BASIS FOR MOTOR LEARNING

Marr and Albus had initially proposed that changes in the strengths of PF-PC synapses could store stimulus-response associations by linking inputs with appropriate motor outputs. The output of Purkinje cells would be the discharge pattern of simple spikes, whereas the complex spikes, whose frequency is too low (1Hz) to influence the motor command, were rather suggested to correspond to an error signal. Mossy fiber signals would be sparsely re-encoded by non-overlapping populations of granule cells and climbing fibers, providing the instructive signal that regulates the strength of PF-PC synapses, would thereby guide the encoding of new stimulus-response associations.

Following this hypothesis, Ito proposed that PF-PC - LTD would select the appropriate microcomplex to trigger the adapted motor program (Figure 31) (Ito, 2001). For example in the case of VOR adaptation, a set of microcomplexes in the cerebellar cortex receive information about head position via the mossy fiber-parallel fiber (MF-PF) pathway. All of these microcomplexes are originally activated by a common MF-PF pathway, and Purkinje cell inhibition dominates in nuclear neurons. During the VOR adaptation task, the retinal-slip signal is brought by the climbing fibers. Since LTD has been shown to require the coincidence of both inputs in a restricted time window, LTD would only occur in the micro-complexes where mossy fiber and climbing fiber combines temporally, i.e. in the microcomplexes that were activated by a specific position of the head at the occurrence of the retinal slip. In these microcomplexes, reduced excitatory action of PF-PC synapses would release nuclear neurons from Purkinje cell inhibition and allow them to activate motor neuron responsible for eye movements.

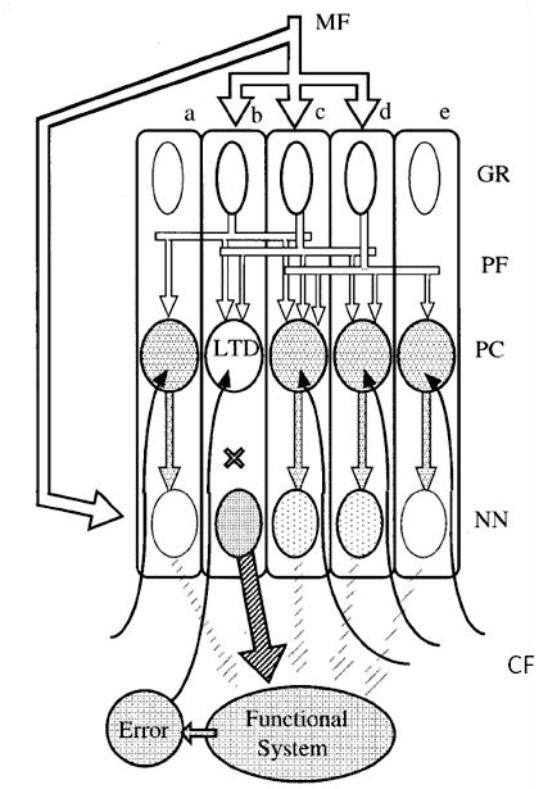

Figure 31. Initial model of LTD involvement in cerebellar motor learning: the selection of the appropriate microcomplex.

Multiple microzone structure of the cerebellum. a–e, Five neighboring microzones are assumed to be associated with a functional system. All of these microzones are originally activated by a common mossy fiber-parallel fiber (MF-PF) pathway, and Purkinje cell (PC) inhibition dominates in nuclear neurons (NN). Drives through the MF-PF pathway, therefore, will not yield output signals of nuclear neurons. When errors involved in the repeated operation of a functional system are fed to microzone b, LTD releases its nuclear neurons from PC inhibition. Microzone b would then operate with the functional system. Despite divergence of the MF-PF pathway to multiple microzones, specificity of each microzone will be secured in this way by the information conveyed by CFs.

MF mossy fiber; GR granule cell; PF parallel fiber; PC Purkinje cell; NN nuclear neuron; CF climbing fiber.

(Ito 2001)

The generation of several mouse mutant lines with specific molecular deficits affecting the cerebellum allowed to bring experimental arguments to this theory. This approach consisted in correlating impaired cellular mechanism and altered performances in the VOR adaptation and eyeblink conditioning tasks. Thus a series of transgenic mouse models targeting signaling pathways involved in cerebellar LTD such as the protein kinase C (PKC) (De Zeeuw et al., 1998a), cGMP-dependent protein kinase type I (cGKI) (Feil et al., 2003) the GluR-delta 2 receptor (Katoh et al., 2005) or the αCaMKII enzyme (Hansel et al., 2006) showed impairments in the VOR adaptation task. Similarly, performances in the eyeblink conditioning task were impaired in models impaired for LTD, due to the lack of mGluR1 receptors (Aiba et al., 1994), GFAP protein (Shibuki et al., 1996), or PKC activity (Koekkoek et

al., 2003). These findings led to the consensus that postsynaptic parallel fiber–Purkinje cell LTD did underlie motor learning in the cerebellum.

2.3 THE ROLE OF CEREBELLAR LTD IN MOTOR LEARNING CALLED INTO QUESTION

However, the view of the postsynaptic PF-PC LTD as the unique cellular mechanism underlying cerebellar motor learning was questioned by a series of recent observations.

First the causal relation between cerebellar LTD and VOR adaptation was not unequivocal. In all the mouse models mentioned above, the genetic alteration could go beyond the alteration of LTD and these additional disruptions might participate to the observed VOR adaptation deficits. Some mouse models (like the GluRdelta2) also show intrinsic motor deficits which may explain the poor learning performances (Katoh et al., 2005). Additionally, pharmacological inactivation of cerebellar LTD was not found to be accompanied by a deficit in other cerebellar dependent learning (eye blink conditioning and rotarod, (Welsh et al., 2005)). In accordance with these findings, the use of three different transgenic mouse models targeting specifically late events in the LTD signaling cascade confirmed the dissociation between LTD and simple motor learning tasks (Schonewille et al., 2011).

Second, the design of a VOR adaptation task with training conditions which did not elicit instructive signals from the climbing fibers (by pairing head movement with oppositely directed motion of a visual target and background), thus preventing heterosynaptic LTD, resulted in a completely normal motor learning (Ke et al., 2009). Third, the discovery of PF-PC *LTP* (Lev-Ram et al., 2002) along with the observation of independent alteration of VOR gain increase and gain decrease (Boyden et al., 2006) led the authors to propose that bi-directional plasticity at the same set of synapses would control VOR gain adaptation in one or the other direction (i.e. the PF-PC LTD would increase VOR gain whereas PF-PC LTP would decrease VOR gain). L7-PP2B mice, lacking PF-PC LTP due to the lack of phosphatase 2B, are indeed dramatically affected in both VOR adaptation and eyeblink conditioning tasks (Schonewille et al., 2010). However, this model based on bidirectional plasticity had to be revised to take into account the new data concerning cerebellar cortical plasticity.

Indeed, additional plasticity sites were identified in the cerebellar cortex (as described previously) and some corresponding mouse models impaired for these plasticities have been generated such as NR2a-/- mice and NR2a ΔC/ ΔC mice with altered mossy fiber-granule cell LTP (Andreescu et al., 2011) and A6 –ΔKKC2 mice affected for granule intrinsic plasticity (Seja et al., 2012). Both Nr2a−/− mutants and Nr2aΔC/ΔC mice have significant deficits in phase reversal adaptation of the VOR (i.e. a mismatch training where the mouse has to make a compensatory eye movement that is opposite to the previous direction) (Andreescu et al., 2011). A6-ΔKcc2 mice show a moderate impairment in phase reversal learning of the VOR and a virtually absent consolidation of this long-term phase learning (Seja et al., 2012). This

suggests that plasticities in the granule cell network may also contribute to motor learning in the VOR adaptation task.

2.4 DISTRIBUTED SYNERGISTIC PLASTICITY

The fact that most of these mutant models displayed alteration in various aspects of the VOR adaptation task (learning, reversal or consolidation) led to the concept of distributed synergistic plasticity (Gao et al., 2012). It refers to the combination of different types of plasticity, at different sites of the cerebellar network, which could act synergistically or antagonistically. These plasticities can be involved in a serial manner (such as plasticity in granule cell network and plasticity in Purkinje cell network) or in parallel manner (such as plasticity at PF-PC synapses and that at PF– molecular layer interneuron synapses).

The authors propose that the granule cell network would re-encode mossy fiber signal to increase the diversity of the activity patterns while the Purkinje cell network, through the climbing fiber guided plasticities, would select the appropriate pattern in order to shape Purkinje cell simple spike output. The diversity role of the granule cell network is supported by different findings: first, the huge number of granule cells, able to sparsely re-encode mossy fibers patterns in none-overlapping populations; second, the presence of Golgi cell which, through feedforward inhibition and feed forward excitation (see Appendix) are able to increase the firing rate for specific short periods, to induce delays in firing rate changes and to generate prolonged periods of increased firing (D'Angelo and De Zeeuw, 2009) and the presence of UBC, which through feed forward excitation, also contribute to increase diversity in activity patterns of granule cell; third, LTP, LTD and intrinsic plasticities at these different sites further increase the possibility to modify mossy fiber patterns that enter the cerebellar cortex.

In the PC network, climbing fiber activity may not only reduce Purkinje cell activity by inducing LTD at the PF-PC synapse but also by promoting potentiation at the PF–molecular layer interneuron synapse, the molecular layer interneuron–PC synapse and probably even at the PF–Golgi cell synapse. Conversely, the absence of climbing fiber input can increase Purkinje cell activity by permitting LTP at the PF-PC synapse, by increasing the intrinsic excitability of Purkinje cell dendrites and by promoting LTD at PF– molecular layer interneuron synapses.

These observations are in line with – and provide the cellular basis for - the general view of the cerebellar micro-circuit as an adaptive filter.

2.5 THE CEREBELLAR MICRO-CIRCUIT AS AN ADAPTIVE FILTER

Dean and Porrill proposed that the cerebellar microcircuit constitutes an adaptive filter (Dean et al., 2010). In signal processing, a filter is a process that transforms an input signal into an output signal. They propose that the cerebellar microcircuit can be mapped onto an adaptive filter structure (Figure 32): the filter inputs (MF activity) are analyzed into component signals (PF activity), which are then weighted (at the PF–PC synapses) and recombined to form the filter output (the PC simple spike rate). The filter is adaptive because the weight of the modules, corresponding to the synapse efficiency, can be modified through bi-directional plasticity (LTP and LTD), under the control of a teaching or error signal (the climbing fiber input). This adjustment follows the covariance rule: a PF signal that is positively correlated with an error signal has its weight reduced (through LTD), whereas a signal that is negatively correlated with an error signal has its weight increased (through LTP).

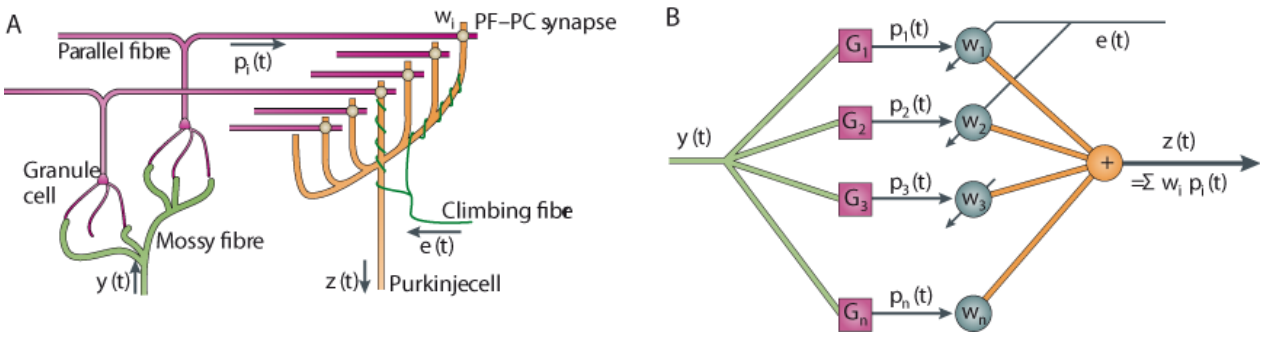

Figure 32. A simplified cerebellar microcircuit as an adaptive filter.
A. A mossy fibre (MF) input signal is distributed over many granule cells, the axons of which form parallel fibers (PFs) that synapse on Purkinje cells (PCs). In Marr–Albus-type models, correlated firing of a PF and the climbing fiber (CF) alters the strength of the PF–PC synapse. Note that this figure omits a number of the microcircuit features, in particular the inhibitory projection from granule cells to PCs via stellate and basket cells.
B. The structure of this microcircuit can be identified with that of an adaptive filter as follows: the processing of a sensory input or motor signal input (y(t)) by the granule cell layer is interpreted as analysis by a bank of modules (Gi). PC output is modeled as a weighted sum of these PF inputs, with the weights (Wi) corresponding to synaptic efficiencies. The CF input is interpreted as a teaching signal (e(t)) that adapts synaptic weights using the covariance learning rule.
(Dean et al. 2010)

Dean and Porrill argue that most of the theoretical models derived from the Marr-Albus models have the core characteristics of an adaptive filter. They also show that the recently

described properties of the cerebellar micro-circuit are consistent with the requirements for fulfilling the basic computational features of adaptive filters:

- the bidirectional plasticity (reciprocal LTP and LTD) that implements the covariance rule
- the existence of a parallel pathway (parallel fiber-Interneurons-Purkinje cell) that allows a signal to have a negative influence onto the output signal and that follows the inverse covariance rule
- the preponderance of silent synapses
- the recurrent architecture, i.e. the fact that a cerebellar microzone receives MF inputs that are related to the microzone's own output.

The view of the cerebellar microcircuit as an adaptive filter implies that the function of this network is to decorrelate the input from a teaching or error signal, that is to say, to silence the inputs which are irrelevant and maintain or potentiate the inputs which are pertinent (these notions having a different meaning depending on the task or type –motor or sensory- of information processed). It also underlies that such a processing is not confined to motor control but could also be used in sensory processing. Thus the function of a particular microzone is determined by its external connection (MF and CF inputs, PC output targets). This means that, according to the recent increase in studies showing new anatomical connections between the cerebellum and non-motor cortical areas in the forebrain, the cerebellum might be involved in a multitude of functions in addition to its well described involvement in motor learning (see for instance Strick et al., 2009). The next chapter exposes how cerebellar processing of information contributes to the different processes of navigation.

Part III. Cerebellar information processing for spatial navigation

I will first review the current evidence showing the involvement of the cerebellum in spatial navigation. Then I will expose several computations performed by the cerebellum that are likely to be of striking importance for navigation.

1 THE ROLE OF THE CEREBELLUM IN SPATIAL NAVIGATION

1.1 FIRST EVIDENCE OF A ROLE OF THE CEREBELLUM IN SPATIAL NAVIGATION

1.1.1 HUMAN STUDIES

In humans, neural correlates of spatial navigation can be investigated by combining functional brain imaging with navigation in virtual reality paradigms. During navigation in a complex virtual reality town, bilateral activation of the cerebellum - among a network of structures - has been reported in navigation trials compared to the static scene trials (Figure 33) (Maguire, 1998). Also, the right cerebellum and frontal gyrus were specifically activated during successful detour navigation compared to direct navigation(Maguire, 1998). Other studies using simulated driving reported cerebellar activation during active driving compared to the passive viewing of the scenes (Walter et al., 2001; Calhoun et al., 2002; Horikawa et al., 2005). However, these findings are often interpreted as a cerebellar role in attention (Allen, 1997) or motor preparation (Thach et al., 1992). Interestingly, in the starmaze task, a spatial navigation task requiring spatio-temporal organisation of sensory information (Iglói et al., 2010), distinct sub-regions of the cerebellum were selectively activated depending on the navigation strategy used to solve the task. When the subject relied on external information, temporally correlated activation was observed in the left cerebellum and the posterior parietal cortex. On the opposite, when the subject navigated using route information (the sequence of turns), right cerebellum, left hippocampus, and medial prefrontal cortex were activated in temporally correlated way (Igloi et al., 2012)

Along with the correlational findings from the imaging studies, data from cerebellar patients reveal a deficit in the angular but not linear control of locomotion during a circular walking task (Goodworth et al., 2012). Otherwise most of the studies focus of visuo-spatial abilities (Schmahmann and Sherman, 1998; Molinari et al., 2004), often confined to the reproduction of complex figures (Rey's complex figure for example) or the pointing of items in a given spatio-temporal order. Their interpretation is also debated, some authors linking them to unspecific attentional impairment (Frank et al., 2007).

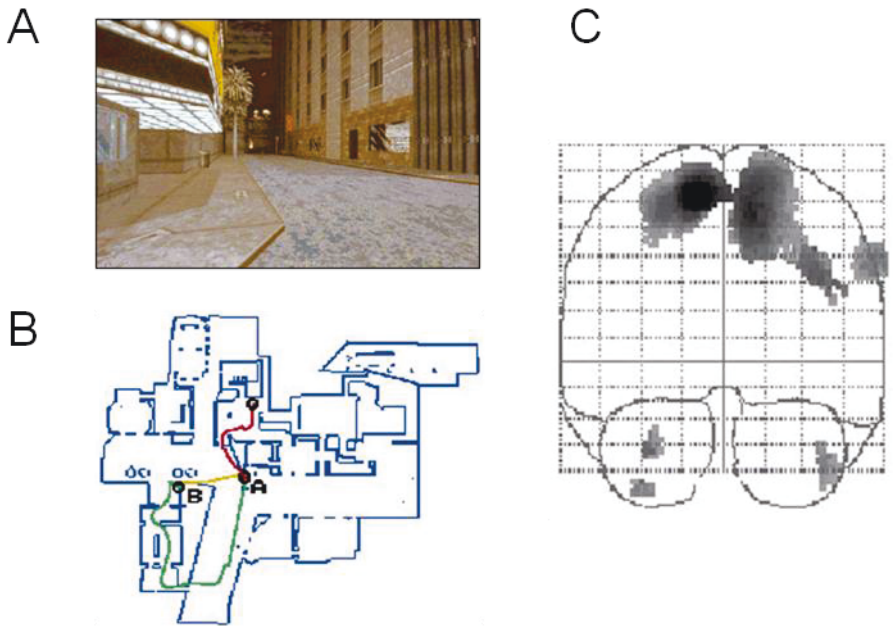

Figure 33. Cerebellar activation in a virtual reality navigation task
A. Example of view from inside the virtual town.
B. The virtual environment is shown from an aerial perspective, demonstrating the complexity of the town and the many possible paths between the various places. Three trajectories between the screens at A and B (18 m apart) are shown from the range of subjects' behavior: an accurate trajectory (yellow), an inaccurate but successful trajectory (green), and an inaccurate "lost" trajectory (red)
C. Areas of significant change in brain activity, in the coronal plane associated with comparison of movement tasks (direct or detour navigation) with the static scenes task, displayed on a transparent brain to facilitate viewing of all significant activations that are on different planes. Statistical Parametric Mapping for activated areas: left medial parietal cortex (-16,-52, 54; z = 4.48); right medial parietal cortex (12,-68, 48; z = 4.02); right inferior parietal lobe (56, -38, 32; z = 6.30); left cerebellum (-34, -40, -40; z = 3.89); and right cerebellum (49, -36, -38; z = 4.22).

1.1.2 ANIMAL STUDIES

The role of the cerebellum in spatial navigation has also been investigated using watermaze tasks in rodents, which provided the possibility to study the consequences of lesions or spontaneous cerebellar mutations (Rondi-Reig and Burguière, 2005). Because cerebellar alterations are often associated with motor deficits, a recurrent problem has been to dissociate between the navigation process deficit *per se* and the motor-related impairments. Therefore, in addition to the spatial Morris watermaze task, rodents were also tested in the cued paradigm, where the platform was indicated by a prominent visual cue, in order to evaluate their visuo-motor abilities independently from spatial learning. A deficit in the spatial version but not cue version of the watermaze allowed to conclude for a spatial impairment. Several cerebellar mutant mice presented a deficit only in the spatial version of the watermaze: the pcd mutant, in which the mutation of the Nan1 gene leads to a postnatal specific degeneration of virtually all cerebellar Purkinje cell (Goodlett et al., 1992), the

nervous mutant, mutated for the nr gene, and displaying an almost complete Purkinje cell loss in the cerebellar hemisphere. Similarly, lesions to the lateral cerebellar cortex (Colombel et al., 2004), the dentate nucleus, (Joyal et al., 2001) or selective destruction of the Purkinje cells (Gandhi et al., 2000) revealed a specific impairment in the spatial version of this task.

To understand the relative contribution of the two major cerebellar inputs, the climbing fiber (CF) and the parallel fiber (PF) input, Rondi-Reig and collaborators (2002) tested rats in the watermaze with different combinations of partial/total lesion of CF and/or PF (Rondi-Reig et al., 2002). None of the group was affected in the cue paradigm. Using a 'fixed departure-fixed arrival' protocol in the spatial paradigm, they examined the animals' ability to orient their bodies toward the platform at the initiation of the trajectory, a behavior rapidly acquired by control animals. Interestingly, a total lesion of PF systematically prevented the animals from correctly orienting toward the goal whereas in animals with a total lesion of CF, the deficit depended on the proportion of preserved PF (being absent if PF were intact and only delayed if PF were partially lesioned). These observations suggest a crucial role of PF input for the acquisition of such a behavior in the context of spatial learning.

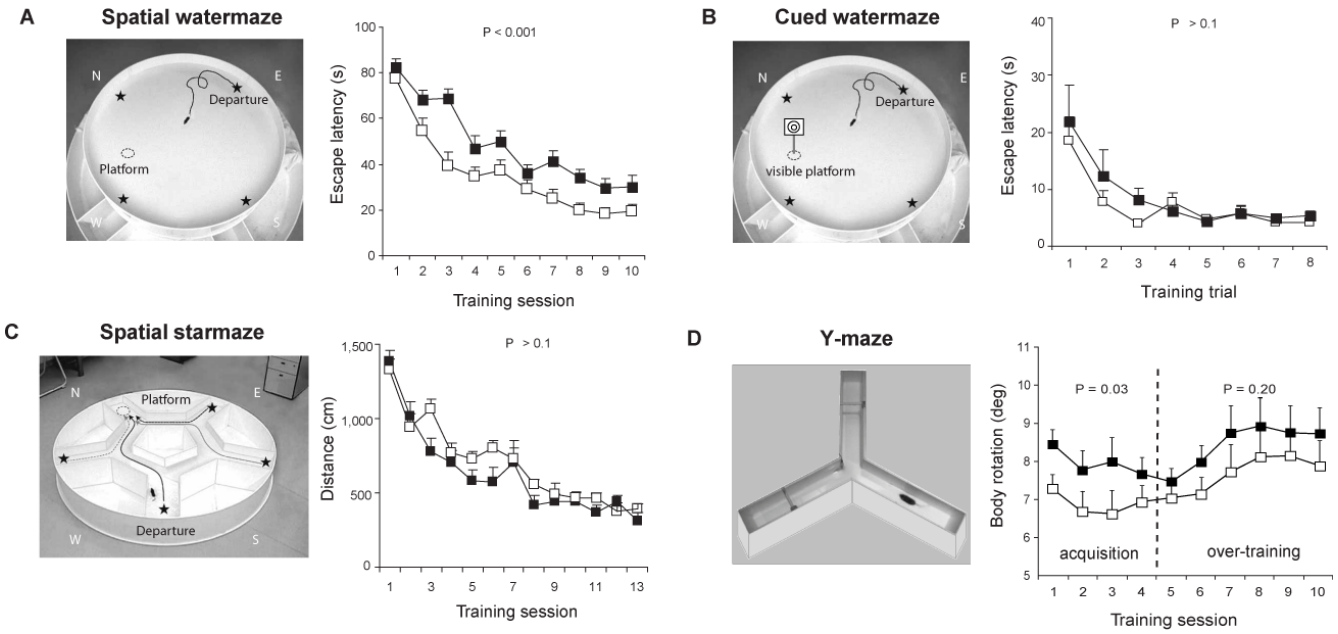

Figure 34. Overview of the different paradigms used in L7-PKCI mice to assess their spatial navigation performances

A. The spatial version of the Morris watermaze, in which a hidden platform can be found using the configuration of distal visual cues around the maze revealed spatial learning deficits in L7-PKCI mice.

B. These lower performances are not due to a deficit in visual guidance abilities, as revealed by subsequent training in the cued version of this maze. In this task, L7-PKCI mice correctly found the platform location indicated by a proximal visual cue.

C. The absence of deficit in the starmaze, in which alleys help to execute efficient trajectories towards an invisible platform, suggests that while L7-PKCI can learn to locate a goal using distal visual cues, they are unable to execute a direct trajectory toward it.

D. The use of a single intersection maze called the Y-maze enables to analyze trajectories quality. Trajectories optimization was quantified by the body rotation parameter which measures the angle between 3 successive points of the trajectory and is averaged over the whole path. Body rotation was specifically impaired in L7-PKCI mice during the acquisition of the task.

N, W, E, S: north, west; east and south respectively. Stars on the pictures in A, B and C indicate each possible departure point.

1.2 CEREBELLAR PLASTICITY AND SPATIAL NAVIGATION

New insights regarding the cellular mechanisms of cerebellar participation in spatial navigation come from the use of genetically modified models, targeted for specific molecular pathways. In the L7-PKCI transgenic model, the protein kinase C activity is specifically inhibited in the Purkinje cells, preventing the establishment of long term depression (LTD) at the PF-PC synapses (De Zeeuw et al., 1998a). Importantly, L7-PKCI mice do not display any motor coordination deficits, allowing to study their spatial behavior independently from any motor-related impairment. L7-PKCI mice were deficient in the ability to find the platform in the spatial but not the cued version of the watermaze (Figure 34, A-B) (Burguière et al., 2005). Interestingly, they did not display any deficit in the starmaze, a complex alley maze in which the mice also have to use the configuration of visual cues to locate the platform but where the number of possible trajectories is reduced by the guiding alleys (Figure 34.C). This pointed toward a participation of the cerebellum in producing an optimal trajectory toward a goal. Studied in an operant conditioning task in an aquatic Y-maze, L7-PKCI mice were shown to be unable to adopt an optimal trajectory toward the platform. Indeed, the body rotation parameter – measuring the angular deviation between successive points of the trajectory, was higher for L7-PKCI than for control mice during the acquisition phase of the task. This added further support to a role of the cerebellum in the optimization of a motor response during goal-directed navigation (Burguière et al., 2010).

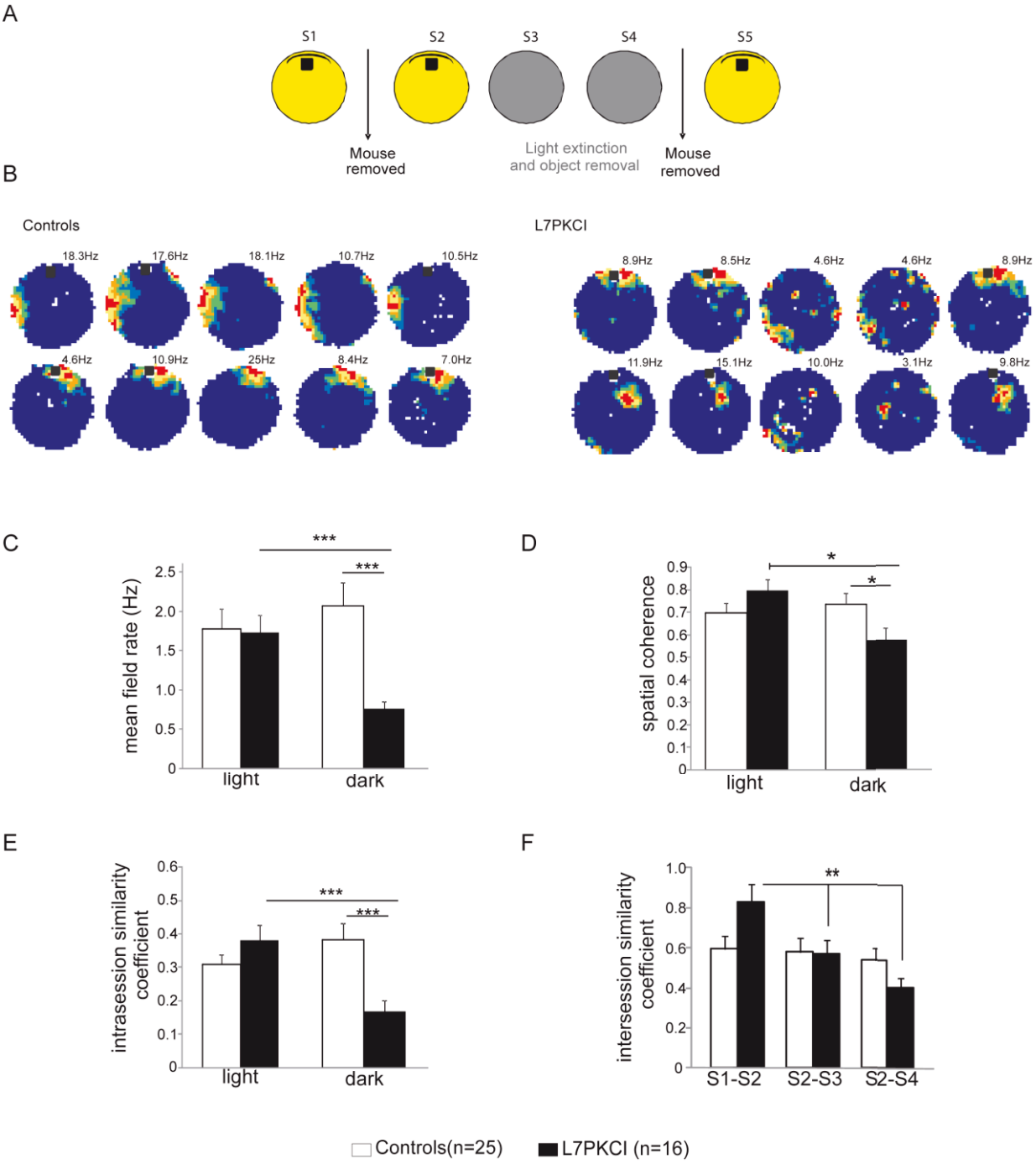

Figure 35. The compulsory use of self-motion cues affects hippocampal place cell properties in L7-PKCI mice.

A. Schematic diagram of the protocol used to assess the effect of self-motion stimulation on place cell properties. After two consecutive standard sessions (S1 and S2), light was turned off (S3 and S4) and objects were removed from the arena. S5 was similar to S1 and S2.

B. Examples of color-coded rate maps showing firing activity of control and L7-PKCI single CA1 pyramidal cells over the five consecutive sessions; color coding ranges from blue (silent) to red (peak activity). Peak firing rates are indicated for each rate map.

C-F. Analysis of place cell characteristics shows that specifically in L7-PKCI mice, the suppression of external cue inputs significantly alters the mean field rate (C), spatial coherence (D) and place field stability, as measured within (E) or across (F) sessions.

***P < 0.05, **P < 0.01, ***P < 0.001 with a Newman-Keuls post hoc analysis. Error bars represent SEM**

In addition to this optimization deficit, electrophysiological recordings in freely exploring L7-PKCI mice revealed an implication of cerebellar LTD in maintaining the hippocampal spatial map when relying on self-motion information (Figure 35) (Rochefort et al., 2011). Indeed, during free exploration of a circular arena in the light, in the presence of a proximal cue (a card and a bottle attached to it), L7-PKCI mice presented hippocampal place cell firing properties similar to their control. However, in the absence of external cue information, L7-PKCI place cell firing properties were strongly affected: their firing rate and spatial coherence decreased in the dark (Figure 35.C-D). Contrarily to the control mice which maintained stable place fields throughout the whole protocol, the stability of their firing pattern, measured either within or across sessions, gradually decreased over sessions in the dark (Figure 35.E-F).

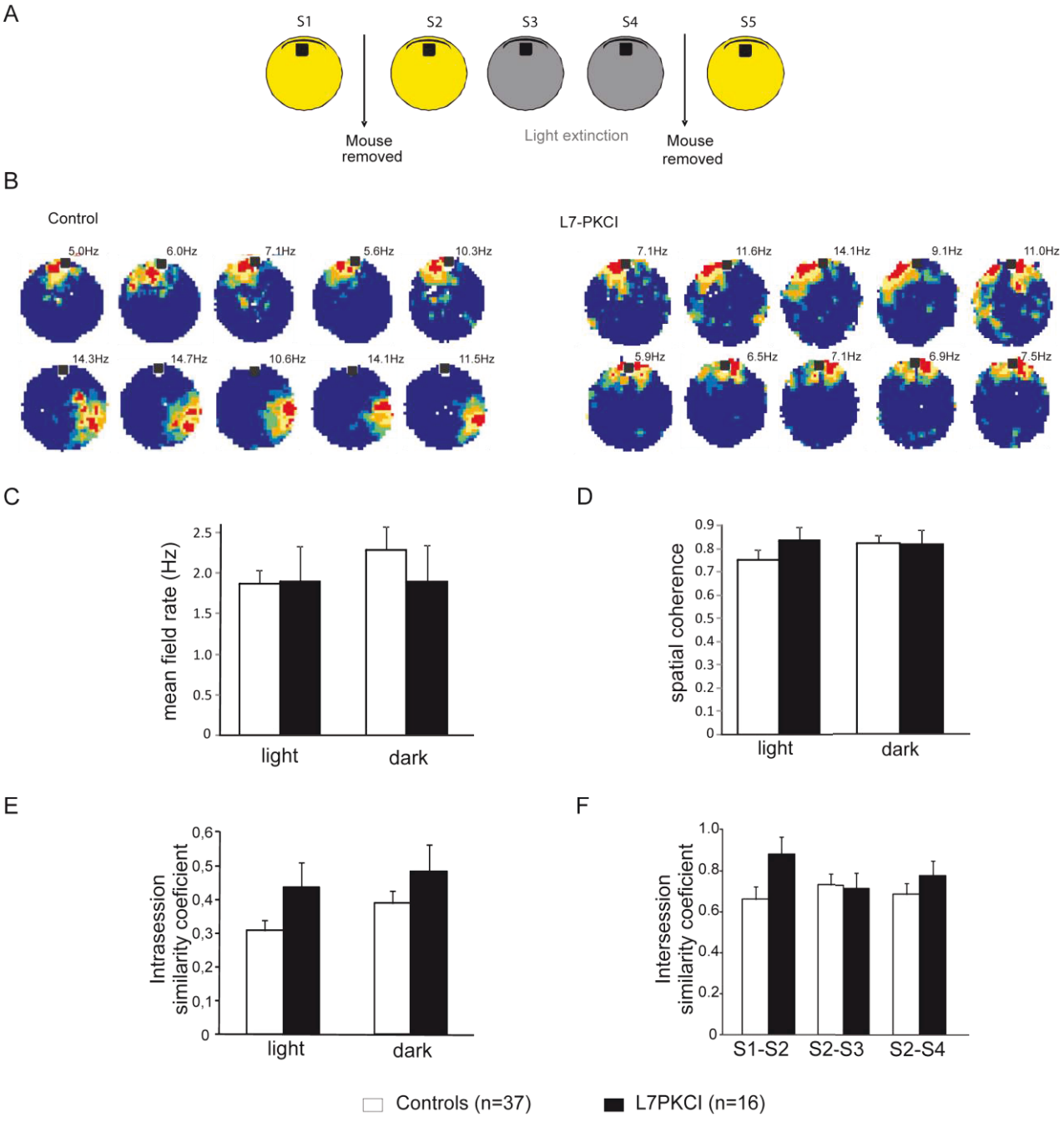

Figure 36. Preserved hippocampal place cell properties in L7-PKCI mice when external cues are available in the dark.

A. Schematic diagram of the protocol used to assess the effect of self-motion stimulation on place cell properties. After two consecutive standard sessions (S1 and S2), light was turned off (S3 and S4) and the cue was maintained in the arena. S5 was similar to S1 and S2.

B. Examples of color-coded rate maps showing firing activity of control and L7-PKCI single CA1 pyramidal cells over the five consecutive sessions; color coding ranges from blue (silent) to red (peak activity). Peak firing rates are indicated for each rate map.

C-F. Analysis of place cell characteristics shows that in the presence of external cue information in the dark L7-PKCI mice display a mean field rate (C), spatial coherence (D) and place field stability, as measured within (E) or across (F) sessions, similar to their controls.

***P < 0.05, **P < 0.01, ***P < 0.001 with a Newman-Keuls post hoc analysis. Error bars represent SEM**

Noticeably, when the object was kept in the arena during the dark session (tactile and olfactory cue information from the object being thus available), the firing parameters and place field stability were not affected in L7-PKCI mice (Figure 36.C-D). These results suggest that in the dark and in absence of the cue, the place cell system of L7-PKCI mice failed to use self-motion information to maintain stable place fields, a deficit which was compensated when they had the possibility to update their position in the dark by using the cue information. Consistent with this hypothesis, in a conflict situation in which control animal use self motion information to maintain stable place fields, L7-PKCI also displayed a prominent deficit (Figure 37). Indeed, a 180° rotation of the single visual cue in the absence of the animal reliably triggers an equivalent rotation of the place field for both L7-PKCI and control mice (Figure 37.B,C,E). However, the same rotation performed in the presence of the animal – thus producing a conflict between self-motion and external information – induced remapping at a random location for most of the L7-PKCI place fields (Figure 37.B,D,F). The inability to maintain stable place fields in L7-PKCI mice strengthens the idea of a deficit in the use of self-motion cues.

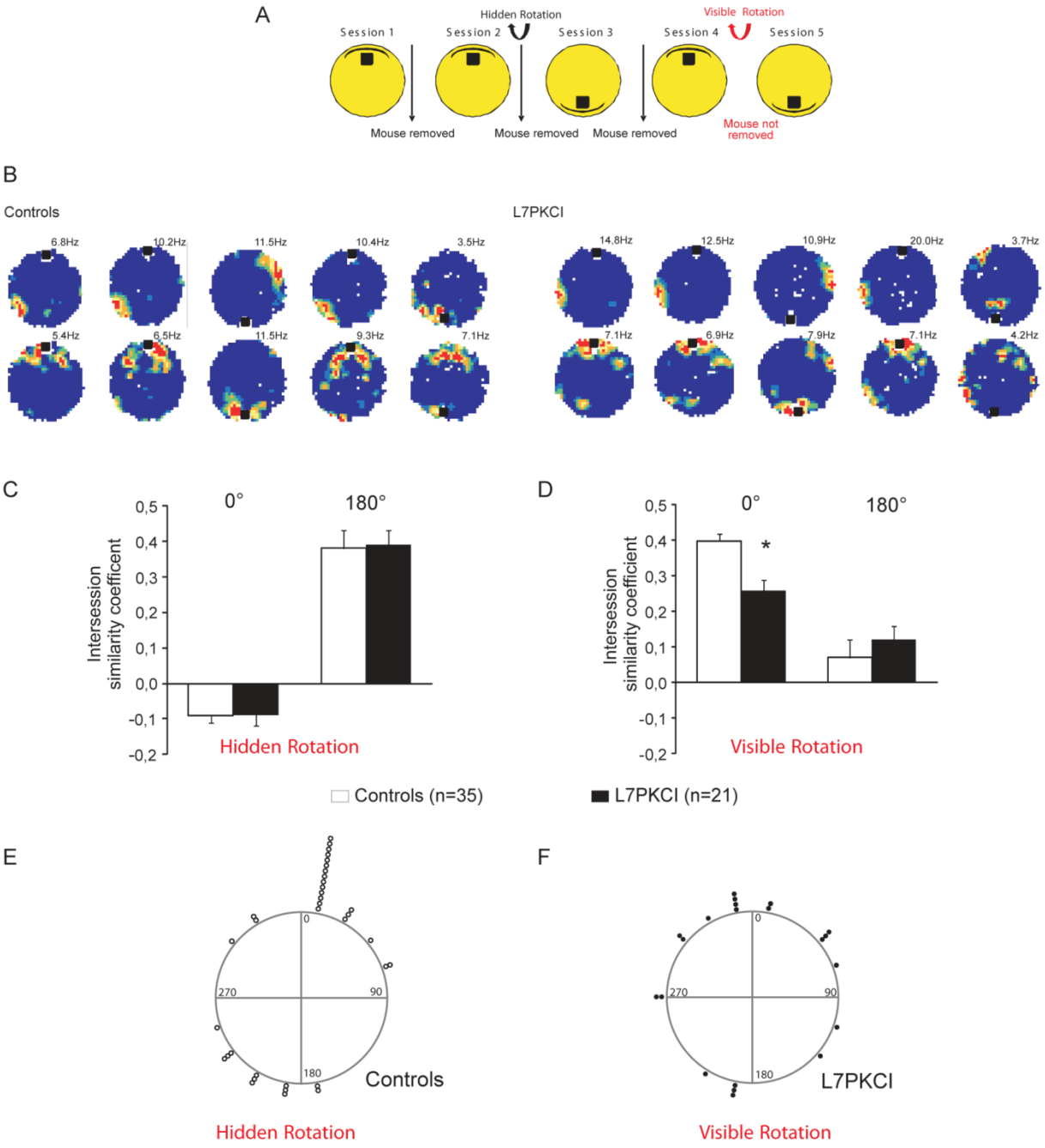

Figure 37. Field locations are not efficiently controlled by self-motion cues in L7-PKCI mice.

A. Schematic diagram illustrating the protocol used to assess the effect of a 180° rotation of the cue in the absence (hidden rotation) or presence (visible rotation) of the mouse in the arena on place cell firing.

B. Color-coded rate maps showing firing activity of control and L7-PKCI single CA1 pyramidal cells over the five consecutive sessions.

C-D. Histogram showing the intersession similarity coefficient score associated to a 0° or to a 180° field rotation after a hidden (C) or a visible (D) rotation of the cue. Field stability significantly decreased in L7-PKCI after a visible rotation of the cue (D).

E-F. Polar distribution of the place field rotation angles after the visible rotation control mice (E) and in L7-PKCI (F).

***p<0.05, Student t-test. Error bars represent SEM.**

Subsequently, mice were tested in a path integration task, in which they had to find a platform in a constant location and from a fixe departure point with an alley guiding the initial orientation of the body. Mice first learned the path in the light and then had to reproduce it in the dark (Figure 38.A). Consistently with their hippocampal place cell alteration, L7-PKCI mice were unable to navigate efficiently towards a goal in the absence of external information (Figure 38.B-E) (Rochefort et al., 2011).

These data suggest that cerebellar LTD is involved in the processing of self-motion information, and that this is required for the construction of the mental representation of space in the hippocampus. These findings also raise the question of the processes performed by the cerebellum. The next chapter is focused on describing the mechanisms by which the cerebellum might participate in navigation by processing and combining multimodal self-motion information and give pertinent information about body's location in space.

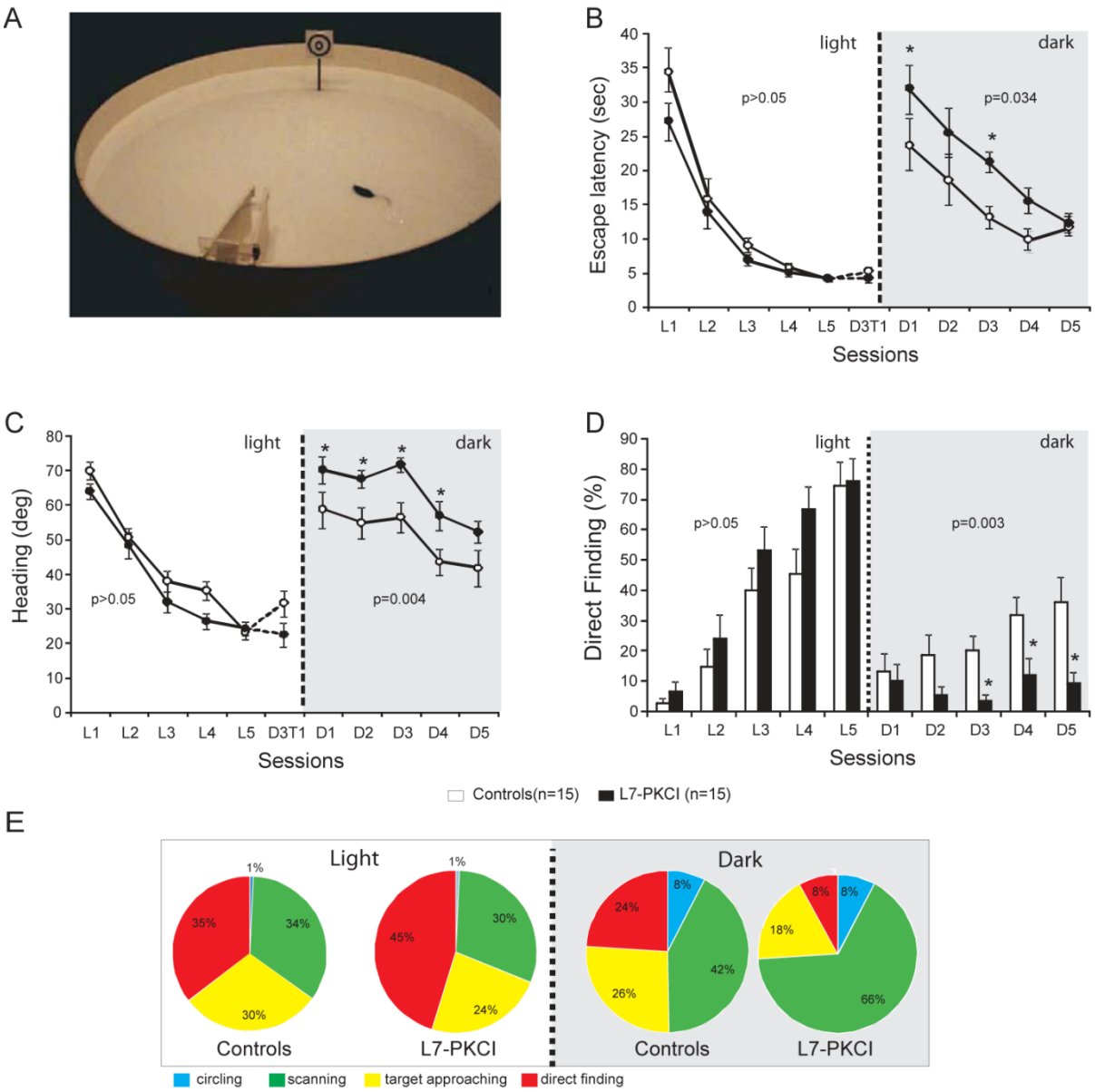

Figure 38. Inactivation of PKC-dependent cerebellar LTD deteriorates path integration.

A. Design of the experimental space developed to evaluate navigation abilities using self-motion cues.

B-C. Quantification of escape latencies (B) and heading (C) in Control and L7-PKCI mice during both light and dark conditions. In the light condition, control and L7-PKCI mice improved their performances significantly over sessions without genotype effect. In the dark condition, both groups improved their performance over time, but the performance of L7-KPCI mice was significantly poorer than that of their control littermates.

D-E. Swim path analyses during both light and dark conditions. The direct trajectory was significantly impaired in L7-PKCI mice during the dark condition (D). L7-PKCI mice cannot perform optimal trajectories during path integration, as highlighted by the differences between control and L7-PKCI mice in the type of trajectory used in the dark but not in the light condition (E).

The P values indicated in (B) to (D) correspond to the genotype effect.

***P < 0.05 with Newman-Keuls post hoc analysis. Error bars represent SEM.**

2 CEREBELLAR ROLE IN SENSORY PROCESSING REQUIRED FOR BUILDING A SPATIAL REPRESENTATION

2.1 THE CEREBELLAR CORTEX IS RESPONSIBLE FOR THE CHANGE OF REFERENCE FRAME OF VESTIBULAR SIGNALS

As explained in chapter I, spatial navigation is an active process that requires the accurate and dynamic representation of our location, which is given by the combination of both external and self-motion cues. Vestibular information has been shown to be crucial for spatial representation (Stackman et al., 2002), spatial navigation (Stackman and Herbert, 2002) and specifically path integration (Wallace et al., 2002). However, vestibular information by itself does not provide sufficient information to properly locate in an environment. Coherent body motion information is indeed given by the combination of multiple sources of self-motion information including vestibular, proprioceptive, optic flow, and motor command efference copy signals.

Vestibular information is first detected in the inner ear by the otoliths organs for the linear component and by the semi-circular canals for the rotational component. As receptor cells are fixed to the head bone, vestibular signals are detected in a head reference frame (Figure 39). This means for example that based on semicircular signals only, a rotation of the head upright relative to the vertical axis cannot be distinguished from a rotation of the head horizontal relative to the horizontal axis. In other words, semicircular canal information alone does not discriminate vertical or horizontal body position. To compute the movement of the body in space, vestibular information needs to be integrated relative both to the body (taking into account the relative position of the head and the body, given by the neck curvature) and to the world, converting the signal initially in head-fixed coordinates into a signal in world-frame coordinates (taking into account gravity). These computations are not necessarily successive and result from the integration of different types of signals. Several recent studies showed that these two reference frame transformations occur in different cerebellar subregions. An elegant report recently pointed out that the cerebellar cortex computes the head-to-world reference frame conversion by combining semicircular and otolith organs inputs (Yakusheva et al., 2007). This computation takes place in the lobules 9 and 10 of the cerebellum and involves GABA transmission (Angelaki et al., 2010).

Head-to-body frame transformation seems to occur in the cerebellar fastigial nucleus. This region contains indeed a subpopulation of neurons (50%) - one synapse downstream the Purkinje cells – that has been shown to encode motion in body coordinates (Kleine et al., 2004; Shaikh et al., 2004). More recently, this idea has been further supported by the demonstration that fastigial neurons respond to both vestibular and neck proprioception, and specifically encode body movement in space (Brooks and Cullen, 2009). However, since head-to-body position has also been shown to modulate Purkinje cell activity

in the cerebellar anterior vermis in decerebrate cats (Manzoni et al., 1999), meaning that Purkinje cells also receive neck proprioceptive information, one cannot exclude that the head to body frame transformation might also take place in the cerebellar cortex.

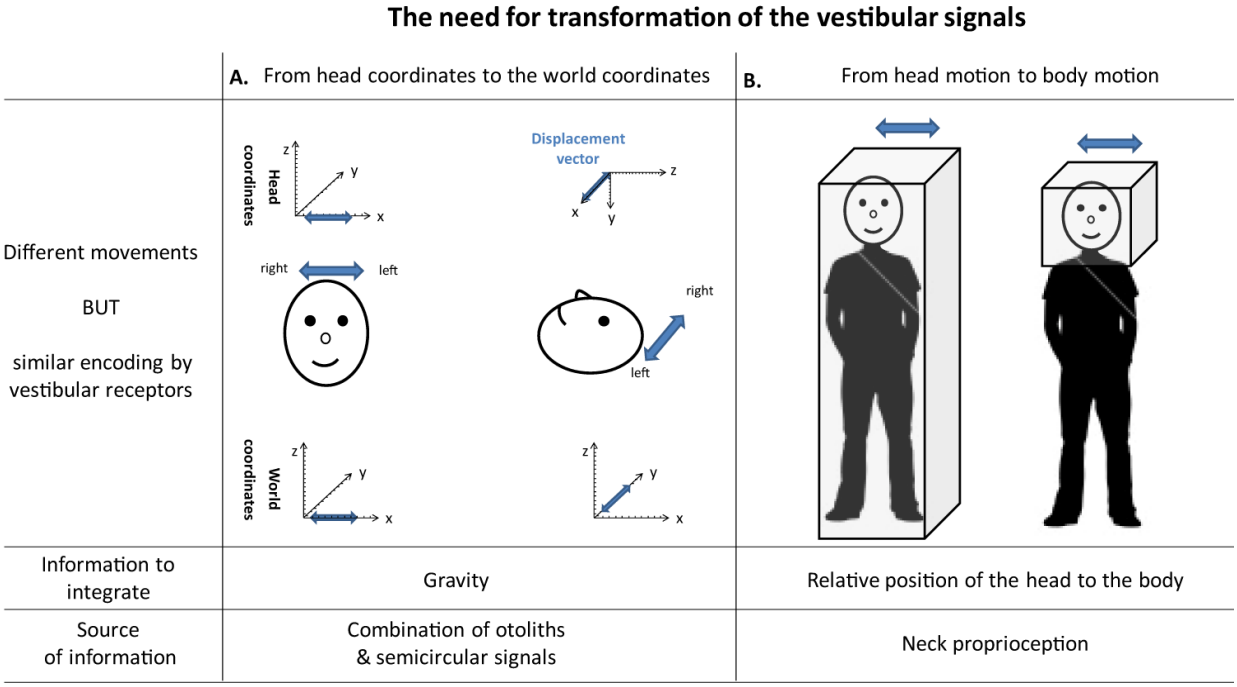

Figure 39. The need for transformation of the vestibular signals
As the vestibular organs are located in the head, vestibular signal is detected in head coordinates. This implies several transformations of the vestibular signal to correctly compute body motion in space. This figure gives two examples of different movements similarly encoded by vestibular receptors.
In column A is a linear displacement from left to right, with the head either vertical or horizontal. Indeed both movements are identical in the head reference frame (displacement vectors (in blue) project onto the x-axis) whereas they are different in the world coordinates (displacement vectors project either onto the x-axis or onto the y-axis). These two movements can be distinguished by taking into account the head position in space, which can be extracted from the combination of semicircular and otolith organs signals (Yakusheva et al., 2007)
Column B illustrates two movements corresponding to the same head motion in space, but different body motions in space (i.e. on the right the body is stationary). These two movements can be distinguished by integrating information about the position of the head relative to the body (that is, the neck curvature, given by neck proprioceptors).
(Rochefort et al. 2013)

2.2 THE CEREBELLAR CORTEX IS RESPONSIBLE FOR THE CANCELLATION OF SELF-GENERATED SIGNALS

2.2.1 A CANCELLATION SIGNAL FROM THE CEREBELLUM

Another implication of the cerebellum in the sensory processing involved in spatial navigation has been highlighted by studies on the cancellation of self-generated vestibular signals. During spatial navigation, displacement of the body in the environment undoubtedly generates stimulations of vestibular receptors. This includes translational stimulations corresponding to the displacement vector as well as rotational stimulations due to head and body reorientation. However, vestibular stimulations are not perceived, meaning that these self-generated signals have been cancelled out, enabling reliable detection of stimuli from external sources. Crucial to navigation, the ability to distinguish self-generated vestibular signals coming from an active movement allows proper integration with other types of self-motion signals to produce an accurate estimate of body movement, which forms the basic computation for path integration.

A particular population of neurons within vestibular nuclei, termed Vestibular Only (VO), are selectively active during passively applied movements (Figure 40.A) (McCrea et al., 1999; Roy and Cullen, 2001). The lack of response of these VO neurons during active movements implies that self-generated vestibular signals are indeed cancelled. Such cancellation requires knowledge about the currently performed movement provided by the combination of the different self-motion signals, and in particular the efference copy of the motor command and proprioception. Because the VO neurons are neither modulated by proprioceptive inputs nor by efference copy of motor command when presented in isolation to alert animals, some authors suggested that a cancellation signal arrives from higher structures in the case of active movements (Figure 40.B) (Roy and Cullen, 2003, 2004). Moreover, Roy and Cullen (2004) showed that during active movements, this cancellation signal occurs only if the actual movement matches the intended one. These authors proposed that, using the efference copy of motor command, an internal model of proprioception is computed and compared to the actual proprioceptive signal. If it matches, a cancellation signal is generated and sent to the vestibular nuclei (Figure 40.B) (Cullen and Roy, 2004). The exact location of the cancellation signal generation remains to be determined. Very recently, neurons in the fastigial nuclei were shown to specifically encode the passive component of the vestibular stimulation during a combination of active and passive movement (Brooks and Cullen, 2013). The fastigial nuclei sending massive projections to the vestibular nuclei, the fastigial neurons are strongly suggested to participate in the selectivity of the VO neurons in the vestibular nuclei.

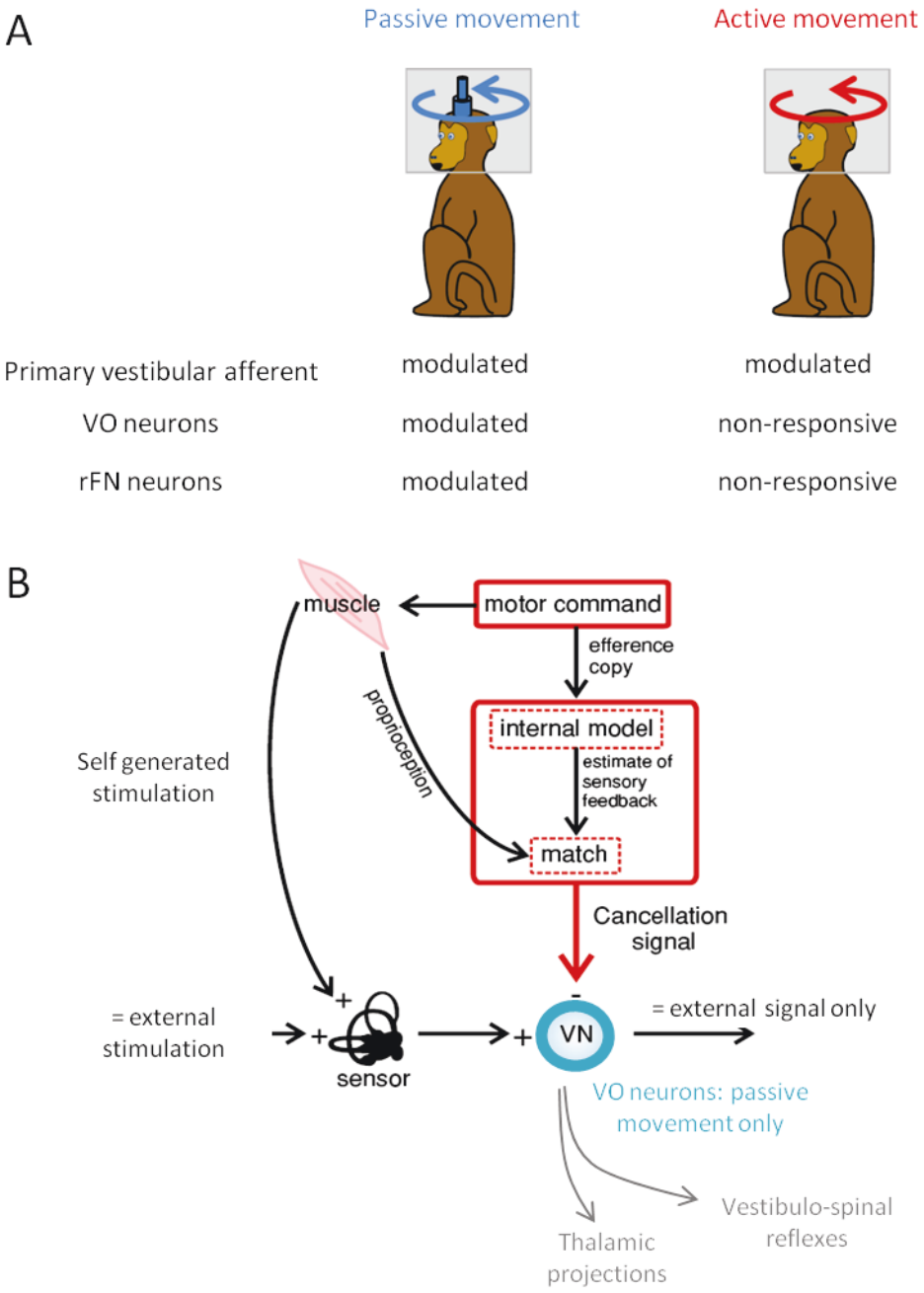

Figure 40. Cancellation of self-generated vestibular inputs in the primate cerebellum

A. Responsiveness of the primary vestibular afferents, vestibular-only (VO) neurons from the vestibular nuclei and neurons from the rostral fastigial nuclei (rFN) ,recorded during passive or active head rotations. Note that for the vestibular and fastigial neurons, the responses correspond to neurons encoding head movement (neurons encoding body movement are not presented).

B. Proposed mechanisms for the attenuation of self-generated vestibular Inputs. During the active head movements, an efference copy is processed by an internal model, which computes the expected sensory consequence of the motor command. Neck proprioceptive inputs are compared with this estimate of sensory feedback in a putative matching center in the cerebellum. If these signals match, a cancellation signal is sent to vestibular-only neurons in the vestibular nuclei.

Adapted from Cullen et al 2011

In fact it has been suggested that the generation of the sensory consequences of the intended action might be a general role of the cerebellum. In the context of motor control, the comparison of this prediction with the actual sensory feedback allows to generate an error signal, which is then used to modify the motor command in order to adjust the movement. In the context of sensory perception, this might decrease the self-generated signals, to enable accurate perception of external signals. An example of such differential perception is the observation that people cannot tickle themselves (Weiskrantz et al., 1971; Claxton, 1975). Using a robotic interface, it has been shown that self-produced and externally produced tactile sensations are perceived differently. Subjects consistently rated a self-produced tactile sensation on their right palm as being significantly less 'tickly', 'intense' and 'pleasant' than an identical stimulus produced by a robot. Functional imaging during the task revealed that in the cerebellum, less activity was associated with a movement that generated a tactile stimulus than with a movement that did not (Blakemore et al., 1998). This difference suggests that the cerebellum is involved in predicting the specific sensory consequences of movements, providing the signal that is used to cancel the sensory response to self-generated stimulation.

Interestingly it was shown in monkeys that this suppression system seems to be able to rapidly adapt when the relationship between the indented movement and the actual one is systematically altered (Brooks and Cullen, 2011). Vestibular and fastigial neurons were recorded while a torque motor systematically altered the relationship between the motor command and the actually produced head movement. Consistent with Roy and Cullen's proposal, VO neuron sensitivity was initially increased such that it was comparable to that observed during passive motion. Then, as the monkey produced a larger motor drive to compensate for the load, neural sensitivities gradually decreased. Finally, when the load was removed, both head velocities and VO neuron sensitivities initially increased providing further evidence that learning occurred in the neural circuit. These results suggest that the internal model of the sensory consequences of motor commands is rapidly updated when the relationship between the motor command and head movements is altered.

The mechanisms of such adaptability remain an open question. In particular, whether plasticity in the cerebellar cortex is responsible for such an adaptation remains to be demonstrated. However, some clues come from studies in the mild electric fish.

2.2.2 A ROLE OF PLASTICITY IN THE UPDATING OF THE INTERNAL MODEL - INSIGHTS FROM THE ELECTRIC FISH CEREBELLUM-LIKE STRUCTURES

Weakly electric fish like mormyrid fish use electro-reception to get information from their environment (Figure 41.A). An electric organ located in their tails produces an electric organ discharge (EOD) whose consequences in the electric field are detected by electro-receptors on the whole body surface. Any object in their environment with an electric conductivity different from the water will disrupt the electric field, increasing or decreasing the stimulation of electro-receptors. However, fish swimming movements alter the position of the electric organ relative to the electro-receptors of the sensory surface, dramatically affecting their responses – that is, increasing the response of electro-receptors located on the ipsi-lateral side while decreasing the response of those on the contra-lateral side of the body. As these changes in the electroreceptor activity might be substantially larger than those of external relevant stimuli, the appropriate detection of the environment requires the cancellation of the electro-sensory consequences of tail bending.

To understand how the work done in cerebellum-like structures can give insights to the functioning of the mammalian cerebellum concerning the multi modal integration, we need to put in parallel the organization and functional properties of their cellular networks (see for review Bell et al., 2008; Sawtell and Bell, 2008). Briefly, cerebellum and cerebellum-like structures share a common cellular architecture including granule cells and their parallel fibers, Golgi cells, stellate cells and unipolar brushed cells (Figure 41.B). Principle cells of cerebellum-like structures are called MG cells or Purkinje-like cells. As Purkinje cells, they receive two types of inputs, peripheral sensory input and parallel fiber inputs, and provide inhibitory signals to the efferent cells which are thus the functional equivalent of deep cerebellar neurons. Purkinje-like cells display narrow and broad spikes very similar to simple and complex spikes of Purkinje cells (Bell et al., 1997). Parallel Fiber- Purkinje-like cell synapses also exhibit associative depression as well as non-associative potentiation, two reciprocal mechanisms (Han et al., 2000).

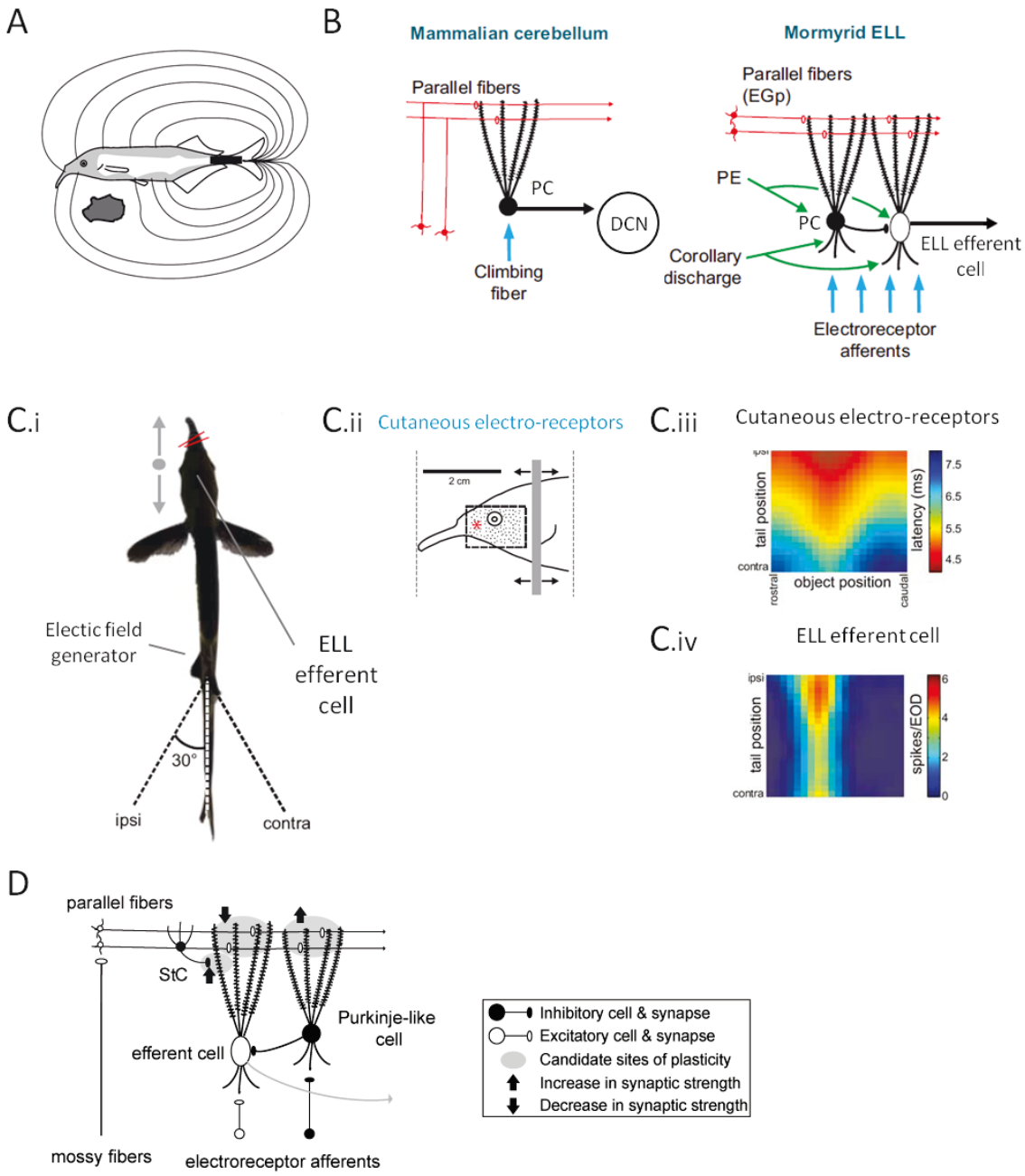

Figure 41. Cancellation of self-generated electro-sensory inputs in the electric fish electro-sensory lobe

A. Schematic diagram of active electro-location in the Mormyrid fish. The black bar in the tail represents the electric organ, which create an electric field around the body by emitting electric organ discharge s (EOD). The electric filed is detected by electro-receptors located on the body surface. Electrical field lines are drawn as thin lines. The scheme shows how potential field is disrupted by any object in the environment with an electric conductivity different from the water (Von der Emde 1999).

B. Comparative architecture of the mammalian cerebellum and the mormyrid electro-sensory lobe. Granule cells and parallel fibers are in red, afferent input from the periphery is in blue, and the additional inputs to the mormyrid ELLs are in green. The Purkinje-like cells of the mormyrid ELL and the Purkinje cells of the mammalian cerebellums are black. Mammalian deep cerebellar nuclei (DCN) as well as excitatory efferent cells are white. PE: nucleus preeminentialis dorsalis (higher-order electro-sensory nucleus just rostral to ELL) (Bell and Sawtell 2008).

C. Recordings of the cutaneous electro-receptors and EEL efferent cells. C.i .Schematic illustrating the experimental design. A small metal cylinder was moved alongside the fish while the tail was simultaneously displaced through an arc of 30°. C.ii Lateral view of the fish indicating the range of object movement (gray bar) relative to the receptor surface. C.iii-iv. Response changes to the modulation on tail and object displacement as measured as the latency of cutaneous electro-receptors (C.iii) and spike numbers of efferent cells (C.iv). (Sawtell & Williams 2008)

D. Multiple sites and mechanisms of plasticity potentially involved in the cancellation of self-generated sensory inputs. (Sawtell & Williams 2008)

To understand how self-generated stimulations are removed during electro-sensory processing, electro-receptors and electro-sensory lobe (ELL) efferent cells were recorded while displacing an external object in the presence of tail movements (Figure 41..Ci). Whereas cutaneous electro-receptor afferents were modulated by both tail position and object position (Figure 41..Cii), ELL efferent cells consistently encode object position regardless tail bending (Figure 41..Ciii). This shows that the modifications of the electric field due to the change in tail position relative to the electro-receptors were indeed suppressed, a process that could occur in the cerebellar structure network, by the subtraction of learned associations between central inputs and their sensory consequences (a process called negative image formation). Indeed, parallel fibers convey proprioceptive, electro-sensory signals and the efference copy of the motor command responsible of the electric organ discharge (EOD) that could be used for such computation. Experimentally, by shunting the electric signal, ELL efferent cells were shown to be modulated by the proprioceptive inputs (i.e. the tail position), on the opposite direction of the electro-sensory consequences of tail bending: ipsilateral bending (normally associated with an increase of electric field) produced a decrease in ELL firing whereas contralateral bending (normally associated with an decrease of electric field produced a increase in ELL firing (Sawtell and Williams, 2008). Moreover the effects of proprioceptive inputs on efferent cells are plastic. Pairing an electro-sensory stimulus with the electric organ discharge (EOD) motor command at a particular tail position resulted in changes in the response to the EOD motor command that were opposite in sign to the effects of the stimulus and greatest at the paired tailed position. This is consistent with previous similar demonstration in distinct groups of electric fish (Bell, 1981; Bastian, 1996; Bodznick et al., 1999). This adaptability in the cancelation of predictable sensory inputs constitutes an interesting parallel to the rapid adjustment of the suppression system of vestibular signals in monkeys when the relationship between the indented movement and the actual one is systematically altered (Brooks and Cullen, 2011).

At the cellular level, in cerebellum-like structures, sensory input is relayed to the basal region of Purkinje-like cells, whereas predictive signals are relayed by parallel fibers to the apical dendrites of the same cells. In vitro and in vivo studies have demonstrated anti-Hebbian plasticity at parallel fiber synapses onto Purkinje-like cells that likely underlies negative image formation (Bell et al., 1993; Bell and Bodznick, 1997; Han et al., 2000). Many

other plasticity sites have been demonstrated, in particular at the parallel-fiber – efferent cell synapses as well as in the inhibitory pathways parallel fiber – interneuron - Purkinje like cells and parallel fiber – interneuron - efferent cells (Bell and Bodznick, 1997; van den Burg et al., 2007). They are likely to participate to the negative image formation in a synergic way with the plasticities at parallel fiber - Purkinje-like cells plasticity but this is beyond the scope of this introduction (Sawtell and Bell, 2008).

Thus, these works on electric fish demonstrated that the Purkinje-like cells, the principal cells of cerebellum-like structures, are inversely modulated by electric signals and proprioceptive and EOD motor command inputs. The formation of negative images of the expected sensory inputs constitutes a mechanism for the cancelation of the self-generated signals, likely to be underlied by anti-Hebbian plasticity at the parallel fiber-Purkinje cell synapses, at least in part. This work suggests that the cancellation of self generated signals in the mammalian cerebellum might rely on similar synaptic plasticity mechanism. The ability of the cancellation system to rapidly adapt to persistent changes between the intended movement and the sensory consequences (showed in monkeys, Brooks and Cullen, 2011) brings additional supports to this hypothesis. However, the cancellation rule in the mammalian vestibular system is slightly different from those of the electric fish ELL since it includes a comparison step between the consequences of the intended movement and the sensory feedback. The precise location of the generation of the cancelation signal as well as the cellular mechanisms involved remains to be determined.

The cerebellum and specifically PF-PC LTD have been shown to be essential for optimal navigation toward a goal as well as building the hippocampal place cell representation. The participation of the cerebellum is likely to involve the correct processing of self-motion information, in particular the correct transformation of vestibular signals and their integration with other self-motion signals. This combination of self-motion signals showed adaptive characteristics (seen in monkeys and electric fish), suggesting the possible involvement of plasticities in these processes.

3 SCIENTIFIC QUESTION

A striking feature of the different experimental and theoretical models is the reciprocal plasticity at the PF-PC synapses. A legitimate question is thus: do LTD and LTP at these synapses equivalently participate in the cerebellar processing of information? The adaptive filter model (Dean et al., 2010) primarily relies on the bidirectional modulation of synaptic efficiencies. A prediction of this model is that the disruption of either LTD or LTP would similarly alter the bidirectional synaptic modulation and thus the processing capacities of the network. To test this prediction I have investigated the consequences of a lack PF-PC LTP in the context of spatial navigation, with a particular focus on the comparison with data from previous works examining the consequences of a lack of LTD at these synapses.

To do so, I have characterized the L7-PP2B mouse model, specifically lacking LTP at the PF-PC synapses, at both the behavioral and electrophysiological level. I examined its spatial learning abilities and spatial memory in the watermaze as well as its capacity to optimize a trajectory toward a goal in an aquatic Y-maze task. On the other hand, I analyzed the properties of its hippocampal place cell in standard conditions and during environmental cue manipulation.

METHODS

1 THE L7-PP2B MOUSE MODEL

To investigate the consequences of a lack of long term potentiation (LTP) at the parallel fiber-Purkinje cell (PF-PC) synapses in the context of spatial navigation, we used L7-PP2B mice, a genetically modified mouse model, specifically impaired for PF-PC LTP. This model was produced in the laboratory of Chris De Zeeuw (Erasmus MC, Rotterdam) (Schonewille et al., 2010).

1.1 THE BUILDING OF A MOUSE MODEL LACKING PF-PC LTP

1.1.1 A MOUSE MODEL TARGETED FOR THE PP2B PHOSPHATASE

L7-PP2B mice specifically lack the phosphastase 2B (PP2B, also called calcineurine) in Purkinje cells, a protein which has been shown in vitro to be required for the induction of parallel fiber-Purkinje cell LTP (Belmeguenai and Hansel, 2005) (Figure 42). In particular, the PP2B is involved in the same molecular cascade as the protein kinase C and may counteract its effects. Indeed, the PKC phosphorylates the AMPA receptors, leading to their internalization and thus to the depression of the synapse (LTD). To my knowledge the precise molecular pathways downstream the PP2B (leading to long term potentiation) are not fully characterized, but one possibility is that the PP2B dephosphorylates the AMPA receptors, allowing their externalization (Belmeguenai and Hansel, 2005).

1.1.2 GENERATION OF L7-PP2B MICE

In L7-PP2B mice, the selective deletion of PP2B in Purkinje cells was obtained using the Cre-loxP-system: loxP sites flank the DNA sequence of the regulatory subunit (CNB1) of protein phosphatase 2B (referred to as floxed CNB1) (Zeng et al., 2001); these loxP sites are short sequences recognized by the Cre recombinase which catalyzes the recombination of DNA, leading the excision of the sequence between the two loxP sites. L7-PP2B mice were created by crossing floxed CNB1 mice (Zeng et al., 2001) with a L7-Cre line (Barski et al., 2000), in which the Cre transgene is expressed under the L7 promoter, specific for Purkinje cells (Oberdick et al., 1990). Thus the deletion of the CNB1 sequence only takes place in the Purkinje cells (Figure 43.A).

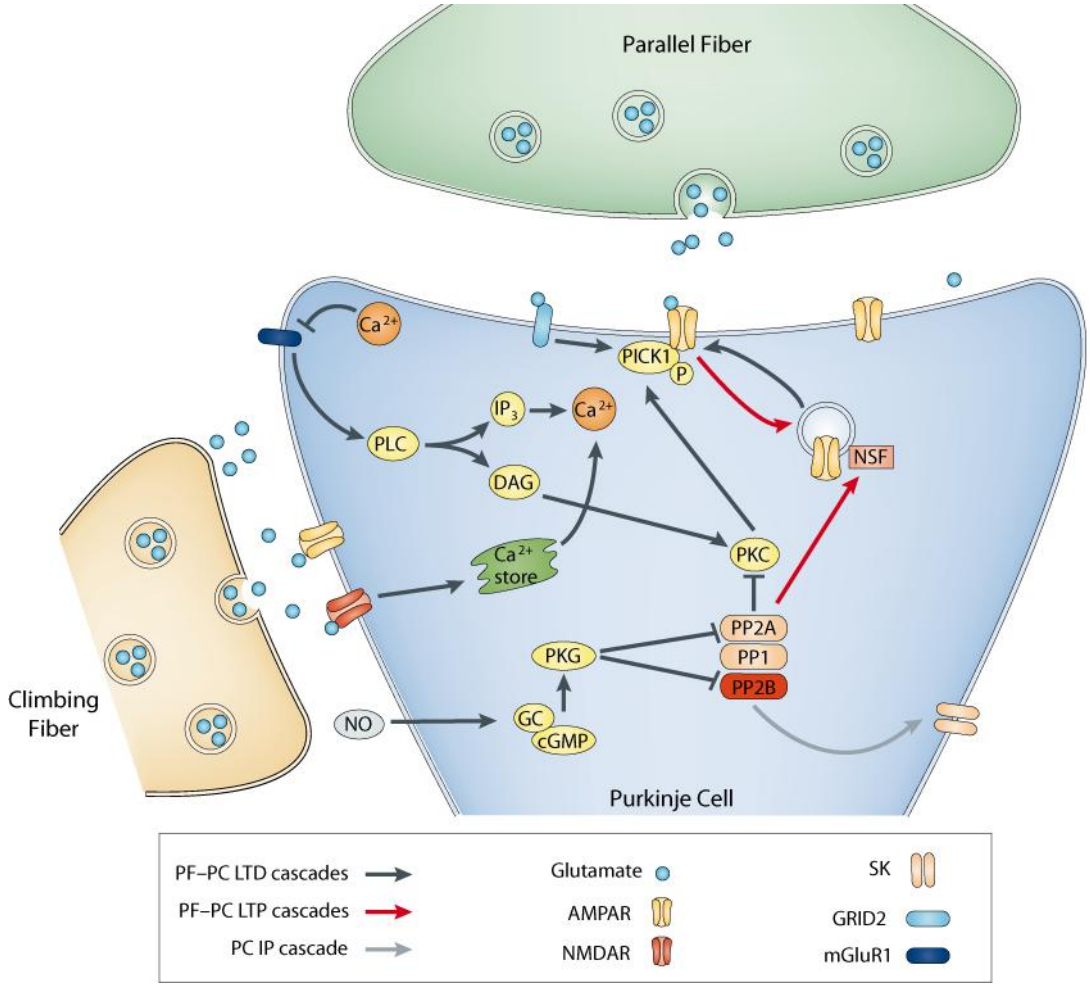

Figure 42. Simplified representation of the postsynaptic molecular mechanisms underlying plasticity in Purkinje cells.

Pathways involved in long-term depression (LTD) at PF–PC synapses are marked in black, and pathways involved in long-term potentiation (LTP) at PF–PC synapses are marked in red. The grey arrow indicates the molecular cascade for intrinsic plasticity (IP).

In conditions of high Ca^{2+} concentration, the PKC is activated and phophorylates the AMPA receptors, leading to their internatlisation, and thus to LTD. Conversely in conditions of low Ca^{2+} concentration, the phosphatases (including PP2B) are activated. Up to date the molecular pathways downstream the PP2B leading to long term potentiation are not fully characterized. Another pathway leading to LTP has also been described in vitro (Wang et al., 2014): it involves cytosolic phospholipase A2 α (cPLA2α)/arachidonic acid (AA) signaling and presynaptic endocannabinoid receptors.

AMPAR, AMPA receptor; cAMP, cyclic AMP ;DAG, diacylglycerol; GABAA, GABA type A receptor; GABAB, GABA type B receptor; GC, guanylyl cyclase; cGMP, cyclic GMP; Glu, glutamate; GluRδ2, glutamate receptor δ2 (GRID2); IP3, inositol trisphosphate; mGluR1, metabotropic glutamate receptor 1; NMDAR, NMDA receptor; NO, nitric oxide; NSF, N-ethylmaleimide-sensitive factor; PICK1, protein interacting with C kinase 1; PKA, cAMP-dependent protein kinase; PKC, protein kinase C; PKG, cGMP-dependent protein kinase; PLC, phospholipase C; PP1, protein phosphatase 1; PP2A, protein phosphatase 2A; PP2B, protein phosphatase 2B; SK, small conductance Ca^{2+}-activated K+ channel;

Adapted from Gao et al.2012

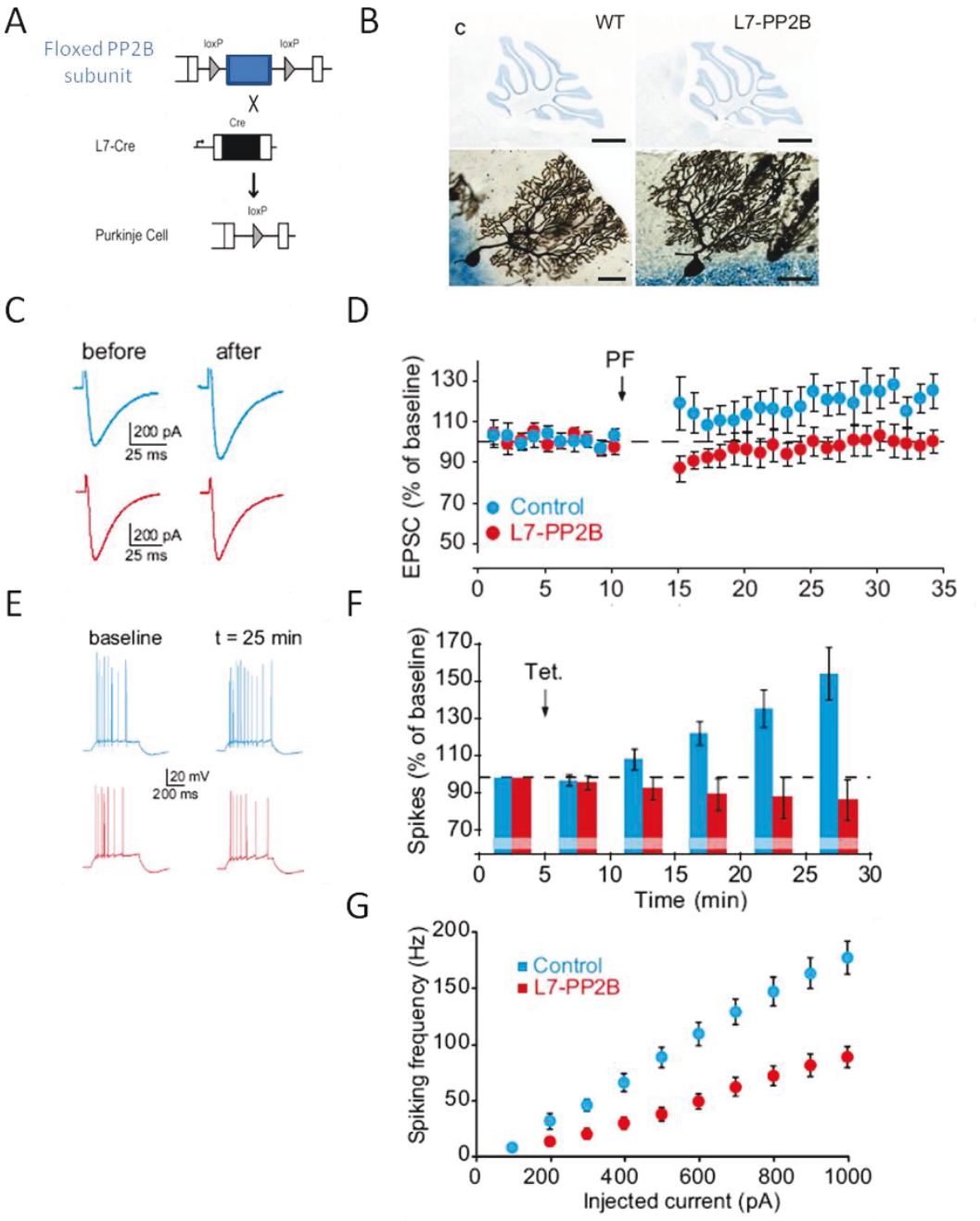

Figure 43. The L7-PP2B mouse model

A. The L7-PP2B mutant mice were created by crossing a floxed calcineurin line with an L7-Cre line.

B. Thionin (upper panel) and Golgi (lower panel) stainings of sagittal sections of the vermis showed no morphological or cytoarchitectural differences between control and L7-PP2B mice

C-D. Induction of PF-PC LTP was significantly (impaired in slices of adult L7-PP2B mice (n=8) compared with those of controls (n=7) ($p < 0.03$; t test). C, sample traces before and after induction.

E-F. Following tetanization (150–300 pA at 5 Hz for 3 s), the spike rate evoked with 550 ms depolarizing current pulses of 100–200 pA increased in wild-types (n = 9), but not in the L7-PP2B mutants (n = 16; $p = 0.007$; ANOVA for repeated measurements). E, sample traces before and after induction.

G. Basal intrinsic excitability is significantly lower in L7-PP2B mice (n = 7 versus n = 10 for controls), quantified by slope ($p = 0.002$; t test) and intercept with the x axis($p = 0.07$; t test).

Adapted from Schonewille et al. 2010.

1.2 L7-PP2B MICE CHARACTERISTICS

L7-PP2B mice display a normal cerebellar histology. They do not present any alteration in the foliations of the cerebellar cortex or the thickness of its different layers (Figure 43.B). The cytoarchitecture of Purkinje cells is intact: the dendritic tree area of Purkinje cells is normal, as well as the number and size of parallel fiber-Purkinje cell synapses. The climbing fiber elimination during development (producing a one-to-one innervations of Purkinje cells by climbing fibers) is unaffected.

At the synaptic level, as predicted by the pharmacological studies on cerebellar rat tissue (Belmeguenai and Hansel, 2005), in vitro electrophysiological recordings of L7-PP2B mice show no LTP following the stimulation of parallel fibers (1Hz, 5min), in contrast to the reliable potentiation induced in their controls (Figure 43.C,D). However the induction of LTD is preserved, as well as the presynaptic plasticity, as shown by a normal pair-pulse facilitation ratio at the PF synapses and a normal pair-pulse depression ratio at the CF synapses. Noticeably, L7-PP2B mice also display defects in the baseline excitability (i.e. the spiking frequency of the cell following cell membrane depolarization; Figure 43.G) and intrinsic plasticity of Purkinje cells (i.e. cell excitability modification by non-synaptic processes following a tetanic stimulation (see Figure 43.EF). At the behavioral level, L7-PP2B mice show dramatic deficits in both the VOR adaptation and eyeblink conditioning task.

As mentioned previously, the vestibulo-ocular reflex (VOR) allows the stabilization of image on the retina during head movements by producing compensatory eye movement, of the same amplitude, in the opposite direction. The basic performance parameters (the VOR reflex without any experimental manipulation) are moderately affected (Figure 44.A). When the visual stimulus is systematically displaced in the same or in the opposite direction as the turntable, motor learning occurs in control mice, whereas the performances of L7-PP2B mice are drastically impaired (Figure 44.B-C) (Schonewille et al., 2010).

In the eyeblink conditioning task, the repetitive association of an aversive stimulus (an air puff on the cornea) with a tone allows the animal to anticipate the delivery of the aversive stimulus based on the tone (Figure 44.D). In this paradigm, the percentage of conditioned responses of L7-PP2B mice does not increase with time (Figure 44.E) and their responses are not appropriately timed to the stimulus (Figure 44.F) showing that the absence of PF-PC LTP dramatically altered learning in the eyeblink condition task (Schonewille et al., 2010).

Based on these findings, parallel-fiber Purkinje cell LTP was proposed to play a major role in cerebellar motor learning. The authors proposed that the LTP would initiate new motor learning by potentiating synapses transmitting relevant inputs while the LTD depresses the synapses active in the prelearning situation (likely to convey non-relevant inputs).

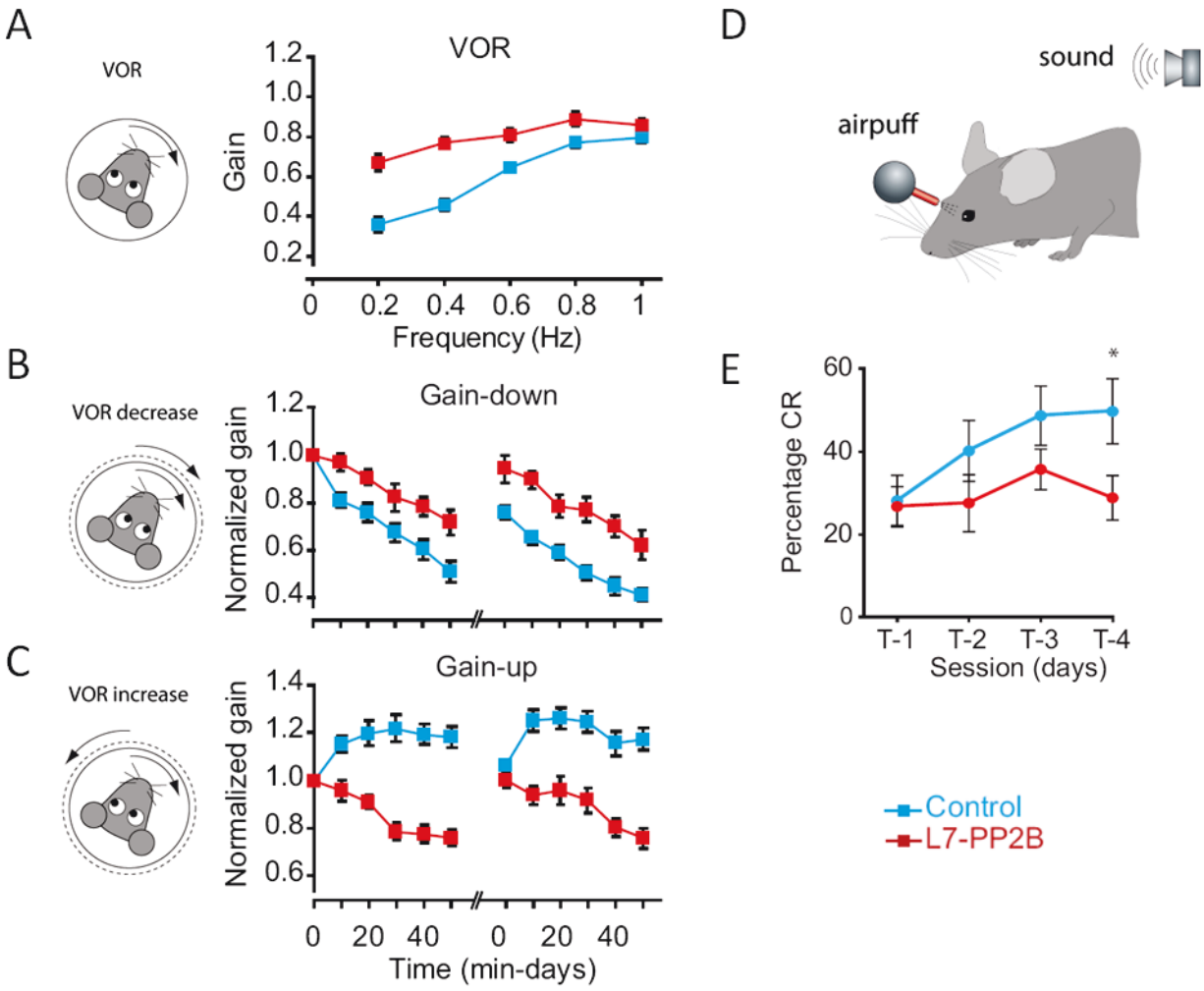

Figure 44. L7-PP2B mice are drastically impaired in motor learning

A. Motor performance during the vestibulo-ocular reflex in the dark (VOR) revealed moderate aberrations in L7-PP2B mice (n = 15) compared to controls (n = 19).

B-C. Motor learning in L7-PP2B mice was severely affected; during 2 days of mismatch training so as to either decrease (E) or increase (F) their VOR gain the L7-PP2B mice (n = 9) learned significantly less than controls (n = 10)

D. The eyeblink conditioning task. An auditory tone is paired with a mild corneal airpuff, allowing the animal to close the eyelid in response to the tone

E. The percentage of conditioned responses (eyelid closure in response to the tone) of L7-PP2B mice (n = 9) does significantly increase with time, in contrast to the controls (n = 9).

Adapted from Schonewille et al. 2010.

2 MATERIAL AND METHODS

2.1 SUBJECTS

Three to six month old transgenic L7-PP2B (n = 29) mice and their wild-type littermate controls (n = 40) were used in this study. All animals were bred in a C57BL/6 mouse strain background and were housed in standard conditions (12h light/dark cycle light on at 7 am water and food *ad libitum*). All data were obtained during the light phase and in compliance with the European ethical animal committee (European directive 86-609). Experiments were carried out in blind conditions with respect to the genotype.

2.2 BEHAVIOR

2.2.1 SUBJECTS

24 transgenic L7-PP2B mice and 36 wild-type littermate controls participated in this study. Mice were used between 3 and 6 months. All mice were submitted to the general sensori-motor evaluation before undergoing a navigation task in the watermaze or Y-maze.

2.2.2 GENERAL ACTIVITY, ANXIETY, EQUILIBRIUM, AND MOTOR COORDINATION TASKS

Animals were kept isolated 7 days prior to, and throughout behavioral experiments in order to limit the inter-boxes variability due to social relationships. All mice were submitted to the S.H.I.R.P.A. protocol by a series of experiments run sequentially (Rogers et al., 1997). The first screen consisted in a set of behavioral tests allowing analysis of general appearance and neurological reflexes. Gross abnormalities that could interfere with behavior in the navigation task were checked in all mice. General appearance was evaluated by periodically weighting the mice, observing the presence of whiskers, the absence of palpebral closure, and pilo-erection. Spontaneous behavior was assessed by placing individually each mouse in an unfamiliar standard mouse cage (22 x 17 x 14 cm) for 3 minutes. Examples of aberrant actions included wild running, abnormal jumping or grooming, and frozen immobility. Finally, the eyeblink, ear twitch and whisker-orienting reflexes were studied according to established protocols (Paylor et al., 1998). In brief, eyeblink and ear twitch reflexes were respectively tested by approaching the eye and touching the ear with the tip of a clean cotton swab. The whisker-orienting reflex test consisted in lightly brushing the whiskers of a freely moving animal with a small paintbrush. All mice tested presented normal appearance and neurological reflexes and were therefore included in the study.

The second screen of the SHIRPA protocol was aimed at detecting potential differences in anxiety, motor control and equilibrium (Rondi-Reig et al., 2001). The classical elevated plus-maze was used to test anxiety (Pellow et al., 1985; Lister, 1987). A cross-shaped maze made of black perspex with a central zone (8 x 8 cm) facing closed and open arms (24 x 8 cm, surrounded by 25 cm walls made of grey perspex), was elevated to a height of 50 cm. The percentage of time spent and the number of entries in the open arms was measured. An entry was considered valid when the 4 paws were present in the arm. The test lasted for 5 min.

Spontaneous locomotor activity was quantified in an arena made of grey perspex (45 x 45 cm) surrounded by red plexiglass walls (30 cm height). Mice were first positioned at the center of the arena and were allowed free exploration for 10 min. Data acquisition was performed at a frequency of 25 Hz using the SMART® video recording system and tracking software. Rearing events were detected manually. Data processing was automated using NAT (Navigation Analysis Tool), a matlab-based software developed in our laboratory (Jarlier et al., 2013). Walking time, travelled distance and number of rearings were then analyzed.

To assess motor coordination, an automatized hole-board was used (Rondi-Reig et al., 1997)**.** It consisted of an experimental box made of transparent altuglass (32 x 32 x 25 cm), in which the floor board made of white altuglass has 36 holes (2 cm in diameter, 2 cm deep) arranged in a 6 x 6 grid. The mouse was placed in the middle of the board and its behavior was recorded during 5 min. The walking time and the frequency of stumbles, a measure of motor coordination were calculated (Rondi-Reig and Mariani, 2002).

Static balance was quantified by using an unstable platform (Hilber et al., 1999). The aim of this test was to evaluate the capabilities of the mice to maintain balance when their displacements were limited. The apparatus consisted of a circular platform (diameter 8.5 cm) made of grey perspex, fixed at its center on a vertical axis (1 m high and 3 cm in diameter) and which could tilt by 30° in every direction. The mouse was placed on the middle of the board (horizontal situation) and the latency before falling (cut-off: 180 s) and the number of slips (when at least one paw was out of the circumference of the platform) were measured. Dynamic balance was evaluated using the horizontal rod test (Rondi-Reig et al., 1997). The aim of this test was to estimate the mouse's ability to maintain its balance while in motion. The apparatus consisted of a horizontal rod (50 cm long, 5 cm in diameter) covered with sticking plaster providing a good gripping surface. It was located 80 cm above a soft carpet to cushion the eventual fall of the animals. Both ends of the beam were limited by white altuglass disk (50 cm in diameter). The mouse was placed on the middle of the rod, its body axis perpendicular to the rod long axis. During the test, the time before falling, the distance travelled and the walking time were recorded. The test ended when the animal fell or after 180 s.

Motor adaptation was assessed using a rotarod task, either on a constant speed protocol (5 and 10 rpm, 4 trials each) or on an accelerating protocol (4 trials). The mouse was placed on the rotating rod, with its body axis perpendicular to the rotation axis at the onset of the training. The trial ended when the animal fell or after 5 min. The trial duration was recorded. In the constant speed protocol, the 5rpm session was separated from the 10 rpm session by 2 hours.

2.2.3 STIMULUS-DEPENDENT WATER Y-MAZE CONDITIONING TASK (SWYM).

Mice were trained in an SWYM apparatus. Each arm, forming a 120° angle with the adjacent arm, was 50 cm long and 10 cm wide, with 30-cm-high side walls (Figure 1.A). Arms were filled with water 10 cm deep. The water was maintained at a temperature of 21°C for the duration of the experiment and made opaque by the addition of an inert and nontoxic coloring agent (Acusol OP 301; Brenntag NV). The symmetric configuration of the maze and the high side walls prevented mice from distinguishing the arms using either the form of the maze or visual distal cues.

Mice were conditioned to turn right or left depending on the Conditioned Stimulus (CS). We used two different CS: a light delivered by a white LED (35,000 candela intensity) or a sound delivered by a loudspeaker (5 kHz, 75 dB). A wrong turn resulted in an air puff on the mouse as an aversive stimulus, which was triggered by the opening of an electromagnetic sluice gate releasing compressed air. This Unconditioned Stimulus (US) forced the animal to turn in the correct direction corresponding to the unconditioned response. An escape platform (8 cm diameter) was located at the end of the correct arm and hidden 1 cm below the surface of the water. The US overlapped with the CS according to a classical delay conditioning paradigm. Our paradigm included elements of operant conditioning since the mice learned to turn left according to the sound and right according to the light to avoid the air puff and find the escape platform. The setup was fully automated using an overhead video camera that monitored the mouse's position, determined by a tracking program (SMART, Bioseb). The electronic apparatus controlling the light, the sound, and the air puff was triggered by the position of the animal tracked via an input/output module.

A day before the start of the training, each animal was put in the water Y-maze apparatus and pretrained with two “forced” right or left configurations in a random order. In these configurations, a barrier blocked the access of one of the two possible arms to force the animal to turn to the open arm. This pretraining day was performed without any stimuli. The aim was to habituate mice to swim in the maze and find the escape platform located at the end of either arm.

The training consisted of two daily sessions of 20 trials each spaced by a minimum of 2h. The intertrials interval was 30 s and a whole session lasted a maximum of 15 min. Two

configurations were designed with the SMART program; the right one associated the light with a right turn and the left one associated the sound with a left turn (Figure 1.B). Each configuration was randomly presented 10 times per session. If the animal made an incorrect turn, an air puff was projected on the mouse at the entrance of the wrong arm. In both configurations, the CS was automatically triggered when the animal crossed the middle of the departure arm and entered the poststimulus zone (Figure 1.B). Three different zones were distinguished in the departure arm: a starting zone where the animal was released, a prestimulus zone beginning 5 cm before the middle distance line, and a poststimulus zone ending 24 cm after the middle distance line.

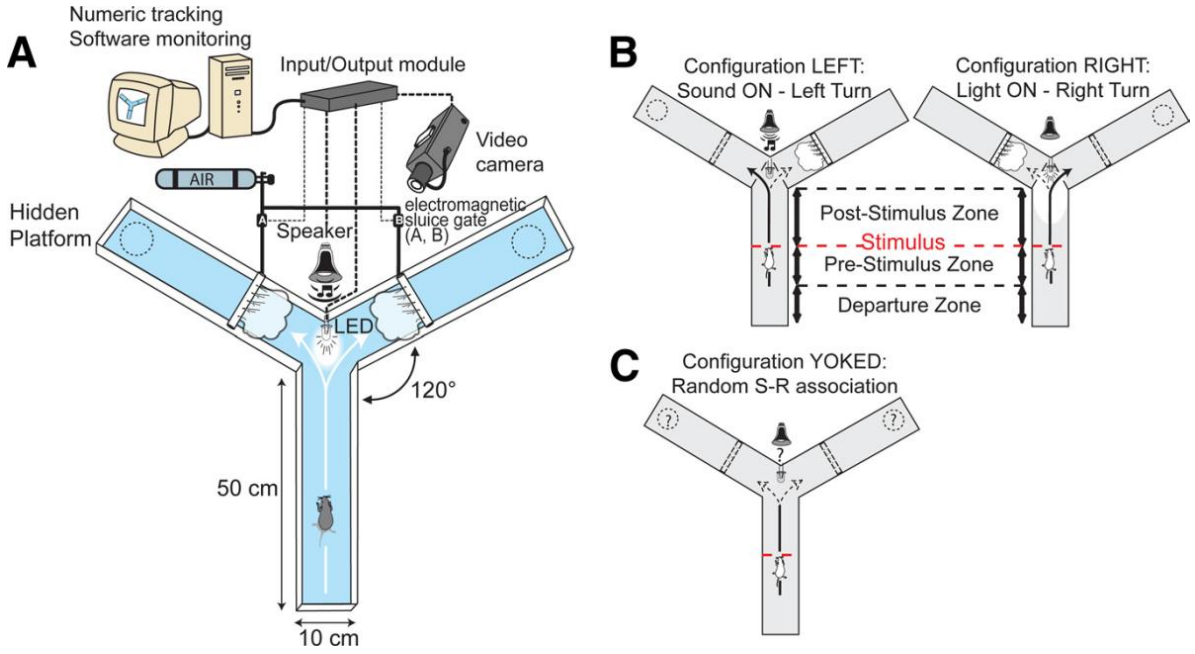

Figure 45. The SWYM conditioning task.
A, The setup was fully automated by electronic apparatus (LED, speaker, electromagnetic sluice gates) triggered by an input/output module and monitored by a video tracking system.
B, Two configurations were designed with the tracking program: one associated a sound with a left turn and the other associated a light with a right turn. In case of a wrong choice, mice received an air puff caused by the opening of an electromagnetic sluice gate releasing compressed air on the mice. When a mouse performed the appropriate choice, it could escape from the water by climbing on a hidden platform located at the end of the correct arm (dotted circle).
C, A yoked task was used to test behavioral response when random S-R associations were proposed. Data analysis focused on the departure arm, which was divided into three different zones. A starting zone corresponded to the location where the animal was released. The prestimulus and poststimulus zones are defined as the areas that are used before and after the stimulus occurrence, respectively.

Since we were particularly interested in the conditional response induced in this protocol, we needed a control experiment mimicking the learning performances but without

any conditioning. To do so we trained two other groups of animals (mutants and control) in a yoked task with the same general conditions as their trained partners but without consistent association between stimulus and response (Figure 1.C). For this purpose, we used the performances of conditioned animals to calculate the mean percentage of correct turns for each session of the entire population. With these theoretical values, the mice were exposed to the same amount of light or sound stimulus (randomly presented), air puff, and reward, but without a consistent link between the occurrence of stimulus and the choice of turn. Thus, the mice could not develop an association between CS and the location of the platform at the end of one arm. In the yoked task, a large majority of mice showed a lateralization over the training.

The sampling of the data was performed at a frequency of 25 Hz (SMART). Data processing was automated using NAT (Jarlier et al., 2013). Several parameters were used to characterize the behavior of mice in the SWYM task. The learning of the association rule was measured by the percentage of correct turns in each session. To assess the mice's abilities to adjust their trajectory during the training, we evaluated the ability of a mouse to reproduce its own path. For this, we measured for each mouse the dispersion of its trajectories over a given session. The mean trajectory performed by an animal was estimated by dividing the maze in small bins along the y-axis (Figure 2). For each y-bin, the barycenter of all points in the bin is estimated and the dispersion (standard deviation) of points around the barycenter is computed. For each session, the dispersion values were averaged across mice.

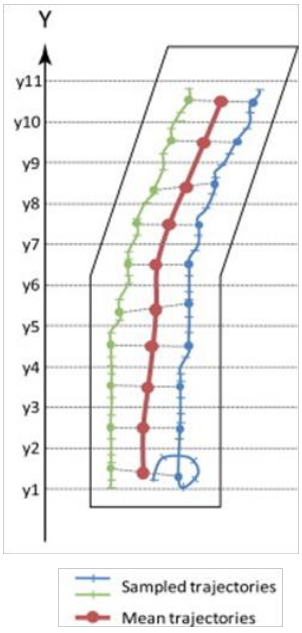

Figure 46. Example illustrating the calculation of the mean trajectory. The mean trajectory performed by an animal was estimated by dividing the maze in small bins along the y-axis. For each y-bin, the barycenter of all points in the bin is estimated and the dispersion (standard deviation) of points around the barycenter is computed.

2.2.4 THE MORRIS WATER MAZE TASK.

Mice were trained in a circular water tank (150 cm in diameter, 40 cm high) to find an escape platform (10 cm of diameter) hidden 0.5 cm below the surface of the water at a fixed location. The pool contained water (21 °C) made opaque by the addition of an inert and nontoxic product (Accusan OP 301). Both the pool and the surrounding distal cues were kept fixed during all experiments. A first batch of mice underwent a 10-day protocol (Figure 3.A), consisting in one training session per day, four trials per session. The starting position (North, East, West, or South) was randomly selected with each quadrant sampled once a day. At the beginning of each trial, the mouse was released at the starting point and made facing the inner wall. Then, it was given a maximum of 90 s to locate and climb onto the escape platform. If the mouse was unable to find the platform within the 90 s period, it was guided to the platform by the experimenter. In either case, the mouse was allowed to remain on the platform for 30 s. To assess spatial memory, a probe test was given 24 hours after the end of training. The platform was removed and the mouse, starting from the opposite quadrant, was allowed a 1-min search for the platform. To check for visuo-motor abilities, mice then underwent a cue task. A flag was placed on the top of the platform, which was positioned at one of four possible locations (North, East, West, and South). To solve this task, animals had to learn that the proximal cue indicated the location of the platform. The starting position of the animal was fixed and located at the center of the circular water tank. The test was performed during two consecutive days with four trials a day. The four possible locations of the platform were randomly sampled each day.

A second batch of mice underwent a 3 phase training protocol (Figure 3.B): cue training (5 days), spatial training (5 days), reversal training (4 days). As previously, during the cue training, an object (11 cm high) was used to mark the platform (which was randomly placed at different locations across trials), and the pool was surrounded by blue curtains to occlude extramaze cues. During spatial training, prominent extramaze cues placed around the testing room enabled the animals to learn the platform's location (fixed over training). After the first spatial training, the location of the platform was moved to the opposite quadrant, and the mice were trained again in the environment during 4 days (reversal training). This last phase aimed at evaluating mice ability to adapt their goal-oriented behavior in a known environment. Each mouse underwent one training session per day consisting of four trials. Like previously, the mouse started from a random position and was given a maximum of 90 s to locate and climb onto the escape platform. To assess spatial memory, a probe test was given 24 hours after the end of spatial and reversal training phase.

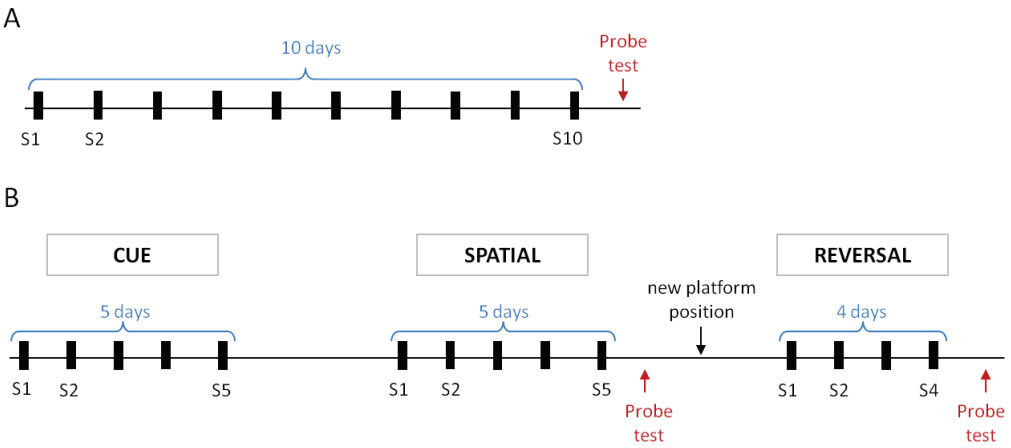

Figure 47. Design of the behavioral assays.
A. Ten-day protocol. The mice had to use the configuration of environmental cues to find a platform hidden below the water surface (at a fixed position).
B. Three phase protocol. The Cue phase consists in reaching a visible platform (cued with a flag) randomly located, in the absence of environmental cues. The spatial training phase is similar to the 10 day protocol (hidden platform, at a fixed position). After spatial training, the location of the platform was moved to the opposite quadrant, and the mice were trained again in the environment during 4 days (reversal).
In both paradigms, each mouse underwent one training session per day (represented by a black bar) consisting of four trials. To assess spatial memory, a probe test was given 24 hours both after the end of each spatial training phase

Data acquisition was performed at a frequency of 25 Hz using the SMART® video recording system and tracking software. Data processing was automated using NAT (Jarlier et al., 2013). The measured parameters were: the average time necessary to reach the platform (i.e., mean escape latency), the traveled distance to reach the platform, the average speed, the mean distance of the mouse relative to the platform, and the percent of time spent in the target quadrant.

2.3 ELECTROPHYSIOLOGY

2.3.1 SUBJECTS

Five transgenic L7-PP2B mice and four wild-type littermate controls were recorded in this study. Mice were implanted at 2.5 months and recorded until 6 months. All mice were submitted to all recording protocols. The mice were housed individually starting from one week before surgery.

2.3.2 SURGERY

L7-PP2B and control mice were deeply anesthetized by injection of Xylasine (10 mg/kg) and Ketamine (100 mg/kg) and then placed on a stereotaxic apparatus. Levels of anaesthesia

were monitored regularly by testing toe and tail pinch reflexes. An implant included 4 tetrodes (each consisting of 4 twisted 25-µm Formvar-insulated nichrome wires) inserted into a single 25-gauge guide cannula. Each wire was attached to a pin of an EIB-18 (Electrode Interface Board-18, Neuralynx Inc, USA). Wires impedance was lowered to 200 kΩ using a gold plating solution enriched with polyethylene glycol (Ferguson et al., 2009). Three steel electric wires were used as reference electrodes and connected as well to the connector. Reference wires were positioned at the brain surface above the right or left cerebellar cortex (1 and 2 wires respectively). A midline incision of the scalp was made, and the skin and muscle were carefully retracted to expose the skull. Tetrodes tips were positioned above the right hippocampus (AP, -2 mm; L, -2 mm, relative to the bregma and DV, -0.9 mm relative to the brain surface). The microdrive was secured to the skull using dental cement (SuperBound C&B, UNIFAST Trad) and protected by successive layers of plastic paraffin film (Parafilm) and dental cement. After implantation, the electrodes and cannula were progressively lowered in the brain by screwing the screw into the Teflon cuff.

2.3.3 DATA COLLECTION

Starting 5 days after surgery, the activity from each tetrode was screened daily while the mice explored the recording cylinder. If no waveforms of sufficient amplitudes were detected, the tetrodes were lowered by 60 µm steps until hippocampal units could be identified. Signals were amplified 2,000 times, filtered (band-pass 0.6 to 9 kHz) using amplifiers and processed with the animals' position signals using Datawave SciWorks acquisition software. Waveforms of identified units were sampled at 32 kHz and stored. Video recording was performed using a CCD camera (Mintron, PAL) fixed to the ceiling above the arena and the mouse position was tracked by contrast, at a sampling rate of 25 Hz. Along with unit data, hippocampal pyramidal LFPs (amplified 1,000 times, filtered between 1.0 and 400 Hz) were recorded from one electrode.

Hippocampal activity was recorded while animals explore a white circular arena (50 cm diameter, 30 cm high, made of white polypren and the floor covered with white linoleum). The arena was placed on a white elevated platform in the center of the recording room (1.90x1.40m) and surrounded by a black circular curtain. The intramaze cue included a prominent light blue plastic card (29 x 21 cm) placed on the wall of the arena and a white plastic bottle (16 cm high) located against the card center. The apparatus was lit with two lights symmetrically attached to the ceiling, providing a homogeneous light over the whole arena (50lux), as well as an infra-red light to allow tracking in the dark. A white noise generator was also installed to the ceiling in order to mask potential auditory cues (75Db). Unlike rats, no food motivation was used to stimulate exploratory activity throughout the recording sessions.

2.3.4 EXPERIMENTAL PROTOCOLS

After identification of recordable cells, a sequence of five consecutive 12-min recording sessions with 4 min inter-session intervals was run. Two different cue manipulation tests were performed: cue removal or cue rotation. For each recording session, the type of the test to be applied was chosen on a pseudorandom basis. Each time that the mouse was removed between two sessions, it returned to its home cage and the arena and the cue were cleaned with soapy water to homogenize potential odor-cues.

Environmental cue removal. In this experiment, we examined the influence of external information on place cell firing by recording place cells in the absence of light and intramaze cue-related information. First the mouse was given two standard sessions (S1 and S2) similar to the screening condition; i.e., with light and environmental cues (the mouse being disconnected and removed from the arena between session S1 and S2) (Figure 4.A). Then, as the mouse stayed in the arena, the light was then turned off, the cue (card + object) was removed and sessions 3 and 4 were run. A last standard session (S5) similar to S1 and S2 was run to check that, whatever the changes in cell firing observed during the cue manipulation sessions, the initial firing pattern could be restored. The animal was removed from the arena between S4 and S5. In the dark condition, the mouse position was tracked by contrast, using infra-red light. To distinguish between the use of visual information and non-visual cue-related information, an additional protocol was run, during which the cue was left in the arena during the two dark sessions (in S3 and S4, Figure 4.B).

Environmental cue rotation. In this experiment, we examined the respective influence of external and self-motion information on place cell firing by using a conflicting situation. Previously developed in rats (Rotenberg and Muller, 1997)**,** this experiment involved two types of object rotations. As in the cue removal condition, two first recording sessions were performed in the standard conditions. After S2, the mouse was removed from the cylinder and the cue (card + object) were rotated by 180° relative to the center of the arena (“hidden rotation”). Such manipulation has been repeatedly shown to induce an equivalent rotation of the place fields. The fourth session was similar to S1 and S2 and was expected to result in return of the place field at its initial position. Following S4, the animal was left in the cylinder and the cue was rotated 180° clockwise at a slow speed (6-9°/s) (“visible rotation”) therefore creating a conflict between self-motion and external information (Figure 4.C). Rotenberg and Muller have shown that after 180° visible rotation the place fields did not rotate 180° as in the "hidden rotation" condition but remained stable relative to their previous position in S4, thus indicating that the place fields were controlled by self-motion rather than external information (Rotenberg and Muller, 1997).

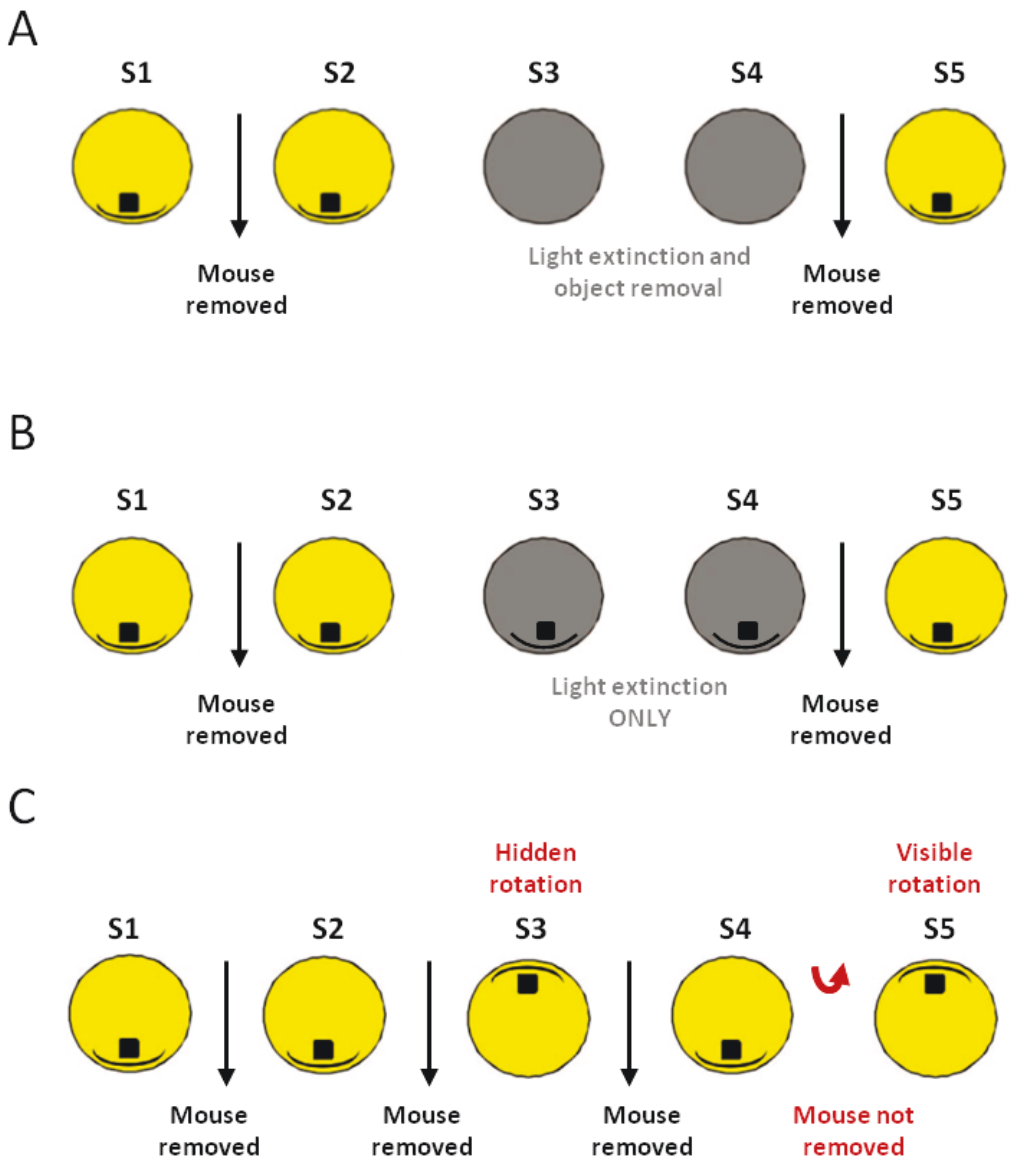

Figure 48. Design of the electrophysiological protocol.

A. Cue removal protocol. First the mouse was given two standard sessions (S1 and S2) i.e. with light and environmental cues (the mouse being disconnected and removed from the arena between session S1 and S2). Then, as the mouse stayed in the arena, the light was then turned off, the cue (card + object) was removed and sessions 3 and 4 were run. A last standard session (S5) similar to S1 and S2 was run to check that, whatever the changes in cell firing observed during the cue manipulation sessions, the initial firing pattern could be restored.

B. Dark only protocol. This protocol was run like the Cue removal protocol but the cue was left in the arena during the two dark sessions (in S3 and S4).

C. Cue conflict protocol. After the two standard sessions (S1 and S2), the mouse was removed from the cylinder and the cue (card + object) were rotated by 180° relative to the center of the arena (hidden rotation). The fourth session was similar to S1 and S2. Following S4, the animal was left in the cylinder and the cue was rotated 180° clockwise at a slow speed (6-9°/s) (visible rotation) therefore creating a conflict between self-motion and external information.

2.3.5 DATA ANALYSIS

Spike sorting and cell classification

Simultaneously recorded units were clustered manually using Plexon Offline Sorter software. Clustering on each tetrode was based on all possible X-Y combinations of characteristic features including maximum and minimum spike voltage, time of occurrence of maximum spike voltage, principal components (1 to 3 usually). Auto-correlograms were used to select only well-discriminated clusters (absence of detected event in the refractory period). Cross correlogram and auto-correlogram comparisons allowed checking unit identity. Unit activity separation for the successive sessions in the recording sequence was based on the initial cluster cutting created for session 1. In some cases, however, the cutting had to be adjusted to slight fluctuations in the signal.

Pyramidal cells and interneurons were distinguished on the basis of their average firing rate, spike shape (spike length, initial slope of valley decay), and firing pattern (auto-correlogram). Among the pyramidal cells that were recorded, only cells with clear location-specific activity, i.e. with a place field, were categorized as place cells and included in the data set.

Analysis of position data

All data were speed-filtered, i.e. only epochs with instantaneous running speeds of 2.5 cm/s or more were included. Final positions were defined by deleting position samples that were displaced more than 100 cm/s from the previous sample (tracking artefacts), interpolating any missing position points with total durations less than 1 s, and then smoothing the path with a Robust Lowess method (linear fit, span=11) (Hen et al., 2004). To characterize firing fields, the position data were sorted into 2.5 cm × 2.5 cm bins. Data from a particular session were only accepted for analysis if more than 80% of the bins were covered by the animal.

Rate maps and analysis of place cells

Firing rate distributions were determined by counting the number of spikes in each 2.5 cm × 2.5 cm bin as well as the time spent per bin. Maps for number of spikes and time were smoothed individually using a boxcar average over the surrounding 5 × 5 bins. Weights were distributed as follows:

box = [0.0025 0.0125 0.0200 0.0125 0.0025;
0.0125 0.0625 0.1000 0.0625 0.0125;
0.0200 0.1000 0.1600 0.1000 0.0200;
0.0125 0.0625 0.1000 0.0625 0.0125;
0.0025 0.0125 0.0200 0.0125 0.0025;]

Firing rates were determined by dividing spike number and time for each bin of the two smoothed maps.

A place field was defined as a set of at least 10 contiguous pixels with a firing rate above the overall mean firing rate. Color-coded firing rate maps were then constructed for each session to visualize the positional firing distribution. In such maps the highest firing rate is coded as red, the lowest as blue, intermediate rates are coded as green, yellow and orange, and unvisited pixels are shown in white.

In addition to the qualitative description of the place cell firing provided by the maps, several numerical measures were used to analyze spatial firing of place cells including the (i) mean field firing rate; (ii) field peak firing rate; (iii) spatial coherence, which measures the local smoothness of firing rate contours (iv) information content, which expresses the amount of information conveyed about spatial location by a single spike (Rotenberg and Muller, 1997), (v) intra-session stability and (vi) inter-session stability.

Spatial coherence was estimated as the first order spatial autocorrelation of the place field map, i.e. the mean correlation between the firing rate of each bin and the averaged firing rate in the 8 adjacent bins (Muller and Kubie, 1989). Spatial coherence was calculated from unsmoothed rate maps.

For each cell, the spatial information content in bits per spike was calculated as information content: $I=\Sigma_i(\lambda_i/\lambda) \times \log_2 (\lambda_i/\lambda) \times P_i$ where λ_i is the mean firing rate in each pixel, λ is the overall mean firing rate, and P_i is the probability of the animal to be in pixel i (i.e. occupancy in the *i*-th bin / total recording time).

The inter-session stability i.e. the spatial correlation between consecutive sessions was estimated for each cell by correlating the rates of firing in corresponding bins of the pair of smoothed rate maps.

Intra -session stability was estimated by computing spatial correlations between rate maps for the

first and second halves of the trial.

The place field angular shift between 2 sessions was measured by performing a cross-correlation as the firing rate array of the first session was rotated in 6° steps relative to the firing rate array of the second session. The angle associated with the highest correlation was taken as the rotation angle of the place field between the 2 sessions.

Exploration characterization

To analyze mice behavior during exploration of the recording chamber, the track was used to compute several parameters. The exploration of the cue (object + card) was evaluated by the percent of time spent in the object zone (a restricted zone 8cm around the

object), the number of entries in this zone, the mean distance to the object (averaged over the track), and the latency to enter the object zone. To control for the specificity of the object-related behavior, the percent of time spent and the number of entries were also computed for a control zone, a zone of the same area on the opposite side of the arena. These analyses were performed on the two first minutes of the recording session to avoid a diluting effect of the 12-minute session.

To detect a difference in the behavior of mice between sessions S1 and S2 and take into account inter-subject variability, we computed a ratio between the values obtained for session S2 and those obtained for the preceding session S1.

Statistics

All statistics were carried out with Matlab statistics toolboxes and the Statview 5.0 software. When the data were normally distributed, a repeated measure analysis of variance (ANOVA) was followed by a Newman-Keuls post-hoc analysis. Kruskal-Wallis and Mann-Whitney tests were used otherwise. Unpaired Student's t tests were used to compare sensori-motor properties of control and L7-PP2B mice. Distributions of similarity coefficients were compared by a Kolmogorov-Smirnov test. Circular statistics was made using Circstat, a matlab toolbox for circular statistics (Berens, 2009). The significant threshold was fixed at 5 % ($p < 0.05$ was significant). All data are presented as mean ± S.E.M.

RESULTS

All the results presented here were analyzed with NAT (Navigation Analysis Tool), a matlab-based software developed in our laboratory. I contributed to its development during my PhD. In particular, with Frederic Jarlier, we coded the program computing the parameter of deviation to mean trajectory and developed a speed filter, required for the extension of NAT to dry paradigms (used in this study in the quantification of mice behavior in the sensori-motor tasks). This software was recently published (Jarlier et al., 2013), and is attached at the end of this manuscript.

1 ANXIETY, GENERAL ACTIVITY, AND SENSORI-MOTOR ABILITIES

To assess the contribution of parallel fiber-Purkinje cell LTP in spatial navigation, we tested L7-PP2B mice in several navigation tasks. However, cerebellar deficits are classically associated to motors impairments and are likely to impact the performances of mice in navigation tasks (Lalonde and Strazielle, 2003). To control for a potential motor bias, all mice were first submitted to a large battery of sensori-motor tests (SHIRPA protocol). None of these tests revealed a deficit in L7-PP2B mice (Student t-tests, all $p>0.5$, see table in Figure 49.A). Indeed, L7-PP2B mice level of anxiety was comparable to control mice, according to the percent of time spent in the open arms of the elevated plus maze ($p=0.94$). They showed no deficit in the spontaneous locomotor activity in the actimeter as indicated by a traveled distance ($p=0.56$) and rearing frequency ($p=0.25$) equivalent to the controls. Moreover, they did not display any motor coordination deficit, as measured by the slipping frequency on the holeboard ($p=0.32$). Their balance, evaluated in a static (the unstable platform) and a dynamic paradigm (the elevated horizontal rod) was also preserved as they stayed as long as the control on the unstable platform ($p=0.72$) and traveled the same distance on the elevated rod ($p=0.32$).

However, their motor adaptation abilities were affected. Indeed, after the sensori-motor evaluation, mice were trained on the rotarod, either on a constant speed protocol or an accelerating protocol (Figure 49.B). L7-PP2B were affected in both versions of the tasks since they fell from the rod earlier than the controls at 5rpm (ANOVA, genotype effect, $F_{1,40}= 4.82$, $p=0.034$) and in the accelerating version (ANOVA, genotype effect, $F_{1,15}= 8.79$, $p=0.010$). It is worth noting than after the 5rpm protocol, L7-PP2B mice did not perform differently from their controls in the 10 rpm protocol (ANOVA, genotype effect, $F_{1,40}= 0.01$, $p=0.921$), suggesting a compensatory effect of training (Figure 49.B).

A

Task	Measure	Controls (n=36)	L7-PP2B (n=24)	*t-test (p)*
Anxiety	% Time in open arms	45.9 ± 4.5	45.3 ± 5.4	0.94
Spontaneous locomotor activity	Speed (cm/s)	13.8 ± 0.3	13.5 ± 0.4	0.56
	Travelled distance (m)	27.5 ± 1.7	26.0 ± 1.7	0.57
	Rearing number	32.9 ± 3.3	27.1 ± 3.5	0.25
Motor coordination	Walking time (min)	1.4 ± 0.1	1.3 ± 0.1	0.65
	Slip frequency	5.5 ± 0.5	6.2 ± 0.6	0.32
Static balance	Falling latency (s)	125.5 ± 6.4	129.1 ± 7.7	0.72
Dynamic balance	Falling latency (s)	180.0	180.0	-
	Travelled distance (m)	18.5 ± 1.0	16.9 ± 1.2	0.32
	Speed (cm/s)	11.6 ± 0.3	10.8 ± 0.5	0.16

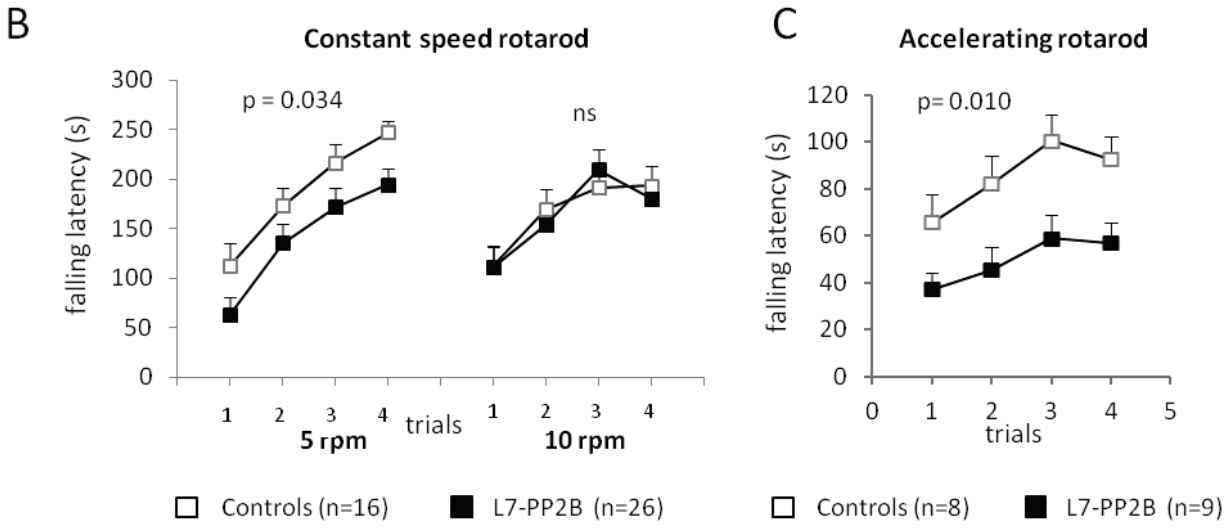

Figure 49. L7-PP2B mice have preserved general sensori-motor properties but impaired motor adaptation abilities.

A. Table showing the basic sensori-motor abilities of controls and L7-PP2B mice.

B,C. Motor adaptation performances expressed as a latency to fall from a rod rotating at a constant (B) or accelerating (C) speed in both controls and L7-PP2B mice. ANOVA, genotype effect, 5rpm $F_{1,40}$= 4.82, p= 0,034 ; 10 rpm $F_{1,40}$= 0.01, p=0.92, C. Accelerating protocol. ANOVA, genotype effect, $F_{1,15}$= 8.79, p= 0,0097.

2 TRAJECTORY OPTIMIZATION

Parallel fiber-Purkinje cell LTD has been previously shown to be important to perform optimal trajectory toward a goal (Burguière et al., 2005, 2010). L7-PKCI mice, that specifically lack LTD at parallel fiber-Purkinje cell synapses were shown to be impaired in their ability to optimize their trajectories in an aquatic Y-maze task. To assess the potential contribution of parallel fiber-Purkinje cell LTP in trajectory optimization, L7-PP2B mice were trained in the same Stimulus-dependent water Y-maze conditioning task.

Like mice lacking cerebellar LTD, L7-PP2B mice learned the task as efficiently as their controls, as the percentage of correct turns increases over training in a similar way (Figure 50.B, ANOVA session effect $F_{9,16}$= 61.51, p <0.0001, genotype effect, $F_{1,16}$= 0.153, p= 0.701, interaction, $F_{9,16}$= 0.632, p=0.768). However, their ability to optimize their trajectories to reach the goal seemed to be affected. Indeed, the overlap plot of 20 tracks (10 left, 10 right) from a control mouse and a mutant mouse during the last session of training (Figure 50.C) evidences that the control mouse always followed the same trajectory in the maze whereas it is less obvious for the mutant mouse. To quantify this ability of a mouse to reproduce its own path, the mean trajectory was computed for each mouse at each session and the deviation relative to the mean trajectory was measured (Figure 50.C, Deviation is computed separately for right and left trajectories, individual values are indicated on the sides of the maze). Averaged across mice, the deviation to mean trajectory decreases over training for both genotypes (Figure 50.B, ANOVA session effect $F_{9,16}$= 9.76, p<0.0001, interaction $F_{9,16}$= 0.348, p=0.957) but was significantly higher for L7-PP2B mice than controls mice (ANOVA, genotype effect, $F_{1,16}$= 12.57, p=0.003). To understand if this deficit in trajectory reproducibility was due to an altered capability to learn an optimal goal oriented behavior over the conditioning, a new group of mice was trained, with the help of Frederic Jarlier, in a yoked paradigm. This protocol aimed at mimicking the learning performances but without any conditioning. Mice received the same number of trials, air puffs, and rewards but with no consistent association between a turn and a stimulus. Similarly, the deviation to mean trajectory was significantly higher for L7-PP2B than controls mice (ANOVA, genotype effect, $F_{1,8}$=6.03, p=0.0396). This last result shows that the impairment of trajectory optimization in L7-PP2B mice was not linked to the learning of a conditioned response to a stimulus. In conclusion, L7-PP2B mice display a deficit in trajectory optimization which was present initially and maintained over the learning of the task, and is thus likely to be related to the motor adaptation deficit revealed on the rotarod.

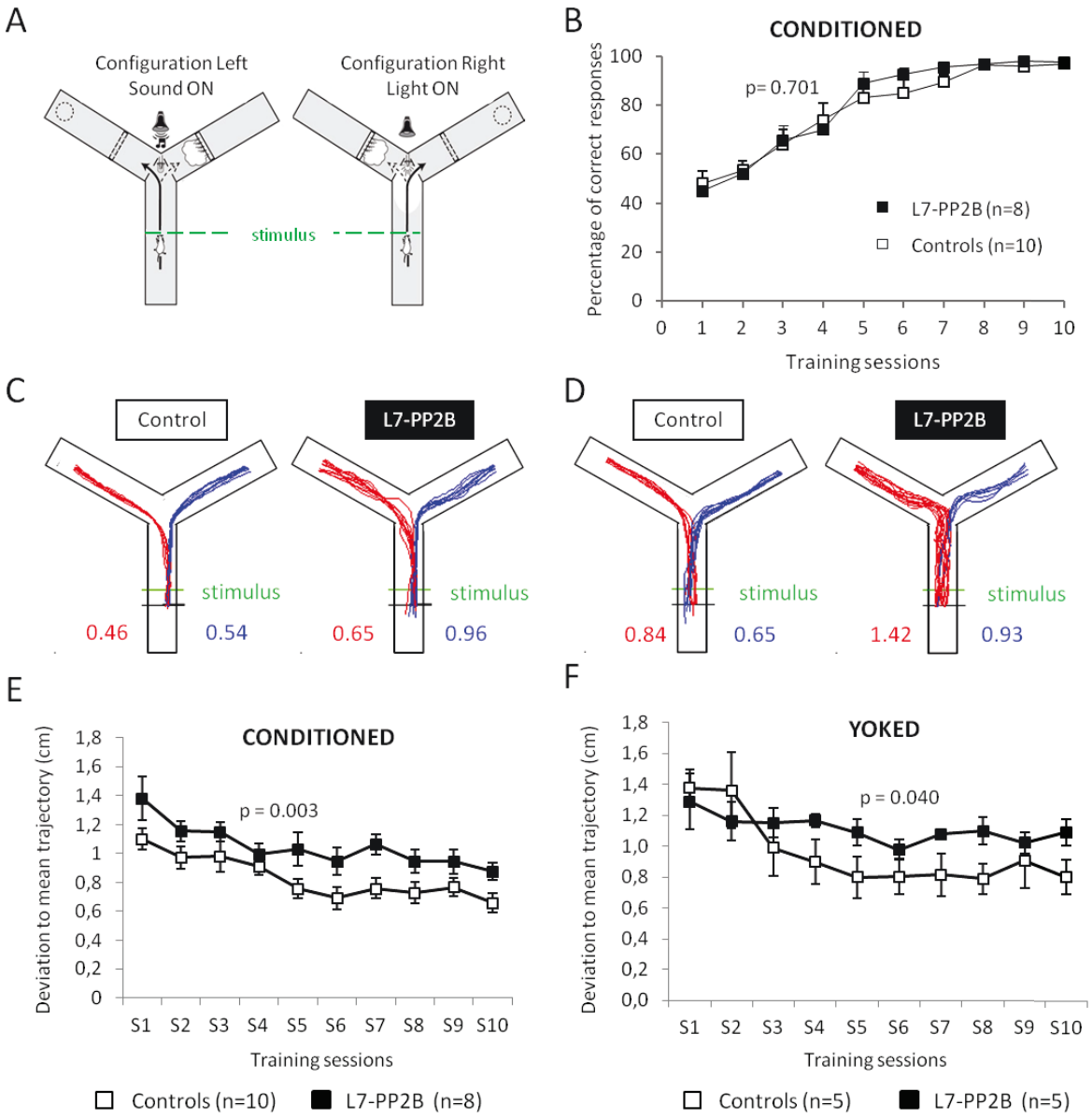

Figure 50. Trajectory optimization in the Y-maze task is affected in L7-PP2B mice.

A. Schematic diagram of the conditioning paradigm. Mice had to turn left or right depending on the stimulus: left for the sound, right for the light. Mice could escape from the water by climbing on a hidden platform located at the end of the correct arm. In case of a wrong choice, mice received an air puff and had to go to the correct arm.

B. Percentage of correct turns during training in the conditioned protocol. ANOVA genotype effect, $F_{1,16}$= 0.153, p= 0.701.

C-D. Overlap of all trajectories (red, left turns; blue right turns) from session 10 for one representative control and mutant mouse in the conditioned (C) or the yoked (D) protocol. The numbers in red and blue represent the deviation to mean trajectory, which quantifies the reproducibility of the path, separetly for left (red) and right (blue) trajectories. E-F. Deviation to mean trajectory over training sessions in the conditioned (E) or the yoked (F) protocol for controls and mutants mice. Conditioned protocol, ANOVA session effect, for controls $F_{9,9}$=7.782, <0.0001, for mutants $F_{7,9}$=3.521 p= 0.001, genotype effet $F_{1,16}$= 12.57, p= 0.003. Yoked protocol, ANOVA session effect, for controls $F_{4,9}$=3.78, p=0.002, for mutants $F_{4,9}$=1.541 p= 0.171, genotype effet $F_{1,8}$=6.03, p= 0.040.

3 SPATIAL LEARNING IN THE WATERMAZE

We further investigated spatial navigation performances of L7-PP2B mice using the Morris watermaze task. Mice were trained to find a platform hidden below the water surface at a fixed location by using the configuration of environmental cues around the pool. They received 4 trials a day during 10 days (Figure 51, this training protocol was carried out by Julien Schmitt). As the control mice, L7-PP2B mice progressively learn the position of the platform, as shown by the traveled distance which decreases over training (ANOVA, session effect, $F_{9,24}$=20.461, p<0.0001, genotype effect, $F_{1,24}$=1.628, p=0.214, interaction, $F_{9,24}$=1.796, p=0.070). Correlatively, their research becomes more focused around the platform area, as revealed by the decrease in the mean distance to the platform (ANOVA, session effect, $F_{9,24}$=27.945, p=<0.0001, genotype effect, $F_{1,24}$=0.149, p=0.703, interaction, $F_{9,24}$=0.333, p=0.963). To assess spatial memory, a probe test was given 24 hours after the end of training. The platform was removed and the mouse was allowed a 1-min search. Heat plots represent the searching area for control and mutants mice (Figure 51. E). The time spent in the target quadrant tends to be lower for L7-PP2B mice compared to theirs controls (Mann-Whitney, U=43, p=0.051) but the mean distance to the platform does not differ between genotypes (Mann-Whitney, U=57, p=0.225). Given the discrepancy between the parameters quantifying the probe test as well as the difference in the plateau reached by the mice at the end of training (stats on the 3 last days required), the spatial learning abilities of L7-PP2B mice remain unclear.

However, during this 10 days protocol, mice had to learn simultaneously the different aspects of the task: the spatial arrangement of visual cues to localize the platform but also the non-spatial components of the task (recognize the platform as the escape from the pool, swimming toward the platform, climbing onto it) (Vorhees and Williams, 2006). Besides, L7-PP2B mice display a mild motor deficit, revealed in the rotarod. They also tend to swim slower in the watermaze during both the spatial training (Mann-Whitney, U=47, p=0.082), and the subsequent cue training (data not shown, Mann-Whitney, U=41, p=0.039), suggesting that it could be related to their motor deficit. Thus, L7-PP2B mice might be affected in the non-spatial components of the task, which could slow down their spatial learning processus or affect their persevering search in the platform area during the probe test.

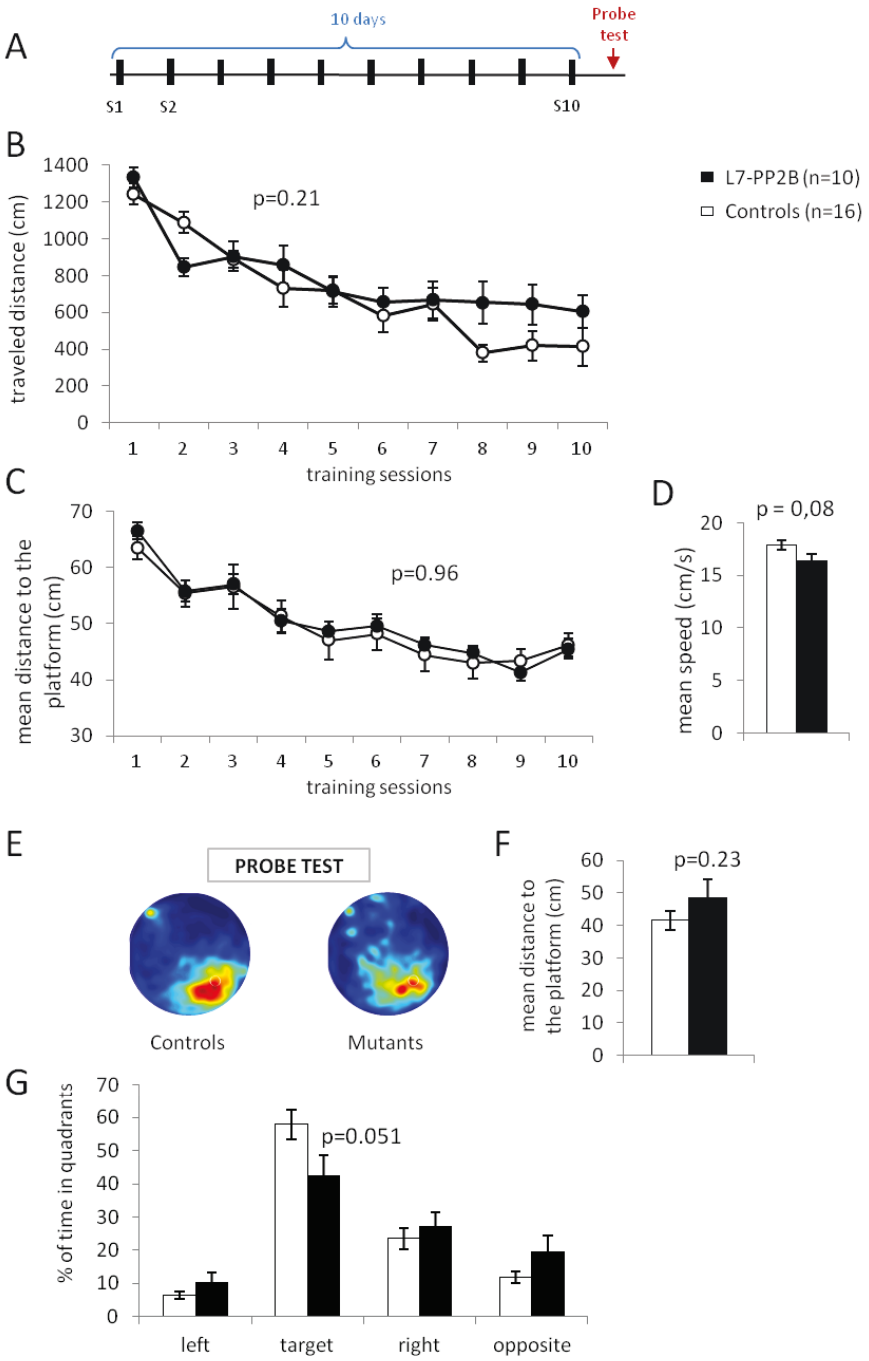

Figure 51. Spatial learning in the watermaze.

A. Schematic representation of the training protocol. The mice had to use the configuration of environmental cues to find a platform hidden below the water surface.

B. Traveled distance to find the platform. ANOVA, genotype effect, $F_{1,24}$=1.628, p= 0.214.

C. Mean distance to the platform ANOVA, genotype effect, $F_{1,24}$=0.149, p= 0.703.

D. Mean swimming speed. Mann-Whitney, U=47.0, p=0.08.

E. Probe test E. Heat plot representation of the time spent in the different quadrant during the 60s probe test for controls (left) and mutant (right).

F. Mean distance to the platform computed during the probe test . Mann-Whitney, U=57.0, p=0.23.

G. Percent of time spent in each quadrant during spatial probe test. Mann-Whitney, U=43.0, p=0.051. This training protocol was carried out by Julien Schmitt.

To investigate more specifically their spatial learning abilities we modified the training protocol by adding a cue phase (5 days) before the spatial training. Cue learning consists in finding a platform indicated by a prominent cue on the platform, in the absence of distal environmental cues. This first training allows the mice to acquire all the non-spatial skills of the task before the beginning of spatial training. Like the control mice, L7-PP2B mice learned the cue task, as shown by the decrease in the traveled distance to find the platform (Figure 52. B, ANOVA, genotype effect, $F_{1,20}$=1.867, p=0.187, session effect, $F_{1,20}$=103.88, p=<0.0001, interaction $F_{1,20}$=4.61, p=0.005) and reached the same plateau. Spatial learning was then evaluated for two positions of the platform in the same learning environment (Spatial and Reversal phases). None of these trainings revealed a deficit in L7-PP2B mice for spatial learning. In both cases, L7-PP2B mice learn to locate the platform as efficiently as their controls, as shown by the similar decrease in the traveled distance to find the platform (Figure 52. B, ANOVA, genotype effect, spatial training, $F_{1,20}$=2.331, p=0.143, reversal training, $F_{1,20}$=0.419, p=0.525). In both groups, the research becomes more focused around the platform area, as revealed by the decrease in the mean distance to the platform (Figure 52. C, ANOVA, session effect, $F_{4,20}$=15.76, p<0.0001, reversal training $F_{3,20}$=40.11, p<0.0001) even if this decrease tended to be slower in the L7-PP2B mice during spatial training (genotype effect, spatial training, $F_{1,20}$=3.717, p=0.061, reversal training, $F_{1,20}$=1.615, p=0.218). Spatial memory was evaluated during the probe test given 24h after the end of each training phase. As shown by the heat plots representing the searching area for control and mutants mice (Figure 52.E,G), L7-PP2B mice searching behavior was as pertinent as the one of control mice: neither the mean distance to the platform nor the percent of time spent in the target quadrant differs between genotypes. This was observed both after the spatial training (Mann-Whitney, mean distance to the platform, U=44, p=0.291, percent of time in target quadrant, U=43, p=0.262) and after reversal training (Mann-Whitney, mean distance to the platform, U=43.5, p=0.277, percent of time in target quadrant, U=47, p=0.391).

This first part led us to two main conclusions. L7-PP2B mice display a deficit in trajectory optimization in a maze with alleys, potentially related to the motor adaptation deficit revealed on the rotarod. Correlatively they were impacted in their swimming abilities in the watermaze task without affecting their spatial learning abilities.

Importantly, previous data have shown that L7-PKCI mice lacking cerebellar LTD were not only impaired in the ability to perform optimal trajectory toward a goal but also in the hippocampal spatial representation (Rochefort et al., 2011). Therefore, it remained unclear if spatial performances deficit was directly a consequence of the impaired hippocampal spatial representation or if the cerebellar circuitry played independent roles in these two processes. L7-PP2B mice provided thus a unique opportunity to investigate the consequence of an altered cerebellar plasticity on hippocampal representation in the absence of a clear behavioral spatial navigation deficit.

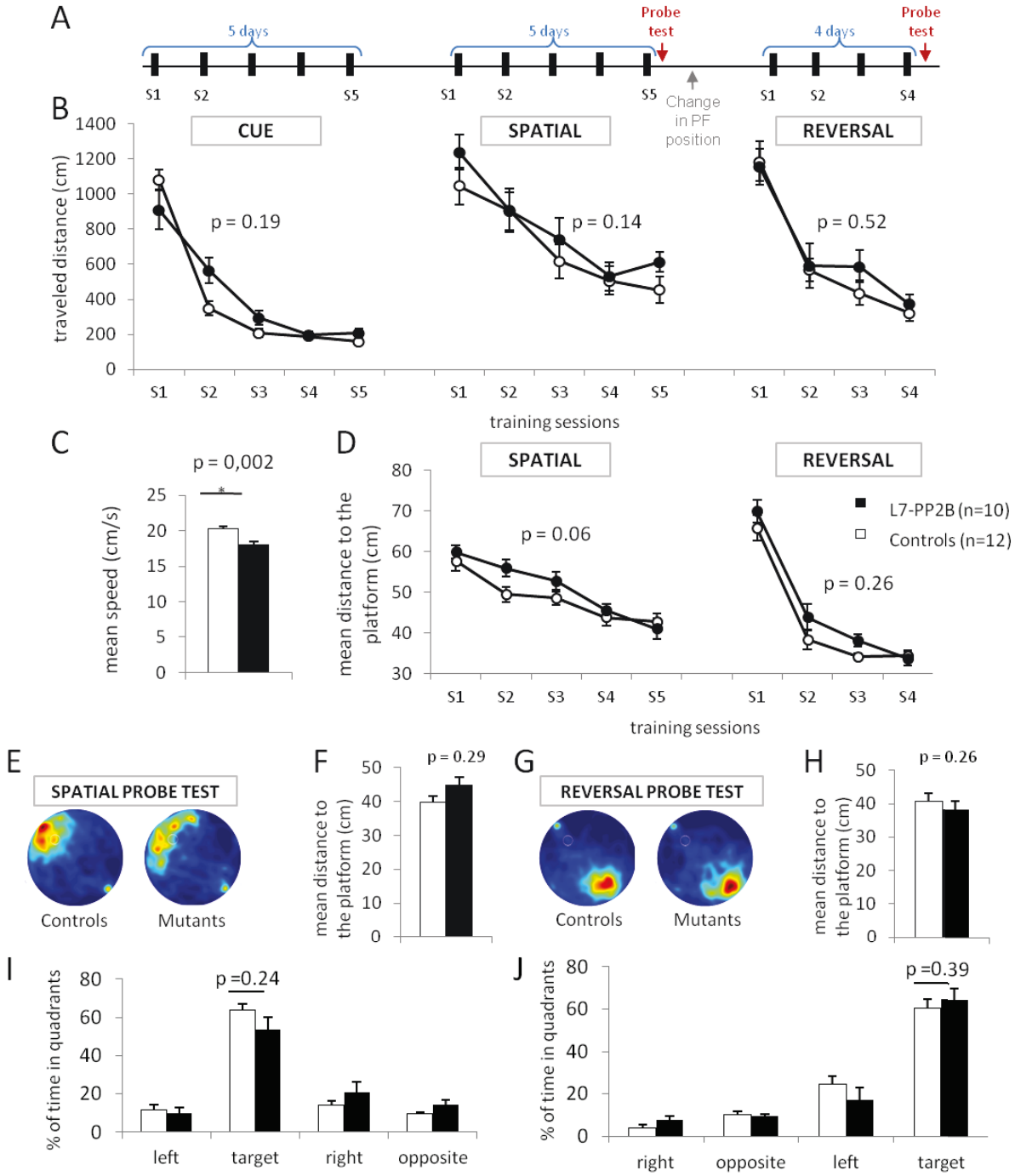

Figure 52. Spatial learning in the watermaze in controls and L7-PP2B mice.

A. Schematic representation of the training protocol. The Cue phase consists in reaching a cued platform in the absence of environmental cues. The spatial training phases require the mice to use the configuration of environmental cues to find a platform hidden below the water surface. After the first spatial training, the location of the platform was moved to the opposite quadrant, and the mice were trained again in the same environment (reversal).

B. Traveled distance to find the platform among the different phases. ANOVA, genotype effect, Cue phase $F_{1,20}$=1.867, p=0.19, Spatial phase, $F_{1,20}$=2.33, p=0.14, Reversal phase, $F_{1,20}$=0.42, p=0.52.

C. Mean swimming speed. Mann-Whitney, U=14, p=0.002. D. Mean distance to the platform (cm). ANOVA, genotype effect, Spatial phase, $F_{1,20}$=3.717, p=0.06, Reversal phase, $F_{1,20}$=1.615, p=0.26.

E. Heat plot representation of the time spent in the different quadrant during the 60s probe test after Spatial training for controls (left) and mutant (right).
F. Mean distance to the platform computed during the spatial probe test. Mann-Whitney, U=44, p=0.29. G. Same as E. after Reversal training. H. Same as F. for reversal probe test. Mann-Whitney, U=43, p=0.26. I-J. Percent of time spent in each quadrant during spatial probe assessed after the spatial (I) or reversal (J) phase. Spatial probe test, test Mann-Whitney, U=43.5, p=0.24. Reversal probe test Mann-Whitney, U=47, p=0.39

4 HIPPOCAMPAL PLACE CELL PROPERTIES IN MICE LACKING CEREBELLAR LTP

Neural activity from the CA1 field of the dorsal hippocampus was sampled as the mice freely explored a circular arena containing a salient cue (a card with a bottle attached to it) during 12-minute sessions in standard conditions (enlightened arena, sessions S1 and S2). To examine the relative influence of external and self-motion cue information on place cell firing, we used two distinct environmental manipulations in subsequent sessions, cue removal and cue conflict (sessions S3-S5). In the cue removal protocol, the arena was in the dark and the cue was removed (Figure 54.A). In the absence of visual and cue-related information, the mice had to rely on self-motion cues. To distinguish between the use of visual information and non-visual cue-related information, a control protocol (dark only) was also performed with the cue still present in darkness (Figure 55.A). In this protocol, the cue can be used as a landmark using tactile information to anchor the spatial representation in the dark. In the cue conflict protocol, we used a paradigm previously developed in rats, in which the external cue was rotated 180° in the absence (hidden rotation) or in the presence (visible rotation) of the animal (Figure 56.A), therefore producing a conflict between visual and self-motion information (Rotenberg and Muller, 1997). During the conflict, rats maintain place field stability relative to the standard session, thus suggesting the dominant use of self-motion cues (Rotenberg and Muller, 1997).

First, the analysis of the exploration behavior in the recording arena revealed that L7-PP2B mice stayed closer to the cylinder wall, as shown by their lower distance to the wall compared to their controls (in the Dark only protocol, ANOVA, genotype effect, p=0.004, session effect, p=0.005, interaction, p=0.483). Consistently, L7-PP2B mice spent less time in the center of the arena, i.e. the central zone defined as any point at least 10 cm away from the walls, (in the Dark only protocol, ANOVA, genotype effect, p=0.036, session effect, p=0.029, interaction, p=0.834) and entered less often into the central zone (in the Dark only protocol, ANOVA, genotype effect, p=0.041, session effect, p=0.006, interaction, p=0.476). Noticeably, this tendency to keep close to the walls did not vary across conditions, as shown by the absence of genotype x session interaction. Identical effects were found in the Cue removal and Cue conflict protocols. This was not due to a tendency to stay immobile next to the wall, since the general level of exploration was unaffected in L7-PP2B. They traveled a similar distance (in the Dark only protocol, ANOVA, genotype effect, p=0.170, session effect,

p=0.112, interaction, p=0.169), and displayed a similar running time (in the Dark only protocol, ANOVA, genotype effect, p=0.416, session effect, p=0.323, interaction, p=0.0.093) and number stops to their controls (in the Dark only protocol, ANOVA, genotype effect, p=0717., session effect, p=0.069, interaction, p=0.022). Identical effects were found in the Cue removal and Cue conflict protocols.

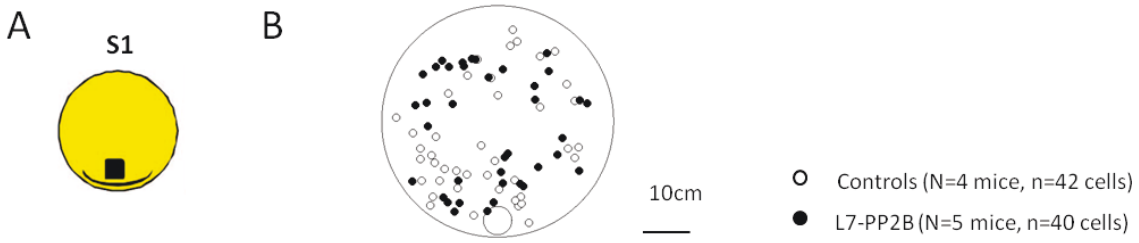

C

	Field size (cm2)	Mean field rate (Hz)	Peak rate (Hz)	Spatial coherence	Spatial Information
Controls (n=42)	562 ± 41	3.27±0.34	6.67 ± 0.64	0.54 ± 0.03	0.93 ± 0.09
L7-PP2B (n=40)	619 ± 36	3.37 ± 0.29	7.27 ± 0.83	0.52 ± 0.04	0.88 ± 0.06
Mann Whitney, p	0.362	0.868	0.943	0.654	0.989

Figure 53. Basic properties of hippocampal place cells are preserved in the L7-PP2B mice.
A. Schematic diagram of the standard recording conditions in which the arena is enlightened and contains a cue formed by a card and bottle attached to it.
B. Distribution of the place field barycenters from place cells recorded in controls (N=4 mice, n=42 cells) and L7-PP2B mice (N=6 mice, n=40 cells) in standard sessions S1 and S2 from the Cue removal protocol.
C. Table of basic place cell properties recorded during 12-minute sessions of free exploration of the circular arena in standard conditions.

The basic firing properties of place cells were first examined in standard conditions (sessions S1 and S2 from the Cue Removal protocol, Figure 53.A). For both genotypes, the place fields were homogeneously distributed over the arena (see the spatial distribution of place field barycenters in Figure 53.B), and the mean distance from the object was similar between groups (controls, 19,1±1.6cm, L7-PP2B 20,1±1.7cm, Mann-Whitney, z=0.508, p=0.613). None of the basic firing properties of place cells was affected in L7-PP2B mice compared to control mice in standard conditions (see table, Figure 53.C, Mann-Whitney tests, all p>0.05). Place fields displayed a similar size (z=0.912, p=0.362), mean and peak firing rate (respectively, z=-0.166, p=0.868 and z=0.071, p=0.943). Place cell firing patterns had the same spatial coherence (z=-0.448, p=0.654) and information content (z=0.014, p=0.989). This allowed us to evaluate the effect of cue manipulation on place cells firing properties. We analyzed only place cells with a clear place field that remained stable between the two standard sessions S1 and S2.

In the Cue removal protocol, following two standard sessions (S1 and S2), the mouse stayed in the arena and sessions 3 and 4 were run in the dark and in the absence of the object. A last standard session (S5) similar to S1 and S2 was run to check that, whatever the changes in cell firing observed during the cue manipulation sessions, the initial firing pattern could be restored (Figure 54.A). None of the examined firing properties of place cells was affected in the dark in a different way in L7-PP2B mice relative to their controls (See Figure 54, ANOVA, genotype and interaction effect, all $p>0.05$). In the dark like in the light, the place cells recorded in L7-PP2B mice displayed a similar mean field rate (Figure 54.C, genotype effect, $F_{1,1}= 0,249$, $p=0.618$, interaction, $F_{1,1}= 0,941$, $p=0.334$) and spatial coherence (Figure 54.D, genotype effect, $F_{1,1}=0,766$, $p=0.382$, interaction, $F_{1,1}= 0,127$, $p=0.722$) compared to their controls.

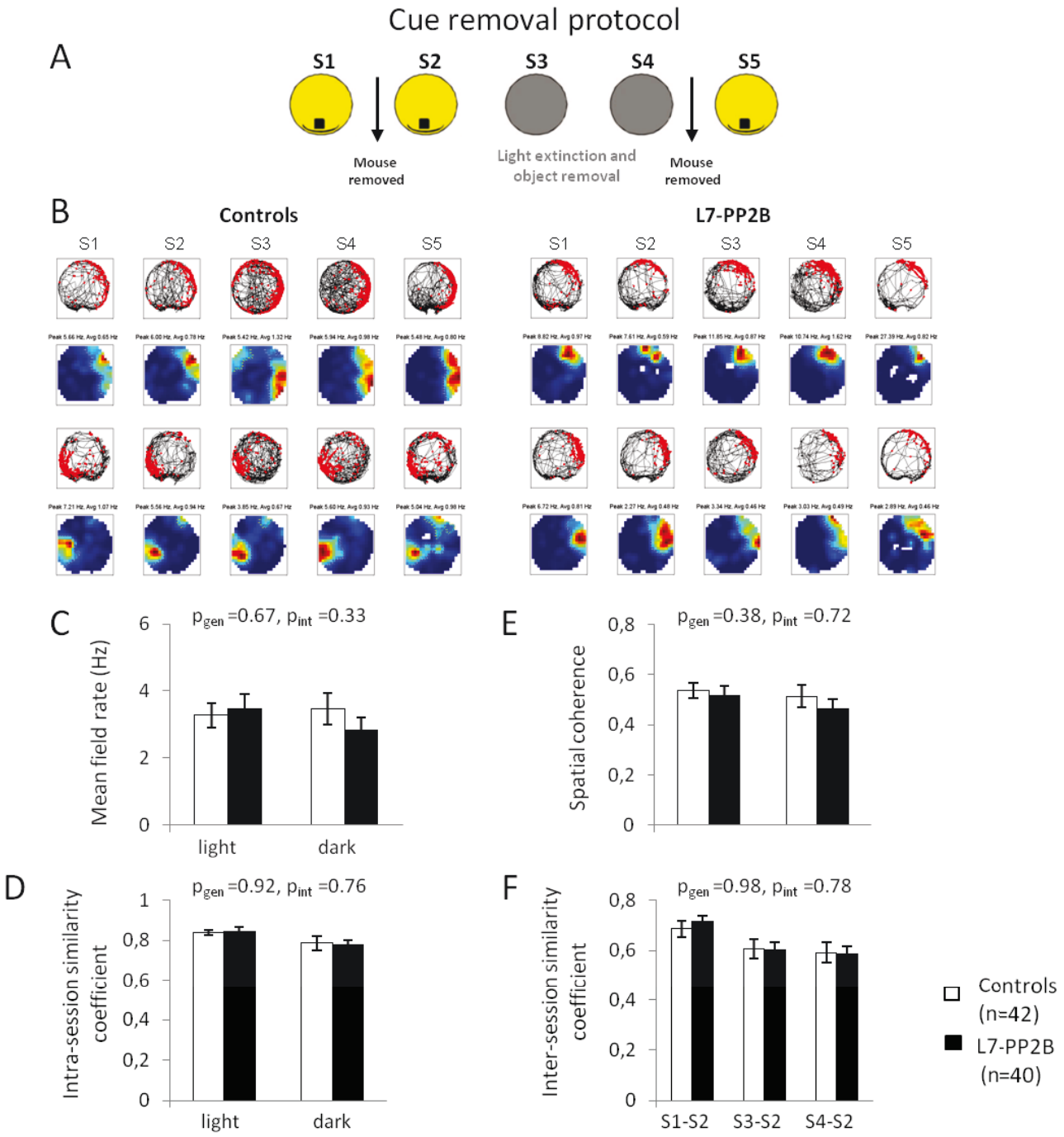

Figure 54. L7-PP2B place cells properties are preserved in the absence of visual and cue information.

A. Schematic diagram of the Cue removal protocol, used to assess the effect of self-motion information on place cell properties. After 2 standard sessions (S1 and S2), the light was turned off, the cue (card + object) was removed and sessions 3 and 4 were run. A last standard session (S5) was run to check that the initial firing pattern could be restored.

B. Examples of color-coded rate maps showing firing activity of control (left) and L7-PP2B (right) single CA1 pyramidal cells during the cue removal protocol; color coding ranges from blue (silent) to red (peak activity). Peak and mean field firing rates are indicated for each rate map.

C-F. Analysis of place cell firing characteristics shows that the suppression of external cue inputs does not affect L7-PP2B place cell properties such as the mean field rate (C), spatial coherence (D) and place field stability, as measured within (E) or across (F) sessions. Error bars represent SEM.

Interestingly place field stability, measured within or across session, was affected in the dark condition in both control and mutant groups: a similar decrease was observed between genotypes for intra-session similarity (Figure 54.E, session effect, $F_{1,2}$= 5,4101, p=0.021, genotype effect, $F_{1,2}$=0,009, p=0.923, interaction, $F_{1,1}$= 0,0879, p=0.767), and inter-session similarity (Figure 6.F, session effect, $F_{1,1}$=10.47, p<0.0001, genotype effect, $F_{1,1}$=$2.53.10^{-4}$,p=0.987 interaction, $F_{1,1}$=0.243, p=0.785). This decrease was not observed during the Dark only protocol either for intra-session (Figure 55.E, session effect, $F_{1,1}$=0,123, p=0.726, interaction, $F_{1,1}$=0,132, p=0.718) or inter-session similarity (Figure 55.F, session effect, $F_{1,2}$=0.114, p=0.892, interaction $F_{1,2}$=0.464, p=0.630). This specific degradation of place field stability in the absence of object cue suggests that mice do use the cue as a landmark to anchor their spatial representation.

In the Dark only protocol we observed a higher mean field rate for place cells recorded in L7-PP2B mice compared to control mice both in light and dark conditions (Figure 55.C, ANOVA genotype effect, $F_{1,1}$=5,312, p=0.023, session effect, $F_{1,1}$=0,7304, p=0.394, interaction, $F_{1,1}$=0,215, p=0.643). This difference in the light condition was not observed in the similar light conditions of the cue removal protocol. Since only 25 place cells were recorded in L7-PP2B mice during the dark only protocol, these results might indicate a sampling bias for the L7-PP2B mice. We also noticed an increase in spatial coherence in the dark, in a similar way for both genotypes (Figure 55.C, ANOVA, session effect, $F_{1,1}$=9,601, p=0.023, interaction, $F_{1,1}$=0,215, p=0.643).

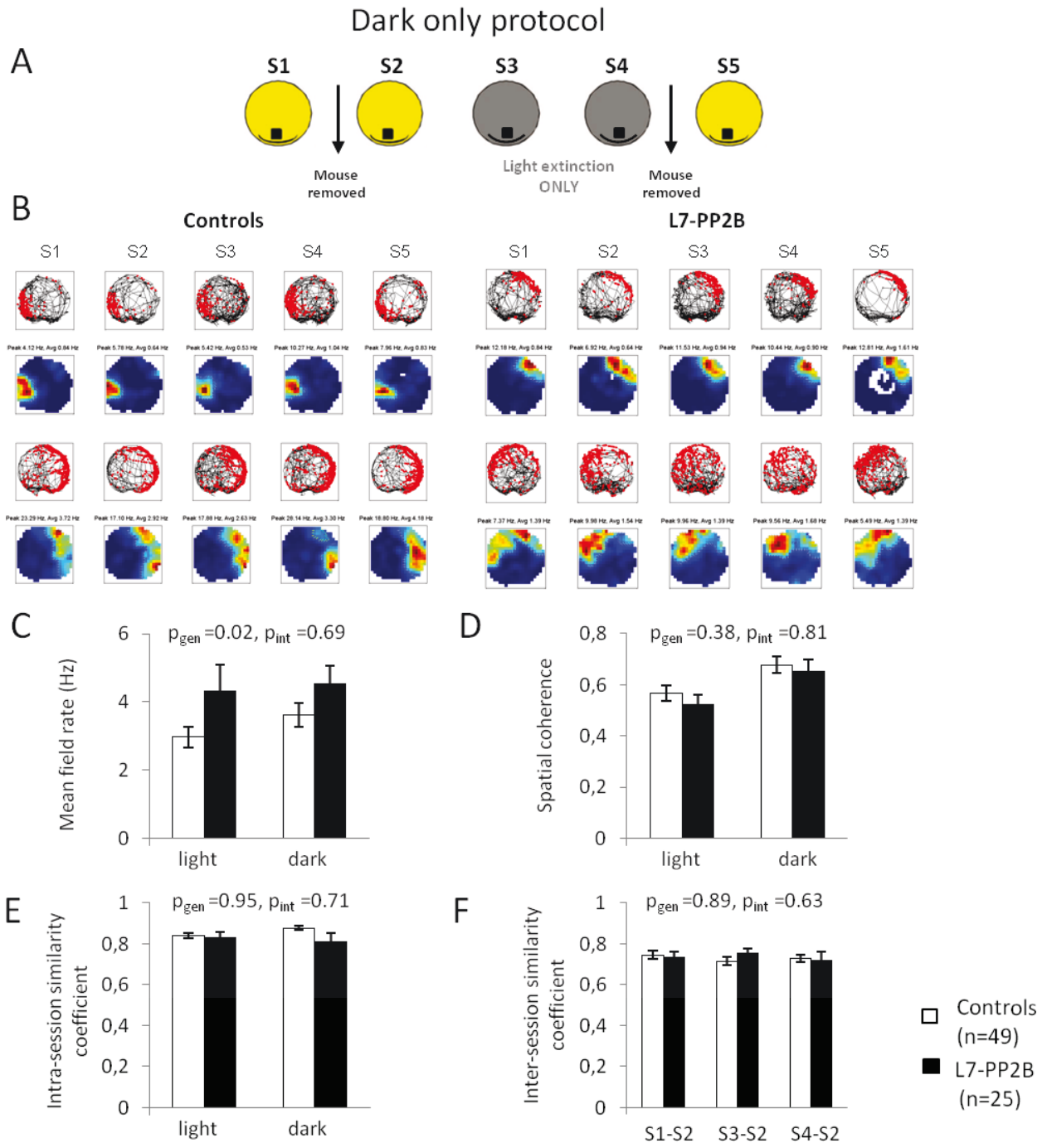

Figure 55. L7-PP2B place cells properties are preserved in the absence of visual information only.

A. Schematic diagram of the Dark only protocol, used as a control protocol, to distinguish between the use of visual information and non-visual cue-related information. After 2 standard sessions (S1 and S2), the light was turned off and sessions 3 and 4 were run. A last standard session (S5) was run to check that the initial firing pattern could be restored.

B. Examples of color-coded rate maps showing firing activity of control (left) and L7-PP2B (right) single CA1 pyramidal cells during the Dark only protocol; color coding ranges from blue (silent) to red (peak activity). Peak and mean field firing rates are indicated for each rate map.

C-F. Analysis of place cell characteristics shows that the suppression of visual inputs does not affect L7-PP2B place cell properties such as the mean field rate (C), spatial coherence (D) and place field stability, as measured within (E) or across (F) sessions. Error bars represent SEM.

To further investigate the respective influence of self-motion and external information on spatial firing pattern in L7-PP2B mice, a cue conflict protocol was conducted (Figure 56.A). Following two standard sessions, a 180° rotation of the cue was performed in the absence of the animal (session S3). This hidden rotation resulted in similar rotation of the place fields in both control and L7-PP2B mice (See examples in Figure 56.B) therefore indicating that the cue efficiently controlled place cell activity. As a result, in both groups, similarity between sessions S3 and S2 at a rotation angle of 180° was comparable to similarity between two consecutive standard sessions (S1 and S2) at a rotation angle of 0° (Figure 56.C, left, genotype effect, $F_{1,1}$=0.926, p=0.340, session effect, $F_{1,1}$=1.549, p=0.219, interaction, $F_{1,1}$=0.039, p=0.845). Visible rotation of the cue was then performed, producing a conflict between external and self-motion sensory information (in session S5). During the conflict, a similar proportion a place cells maintained their place field stable relative to the previous session (0° $\pm$ 30° rotation) (30/44 (68 %) in control mice and 25/33 (76%) in L7-PP2B mice, Fisher exact test, p=0.611), which suggests that in both groups, animals resolved the conflict by relying mainly on self-motion cues (Figure 56.D). In both genotypes, a low percentage of cells exhibited remapping at different locations, resulting in a similar decrease in field stability (measured by intersession similarity coefficient at a rotation angle of 0°) between sessions S4 and S5 (Figure 56.C, ANOVA, session effect, $F_{1,1}$=20.611, p<0.0001, genotype effect, $F_{1,1}$=0.084, p=0.773, interaction, $F_{1,1}$=0.231, p=0.633). Consistently, the distribution of place field rotation angles after the visible rotation was not different between genotypes (Circular Kuiper test, p>0.1).

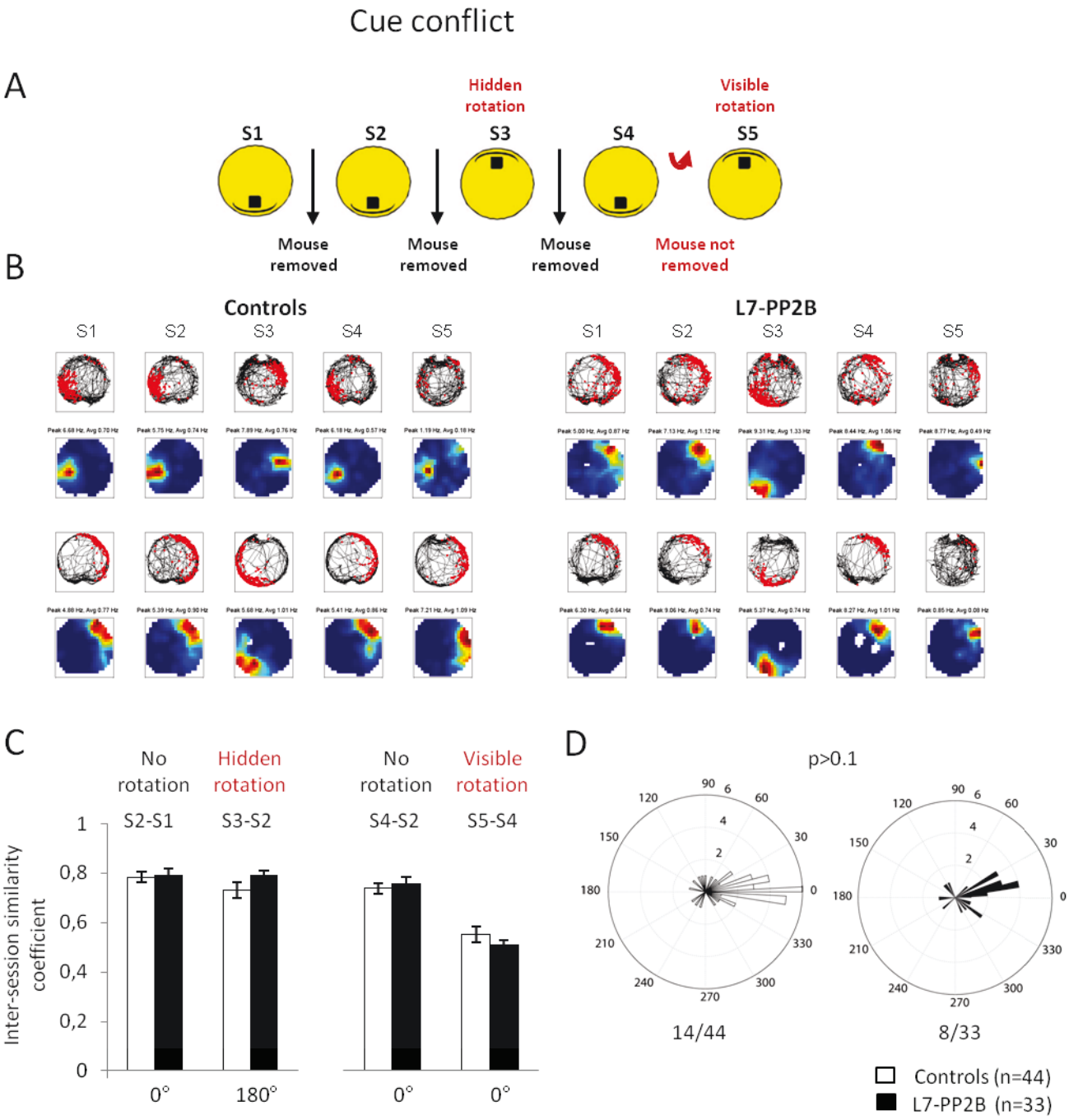

Figure 56. L7-PP2B place cells properties are preserved during cue conflict.

A. Schematic diagram of the Cue conflict protocol, used to assess the effect on place cell firing of a 180° rotation of the cue in the absence (hidden rotation) or presence (visible rotation) of the mouse in the arena.

B. Examples of color-coded rate maps showing firing activity of control (left) and L7-PP2B (right) single CA1 pyramidal cells cue removal protocol; color coding ranges from blue (silent) to red (peak activity). Peak and mean field firing rates are indicated for each rate map.

C. Histograms showing the intersession similarity coefficient score associated to a 0° or 180° field rotation after a hidden or a visible rotation of the cue.

D. Polar distributions of place field rotation angles during visible rotation for control (left) and L7-PP2B (right) mice. The L7-PP2B distribution is not different from the control distribution, Circular Kuiper test, p>0.1. Proportion of place field displaying a rotation angle superior to 30° is indicated below the diagrams. These proportions do not differ between mutant and controls, Fisher exact test, p=0.61.

5 INSTABILITY OF THE SPATIAL REPRESENTATION IN L7-PP2B MICE

As mentioned previously, analysis on cue removal and cue conflict condition included only place cells with a place field location stable between consecutive standard sessions S1 and S2. Surprisingly, this criterion led us to exclude an important number of sessions in L7-PP2B mice compared to control mice. In an unpredictable manner, in L7-PP2B mice, many cells with a clear place field in S1 displayed a different place field location in session S2. This resulted in a very low similarity coefficient between rate maps from sessions S1 and S2 (often below 0, see examples in Figure 57.B). The analysis of the whole population of place cells revealed that the distribution of S1-S2 similarity coefficients differed between control and mutant groups (Figure 57.C, Kolmogorov-Smirnov test, $p = 4{,}096.\ 10^{-5}$). The cells displaying a S1-S2 similarity coefficient below 0.2 were then qualified as unstable cells (threshold determined by a k-mean analysis on the distribution of S1-S2 similarity coefficients in L7-PP2B). According to this criterion, we did not find any unstable place cell in control mice.

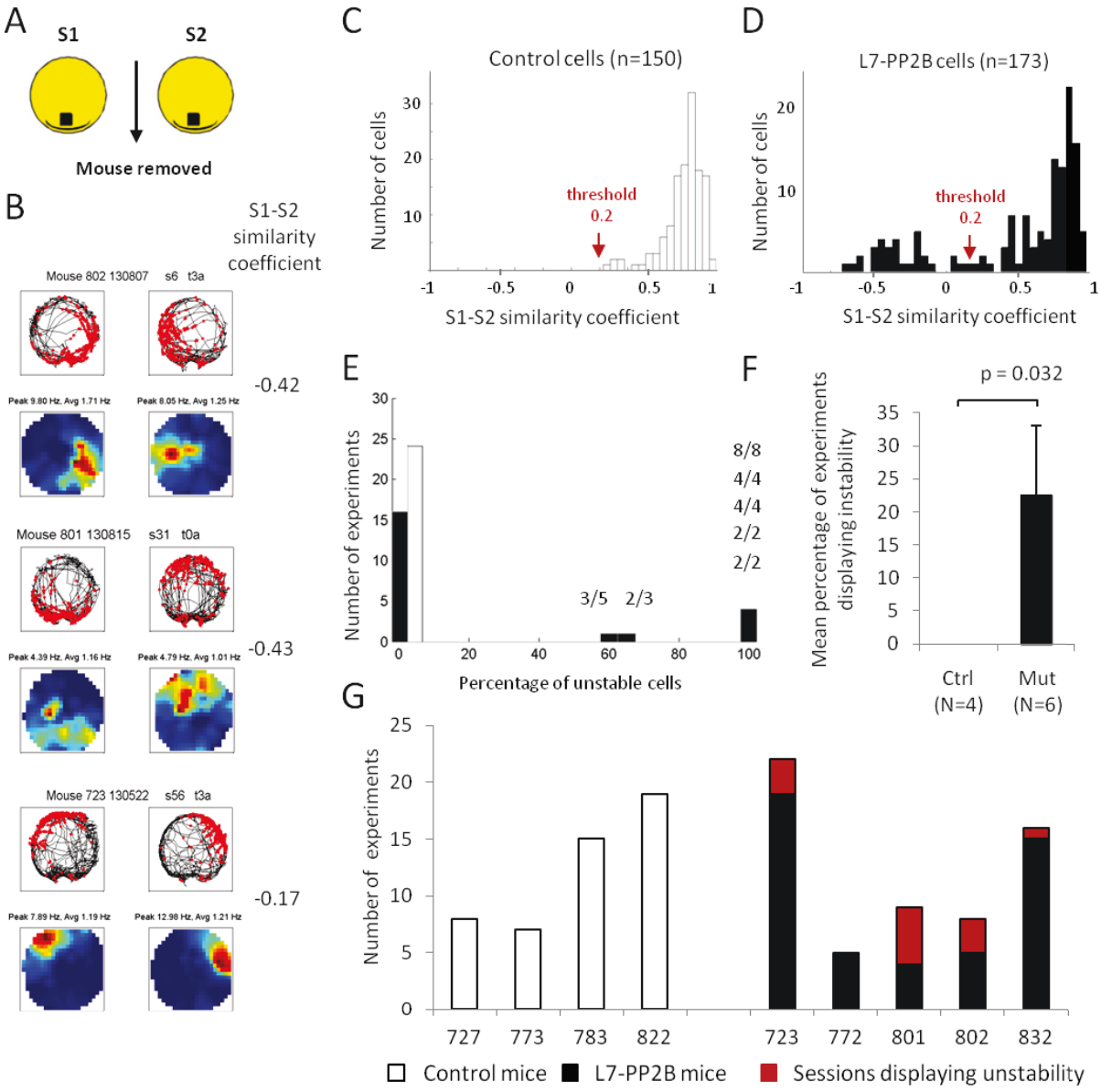

Figure 57. L7-PP2B mice display unstable place fields in a familiar environment.

A. Schematic diagram of the standard recording conditions.

B. Examples of color-coded rate maps showing place cells recorded during two consecutive sessions in standard conditions. S1-S2 similarity coefficients are indicated on the right.

C-D. Distribution of S1-S2 similarity coefficients in the whole population of place cells recorded in control (C) and mutant (D) mice. These distribution are significantly different, Kolmogorov-Smirnov test, $p = 2.08 .10^{-7}$.

E. Distribution of experiments in function of the percentage of unstable cells (S1-S2 similarity coefficient below 0.2) recorded in the experiment. Only experiments in which a minimum of 3 place cells were recorded simultaneously are included in the histogram. For experiments displaying a percentage of unstable cells different from zero, the number of unstable cells is individually plotted.

F. Percentage of experiments displaying instability is computed for each mouse and averaged over the group of control (N=4) and mutant (N=6) mice. This percentage is significantly higher for mutant mice compared to their controls, Mann-Whitney, U=2, p = 0.0318.

G. Number of sessions displaying instability for each control and L7-PP2B mouse. For each mouse the proportion of sessions displaying instability is represented in red.

Importantly, two observations led us to analyze these instabilities at the level of the recording sessions rather than the cell level. First, in some cases we were able to record the same place cell over several days (see examples Figure 58). Depending on the recording day, a given place cell could display either a similar or a different place field between S1 and S2. Thus a classification based on the cell phenotype would alternatively categorize it as stable or unstable. Secondly, we examined the distribution of unstable cells across the experiments (an experiment being defined as a S1-S2 pair). Our data reveals that in a given experiment, the place cells are either all stable or most of them unstable (Figure 57.C). The two experiments displaying an intermediate proportion of unstable cells will be discussed later. This indicates that when instability was observed, most of the simultaneously recorded place cells were affected. Instabilities were thus referred as events in the following part of this study.

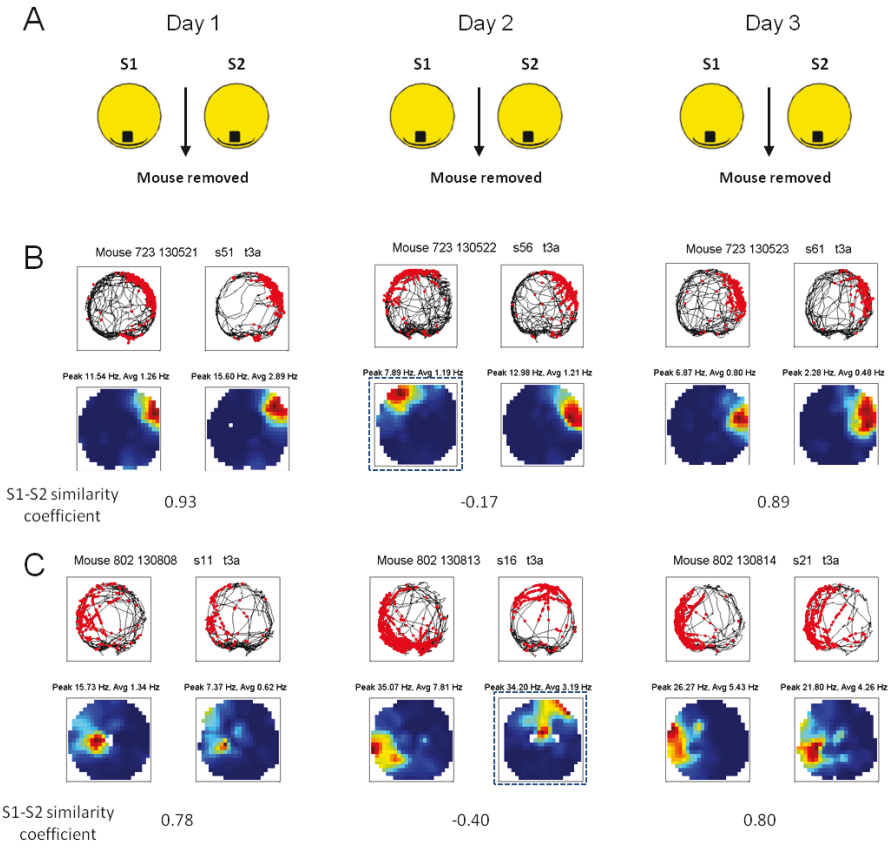

Figure 58. In L7-PP2B, a given place cell can display stability or instability in an independent way from one day to the other.

A. Schematic diagram of the standard recording conditions. B. Examples of color-coded rate maps showing a given place cell recorded during three consecutive days in two consecutive sessions in standard conditions (unit t3a, recorded in mouse 723) . Respective S1-S2 similarity coefficients are indicated below. C. Same as B for another place cell (unit t3a, recorded in mouse 802).

Instability between S1 and S2 was observed in 12/60 experiments in the L7-PP2B group. They were recorded in all but one of the L7-PP2B mice (Figure 57.G). The frequency of these instability events for each mouse was quite variable (ranging from 0 to 56%) but the mean percentage (22.6 ± 10.4 %) was significantly higher than in the control group (Figure 57.H, Mann-Whitney, p=0.0318). To further characterize these instability events, we analyzed the modifications in the firing pattern between standard sessions S1 and S2. First observed by Muller and Kubie in 1987, the change in the firing pattern of place cells in response to changes in sensory or cognitive inputs is called remapping (Muller and Kubie, 1987; Colgin et al., 2008). Two main categories of remapping have been reported, rate remapping and global remapping (Leutgeb et al., 2005). Rate remapping is defined as substantial changes in firing rate accompanied by little to no shift in place field location whereas global remapping (also called "complete remapping", (Muller et al., 1991)) refers to arbitrary changes in both firing rate and field location. During global remapping a place cell displays unrelated place fields in the two conditions or a place field in one condition but not in the other (Colgin et al., 2008). Consequently, the spatial relationships between place fields from different place cells in one condition are altered in the second one. Some authors also observed rotational remapping (in mutant mice lacking zif-268, (Renaudineau et al., 2009)), characterized by the formation in the recording arena of a place field with the same shape, but with a different orientation according to an external cue (Renaudineau et al., 2009). Rotational remapping was observed for cell ensembles, meaning that the spatial relationships between place fields of simultaneously recorded cells were preserved during the sessions displaying rotation. A schematic diagram illustrates the properties of these different types of remapping in Figure 59.

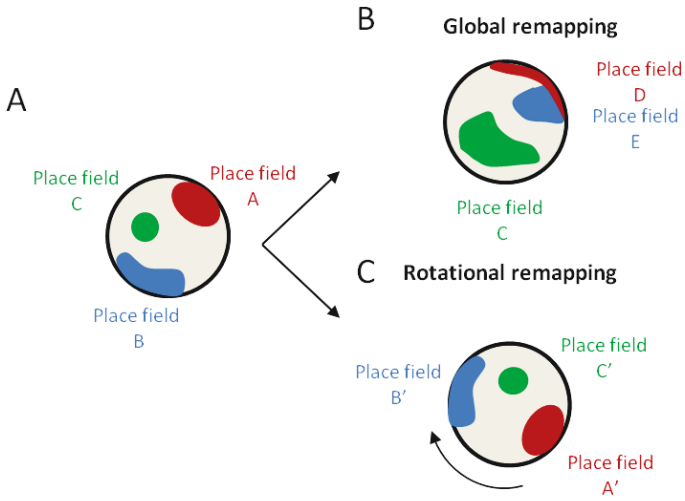

Figure 59. Low rate map similarity between consecutive standard condition sessions can correspond to different events.

A. Schematic diagram showing the place fields (A,B,C) of three simultaneously recorded cells in standard conditions (cells are represented in red, blue, and green).

B. In a remapping event, place cells display a new spatial specificity (place fields C,D,E). These modifications are independent from cell to cell and include a new shape and a new location of the place fields (Muller and Kubie, 1987, Colgin et al 2008).

C. In a rotation of the spatial representation (rotational remapping), all place fields are rotated by a similar angle compared to the preceding recording session (place fields A',B',C'). This event is characterized by a conservation of the place field shapes and the spatial relationships between place fields.

Interestingly, visual examination of the rate maps of the cells displaying a different field location between S1 and S2 suggested that numerous place cells underwent rotational remapping (Figure 57.B and Figure 58). To investigate this possibility, we first quantified place field shape similarity during instability events. To do so, we computed the correlation coefficient between S1 and S2 rate maps, corresponding to the rotation angle that maximizes the correlation (Figure 60). The correlation coefficients were calculated for consecutive sessions of the same cell (self-correlation) as well as for randomly chosen cells (random correlation). The mean self-correlation coefficient computed on place cells displaying instability between S1 and S2 was significantly higher than the mean random coefficient (Student t-test, t_{37}=3.974, p=0.0003). This indicates that during an instability event, the shapes of place fields were preserved between consecutive standard sessions.

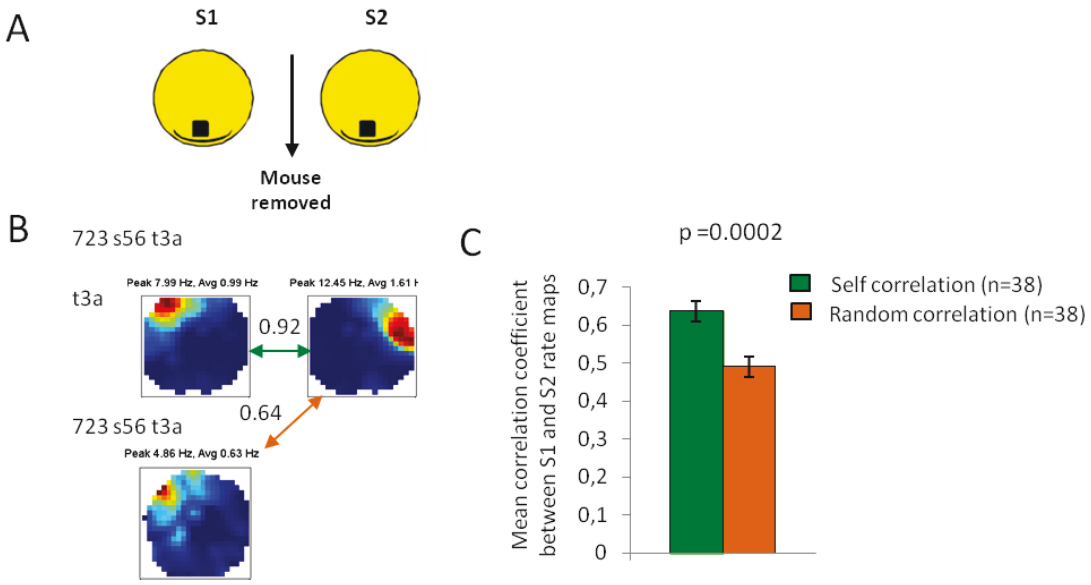

Figure 60. Place field shape is preserved during instability events in L7-PP2B mice.

A. Schematic representation of the recording conditions.

B. Color-coded rate maps showing two simultaneously recorded L7-PP2B place cells during two consecutive standard sessions. Place field shape similarity was obtained by the correlation coefficient between S1 and S2 and corresponding to the rotation that maximizes the correlation. The correlation coefficients were calculated for consecutive sessions of the same cell (unit t1a, self-correlation, green arrow) as well as for randomly chosen cells (unit t1a S2 compared to unit t3a S1, random correlation, orange arrow).

C. Mean place field shape similarity computed for consecutive sessions of the same cell (green) as well as for randomly chosen cells (orange). Student test, t_{37}=3.974, p=0.0003.

To further describe the remapping that occurs during instability events, we investigated the behavior of ensembles of simultaneously recorded place cells. We first computed for each place cell the rotation angle, i.e. the angle that maximized the correlation coefficient between S1 and S2 rate maps (see Figure 61.B,E,H). We then calculated the circular standard deviation of the mean rotation angle corresponding to each set of simultaneously recorded place cells. This circular standard deviation was then averaged over the experiments and compared to chance level by a permutation test. To do so, for each set of rotation angles, a corresponding set of angles was selected from shuffle data and used to compute a random standard deviation. This permutation procedure allowed to compute a mean random standard deviation and was repeated 100 times. Mean standard deviation computed on data falls into the extreme 2.5% of the distribution of random standard deviation (Figure 61.J), showing that it was indeed below chance level. This indicates that place field rotations in an ensemble of simultaneously recorded place cells occurred in a coherent manner. Thus, instability events observed in L7-PP2B mice correspond to rotational remapping of the whole spatial representation.

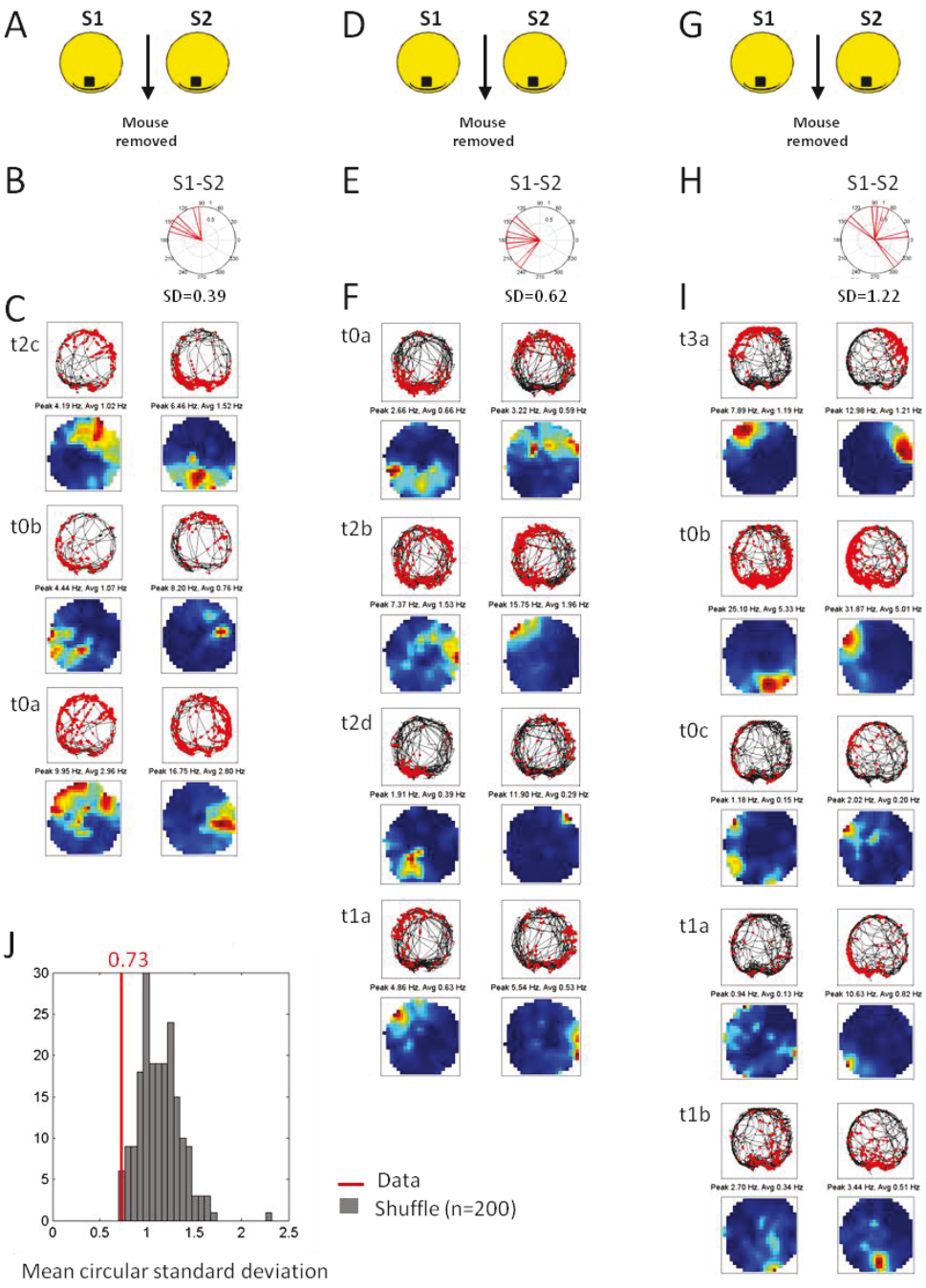

Figure 61. Place cells unstability of L7-PP2B mice is consistent in a given experiment.

A-I Three examples of experiments during which place field instability was observed between S1 and S2.

A. Schematic diagram of the recorded sessions.

B. Polar distribution of the rotation angles between S1 and S2 for all simultaneously recorded place cells. Circular standard deviation is plotted below each distribution.

C. Color-coded rate maps showing all simultaneously recorded place cells of the example.

D,E,F and G,H,I, same as A,B,C for examples 2 and 3.

J. Standard deviation of rotation angles has been computed for each experiment and for its paired shuffled set of rotation angles (shuffling procedure repeated 100times). Mean standard deviation computed on data is plotted in red and is compared to the distribution of mean standard deviation computed on shuffled data. Mean standard deviation computed on data falls into the extreme 2.5% of the distribution of shuffled values.

Therefore, in the standard sessions displaying instability, the spatial relationships between the spatial representation of the mouse and the cue (which is always at the same position in the arena), were modified. Previous studies showed that a spatial rearrangement of objects in the recording arena was accompanied by an increased exploration of the object (Ennaceur et al., 2005; Lenck-Santini et al., 2005). Since place cells are thought to underlie the navigational function of hippocampus, we wondered if the new position of the place fields relative to the cue could be interpreted by the mice as a change in cue position. In such case, it would result in an increase of cue investigation. Mice behavior was analyzed during the two first minutes of the recording session to avoid a diluting effect of the 12-minute session. To detect a difference between sessions S1 and S2 and take into account inter-subject variability, we computed a ratio between the values obtained for session S2 and those obtained for the preceding session S1.

In a general way, during experiments displaying instability, L7-PP2B mice were closer to the object in session 2 compared to session 1 (as shown by the mean distance ratio lower than 1, Student t-test, t_{11}= -3.163, p=0.009,Figure 62.D) whereas this was not the case for the same mice during classic sessions (mean distance ratio compared to 1, Student t-test, t_{35}=0.549, p=0.587). Similarly, during experiments displaying instability L7-PP2B mice spent more time and entered more often in the cue zone in session 2 compared to session 1 (Student t-test comparison to 1, percent of time in object zone ratio, t_{11}=2.816, p=0.017, entries in object zone ratio, t_{11}=2.319, p=0.040) but this was not observed during classic experiments (Student t-test comparison to 1, percent of time in object zone ratio, t_{35}=0.710, p=0.482, entries in object zone ratio, t_{35}=1.447, p=0.16). The comparison of ratio between classic sessions and sessions displaying instability also supports these observations (Figure 62.C,D,F, Mann-Whitney test, mean distance to the object, p=0.01, percent of time in object zone, p=0.01, entries in object zone, p=0.11). Conversely for the control zone, the ratio of percent of time and entries tend to be lower in sessions displaying instability compared to classic sessions (Figure 62.E,G, Mann-Whitney test, percent of time in control zone, p=0.09, entries in control zone, p=0.08). All these parameters show that during sessions displaying spatial representation rotation, L7-PP2B mice displayed an increase of the object-oriented behavior.

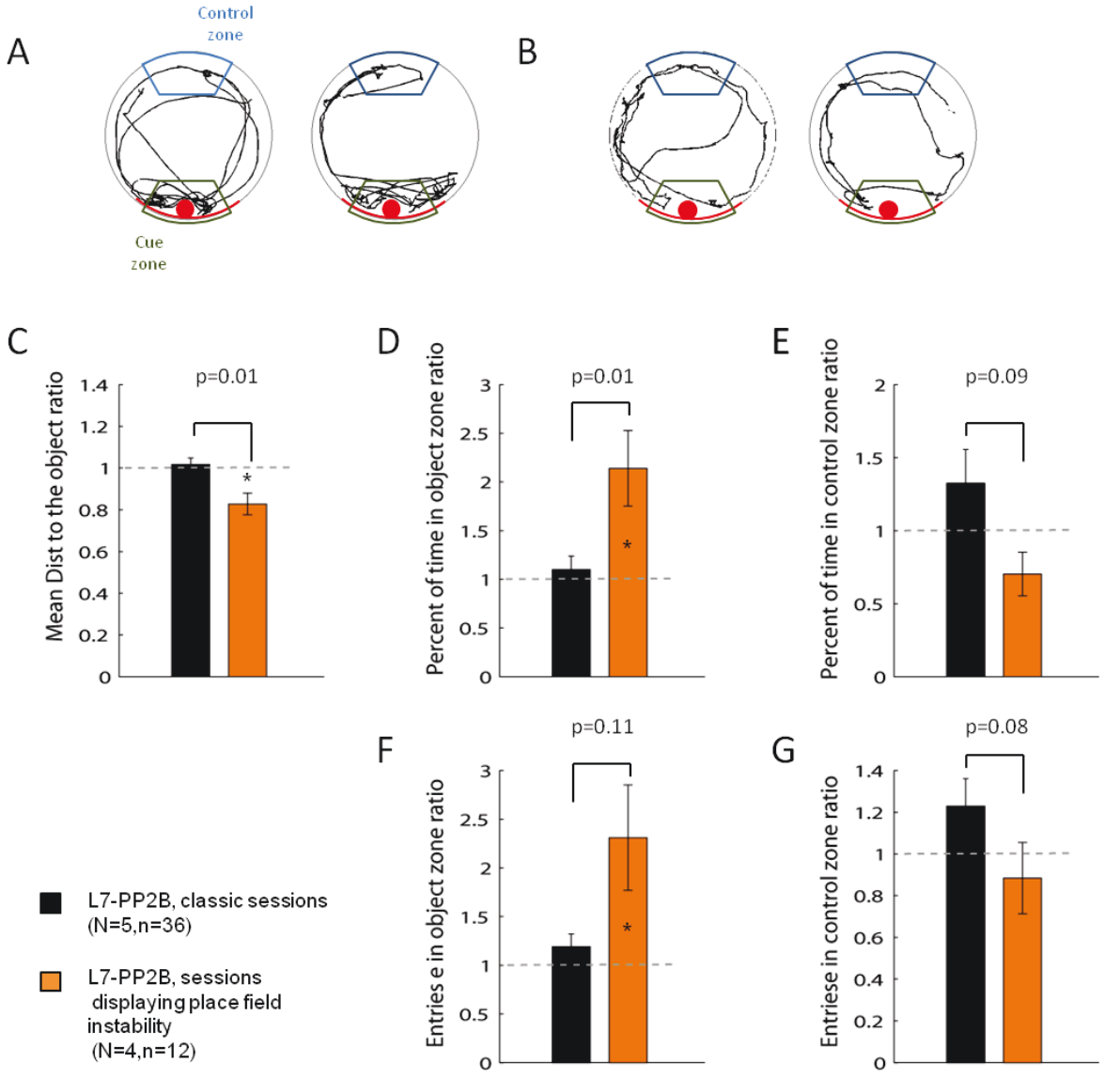

Figure 62. Rotations of the spatial representation are associated with an increase of the object-oriented behavior.

A. Representative examples of track during the first 2 min of a session displaying instability. The object zone is used in the analysis of the tracks to quantify the behavior relative to the object cue. The control zone, a zone of the same area on the opposite side of the arena, allows to control for the specificity of the object-related behavior.

B. Representative examples of track during the first 2 min of a classic session from the same mouse.

C-G. Parameters computed on the mouse track during the two first minutes of exploration. The ratio between the values obtained for session S2 and those obtained for the preceding session S1 are plotted. These ratio are compared to 1 by a one sample t-test. *p<0.05. Mann-Whitney tests were used to compare the ratio of classic sessions to sessions displaying place field instability (p value are indicated).

C. Mean distance to the object, p=0.01. D. Percent of time spent in the object zone p=0.01. E. Percent of time spent in the control zone. p=0.09. F. Latency to enter the object zone, p=0.11. G. Number of entries in the object zone, normalized by the traveled distance, p=0.11. H. Number of entries in the control zone, normalized by the traveled distance p=0.08.

DISCUSSION

This study aimed at understanding the contribution of parallel fiber –Purkinje cell (PF-PC) LTP to the different processes involved in spatial navigation. For this, we analyzed the consequences of an absence of such plasticity by characterizing L7-PP2B mice, specifically impaired for PF-PC LTP, in various spatial navigation paradigms. First and foremost, L7-PP2B mice do not display any basic motor deficit in the broad range of motor tasks in which they were tested. However, they presented a motor adaptation deficit on the rotarod task as well as defects in trajectory optimization, revealed in the aquatic Y-maze task. In spite of these moderate alterations, spatial learning of L7-PP2B mice was not impaired in the watermaze task. The characterization of their hippocampal place cell properties during exploration of a circular arena showed no impairment when mice had to rely on self-motion cues. But surprisingly, L7-PP2B place cells displayed instability in the absence of any cue manipulation in 23 % of the recording sessions. This instability was unpredictable and characterized each time by a coherent angular rotation of the whole set of recorded place cells. This work confirmed the involvement of cerebellar plasticity in the building of a spatial representation and suggests that the absence of LTP specifically affects the stability of this representation.

1 COMPARATIVE STUDY WITH L7-PKCI

1.1 BEHAVIORAL RESULTS

1.1.1 OPTIMIZATION DEFICIT IN THE Y MAZE

In the Y-maze task, the control mice followed the same trajectory in the maze with a high degree of reproducibility from trial to trial. This observation inspired the analysis we made regarding the deviation to individual mean trajectory. In this approach, the mean trajectory per individual mouse is considered as a biological optimal trajectory. An alternative way of estimating an optimal trajectory could have been through the calculation of a theoretical optimal trajectory, taking into account the speed and acceleration of the mouse at defined points in the maze (departure, intersection, arrival) (Hogans and Flash, 1985). However, the relevance of the theoretically estimated trajectory is not easy to evaluate. For example, this method is based on the assumption that an optimal trajectory is as smooth as possible, but this is not necessarily the case. Additionally, by computing the mean trajectory of each individual, our method takes into account the possibility that each mouse has its own optimal trajectory, i.e. it does not supposes that trajectories of all mice progressively converge to one single efficient trajectory (a global optimal). The variety of final trajectories across control mice argue for such an approach. Besides, this parameter of deviation to mean trajectory overcomes the drawbacks of the body rotation parameter, which highly correlates with the swimming speed of the mice. It can thus be used only in the absence of swimming speed differences between mutant and control as it was the case in

the study with L7-PKCI mice that lack cerebellar LTD Since L7-PP2B mice have a significantly lower swimming speed (in contrast to the L7-PKCI mice), this parameter was thus non-appropriated to evaluate trajectory optimization.

L7-PP2B mice displayed an impaired ability to reliably reproduce their own trajectories toward the platform, as shown by a higher deviation to their mean trajectory compared to the controls (Figure 50). As the impairment of trajectory optimization in L7-PP2B mice was observed in both the conditioned and yoked versions of the task, it is not linked to the learning of a conditioned response to a stimulus. Consistently, in the conditioning task, the attempts to correlate the reduction of deviation to mean trajectory with the learning of the task revealed that the correlation of this parameter with the percentage of correct responses (the knowledge of the rule) was lower than the correlation of this parameter with the number of sessions (the course of training). This suggested that the progressively reduced dispersion of trajectories was rather due to the repetition of the trajectory in the maze than to the learning of the task's rule.

On the opposite, our results show that the learning of the associative rule was not affected in L7-PP2B mice, similarly to L7-PKCI mice. Previous studies in T-mazes have shown that cerebellar lesions of the interposed nuclei did not prevent the ability to associate cues with a reward (Callu et al., 2013), but altered the formation of habits (Callu et al., 2007). Could the deficit in trajectory optimization be related to an impaired automation of the task? The percentage of correct responses reached a plateau, suggesting that the stimulus-response association have been automated; however, habit formation has not been specifically tested in our task (it would require for example outcome devaluation experiment). Besides, since the deficit in trajectory optimization was present from the beginning of the task (thus including the acquisition phase) and was not modified in amplitude over training, it is unlikely that it corresponds to a deficit of habit formation and is rather probably related to the motor adaptation deficit revealed on the rotarod.

Thus, L7-PP2B mice may have a subtle motor deficit that would not affect their basic motor performances but would be unraveled under high-demanding conditions. This is consistent with the findings of previous studies which showed that L7-PP2B mice are not ataxic (Schonewille et al., 2010) but present altered performances on the rotarod (Galliano et al., 2013). Accordingly, their lower swimming speed in the watermaze could be related to their motor deficit and fit this interpretation. The reading of the trajectory optimization deficit in L7-PP2B mice as a consequence of a motor related impairment is in accordance with the long standing view of the cerebellar involvement in motor control.

1.1.2 ABSENCE OF SPATIAL NAVIGATION DEFICIT IN THE WATERMAZE?

L7-PP2B mice did not show any significant deficit in their spatial learning abilities in the watermaze. It has to be noted that all experiments were carried out in a different laboratory

than the one done with L7-PKCI. All attempts were made to reproduce the experimental protocols previously performed on the L7-PKCI mice, but we cannot totally rule out the possibility that some slightly different parameters have prevented us from detecting a deficit in L7-PP2B mice. In particular, the configuration of visual cues in the watermaze experiment was completely different and might have been easier to learn, thus decreasing the probability to observe deficient performers.

Nevertheless it can be noted that during the 3 phase training protocol (Figure 52, spatial phase) their mean distance to the platform tends to be higher than the controls, suggesting a less pertinent research area. This could be interpreted with regard to the trajectory optimization deficit in the Y-maze: if the trajectory is less efficiently controlled in L7-PP2B mice, it may delay their approach to the target, thus reducing the mean distance to the platform (which is averaged over the track). However, cautious should be taken since the task's constrains are very different: the Y-maze task allows the description of a stereotyped trajectory in a 10 cm corridor whereas the watermaze task involves trajectories expanding in a 160 cm diameter circular pool, which are never reproduced. Determining whether this subtle difference corresponds to a non-optimal behavior to reach the platform would probably require a larger group of subjects ($n \leq 12$ in each group). Interestingly this would parallel (to a lower extend) the deficit found in the L7-PKCI mice. Indeed L7-PKCI mice are deficient in the ability to find the platform in the watermaze, but not in the Starmaze, a complex maze in which the number of possible trajectories is reduced by the guiding alleys, suggesting a specific impairment in the production of optimal trajectories toward a goal (Burguière et al., 2005).

These results complement those from another study assessing the spatial performances of L7-PP2B mice in the watermaze, with a protocol including a short term memory component (Galliano et al., 2013). In this paradigm, mice were placed on the platform for 30s before each trial, as well as before the probe test. The other differences included (1) the ratio between the platform and pool surface area, which determines the difficulty of task (the ratio area $_{platform}$/area $_{pool}$ was 8.5‰ instead of 3.9‰ in our study) and (2) the training intensity (2 trials per day instead of 4 in our study). These differences are likely to counterbalance each other and control mice were able to learn the platform location in 7 days. In spite of these discrepancies in procedures, both studies agree on the absence of deficit in the spatial learning and spatial memory of L7-PP2B mice.

A complementary approach would be to test the spatial learning abilities of L7-PP2B mice in non aquatic paradigms. Indeed, L7-PP2B mice swim slower than their controls and the extent to which this impacts their capacity to gather information about the environment remains difficult to estimate. Previous work in the watermaze mentioned an inverted U-curve modulation of swimming speed over training, with a high speed during the exploration phase, a slower speed during the acquisition phase, and a increase of speed once the task is mastered (Verbitsky et al., 2004). On the opposite, in dry conditions, L7-PP2B mice did not

display any difference in their exploratory behavior compared to their controls (assessed by the mean running speed, the traveled distance and the number of rearing, Figure 49.A). Spatial learning abilities could be assessed in the radial maze task (Olton and Samuelson, 1976) or in the conditioned place preference task using intracranial self stimulation (De Witte and Gewiss, 1987; Carlezon and Chartoff, 2007). Since L7-PP2B mice did not present any locomotor deficit in dry paradigms, I expect them to perform these tasks as efficiently as their controls.

The absence of deficit of L7-PP2B mice in the watermaze in spite of the instabilities of their place cells in a familiar environment may seem surprising. Given that the spatial representation instabilities occurred in only 23% of the cases, this might be due to our inability to detect their consequences at the behavioral level. In fact, other genetically modified mouse models have been shown to display place cell alterations without any deficit in spatial memory in the watermaze task (Zamanillo et al., 1999; Reisel et al., 2002). Besides, the recording arena contains a single cue whereas the watermaze environment consists in a complex configuration of numerous visual cues that might help to stabilize the spatial representation. Lastly, it has been shown that place cell stability depended on the spatial demand of the task (Kentros et al., 2004): using several recording conditions ranging from free exploration to an operant place preference task requiring the use of visual information, they showed that long term stability of place fields increased with the degree of attentional demand. Thus, the need to find the platform might have contributed to the stability of the place cell representation and thus to the preserved performances of L7-PP2B mice in the watermaze.

1.2 PRESERVED HIPPOCAMPAL PLACE CELL PROPERTIES DURING CUE MANIPULATION

We characterized hippocampal place cell properties of L7-PP2B mice during free exploration of a circular arena. We run three protocols to manipulate the sensory information available to the mice and analyze their consequences on hippocampal spatial representation. In contrast to the results previously obtained in L7-PKCI mice, we did not find any deficit in L7-PP2B hippocampal place cell properties during cue manipulation.

During the protocol in which mice had to navigate in darkness in the absence of object, they had access to self-motion information but also to tactile information from the wall and odor cues left on the floor. A previous study using a very similar protocol demonstrated the importance of these olfactory cues (Save et al., 2000). Using a combination of light/dark and cleaning/no cleaning conditions, they showed that whatever were the light conditions, the place fields were unstable when the odors traces were removed (in the dark/cleaning and light/cleaning conditions) whereas they remained stable otherwise (in the dark/no cleaning and light/no cleaning conditions) (Figure 63). The authors suggested that self motion

information is not sufficient to maintain stable place field in the absence of olfactory information. On the other hand, the identical properties of place cells between the dark/no cleaning and light/no cleaning conditions suggested that the path integration system interacts with an olfactory-based representation to cope with the absence of visual cues.

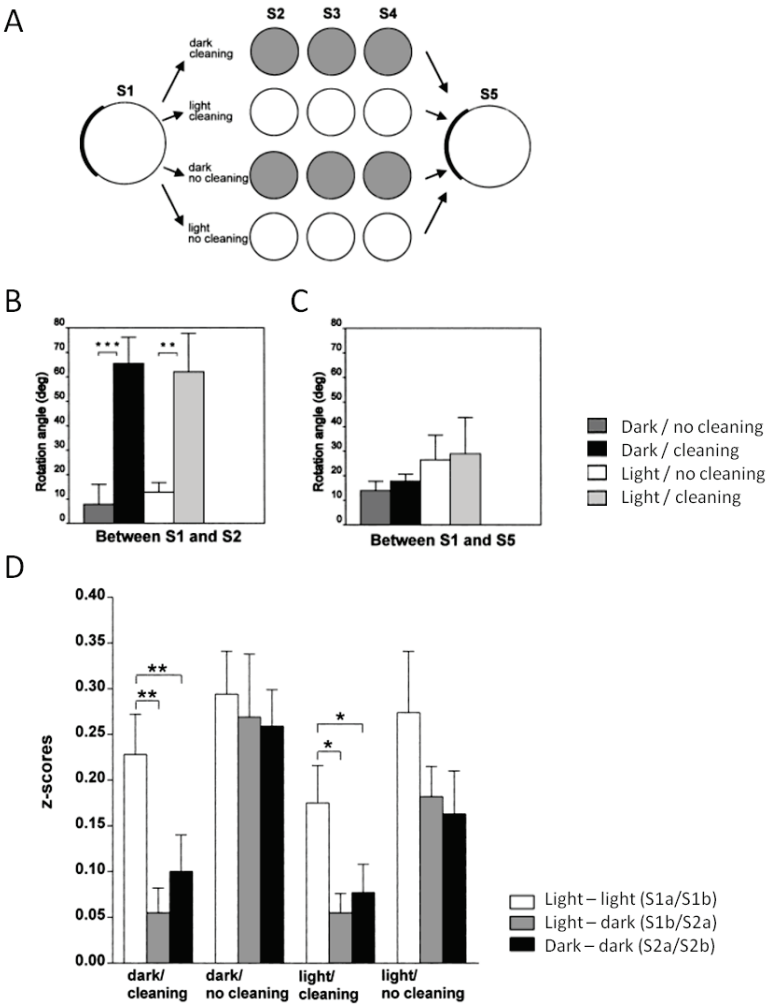

Figure 63. The role of odor cue during free exploration in the dark

A. Schematic representation of the four experimental conditions. Each circle represents the recording cylinder viewed from above. The cue card is shown as a thick curved line segment. The initial session (S1) was conducted with the lights on. Following S1, the cue card was removed and the lights were either turned off or left on and the floor was cleaned or left unchanged according to the experimental condition. The final session (S5) was a replication of S1.

B,C. Between-sessions rotation angles of the place fields in each condition, for two pairs of session: S1 and S2 (B), and S1 and S5 (C). **P F 0.01, ***P F 0.001 (unpaired two-tailed t-tests).

C. Z-scores of cross-correlations between pairs of firing rate arrays in each condition. These pairs were either two successive 8-min periods of a given session (S1a/S1b or S2a/S2b) or the last 8 min of S1 (S1b) and the first 8 min of S2 (S2a). The S1a/S1b correlation coefficient provides the reference measure for place field stability when no experimental manipulation occurs. *P F 0.05, **PF0.01 (paired two-tailed t-tests).

In our study, the comparison of the place properties between the Cue removal and the Dark only protocols adds some arguments to this hypothesis. In the Cue removal protocol,

place field stability, measured either within or between sessions, decreases in the dark but this is not observed in the Dark only (with object) protocol (Figure 54, Figure 55). This specific degradation of place field stability in the absence of object cue is consistent with the participation of the path integration system in the maintenance of place fields and with the use of the object to anchor the spatial representation. Indeed in a circular arena, a position can be referred as a distance from the center (or the walls) and an angle relative to a landmark. In the absence of object, information about the distance from the walls is available when the mouse touches the walls and can be estimated by path integration processes when running away from the walls. As the mouse touches the walls quite often, the accumulation of errors on this parameter is limited. On the opposite, the angular position has to be computed by path integration from a remembered position of the object, which is likely to accumulate errors over time. In the Dark only protocol, the contact of the object can be used to reset the estimation of the angular position, thus limiting the accumulation of errors on this parameter. These considerations underlie the fact that in spite of the presence of olfactory traces, our protocol is adapted to assess the influence of path integration system (and thus self-motion processing) in the maintenance of place fields in control and L7-PP2B mice.

Interestingly, these results are nicely paralleled by those of a simulation study, examining the maintenance of a cognitive map in darkness (Cheung et al., 2012). Modeling head direction signal (including its intrinsic noise), they showed that pure self motion information (path integration) cannot be used to maintain a stable spatial representation in the absence of visual information. However, combining it with boundary knowledge enabled place and grid cell stability over prolonged periods. Their results also indicate that place field stability is drastically higher in squared arena compared to a circular arena of the same area (Cheung et al., 2012). This could be explained by the presence of corners in the squared arena, providing punctual landmarks which discretize the boundaries (oppositely the continuous wall of the circular arena) and may serve a similar role as the object in our recording arena.

Thus, the place cell properties of L7-PP2B mice were similar to those of their controls in all points of the three protocols: place fields remained stable in the dark as well as during the conflict situation (Cue conflict protocol, S5). This suggests that, in contrast to the L7-PKCI mice, the place cell system of L7-PP2B mice might correctly use self-motion information to maintain stable place fields.

1.3 DISTINCT ROLES OF CEREBELLAR LTD AND LTP IN SPATIAL NAVIGATION?

This work aimed at testing a prediction of the adaptive filter model of the cerebellar circuit proposed by Dean and colleagues (Dean et al., 2010). In such model the input signal is transmitted to a range of independent modules, whose efficiency is individually adjusted through bidirectional plasticity (reciprocal LTP/LTD). According to this view, one could expect that disrupting bidirectional plasticity by suppressing either LTD or LTP would produce a similar alteration of the processing capacities of the cerebellar network and lead to comparable phenotypes in mice.

However, at the behavioral and physiological level, we did not observe the same impairments in mice lacking LTP and LTD. These findings suggest that altering LTP or LTD does not have the same consequences on cerebellar processing. This discrepancy between the phenotypes of L7-PP2B and L7-PKCI mice had been previously found in motor learning tasks such as the eyeblink conditioning and VOR adaptation. In these paradigms the L7-PP2B mice had a more pronounced phenotype than the L7-PKCI mice: they had impaired basic reflexes in the VOR task and altered performances on the rotarod, whereas both of which are preserved in L7-PKCI mice (De Zeeuw et al., 1998a; Schonewille et al., 2010). Based on the major cerebellar learning deficits of L7-PP2B mice, the authors proposed that the LTP would initiate new motor learning by potentiating synapses transmitting relevant inputs while the LTD would depress the synapses active in the pre-learning situation (likely to convey non-relevant inputs) (Schonewille et al., 2010). Indeed, since the vast majority of PF-PC synapses are silent (Szapiro and Barbour, 2007), the inability of increase synaptic efficiency ("waken" a synapse) might have more drastic consequences than the incapacity to decrease synaptic efficiency.

However, in the context of spatial navigation, L7-PP2B mice rather seem to display a milder deficit compared to L7-PKCI (they are not impaired for spatial learning and memory, and their self-motion processing is preserved). This does not fit with a prevalent role of LTP upon LTD in cerebellar information processing. To reconcile these data, one could also imagine that these processes depend on computations performed in different modules, among which PP2B involvement in LTP or PKC involvement in LTD is not homogeneous. Indeed, the zebrin stripes of the cerebellar cortex coincide with the expression patterns of numerous other molecular markers, corresponding to various molecular functions (Murase and Hayashi, 1996; Dehnes et al., 1998; Mateos et al., 2001). Some of them might be able to compensate for the absence of PP2B or PKC, leading to a differential alteration of LTP or LTD across modules. Another possibility is that information processing in these modules differentially relies on synaptic plasticities. Indeed, it has been shown that the firing properties of Purkinje cells varied among the cerebellar modules, in correlation with the expression of molecular markers. In particular, Purkinje cells in zebrin negative bands fire at a higher rate (simple spikes and complex spikes) than those of zebrin positive bands (Zhou et

al., 2014). The possibly different functioning of cerebellar modules might explain why L7-PP2B mice seem to have a more drastic deficit than L7-PKCI mice in motor learning but milder impairments in spatial navigation.

Nevertheless, in cases (motor learning and spatial navigation), L7-PKCI and L7-PP2B display a different phenotype, which does not seem to be consistent with the adaptive filter model of the cerebellar cortex.

Alternatively, the lack of similitude between L7-PKCI and L7-PP2B phenotypes could be due to a differential disruption of LTD or LTP in the two mouse models. This could result from a difference in the transgene expression in the two lines. This possibility should not be of major importance since both L7-PKCI (De Zeeuw et al., 1998a) and L7-Cre line (Barski et al., 2000) (used for the L7-PP2B creation) were constructed using the L7ΔAUG promoter (Smeyne et al., 1995). However, some differences cannot be completely excluded since the cloning procedures were performed independently, leading to different numbers of inserted copies of the transgene in the genome and various insertion sites, both of which being able to have a strong influence on the expression level of the inserted gene (this is particularly evidenced by the fact that the positive clones -containing the transgene- produced during the generation process of the transgenic line displayed variable degrees of transgene expression). This being said, in both lineages, the clones retained for the mouse line displayed a very high level of expression of the transgene in almost all Purkinje cells (De Zeeuw et al., 1998a; Barski et al., 2000) as well as a severe impairment of LTD or LTP induction in all recorded Purkinje cells (De Zeeuw et al., 1998a; Schonewille et al., 2010).

We also need to keep in mind that both L7-PKCI and L7-PP2B mice could show disruption of the other pathways downstream the PKC kinase or the PP2B phosphatase, non-related to synaptic plasticity. On the one hand, the PP2B inhibition also affects intrinsic plasticity, which is certainly a key parameter shaping Purkinje cell output (Belmeguenai et al., 2010). On the other hand, PKC signaling pathways are closely linked to the regulation of PC dendritic growth and its arborization during cerebellar development (Metzger and Kapfhammer, 2003). PKC could also modulate the efficacy of GABA receptors (at interneuron–Purkinje cell synapses) by influencing their surface density and sensitivity to positive allosteric modulators and/or by modifying chloride conductance (Song and Messing, 2005).

Surprisingly we found a specific deficit in the L7-PP2B mice regarding hippocampal spatial representation that was not observed in mice lacking cerebellar LTD. Indeed, L7-PP2B mice displayed an unstable spatial representation in a familiar environment, in the absence of any proximal cue manipulation. These results will be discussed in the next chapter.

2 ROTATIONAL REMAPPING

L7-PP2B mice displayed an unstable spatial representation in standard light conditions and in the absence of any proximal cue manipulation, in 23 % of the recording sessions. These events were characterized each time by a coherent angular rotation of the whole set of recorded place cells, associated with an increase of the object-oriented behavior.

2.1 COMMENTS ON WHAT WE OBSERVED

2.1.1 EXPERIMENTAL CONSIDERATIONS THAT MIGHT HAVE REDUCED OUR ABILITY TO RECORD THE INSTABILITY PHENOMENON

At first sight, 23 % of the recording sessions can seem a moderate percentage to sustain such a conclusion. Several observations argue that this percentage might be indeed under-estimated. First, as these instabilities were initially regarded as experimental artefacts preventing a correct analysis of the cue manipulation protocol, the recordings of two mice (801, 802, respectively displaying 55.5% and 37.5% of unstable experiments) were interrupted prematurely (9 and 8 protocols instead of 16 and 22 protocols for 832 and 723). Second, an additional mutant mouse was not included in the analyses because of a small discrepancy in the recording conditions: the black curtain surrounding the arena was hung from a square frame instead of circular frame in the rest of the recordings. Given that the curtain folds made the corners of the squared frame indistinguishable with human eyes, and that mice are known to have drastically lower visual acuity, this could be considered as a minor point. Additionally, in a 50-cm diameter arena with 30-cm high walls, the extra-arena visual cues barely fall in the mouse visual field. This mouse displayed 37.5% of unstable experiments, which would lead the group average from 23% to 25%. Last, for clarity these analyses were performed on instabilities observed on the two first standard sessions of each cue manipulation protocol (S1-S2 pairs, these two sessions being in all points identical between the three protocols), which represented 12 instability events. However, we also observed instabilities between the other pairs of standard sessions (S2-S5 in the Cue removal and Dark only protocols and S1-S4 in the Cue conflict protocol), leading the number of instability events from 12 to 19. Analyses taking into account these instabilities also found significant results for both the occurrence of instabilities and the behavioral correlate.

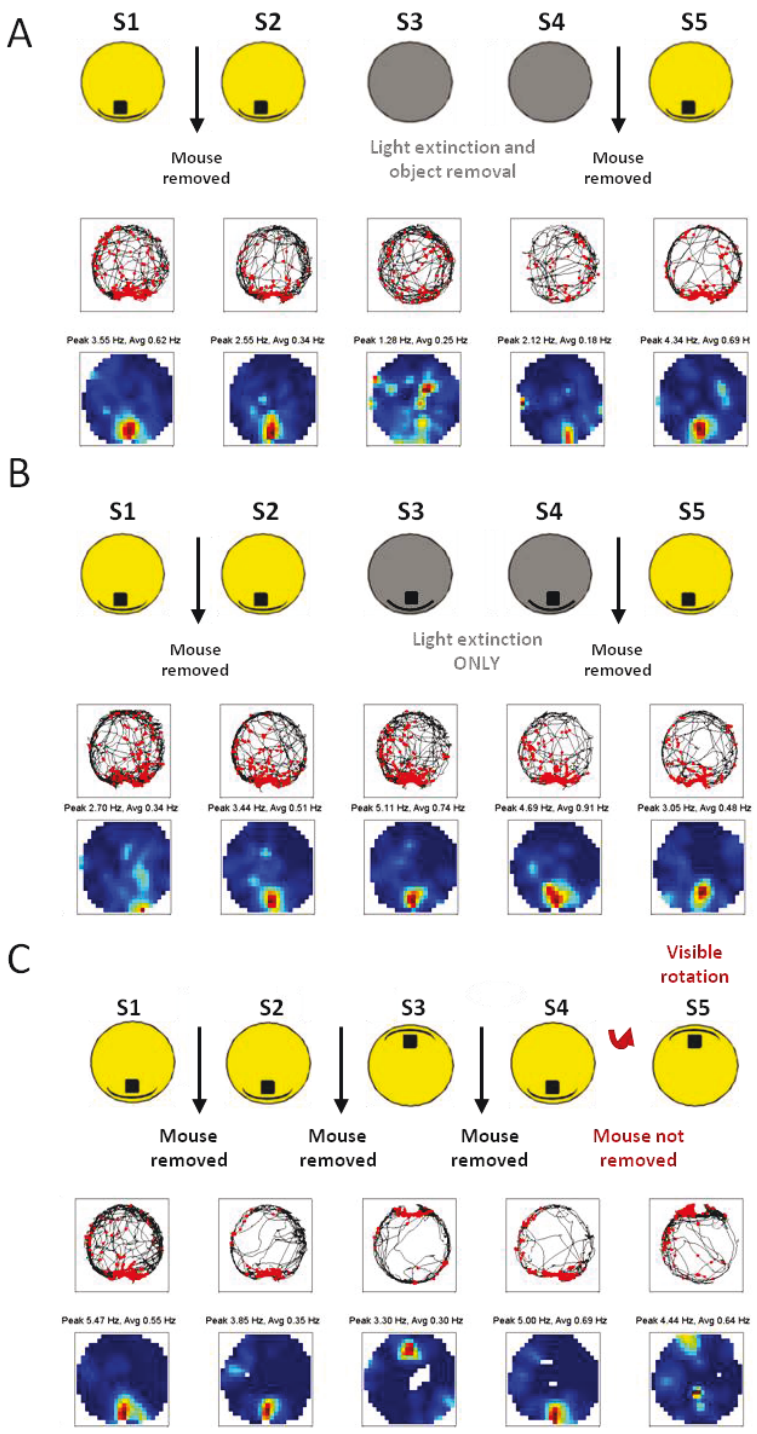

Figure 64. Responses of an object cell recorded in the 3 protocols.

A-C, Top. Schematic diagram of the 3 recording protocols: Cue removal (A), Dark only (B) and Cue conflict protocol (C).

A-C, Bottom. Color-coded rate maps showing the firing activity of unit t1a recorded in mouse 723 in session s61-65(A), s56-60 (B) and s66-70 (C); color coding ranges from blue (silent) to red (peak activity).

2.1.2 EXCEPTION OF CELLS CLOSE TO THE OBJECT

The analysis of instabilities as "event" was based on the observation that in most of the experiments, the percentage of unstable cell was either zero (stable experiment) or 100% (unstable experiment) (Figure 57. E). This statement suffers two interesting exceptions (mouse 723 sessions 56-57: 2/3 unstable cells, mouse 801, sessions 16-17: 3/5 unstable cells). Indeed, further examination of the place fields that failed to be detected as unstable (for which S1-S2 similarity coefficient was above 0.2) revealed that for 2 out 3 cells, the place fields were located very close to the object. The fact that these cells near the object did not rotate with the ensemble of the other recorded place cells but rather stayed stable in an object reference frame could be interpreted as the characteristics of object cells, as those recorded in the study of Rivard et al (2004). Indeed we had the opportunity to record one of these cells in the three protocols: its place field degraded in the dark, only when the object was removed (in Cue removal protocol but not in the Dark only protocol) and rotated with the object during the conflict protocol (Figure 64). The interpretation of these apparent discrepancies (percentage of unstable different from 0 or 100%) as the result of the presence object cells strengthens our approach at the level of event rather than at the level of cell.

2.1.3 INCREASED EXPLORATION OF THE OBJECT

During the instability events, the angular rotation of the whole set of recorded place cells led to a new position of the cue relative to the place fields. During these events, mice showed an increase of the object-oriented behavior, suggesting that the object was associated with novelty, as it would be the case if the object had been displaced (Ennaceur et al., 2005; Lenck-Santini et al., 2005). This enhanced exploration of the object was visible during the 2 first minutes but not over the 12 minutes, suggesting a diluting effect over the whole session. This is consistent with a novelty interpretation of this increased exploration, since the novelty associated to the apparent displacement should progressively fade away. Previous studies have evidenced the link between the modifications of place fields and the behavior of animals (Lenck-Santini et al., 2001, 2002; Kubie et al., 2007). Indeed, in the task of Kubie et al., the rat earned a food reward by pausing in a small unmarked goal zone in the circular arena. When the cues were shifted in the absence of the animal, the zones at which the animals stopped and waited for the reward were accurately predicted by the displacement of the place fields (the goal zone selection and the place fields were shifted by the same displacement vector) (Kubie et al., 2007). Thus, electrophysiological recordings and behavioral measurements converge to suggest that in a familiar environment the spatial representation of L7-PP2B mice is not reliably anchored to the proximal cue.

2.2 INTERPRETATION OF THESE INSTABILITIES

These instabilities were very similar to those observed in the study of Renaudineau et al. (2009). In mutant mice lacking zif-268, a gene involved in maintenance of the late phases of hippocampal LTP and consolidation of spatial memories (Jones et al., 2001; Bozon et al., 2003), exposure to a novel environment induced rotational remapping when mice returned to the familiar environment. The authors proposed that since the formation of a new representation in the novel environment occurred shortly after exposure to the familiar environment, it may destabilize the previously consolidated representation, rendering it labile (or malleable) and vulnerable to interference. In our case, animals never experienced another environment than the circular arena, suggesting that their spatial representation might be unstable even in the absence of any competing representation. It may be interesting to investigate in these mice the formation of representations of different environments and their possible interactions.

2.2.1 DOES IT REVEAL A TENDENCY TO MISTRUST THE OBJECT?

The observation of spatial representation rotations relative to the arena cue raises questions over the stability of the object salience for the animal across trials. Previous studies showed that the influence of visual cues on place fields orientation depended on the previous experience of the animals (Jeffery, 1998; Jeffery and O'Keefe, 1999). In these works, rats were recorded in squared symmetrical arena containing a single salient cue which was rotated either in sight or out-of-sight of the rat. Two groups of rats underwent both manipulations in a different sequence. In the group of rats first submitted to cue rotations out-of-sight of the animal the place fields were mostly oriented by the visual cue (Figure 65). In contrast, in the group of rats which initially saw the cue to be mobile (in-sight rotations), the place fields ceased following the cue and became oriented by the self-motion cue instead (Figure 65) even for the cue rotation that occurred out-of-sight of the animal. This suggests that rats had learned that the visual cue was unreliable. Could such a phenomenon explain the rotational remapping observed in L7-PP2B?

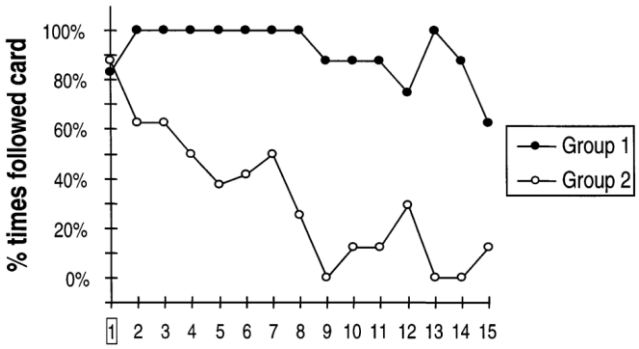

Figure 65. Behavior of place fields from the two groups of rats for all 60 mismatch trials (15 sessions of four trials), in which directional information conveyed by the cue card conflicted with the idiothetic cues. Percentage of trials in which the fields followed the card. Group 1 rats were first submitted to cue rotations out-of-sight of the animal whereas Group 2 rats were first submitted to cue rotations in-sight of the animal. Fields in both groups began by following the card almost all of the time. For Group 1 rats, fields continued to follow the card predominantly, while for Group 2 rats, control of the fields by the card became weakened. (Jeffery 1998)

In our experimental design all types of protocol (Cue removal, Dark Only, Cue conflict) were intermingled. A possibility would have been that the repeated experience of cue rotation in sight of the animal in the cue conflict protocol lead the mice to judge the visual cue as unreliable and to use other cues to anchor their representation. However, in our study, we observed instability events that happen even before any cue conflict experience (Figure 66, mouse 801,802). Moreover these unstable events did not show any tendency to occur more frequently with time (Figure 66). Even if the amount of available data does not suffice to bring a definitive conclusion, the observed rotational remapping might not be explained by a progressive mistrust of the object. This tendency to prefer another type of cue seems rather to be an intrinsic behavior of L7-PP2B mice. Importantly, the type of cue that L7-PP2B mice might use to orient their spatial representation during these events remains an open question. The experiment was designed so that the mice use the object as a single cue and everything was made to minimize the extra-maze, but we cannot exclude that L7-PP2B mice used another type of uncontrolled cue.

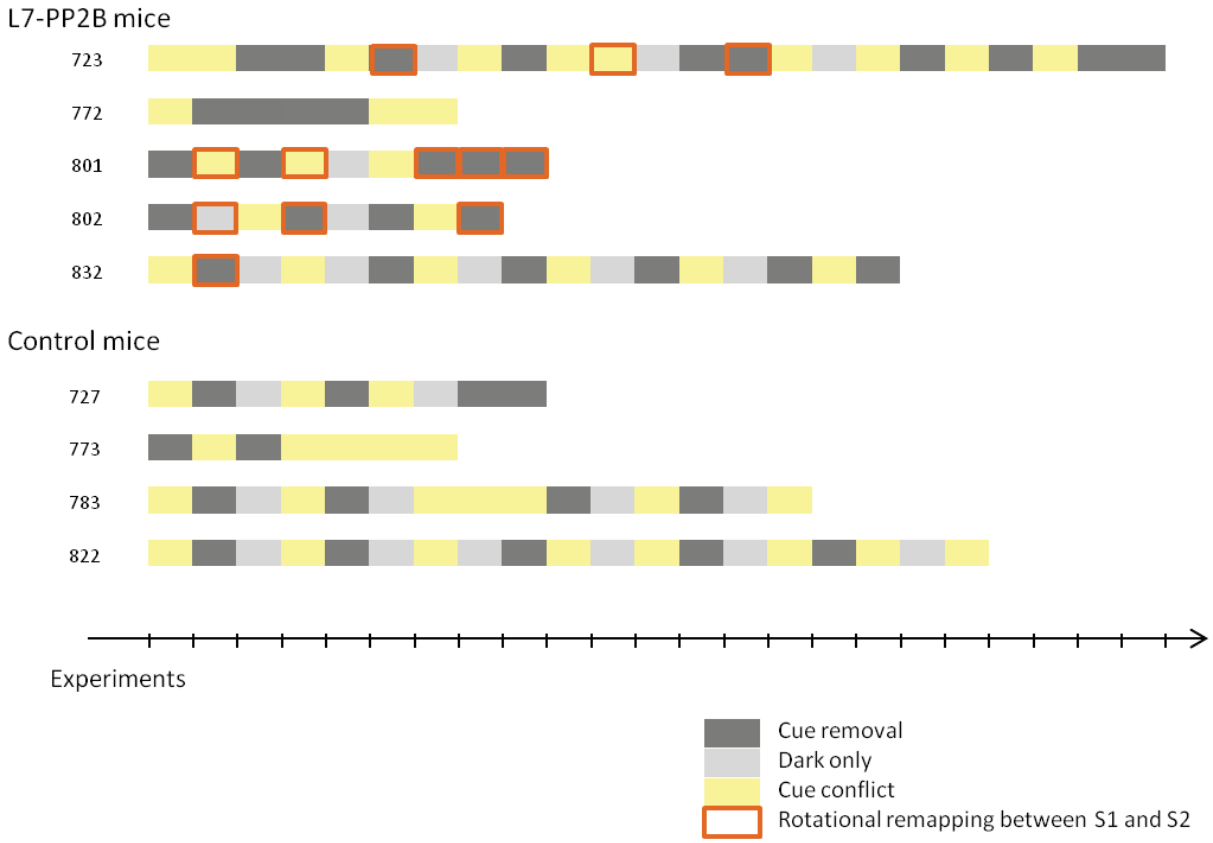

Figure 66. Temporal distribution of rotational remapping events
Schematic representation of the successive protocols underwent by each L7-PP2B (top) and control (bottom) mouse. The type of protocol is color-coded: Cue removal (dark grey), Dark only (light grey), Cue conflict (yellow). The occurrence of rotational remapping is indicated by orange squares.

2.2.2 AN IMPAIRED TACTILE DISCRIMINATION OF THE OBJECT?

Could this deficit of object based orientation be due to a deficiency in the processing of tactile cue related information? Indeed, in the absence of other cues, tactile information has been showed to exert a strong control over place fields (Gener et al., 2013). In an enriched tactile environment, the rotation of the tactile cues triggers an equivalent rotation of 90% of the place fields. Moreover, following tactile deprivation (tactile transmission was blocked by means of lidocaine applied on the whisker pad), the majority of place cells decreased their firing rate and their place fields expanded (Gener et al., 2013). Importantly, Rhamati et al (2014) reported a default of whisker-based object localization in L7-PP2B mice. Indeed, on a go-no go paradigm, mice learned to localize an object with their whiskers, and based upon this location they were trained to lick within a particular period ("go" trial) or refrain from licking ("no-go" trial). L7-PP2B mice were severely impaired in learning this task: fewer L7-PP2B mice were able to learn the task (6 out of 14 against 14 out of 16 for their controls) and those that eventually learned the task were slower in learning (Rahmati et al., 2014). A possible interpretation of the place field rotational remapping observed in our study is that

an altered processing of tactile cue related information renders difficult its use as landmark; or that a noisy representation of the cue impairs the integration of tactile information with other sensory cues, thus the decrease of the cue reliability would lead the animals to ignore or mistrust it to orient themselves.

However, several observations argue against this interpretation. First, in the object localization task of Rhamati et al. (2014), the object consisted in a 1mm bar which was moved horizontally and vertically to reach different positions relative to the whiskers. In the go trials the bar was inside the whisker field whereas in the no-go trials the bar was outside the field during resting period but could be reached during active whisking. Mice had thus to discriminate between two positions spaced by about 1cm. L7-PP2B mice were impaired in such discrimination but not in the preliminary associative task in which the mere detection of the bar (whose location did not vary) predicted the reward. Thus, the precise localization but not the detection of the bar was impaired in L7-PP2B mice. Moreover, in our recording arena, the cue was composed of a 6 cm diameter cylinder and a 29 cm large card. The scale of the tactile stimuli to take into account exceeds by one order of magnitude those of Rahmati's study. Consequently, in addition to the visual cues which were available in the standard light conditions, the localization of the proximal cue is likely to rely on other sensory modalities than pure whisking, such as distance estimation by the path integration system. Besides, we considered a session as unstable if the position of the place fields relative to the cue were modified by an angle superior to 30°, that is to say a distance of 13 cm at the periphery of the arena. Such a large discrepancy is unlikely to be explained by a deficiency in whisker-based object localization.

Further investigation of the role of object tactile information in the orientation of the spatial representation could be made by the analysis of the temporal course of the sessions displaying instability. Is the location of the place field immediately settled when the mouse is put into the arena? Or does it require several minutes to decide which cue to favor to orient its spatial map? Computing the firing rate map on a minute-by-minute basis could allow to answer this question. Specifically, we could see if the rate map computed on the time window preceding the first contact of the object is different from the map computed thereafter. This could provide some clues about the potential use of tactile cue information in the orientation of the map. However, since the mice approach the object within the first 30secondes on average, the low level of sampling (it is likely that many pixels of the map would not be covered within 30 sec) might fail to give a definitive answer to this question.

2.2.3 AN ALTERATION OF ATTENTION TO SPATIAL CUES?

Could this deficit of object based orientation be due to an altered attention? Indeed, cerebellar activation in fMRI has been reported during a visual attention task in humans (Allen, 1997). Besides, attention enhances the stability and retrieval of visuo-spatial representations in the hippocampus (Kentros et al., 2004; Muzzio et al., 2009). In the study

of Muzzio and colleagues, rats were trained in two different paradigms requiring them to pay attention to the configuration of visual cues or to olfactory cues. The place cells were shown to display an increased short term and long term stability in the visuospatial task but in contrast their stability was compromised in the odor-based task (Muzzio et al., 2009) . Could an altered attentional modulation of place cells explain the rotational remapping observed in L7-PP2B mice? This hypothesis is not straightforward since in our paradigm there is no specific task to learn, mice are not required to pay attention to any type of cue. Besides, attention is suggested to modulate the extra-field firing activity of place cells (called over dispersion) rather than its spatial location (Fenton et al., 2010).

2.2.4 A POTENTIAL EXPLANATION: THE EXPERIMENTER AS A DISTANT CUE?

What other cue could be used by the mice to orient their spatial map? We can exclude the hypothesis that L7-PP2B mice used their initial location in the arena to orient their spatial representation since the mice were always placed inside the arena next to the object, facing it. Thus, their initial orientation was very similar across session and could not explain the various rotation angles we observed. Besides, the possibility that they used the side by which they entered the recording chamber is relatively unlikely since mice carried wrapped in towel, preventing them from seeing the environment. Additionally, before putting the mouse inside the arena, the experimenter performed one rotation to mildly disorient the animal.

An alternative is that the experimenter was sometimes used as an external cue to initially orient the map. Indeed, in order to avoid the experimenter position to be encoded in the environment at the beginning of exploration, his position was randomly changed from one session to the other. In particular, the experimenter could approach the arena by two openings in the curtain diametrically opposed, and the opening used was systematically different between S1 and S2. Thus even if the presence of the experimenter was a brief cue (a few seconds) compared to the 12-minute session, it was the only controlled parameter that reliably changed between the two standard light sessions. Moreover, as the animals were manipulated every day during weeks (up to 2 months), the experimenter might have a strong significance for the animal (at least more than a distal uncontrolled cue).

Qualitative recordings of the experimenter position have been done and this will allow a correlation analysis to test this hypothesis. Further experiments using combination of distal and proximal cue manipulation could be performed to investigate the relative contribution of these different types of cues in orienting the spatial representation in L7-PP2B mice.

2.2.5 AN ALTERED INTEGRATION OF SELF MOTION AND PROXIMAL CUE INFORMATION IN THE POSTERIOR PARIETAL CORTEX?

Interestingly, the cerebellum has been shown to project to the posterior parietal cortex (PPC), an area thought to be involved in proximal cue information processing for spatial representation (Save and Poucet, 2009). This disynaptic pathway, from the cerebellar nuclei to the parietal cortex, via the central and ventro-lateral thalamic nuclei has been demonstrated in primates (Amino et al., 2001; Clower et al., 2001; Prevosto et al., 2010) and in rats (Giannetti and Molinari, 2002).

The role of PPC has been studied by examining the consequences of lesions in various navigation tasks. Kolb and colleagues observed that rats with PPC lesions were able to learn the general location of the platform by using room cues but had difficulties in adjusting their movement toward the goal (Kolb and Walkey, 1987; Kolb et al., 1994). They suggested that the PPC would serve to orient the body toward points in space. An alternative is that the PPC participates in the building of the spatial map, by integrating self-motion information and local feature of the environment. Indeed, in another study, rats were trained in different versions of the watermaze task: they had to find a platform based on the configuration of distal cues, or on the configuration of proximal objects placed directly in the pool, or using a single cue placed on the top of the platform (Save and Poucet, 2000). PPC lesioned rats were only impaired in the paradigm using the configuration of proximal cues, suggesting that the PPC is involved in the formation of a spatial representation based on proximal objects.

Similar results were found in an object recognition paradigm (Save et al., 1992). Following several exploration sessions of an arena containing a constant configuration of objects, two objects were displaced. In control animals, such a manipulation induced a renewal of exploration specifically directed toward the displaced objects, suggesting that the animals has formed a representation of the objects configuration and detected novelty associated to the spatial change of objects. PPC lesioned rats did not display such behavior. In contrast, the replacement of one object by a novel object induced a similar renewal of exploration in both groups indicating that PPC lesioned rats were not impaired in object recognition but specifically in the discrimination of their spatial configuration. These findings strengthen the idea that PPC lesioned rats were impaired in elaborating a spatial representation on the basis of the object configuration.

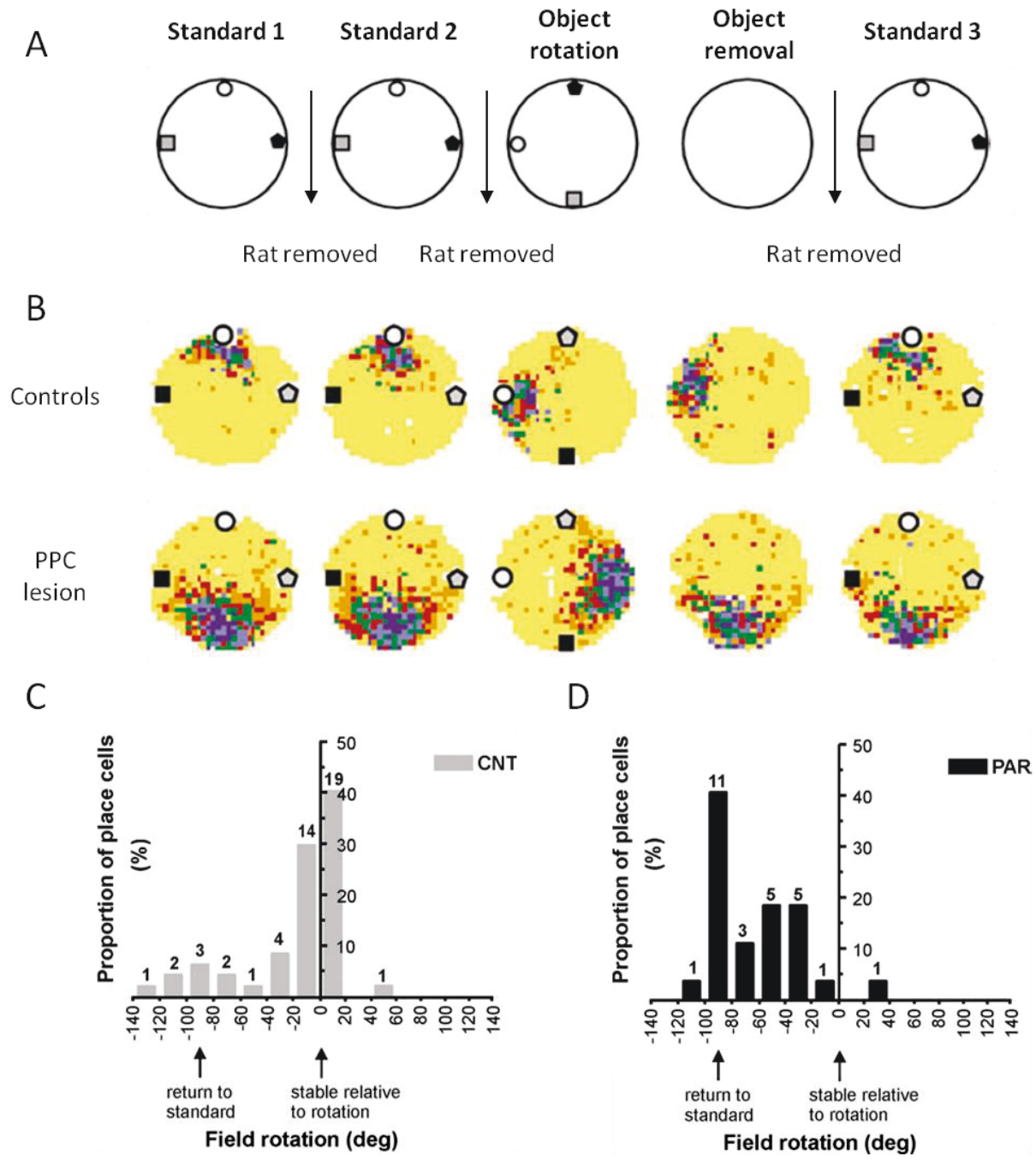

Figure 67. Hippocampal place cell properties following PPC lesions

A. Schematic representation of the protocol. Five successive 16-min recording sessions were run. Between sessions, the rat was removed from the cylinder and the floor was cleaned, except between Object rotation and Object removal sessions

B. Representative examples of firing rate maps in control and parietal rats in a recording sequence. In control rats, most place fields remained stable relative to the rotation session. Note that only one cell in parietal rats was found to display such a response. In parietal rats, most place fields shifted back to their initial location (Object removal = Standard 2).

C-D. Distribution of place field rotations grouped in 20 bins after Object removal in (C) control (n = 47 place cells) and (D) parietal (n = 27 place cells) rats. Cell numbers are displayed above each bar.

(Save et al. 2005)

Further arguments for this hypothesis come from the analysis of hippocampal place cells activity following PPC lesions. Place cells were recorded in PPC lesioned rats as the animals performed a pellet chasing task in a circular arena containing three objects, the room cues being masked by a circular curtain surrounding the arena (Figure 67.A) (Save et al., 2005). 90° rotation of the three objects in the absence of the animal led to a consistent rotation of all place fields in controls animals (Figure 67.B). In PPC lesioned animals, half of the place fields did not rotate with the object but remained stable in the room reference frame, suggesting that they were controlled by background cues (Figure 67.B). In the subsequent session, the removal of the objects did not disrupt the place fields in control animals, which remained stable relative to the preceding session (Figure 67.B-C). In contrast, the analysis of the place fields which had rotated with the objects in PPC lesioned animals revealed that these place fields returned to their initial location at the object removal (Figure 67.B,D), bolstering the hypothesis of a control by extra-maze cues. The authors proposed that because PPC lesioned rats were unable to properly use proximal objects, place cells eventually used non controlled background cues (Save et al., 2005).

A series of studies also proposed a role of PPC in egocentric information processing. Indeed, in a paradigm where rats were trained in the watermaze to reach a platform from in a fixed position in darkness, lesioning the PPC resulted in the inability to orient the trajectories toward the platform, indicating a role of PPC in self-motion processing (Save and Moghaddam, 1996). Similar deficits were found in a homing task, where rats had to explore a large circular platform to find a hidden piece of food and carry it back to the refuge in the absence of any external cues. Rats with parietal lesions were unable to perform straight trajectories to the refuge, suggesting a path integration deficit (Save et al., 2001; Parron and Save, 2004).

These data suggest a role of PPC in processing both allocentric and self-motion information. Actually, a basic function of PPC could be to combine visuo-spatial and self-motion information. It has been suggested that the formation of a spatial map required the integration of local views of the environment with movements connecting these views (Poucet, 1993; Poucet and Benhamou, 1997). This is particularly needed with proximal cues which can produce different views depending on the animal's position relative to the proximal cues (in contrast to the distal cues which give relatively similar visual information from all points of the apparatus).

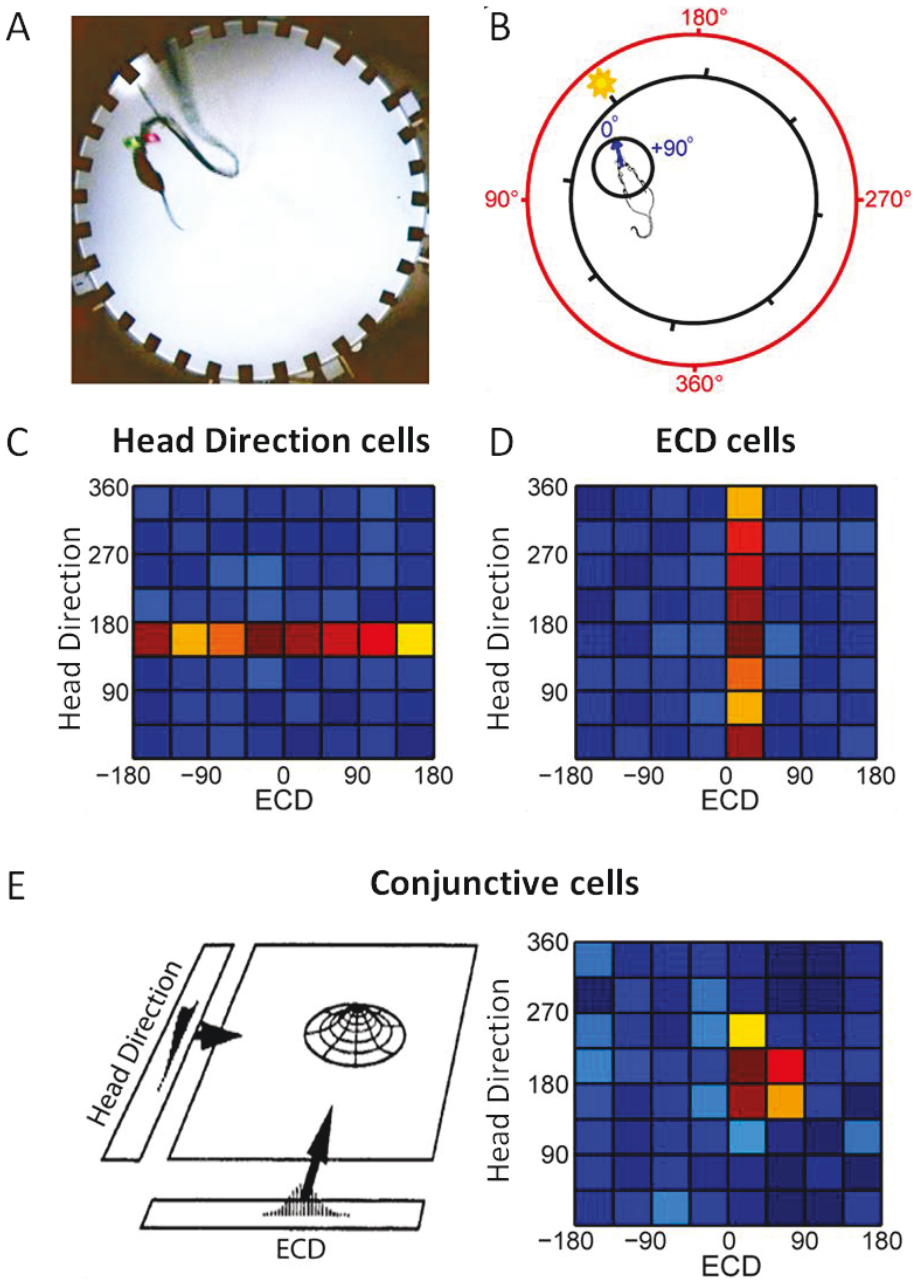

Figure 68. Egocentric Cue Direction (ECD) cells in the posterior parietal cortex

A. Apparatus. Rats are trained to run a random spatial sequence to 32 light locations. This task requires the rat to cover the full range of headings and ECDs at a wide range of spatial locations.

B. Schematic of ECD and head direction for the same video frame. In this example, the ECD (blue) is approximately 10° and the head direction (red) is 160°.

C-D, Color-coded plots (firing rate per 45° of ECD and head direction) for an ideal head direction-only cell (C; horizontal band of high activity spans range of ECDs) and for an ideal ECD-only cell (D; band of high activity spanning range of head directions).

(blue: minimum firing rate, red : maximum firing rate)

D, Left, Head direction and ECD units could combine to produce units which would encode a specific combination of both reference frames (adapted from McNaughton et al., 1995). Right, Color-coded plot of an ideal conjunctive cell. Conjunctive cells encode neither head direction nor ECD but a specific combination of these two reference frames.

(Wilber et al. 2014)

Interestingly a recent study evidenced neuro-correlates of cue position in the PPC that could fulfill such a function (Wilber et al., 2014). This study demonstrated that neurons in the PPC encode cue orientation in an egocentric reference frame (Figure 68). To do so, rats were trained in a large circular platform with 32 light cues evenly distributed around the perimeter (Figure 68.A). All the lights were off and when one lit on, the rat had to approach this cue to receive a reward. All the light cues were successively switched on in a random order. This task required the rat to cover the full range of heading (the orientation of the head in an allocentric reference frame) at a wide range of spatial location. The rats also cover the full range of egocentric cue direction (ECD, i.e. the relative orientation of the head and the object). In the example, heading is ~160° (North Est) whereas ECD is ~10° (about in face of the animal) (Figure 68.B). This study showed that 10 % of PPC cells encode cue direction, 4% encode heading, and 9% are conjunctive cells i.e. cells modulated by both heading and ECD, which fire for a specific combination of cue and head direction (Wilber et al., 2014). For example, a conjunctive cell fires when the animal points its head to the north and has the object on the right (Figure 68.E). Additionally most of these cells are modulated by self-motion, that is to say that their responses are increased when the animal concomitantly displaces in a specific direction (Wilber et al., 2014). These cells encoding the egocentric position of the cue might be responsible for impaired orientation toward the goal that is observed following PPC lesion (Kolb et al., 1994; Save and Poucet, 2000).

This work underlies the fact that visual and self-motion information interact in the parietal cortex. It also emphasizes that cue direction is encoded in an egocentric reference frame. This could underpin the participation of the parietal cortex in the integration of external and self-motion information to build the spatial representation. Indeed the parietal cortex could send information to the hippocampus via the retrosplenial cortex and the entorhinal cortex: the retrosplenial cortex receive dense projections from the parietal cortex (Reep et al., 1994) and projects to the entorhinal cortex (Jones and Witter, 2007).

These findings bring another perspective to our results. Based on the inappropriate anchoring of the spatial representation to the proximal cue in mice lacking PF-PC LTP, we could speculate that an altered processing of self-motion information in the cerebellum (in particular an incorrect change of reference frame of vestibular signals) disrupts the integration of cue-related and self-motion information in the parietal cortex, leading to an erroneous orientation of hippocampal spatial representation relative to the proximal cues. Besides, electrophysiological recordings in monkey showed that vestibular signals are encoded in distinct reference frames in parietal cortex (Chen et al., 2013b). Additionally, simultaneous recordings of cerebellar Purkinje cells and neurons in parietal cortex evidenced a similar tuning to both vestibular and optic flow signals (Yakusheva et al., 2013), strengthening the idea of a functional coupling between these two regions.

An objection to that interpretation comes from the recordings of place cells in the dark and conflict conditions. If self-motion information is incorrectly processed by the cerebellum

in L7-PP2B mice, how could they maintain a stable spatial representation in the dark? As mentioned previously, tactile information and the olfactory traces left on the floor might have been sufficient to compensate for altered self-motion information, and thus allowed to preserve place cell properties in the dark. As far as the conflict condition is concerned, the possible use of background cues may have enabled the mice to maintain stable place fields. Indeed, Save et al. observed that lesioning the PPC resulted in a preferential use of background cues to orient the place fields (Save et al., 2005). Previous studies on head-direction cells had showed that background cues rather than foreground cues (the configuration of proximal objects) controlled overt the directional specificity of head direction cells in rats (Zugaro et al., 2001). The authors hypothesized that contrasts in curtains folds might be used by the animals as a stable reference frame.

However, in our study, we observed inconsistent rotations of the spatial representation relative to the room frame. A possibility is that the animals used the curtains-related information but that given the repetitive structure of curtains folds, this gave confounding information that led to random orientation of the place fields. Alternatively, as previously mentioned, the use of the experimenter as a distal cue would also lead to an unpredictable orientation of the spatial representation. Interestingly, Zugaro et al. showed that the directional specificity of head directional cells was established within the first seconds of the session (Zugaro et al., 2001), a time window which is compatible with the experimenter-hypothesis.

CONCLUSION

During my Ph.D, I have investigated the consequences of the absence of PF-PC LTP in spatial navigation, at the behavioral and physiological level. This work follows previous works on L7-PKCI mice lacking PF-PC LTD which had strongly suggested a role of PF-PC LTD in self-motion information processing that is necessary for the building of the hippocampal spatial representation as well as for optimal navigation.

Like L7-PKCI, L7-PP2B mice lacking LTP displayed a deficit in trajectory optimization, but in their case it is probably linked to their mild motor deficit. However, in contrast to the absence of PF-PC LTD, the absence of PF-PC- LTP impacted neither spatial learning in the watermaze task nor the spatial properties of hippocampal place cells during cue manipulation. This discrepancy between L7-PKCI and L7-PP2B phenotypes seems to contradict what one could expect from the prediction of the adaptive filter model of the cerebellum (i.e. disrupting bi-directional plasticity by either ways would lead to a similar phenotype). Yet, the intrinsic limitations of the mouse genetic models keep us from making a strong conclusion regarding that point.

Surprisingly, hippocampal place cell recordings revealed that L7-PP2B mice displayed unpredictable rotations of their spatial representation relative to the object inside the arena. Importantly, building a spatial map based on proximal cues requires the integration of different views of the environment with the movements connecting these views. This integration is thought to be a basic function of the parietal cortex, a cortical area receiving strong projections from the cerebellum. Recent electrophysiological data highlighted its role in proximal cue and self-motion integration and its functional connectivity with the cerebellum. A possible interpretation of our data is that in mice lacking PF-PC LTP, incorrectly processed self-motion information is sent by the cerebellum to the parietal cortex. This would impair the integration of object-related and self-motion information in the parietal cortex, and subsequently the use of proximal cue information in the building of the hippocampal spatial representation.

This work confirmed the crucial role of the cerebellum in sensory information processing for the formation of a spatial representation. It joins the growing body of evidence suggesting that the cerebellum participates in multiple functions due to its connections with a large network of brain areas and that its implication in these functions is critically dependent on the type of information processed by the structures it is connected to.

Appendix

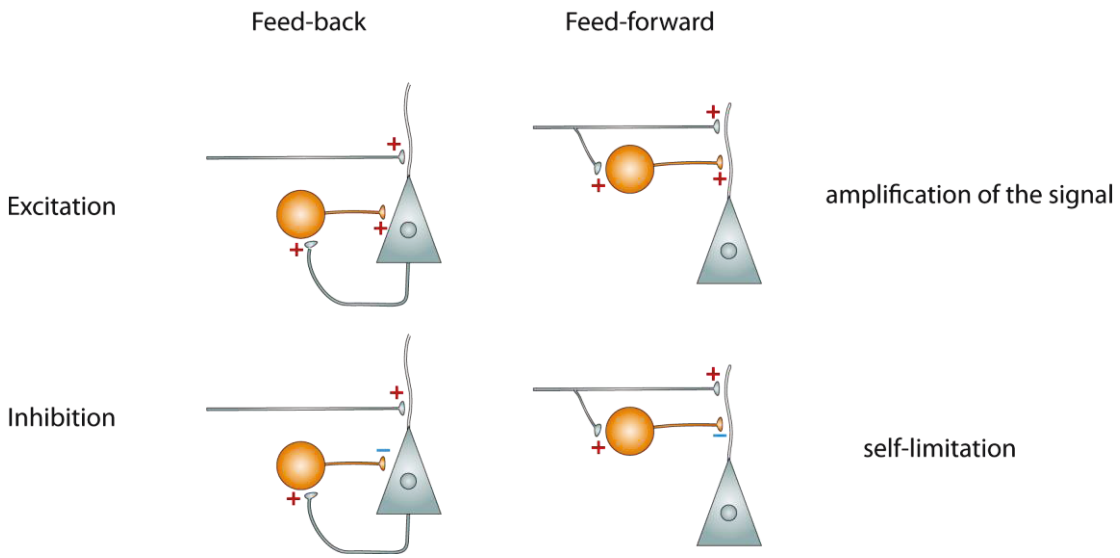

Appendix. Simplified view of the different configurations of interneurons, mediating feed-back or feed-forward influence onto the principal cells.
Feed-back configuration: the interneuron is innervated by recurrent collaterals of local principal cells
Feed-forward configuration: the axons of remote principal cells innervate both the local principal cell and the interneuron. It should be noted such a dichotomy is simplistic that because many cells are excited by both the axon collaterals of local principal cells and by the excitatory axons of more remote structures.
Principal cells are shown in green; inter-neurons are shown in orange. Red excitatory connection, blue inhibitory connection.
Adapted from Kullmann and Lamsa, 2007

BIBLIOGRAPHY

- A -

Ahn AH, Dziennis S, Hawkes R, Herrup K (1994) The cloning of zebrin II reveals its identity with aldolase C. Development 120:2081–2090.

Aiba A, Kano M, Chen C, Stanton ME, Fox GD, Herrup K, Zwingman TA, Tonegawa S (1994) Deficient cerebellar long-term depression and impaired motor learning in mGluR1 mutant mice. Cell 79:377–388.

Aikath D, Weible AP, Rowland DC, Kentros CG (2014) Role of self-generated odor cues in contextual representation. Hippocampus 13:1–13.

Aizenman CD, Linden DJ (2000) Rapid, synaptically driven increases in the intrinsic excitability of cerebellar deep nuclear neurons. Nat Neurosci 3:109–111.

Aizenman CD, Manis PB, Linden DJ (1998) Polarity of long-term synaptic gain change is related to postsynaptic spike firing at a cerebellar inhibitory synapse. Neuron 21:827–835.

Akkal D, Dum RP, Strick PL (2007) Supplementary motor area and presupplementary motor area: targets of basal ganglia and cerebellar output. J Neurosci 27:10659–10673.

Albus J (1971) A theory of cerebellar function. Math Biosci.

Alcami P, Marty A (2013) Estimating functional connectivity in an electrically coupled interneuron network. Proc Natl Acad Sci U S A 110:E4798–807.

Allen G (1997) Attentional Activation of the Cerebellum Independent of Motor Involvement. Science (80-) 275:1940–1943.

Allen K, Gil M, Resnik E, Toader O, Seeburg P, Monyer H (2014) Impaired Path Integration and Grid Cell Spatial Periodicity in Mice Lacking GluA1-Containing AMPA Receptors. J Neurosci 34:6245–6259.

Allen K, Rawlins JNP, Bannerman DM, Csicsvari J (2012) Hippocampal place cells can encode multiple trial-dependent features through rate remapping. J Neurosci 32:14752–14766.

Altman J, Bayer SA (1977) Time of origin and distribution of a new cell type in the rat cerebellar cortex. Exp brain Res 29:265–274.

Alvernhe A, Save E, Poucet B (2011) Local remapping of place cell firing in the Tolman detour task. Eur J Neurosci 33:1696–1705.

Alvernhe A, Van Cauter T, Save E, Poucet B (2008) Different CA1 and CA3 representations of novel routes in a shortcut situation. J Neurosci 28:7324–7333.

Amino Y, Kyuhou S, Matsuzaki R, Gemba H (2001) Cerebello-thalamo-cortical projections to the posterior parietal cortex in the macaque monkey. Neurosci Lett 309:29–32.

Andersen P, Morris R, Amaral D, Bliss T, O'Keefe J (2006) The hippocampus book.

Anderson MI, Jeffery KJ (2003) Heterogeneous modulation of place cell firing by changes in context. J Neurosci 23:8827–8835.

Andreescu CE, Prestori F, Brandalise F, D'Errico A, De Jeu MTG, Rossi P, Botta L, Kohr G, Perin P, D'Angelo E, De Zeeuw CI (2011) NR2A subunit of the N-methyl D-aspartate receptors are required for potentiation at the mossy fiber to granule cell synapse and vestibulo-cerebellar motor learning. Neuroscience 176:274–283.

Angaut P, Cicirata F, Serapide F (1985) Topographic organization of the cerebellothalamic projections in the rat. An autoradiographic study. Neuroscience 15:389–401.

Angelaki DE, Yakusheva T a, Green AM, Dickman JD, Blazquez PM (2010) Computation of egomotion in the macaque cerebellar vermis. Cerebellum 9:174–182.

Aoki E, Semba R, Kashiwamata S (1986) New candidates for GABAergic neurons in the rat cerebellum: an immunocytochemical study with anti-GABA antibody. Neurosci Lett 68:267–271.

Apps R, Garwicz M (2000) Precise matching of olivo-cortical divergence and cortico-nuclear convergence between somatotopically corresponding areas in the medial C1 and medial C3 zones of the paravermal cerebellum. Eur J Neurosci 12:205–214.

Apps R, Garwicz M (2005) Anatomical and physiological foundations of cerebellar information processing. Nat Rev Neurosci 6:297–311.

Apps R, Hawkes R (2009) Cerebellar cortical organization: a one-map hypothesis. Nat Rev Neurosci 10:670–681.

Arleo A, Déjean C, Allegraud P, Khamassi M, Zugaro MB, Wiener SI (2013) Optic flow stimuli update anterodorsal thalamus head direction neuronal activity in rats. J Neurosci 33:16790–16795.

Arleo A, Rondi-Reig L (2007) Navigation strategies for spatial cognition in real and artificial organisms. 6:327–366.

Armano S, Rossi P, Taglietti V, D'Angelo E (2000) Long-term potentiation of intrinsic excitability at the mossy fiber-granule cell synapse of rat cerebellum. J Neurosci 20:5208–5216.

Armstrong CL, Krueger-Naug AM, Currie RW, Hawkes R (2000) Constitutive expression of the 25-kDa heat shock protein Hsp25 reveals novel parasagittal bands of purkinje cells in the adult mouse cerebellar cortex. J Comp Neurol 416:383–397.

Armstrong DM, Schild RF (1970) A quantitative study of the Purkinje cells in the cerebellum of the albino rat. J Comp Neurol 139:449–456.

Asanuma C, Thach WT, Jones EG (1983) Distribution of cerebellar terminations and their relation to other afferent terminations in the ventral lateral thalamic region of the monkey. Brain Res 286:237–265.

Attwell PJ, Rahman S, Yeo CH (2001) Acquisition of eyeblink conditioning is critically dependent on normal function in cerebellar cortical lobule HVI. J Neurosci 21:5715–5722.

Attwell PJE, Cooke SF, Yeo CH (2002) Cerebellar function in consolidation of a motor memory. Neuron 34:1011–1020.

Aumann TD, Rawson JA, Finkelstein DI, Horne MK (1994) Projections from the lateral and interposed cerebellar nuclei to the thalamus of the rat: a light and electron microscopic study using single and double anterograde labelling. J Comp Neurol 349:165–181.

- B -

Barry C, Hayman R, Burgess N, Jeffery KJ (2007) Experience-dependent rescaling of entorhinal grids. Nat Neurosci 10:682–684.

Barry C, Lever C, Hayman R, Hartley T, Burton S, O'Keefe J, Jeffery K, Burgess N (2006) The boundary vector cell model of place cell firing and spatial memory. Rev Neurosci 17:71–97.

Barski JJ, Dethleffsen K, Meyer M (2000) Cre recombinase expression in cerebellar Purkinje cells. Genes New York NY 2000 28:93–98.

Bastian J (1996) Plasticity in an electrosensory system. I. General features of a dynamic sensory filter. J Neurophysiol 76:2483–2496.

Bell C, Bodznick D (1997) The generation and subtraction of sensory expectations within cerebellum-like structures. Brain, Behav ….

Bell CC (1981) An efference copy which is modified by reafferent input. Science 214:450–453.

Bell CC, Caputi a, Grant K, Serrier J (1993) Storage of a sensory pattern by anti-Hebbian synaptic plasticity in an electric fish. Proc Natl Acad Sci U S A 90:4650–4654.

Bell CC, Han V, Sawtell NB (2008) Cerebellum-like structures and their implications for cerebellar function. Annu Rev Neurosci 31:1–24.

Bell CC, Han VZ, Sugawara Y, Grant K (1997) Synaptic plasticity in a cerebellum-like structure depends on temporal order. Nature 387:278–281.

Belmeguenai A, Botta P, Weber JT, Carta M, De Ruiter M, De Zeeuw CI, Valenzuela CF, Hansel C (2008) Alcohol impairs long-term depression at the cerebellar parallel fiber-Purkinje cell synapse. J Neurophysiol 100:3167–3174.

Belmeguenai A, Hansel C (2005) A role for protein phosphatases 1, 2A, and 2B in cerebellar long-term potentiation. J Neurosci 25:10768–10772.

Belmeguenai A, Hosy E, Bengtsson F, Pedroarena CM, Piochon C, Teuling E, He Q, Ohtsuki G, De Jeu MTG, Elgersma Y, De Zeeuw CI, Jörntell H, Hansel C (2010) Intrinsic plasticity complements long-term potentiation in parallel fiber input gain control in cerebellar Purkinje cells. J Neurosci 30:13630–13643.

Bender VA, Pugh JR, Jahr CE (2009) Presynaptically expressed long-term potentiation increases multivesicular release at parallel fiber synapses. J Neurosci 29:10974–10978.

Berens P (2009) A MATLAB Toolbox for Circular Statistics. J Stat Softw 31.

Bjerknes TL, Moser EI, Moser M-B (2014) Representation of Geometric Borders in the Developing Rat. Neuron 82:71–78.

Blakemore SJ, Wolpert DM, Frith CD (1998) Central cancellation of self-produced tickle sensation. Nat Neurosci 1:635–640.

Blot A, Barbour B (2014) Ultra-rapid axon-axon ephaptic inhibition of cerebellar Purkinje cells by the pinceau. Nat Neurosci 17:289–295.

Boccara CN, Sargolini F, Thoresen VH, Solstad T, Witter MP, Moser EI, Moser M-B (2010) Grid cells in pre- and parasubiculum. Nat Neurosci 13:987–994.

Bodznick D, Montgomery J, Carey M (1999) Adaptive mechanisms in the elasmobranch hindbrain. J Exp Biol 202:1357–1364.

Bonnevie T, Dunn B, Fyhn M, Hafting T, Derdikman D, Kubie JL, Roudi Y, Moser EI, Moser M-B (2013) Grid cells require excitatory drive from the hippocampus. Nat Neurosci 16:309–317.

Bosman LWJ, Takechi H, Hartmann J, Eilers J, Konnerth A (2008) Homosynaptic long-term synaptic potentiation of the “winner” climbing fiber synapse in developing Purkinje cells. J Neurosci 28:798–807.

Boyden ES, Katoh A, Pyle JL, Chatila T a, Tsien RW, Raymond JL (2006) Selective engagement of plasticity mechanisms for motor memory storage. Neuron 51:823–834.

Bozon B, Kelly A, Josselyn SA, Silva AJ, Davis S, Laroche S (2003) MAPK, CREB and zif268 are all required for the consolidation of recognition memory. Philos Trans R Soc Lond B Biol Sci 358:805–814.

Braitenberg V, Atwood RP (1958) Morphological observations on the cerebellar cortex. J Comp Neurol 109:1–33.

Brandon MP, Bogaard AR, Libby CP, Connerney MA, Gupta K, Hasselmo ME (2011) Reduction of theta rhythm dissociates grid cell spatial periodicity from directional tuning. Science 332:595–599.

Brochu G, Maler L, Hawkes R (1990) Zebrin II: a polypeptide antigen expressed selectively by Purkinje cells reveals compartments in rat and fish cerebellum. J Comp Neurol 291:538–552.

Brooks JX, Cullen KE (2009) Multimodal integration in rostral fastigial nucleus provides an estimate of body movement. J Neurosci 29:10499–10511.

Brooks JX, Cullen KE (2011) Learning in the neural circuit that underlies the cancellation of vestibular reafference: Evidence for a rapid updating of internal models in the vestibular cerebellum. Poster Sess Present Soc Neurosci Meet Washington, DC; 2011:2011.

Brooks JX, Cullen KE (2013) The primate cerebellum selectively encodes unexpected self-motion. Curr Biol 23:947–955.

Brown IE, Bower JM (2001) Congruence of mossy fiber and climbing fiber tactile projections in the lateral hemispheres of the rat cerebellum. J Comp Neurol 429:59–70.

Brown MW, Aggleton JP (2001) Recognition memory: what are the roles of the perirhinal cortex and hippocampus? Nat Rev Neurosci 2:51–61.

Bruckmoser P, Hepp-Reymond MC, Wiesendanger M (1970) Cortical influence on single neurons of the lateral reticular nucleus of the cat. Exp Neurol 26:239–252.

Buisseret-Delmas C, Angaut P (1993) The cerebellar olivo-corticonuclear connections in the rat. Prog Neurobiol 40:63–87.

Burgess N, Barry C, O'Keefe J (2007) An oscillatory interference model of grid cell firing. Hippocampus 17:801–812.

Burguière E, Arabo A, Jarlier F, De Zeeuw CI, Rondi-Reig L (2010) Role of the cerebellar cortex in conditioned goal-directed behavior. J Neurosci 30:13265–13271.

Burguière E, Arleo A, Hojjati MR, Elgersma Y, De Zeeuw CI, Berthoz A, Rondi-Reig L (2005) Spatial navigation impairment in mice lacking cerebellar LTD: a motor adaptation deficit? Nat Neurosci 8:1292–1294.

Burwell RD, Hafeman DM (2003) Positional firing properties of postrhinal cortex neurons. Neuroscience 119:577–588.

- C -

Caddy KW, Biscoe TJ (1979) Structural and quantitative studies on the normal C3H and Lurcher mutant mouse. Philos Trans R Soc Lond B Biol Sci 287:167–201.

Calhoun VD, Pekar JJ, McGinty VB, Adali T, Watson TD, Pearlson GD (2002) Different activation dynamics in multiple neural systems during simulated driving. Hum Brain Mapp 16:158–167.

Callu D, Lopez J, El Massioui N (2013) Cerebellar deep nuclei involvement in cognitive adaptation and automaticity. Learn Mem 20:344–347.

Callu D, Puget S, Faure A, Guegan M, El Massioui N (2007) Habit learning dissociation in rats with lesions to the vermis and the interpositus of the cerebellum. Neurobiol Dis 27:228–237.

Calton JL, Stackman RW, Goodridge JP, Archey WB, Dudchenko P a, Taube JS (2003) Hippocampal place cell instability after lesions of the head direction cell network. J Neurosci 23:9719–9731.

Calton JL, Taube JS (2005) Degradation of head direction cell activity during inverted locomotion. J Neurosci 25:2420–2428.

Carlezon WA, Chartoff EH (2007) Intracranial self-stimulation (ICSS) in rodents to study the neurobiology of motivation. Nat Protoc 2:2987–2995.

Cerminara NL, Rawson JA (2004) Evidence that climbing fibers control an intrinsic spike generator in cerebellar Purkinje cells. J Neurosci 24:4510–4517.

Chadderton P, Margrie TW, Häusser M (2004) Integration of quanta in cerebellar granule cells during sensory processing. Nature 428:856–860.

Chaumont J (2013) Organisation fonctionnelle de la boucle Olivo-cortico-nucléaire : Influence de l'activité des cellules de purkinje. Thesis.

Chen G, King JA, Burgess N, O'Keefe J (2013a) How vision and movement combine in the hippocampal place code. Proc Natl Acad Sci U S A 110:378–383.

Chen L, Bao S, Lockard JM, Kim JK, Thompson RF (1996) Impaired classical eyeblink conditioning in cerebellar-lesioned and Purkinje cell degeneration (pcd) mutant mice. J Neurosci 16:2829–2838.

Chen LL, Lin LH, Green EJ, Barnes CA, McNaughton BL (1994) Head-direction cells in the rat posterior cortex. I. Anatomical distribution and behavioral modulation. Exp brain Res 101:8–23.

Chen X, Deangelis GC, Angelaki DE (2013b) Diverse spatial reference frames of vestibular signals in parietal cortex. Neuron 80:1310–1321.

Cheung A, Ball D, Milford M, Wyeth G, Wiles J (2012) Maintaining a cognitive map in darkness: the need to fuse boundary knowledge with path integration. PLoS Comput Biol 8:e1002651.

Cho J, Sharp PE (2001) Head direction, place, and movement correlates for cells in the rat retrosplenial cortex. Behav Neurosci 115:3–25.

Chung HJ, Steinberg JP, Huganir RL, Linden DJ (2003) Requirement of AMPA receptor GluR2 phosphorylation for cerebellar long-term depression. Science 300:1751–1755.

Clark BJ, Hamilton D a, Whishaw IQ (2006) Motor activity (exploration) and formation of home bases in mice (C57BL/6) influenced by visual and tactile cues: modification of movement distribution, distance, location, and speed. Physiol Behav 87:805–816.

Claxton G (1975) Why can't we tickle ourselves? Percept Mot Skills 41:335–338.

Clower DM, Dum RP, Strick PL (2005) Basal ganglia and cerebellar inputs to "AIP". Cereb Cortex 15:913–920.

Clower DM, West R a, Lynch JC, Strick PL (2001) The inferior parietal lobule is the target of output from the superior colliculus, hippocampus, and cerebellum. J Neurosci 21:6283–6291.

Coesmans M, Weber JT, De Zeeuw CI, Hansel C (2004) Bidirectional parallel fiber plasticity in the cerebellum under climbing fiber control. Neuron 44:691–700.

Cohen D, Yarom Y (2000) Cerebellar on-beam and lateral inhibition: two functionally distinct circuits. J Neurophysiol 83:1932–1940.

Colgin LL, Moser EI, Moser M-B (2008) Understanding memory through hippocampal remapping. Trends Neurosci 31:469–477.

Colombel C, Lalonde R, Caston J (2004) The effects of unilateral removal of the cerebellar hemispheres on spatial learning and memory in rats. Brain Res 1004:108–115.

Crepel F, Delhaye-Bouchaud N, Dupont JL (1981) Fate of the multiple innervation of cerebellar Purkinje cells by climbing fibers in immature control, x-irradiated and hypothyroid rats. Brain Res 227:59–71.

Crepel F, Mariani J (1976) Multiple innervation of Purkinje cells by climbing fibers in the cerebellum of the Weaver Mutant Mouse. J Neurobiol 7:579–582.

Crepel F, Mariani J, Delhaye-Bouchaud N (1976) Evidence for a multiple innervation of Purkinje cells by climbing fibers in the immature rat cerebellum. J Neurobiol 7:567–578.

Cullen KE, Roy JE (2004) Signal processing in the vestibular system during active versus passive head movements. J Neurophysiol 91:1919–1933.

D'Angelo E, De Zeeuw CI (2009) Timing and plasticity in the cerebellum: focus on the granular layer. Trends Neurosci 32:30–40.

D'Angelo E, Rossi P, Armano S, Taglietti V (1999) Evidence for NMDA and mGlu receptor-dependent long-term potentiation of mossy fiber-granule cell transmission in rat cerebellum. J Neurophysiol 81:277–287.

- D -

De Witte P, Gewiss M (1987) Preference and aversion for brain stimulations estimated by the conditioned place preference. Arch Physiol Biochem 95:147–152.

De Zeeuw CI, Hansel C, Bian F, Koekkoek SK, van Alphen AM, Linden DJ, Oberdick J (1998a) Expression of a protein kinase C inhibitor in Purkinje cells blocks cerebellar LTD and adaptation of the vestibulo-ocular reflex. Neuron 20:495–508.

De Zeeuw CI, Hoebeek FE, Bosman LWJ, Schonewille M, Witter L, Koekkoek SK (2011) Spatiotemporal firing patterns in the cerebellum. Nat Rev Neurosci 12:327–344.

De Zeeuw CI, Simpson JI, Hoogenraad CC, Galjart N, Koekkoek SK, Ruigrok TJ (1998b) Microcircuitry and function of the inferior olive. Trends Neurosci 21:391–400.

Dean P, Porrill J, Ekerot C-F, Jörntell H (2010) The cerebellar microcircuit as an adaptive filter: experimental and computational evidence. Nat Rev Neurosci 11:30–43.

Dehnes Y, Chaudhry FA, Ullensvang K, Lehre KP, Storm-Mathisen J, Danbolt NC (1998) The glutamate transporter EAAT4 in rat cerebellar Purkinje cells: a glutamate-gated chloride channel concentrated near the synapse in parts of the dendritic membrane facing astroglia. J Neurosci 18:3606–3619.

Derdikman D, Whitlock JR, Tsao A, Fyhn M, Hafting T, Moser M-B, Moser EI (2009) Fragmentation of grid cell maps in a multicompartment environment. Nat Neurosci 12:1325–1332.

Dieudonné S, Dumoulin A (2000) Serotonin-driven long-range inhibitory connections in the cerebellar cortex. J Neurosci 20:1837–1848.

Domnisoru C, Kinkhabwala A a, Tank DW (2013) Membrane potential dynamics of grid cells. Nature 495:199–204.

Dow R, Moruzzi G (1958) The physiology and pathology of the cerebellum.

Dugué GP, Dumoulin A, Triller A, Dieudonné S (2005) Target-dependent use of co-released inhibitory transmitters at central synapses. J Neurosci 25:6490–6498.

Duguid IC, Smart TG (2004) Retrograde activation of presynaptic NMDA receptors enhances GABA release at cerebellar interneuron-Purkinje cell synapses. Nat Neurosci 7:525–533.

- E -

Eccles JC, Sasaki K, Strata P (1967) Interpretation of the potential fields generated in the cerebellar cortex by a mossy fibre volley. Exp brain Res 3:58–80.

Emde G Von der (1999) Active electrolocation of objects in weakly electric fish. J Exp Biol.

Eichenbaum H (1999) The hippocampus and mechanisms of declarative memory. Behav Brain Res 103:123–133.

Eijkenboom M, Blokland A, van der Staay FJ (2000) Modelling cognitive dysfunctions with bilateral injections of ibotenic acid into the rat entorhinal cortex. Neuroscience 101:27–39.

Ennaceur A, Michalikova S, Bradford A, Ahmed S (2005) Detailed analysis of the behavior of Lister and Wistar rats in anxiety, object recognition and object location tasks. Behav Brain Res 159:247–266.

Etienne AS, Jeffery KJ (2004) Path integration in mammals. Hippocampus 14:180–192.

Etienne AS, Maurer R, Saucy F (1988) Limitations in the Assessment of Path Dependent Information. Behaviour 106:81–110.

Etienne AS, Teroni E, Hurni C, Portenier V (1990) The effect of a single light cue on homing behaviour of the golden hamster. Anim Behav 39:17–41.

- F -

Feil R, Hartmann J, Luo C, Wolfsgruber W, Schilling K, Feil S, Barski JJ, Meyer M, Konnerth A, De Zeeuw CI, Hofmann F (2003) Impairment of LTD and cerebellar learning by Purkinje cell-specific ablation of cGMP-dependent protein kinase I. J Cell Biol 163:295–302.

Fenton A a, Kao H-Y, Neymotin S a, Olypher A, Vayntrub Y, Lytton WW, Ludvig N (2008) Unmasking the CA1 ensemble place code by exposures to small and large environments: more place cells and multiple, irregularly arranged, and expanded place fields in the larger space. J Neurosci 28:11250–11262.

Fenton A a, Lytton WW, Barry JM, Lenck-Santini P-P, Zinyuk LE, Kubík S, Bures J, Poucet B, Muller RU, Olypher A V (2010) Attention-like modulation of hippocampus place cell discharge. J Neurosci 30:4613–4625.

Fenton AA, Csizmadia G, Muller RU (2000) Conjoint control of hippocampal place cell firing by two visual stimuli. I. The effects of moving the stimuli on firing field positions. J Gen Physiol 116:191–209.

Fenton AA, Wesierska M, Kaminsky Y, Bures J (1998) Both here and there : Simultaneous expression of autonomous spatial memories in rats. Proc Natl Acad Sci U S A 95:11493–11498.

Ferbinteanu J, Shirvalkar P, Shapiro ML (2011) Memory modulates journey-dependent coding in the rat hippocampus. J Neurosci 31:9135–9146.

Ferguson JE, Boldt C, Redish AD (2009) Creating low-impedance tetrodes by electroplating with additives. Sensors Actuators, A Phys 156:388–393.

Floresco SB, Seamans JK, Phillips AG (1997) Selective roles for hippocampal, prefrontal cortical, and ventral striatal circuits in radial-arm maze tasks with or without a delay. J Neurosci 17:1880–1890.

Flourens P (1824) Recherches expérimentales sur les propriétés et les fonctions du système nerveux dans les animaux vertébrés.

Fouquet C, Babayan BM, Watilliaux A, Bontempi B, Tobin C, Rondi-Reig L (2013) Complementary Roles of the Hippocampus and the Dorsomedial Striatum during Spatial and Sequence-Based Navigation Behavior. PLoS One 8:e67232.

Frank B, Schoch B, Richter S, Frings M, Karnath H-O, Timmann D (2007) Cerebellar lesion studies of cognitive function in children and adolescents - limitations and negative findings. Cerebellum 6:242–253.

Fyhn M, Hafting T, Treves A, Moser M-B, Moser EI (2007) Hippocampal remapping and grid realignment in entorhinal cortex. Nature 446:190–194.

Fyhn M, Hafting T, Witter MP, Moser EI, Moser M-B (2008) Grid cells in mice. Hippocampus 18:1230–1238.

- G -

Gall D, Prestori F, Sola E, D'Errico A, Roussel C, Forti L, Rossi P, D'Angelo E (2005) Intracellular calcium regulation by burst discharge determines bidirectional long-term synaptic plasticity at the cerebellum input stage. J Neurosci 25:4813–4822.

Galliano E, Potters J-W, Elgersma Y, Wisden W, Kushner S a, De Zeeuw CI, Hoebeek FE (2013) Synaptic transmission and plasticity at inputs to murine cerebellar Purkinje cells are largely dispensable for standard nonmotor tasks. J Neurosci 33:12599–12618.

Gandhi CC, Kelly1 RM, Wiley RG, Walsh TJ (2000) Impaired acquisition of a Morris water maze task following selective destruction of cerebellar purkinje cells with OX7-saporin. Behav Brain Res 109:37–47.

Gao W, Dunbar RL, Chen G, Reinert KC, Oberdick J, Ebner TJ (2003) Optical imaging of long-term depression in the mouse cerebellar cortex in vivo. J Neurosci 23:1859–1866.

Gao Z, van Beugen BJ, De Zeeuw CI (2012) Distributed synergistic plasticity and cerebellar learning. Nat Rev Neurosci 13:619–635.

Garwicz M, Ekerot C-F, Jörntell H (1998) Organizational Principles of Cerebellar Neuronal Circuitry. News Physiol Sci 13:26–32.

Gener T, Perez-Mendez L, Sanchez-Vives M V (2013) Tactile modulation of hippocampal place fields. Hippocampus 23:1453–1462.

Gerrits NM, Voogd J (1987) The projection of the nucleus reticularis tegmenti pontis and adjacent regions of the pontine nuclei to the central cerebellar nuclei in the cat. J Comp Neurol 258:52–69.

Ghez C (1991) The cerebellum. Appleton and Lange.

Giannetti S, Molinari M (2002) Cerebellar input to the posterior parietal cortex in the rat. Brain Res Bull 58:481–489.

Gibson JJ (1950) The perception of the visual world.

Golob EJ, Taube JS (1997) Head direction cells and episodic spatial information in rats without a hippocampus. Proc Natl Acad Sci U S A 94:7645–7650.

Golob EJ, Taube JS (1999) Head direction cells in rats with hippocampal or overlying neocortical lesions: evidence for impaired angular path integration. J Neurosci 19:7198–7211.

Gonzalez L, Shumway C, Morissette J, Bower JM (1993) Developmental plasticity in cerebellar tactile maps: fractured maps retain a fractured organization. J Comp Neurol 332:487–498.

Goodale MA, Dale RH (1981) Radial-maze performance in the rat following lesions of posterior neocortex. Behav Brain Res 3:273–288.

Goodlett CR, Hamre KM, West JR (1992) Dissociation of spatial navigation and visual guidance performance in Purkinje cell degeneration (pcd) mutant mice. Behav Brain Res 47:129–141.

Goodridge JP, Dudchenko P a, Worboys K a, Golob EJ, Taube JS (1998) Cue control and head direction cells. Behav Neurosci 112:749–761.

Goodridge JP, Taube JS (1995) Preferential use of the landmark navigational system by head direction cells in rats. Behav Neurosci 109:49–61.

Goodridge JP, Taube JS (1997) Interaction between the postsubiculum and anterior thalamus in the generation of head direction cell activity. J Neurosci 17:9315–9330.

Goodworth AD, Paquette C, Jones GM, Block EW, Fletcher WA, Hu B, Horak FB (2012) Linear and angular control of circular walking in healthy older adults and subjects with cerebellar ataxia. Exp brain Res 219:151–161.

Gothard KM, Skaggs WE, Moore KM, McNaughton BL (1996) Binding of hippocampal CA1 neural activity to multiple reference frames in a landmark-based navigation task. J Neurosci 16:823–835.

Granon S, Poucet B (1995) Medial prefrontal lesions in the rat and spatial navigation: evidence for impaired planning. Behav Neurosci 109:474–484.

Gravel C, Eisenman LM, Sasseville R, Hawkes R (1987) Parasagittal organization of the rat cerebellar cortex: direct correlation between antigenic Purkinje cell bands revealed by mabQ113 and the organization of the olivocerebellar projection. J Comp Neurol 265:294–310.

Groenewegen HJ, Voogd J (1977) The parasagittal zonation within the olivocerebellar projection. I. Climbing fiber distribution in the vermis of cat cerebellum. J Comp Neurol 174:417–488.

- H -

Hafting T, Fyhn M, Molden S, Moser M-B, Moser EI (2005) Microstructure of a spatial map in the entorhinal cortex. Nature 436:801–806.

Han VZ, Grant K, Bell CC (2000) Reversible associative depression and nonassociative potentiation at a parallel fiber synapse. Neuron 27:611–622.

Hansel C, de Jeu M, Belmeguenai A, Houtman SH, Buitendijk GHS, Andreev D, De Zeeuw CI, Elgersma Y (2006) alphaCaMKII Is essential for cerebellar LTD and motor learning. Neuron 51:835–843.

Hansel C, Linden DJ (2000) Long-Term Depression of the Cerebellar Climbing Fiber–Purkinje Neuron Synapse. Neuron 26:473–482.

Hansel C, Linden DJ, D'Angelo E (2001) Beyond parallel fiber LTD: the diversity of synaptic and non-synaptic plasticity in the cerebellum. Nat Neurosci 4:467–475.

Hargreaves EL, Rao G, Lee I, Knierim JJ (2005) Major dissociation between medial and lateral entorhinal input to dorsal hippocampus. Science 308:1792–1794.

Hargreaves EL, Yoganarasimha D, Knierim JJ (2007) Cohesiveness of Spatial and Directional Representations Recorded From Neural Ensembles in the Anterior Thalamus , Parasubiculum , Medial Entorhinal Cortex , and Hippocampus. 841:826–841.

Harker KT, Whishaw IQ (2004) Impaired place navigation in place and matching-to-place swimming pool tasks follows both retrosplenial cortex lesions and cingulum bundle lesions in rats. Hippocampus 14:224–231.

Haroian a J, Massopust LC, Young P a (1981) Cerebellothalamic projections in the rat: an autoradiographic and degeneration study. J Comp Neurol 197:217–236.

Hartell NA (1994) Induction of cerebellar long-term depression requires activation of glutamate metabotropic receptors. Neuroreport 5:913–916.

Hartley T, Burgess N, Lever C, Cacucci F, O'Keefe J (2000) Modeling place fields in terms of the cortical inputs to the hippocampus. Hippocampus 10:369–379.

Harvey RJ, Napper RM (1988) Quantitative study of granule and Purkinje cells in the cerebellar cortex of the rat. J Comp Neurol 274:151–157.

Harvey RJ, Napper RM (1991) Quantitative studies on the mammalian cerebellum. Prog Neurobiol 36:437–463.

Häusser M, Clark BA (1997) Tonic Synaptic Inhibition Modulates Neuronal Output Pattern and Spatiotemporal Synaptic Integration. Neuron 19:665–678.

Hawkes R, colonnier M, Leclerc N (1985) Monoclonal antibodies reveal sagittal banding in the rodent cerebellar cortex. Brain Res 333:359–365.

Hawkes R, Leclerc N (1989) Purkinje cell axon collateral distributions reflect the chemical compartmentation of the rat cerebellar cortex. Brain Res 476:279–290.

Heckroth JA (1994) Quantitative morphological analysis of the cerebellar nuclei in normal and lurcher mutant mice. I. Morphology and cell number. J Comp Neurol 343:173–182.

Hen I, Sakov A, Kafkafi N, Golani I, Benjamini Y (2004) The dynamics of spatial behavior: how can robust smoothing techniques help? J Neurosci Methods 133:161–172.

Henriksen EJ, Colgin LL, Barnes C a, Witter MP, Moser M-B, Moser EI (2010) Spatial representation along the proximodistal axis of CA1. Neuron 68:127–137.

Hesslow G (1994) Correspondence between climbing fibre input and motor output in eyeblink-related areas in cat cerebellar cortex. J Physiol 476:229–244.

Hilber P, Lalonde R, Caston J (1999) An unsteady platform test for measuring static equilibrium in mice. J Neurosci Methods 88:201–205.

Hill AJ (1978) First occurrence of hippocampal spatial firing in a new environment. Exp Neurol 62:282–297.

Hogans N, Flash T (1985) The coordination of arm movements: an experimentally confirmed mathematical model. 5:1688–1703.

Hoover JE, Strick PL (1999) The organization of cerebellar and basal ganglia outputs to primary motor cortex as revealed by retrograde transneuronal transport of herpes simplex virus type 1. J Neurosci 19:1446–1463.

Horikawa E, Okamura N, Tashiro M, Sakurada Y, Maruyama M, Arai H, Yamaguchi K, Sasaki H, Yanai K, Itoh M (2005) The neural correlates of driving performance identified using positron emission tomography. Brain Cogn 58:166–171.

- I -

Igloi K, Doeller C, Benchenane K, Berthoz A, Burgess N, Rondi-Reig L (2012) Hippocampus and cerebellum ensure place and route representations together. Poster Sess Present 18th Annu Meet Organ Hum Brain Mapping Beijing, China; 2012.

Iglói K, Doeller CF, Berthoz A, Rondi-reig L, Burgess N (2010) Lateralized human hippocampal activity predicts navigation based on sequence or place memory.

Ito M (1984) The modifiable neuronal network of the cerebellum. Jpn J Physiol 34:781–792.

Ito M (2001) Cerebellar Long-Term Depression: Characterization, Signal Transduction, and Functional Roles. Physiol Rev 81:1143–1195.

Ito M (2006) Cerebellar circuitry as a neuronal machine. Prog Neurobiol 78:272–303.

Ito M, Kano M (1982) Long-lasting depression of parallel fiber-Purkinje cell transmission induced by conjunctive stimulation of parallel fibers and climbing fibers in the cerebellar cortex. Neurosci Lett 33:253–258.

Ito M, Sakurai M, Tongroach P (1982) Climbing fibre induced depression of both mossy fibre responsiveness and glutamate sensitivity of cerebellar Purkinje cells. J Physiol 324:113–134.

Ito M, Shiida T, Yagi N, Yamamoto M (1974) Visual influence on rabbit horizontal vestibulo-ocular reflex presumably effected via the cerebellar flocculus. Brain Res 65:170–174.

- J -

Jarlier F, Arleo A, Petit GH, Lefort JM, Fouquet C, Burguière E, Rondi-Reig L (2013) A Navigation Analysis Tool (NAT) to assess spatial behavior in open-field and structured mazes. J Neurosci Methods 215:196–209.

Jeffery KJ (1998) Learning of landmark stability and instability by hippocampal place cells. Neuropharmacology 37:677–687.

Jeffery KJ, Burgess N (2006) A metric for the cognitive map: found at last? Trends Cogn Sci 10:1–3.

Jeffery KJ, O'Keefe JM (1999) Learned interaction of visual and idiothetic cues in the control of place field orientation. Exp brain Res 127:151–161.

Jensen O, Lisman JE (2000) Position reconstruction from an ensemble of hippocampal place cells: contribution of theta phase coding. J Neurophysiol 83:2602–2609.

Jones BF, Witter MP (2007) Cingulate cortex projections to the parahippocampal region and hippocampal formation in the rat. Hippocampus 17:957–976.

Jones MW, Errington ML, French PJ, Fine A, Bliss T V, Garel S, Charnay P, Bozon B, Laroche S, Davis S (2001) A requirement for the immediate early gene Zif268 in the expression of late LTP and long-term memories. Nat Neurosci 4:289–296.

Jörntell H, Ekerot C-F (2002) Reciprocal bidirectional plasticity of parallel fiber receptive fields in cerebellar Purkinje cells and their afferent interneurons. Neuron 34:797–806.

Jörntell H, Ekerot C-F (2003) Receptive field plasticity profoundly alters the cutaneous parallel fiber synaptic input to cerebellar interneurons in vivo. J Neurosci 23:9620–9631.

Joyal CC, Strazielle C, Lalonde R (2001) Effects of dentate nucleus lesions on spatial and postural sensorimotor learning in rats. Behav Brain Res 122:131–137.

Jung MW, Wiener I (1994) Comparison of Spatial Firing Characteristics Ventral Hippocampus of the Rat. 74.

- K -

Kandel E, Schwartz J, Jessell T (2000) Principles of neural science.

Kano M, Rexhausen U, Dreessen J, Konnerth A (1992) Synaptic excitation produces a long-lasting rebound potentiation of inhibitory synaptic signals in cerebellar Purkinje cells. Nature 356:601–604.

Katoh A, Yoshida T, Himeshima Y, Mishina M, Hirano T (2005) Defective control and adaptation of reflex eye movements in mutant mice deficient in either the glutamate receptor delta2 subunit or Purkinje cells. Eur J Neurosci 21:1315–1326.

Ke MC, Guo CC, Raymond JL (2009) Elimination of climbing fiber instructive signals during motor learning. Nat Neurosci 12:1171–1179.

Kelly J (1991) The sense of balance. Princ neural Sci.

Kelly RM, Strick PL (2003) Cerebellar loops with motor cortex and prefrontal cortex of a nonhuman primate. J Neurosci 23:8432–8444.

Kentros CG, Agnihotri NT, Streater S, Hawkins RD, Kandel ER (2004) Increased attention to spatial context increases both place field stability and spatial memory. Neuron 42:283–295.

Kjelstrup KB, Solstad T, Brun VH, Hafting T, Leutgeb S, Witter MP, Moser EI, Moser M-B (2008) Finite scale of spatial representation in the hippocampus. Science 321:140–143.

Kleine JF, Guan Y, Kipiani E, Glonti L, Hoshi M, Büttner U (2004) Trunk position influences vestibular responses of fastigial nucleus neurons in the alert monkey. J Neurophysiol 91:2090–2100.

Knierim JJ, Hamilton D a (2011) Framing spatial cognition: neural representations of proximal and distal frames of reference and their roles in navigation. Physiol Rev 91:1245–1279.

Knierim JJ, Kudrimoti HS, McNaughton BL (1995) Place cells, head direction cells, and the learning of landmark stability. J Neurosci 15:1648–1659.

Knierim JJ, Rao G (2003) Distal landmarks and hippocampal place cells: effects of relative translation versus rotation. Hippocampus 13:604–617.

Koekkoek SKE, Hulscher HC, Dortland BR, Hensbroek R a, Elgersma Y, Ruigrok TJH, De Zeeuw CI (2003) Cerebellar LTD and learning-dependent timing of conditioned eyelid responses. Science 301:1736–1739.

Koenig J, Linder AN, Leutgeb JK, Leutgeb S (2011) The spatial periodicity of grid cells is not sustained during reduced theta oscillations. Science 332:592–595.

Kolb B, Buhrmann K, McDonald R, Sutherland RJ (1994) Dissociation of the medial prefrontal, posterior parietal, and posterior temporal cortex for spatial navigation and recognition memory in the rat. Cereb Cortex 4:664–680.

Kolb B, Walkey J (1987) Behavioural and anatomical studies of the posterior parietal cortex in the rat. Behav Brain Res 23:127–145.

Krupa DJ, Thompson JK, Thompson RF (1993) Localization of a memory trace in the mammalian brain. Science 260:989–991.

Kubie JL, Fenton A, Novikov N, Touretzky D, Muller RU (2007) Changes in goal selection induced by cue conflicts are in register with predictions from changes in place cell field locations. Behav Neurosci 121:751–763.

Kullmann DM, Lamsa KP (2007) Long-term synaptic plasticity in hippocampal interneurons. Nat Rev Neurosci 8:687–699.

- L -

Lalonde R, Strazielle C (2003) The effects of cerebellar damage on maze learning in animals. Cerebellum 2:300–309.

Lang EJ, Sugihara I, Llinás R (1996) GABAergic modulation of complex spike activity by the cerebellar nucleoolivary pathway in rat. J Neurophysiol 76:255–275.

Langston RF, Ainge J a, Couey JJ, Canto CB, Bjerknes TL, Witter MP, Moser EI, Moser M-B (2010) Development of the spatial representation system in the rat. Science 328:1576–1580.

Larsell O (1952) The morphogenesis and adult pattern of the lobules and fissures of the cerebellum of the white rat. J Comp Neurol.

Larsell O (1953) The cerebellum of the cat and the monkey. J Comp Neurol.

Lavenex P, Schenk F (1996) Integration of olfactory information in a spatial representation enabling accurate arm choice in the radial arm maze. Learn Mem 2:299–319.

Lavenex P, Schenk F (1998) Olfactory traces and spatial learning in rats. Anim Behav 56:1129–1136.

Leitges M, Kovac J, Plomann M, Linden DJ (2004) A unique PDZ ligand in PKCalpha confers induction of cerebellar long-term synaptic depression. Neuron 44:585–594.

Lemkey-Johnston N, Larramendi LM (1968) Types and distribution of synapses upon basket and stellate cells of the mouse cerebellum: an electron microscopic study. J Comp Neurol 134:73–112.

Lenck-Santini P-P, Muller RU, Save E, Poucet B (2002) Relationships between place cell firing fields and navigational decisions by rats. J Neurosci 22:9035–9047.

Lenck-Santini P-P, Rivard B, Muller RU, Poucet B (2005) Study of CA1 place cell activity and exploratory behavior following spatial and nonspatial changes in the environment. Hippocampus 15:356–369.

Lenck-Santini PP, Save E, Poucet B (2001) Evidence for a relationship between place-cell spatial firing and spatial memory performance. Hippocampus 11:377–390.

Leutgeb S, Leutgeb JK, Barnes C a, Moser EI, McNaughton BL, Moser M-B (2005) Independent codes for spatial and episodic memory in hippocampal neuronal ensembles. Science 309:619–623.

Lever C, Burgess N, Cacucci F, Hartley T, O'Keefe J (2002) What can the hippocampal representation of environmental geometry tell us about Hebbian learning? Biol Cybern 87:356–372.

Lever C, Burton S, Jeewajee A, O'Keefe J, Burgess N (2009) Boundary vector cells in the subiculum of the hippocampal formation. J Neurosci 29:9771–9777.

Lev-Ram V, Mehta SB, Kleinfeld D, Tsien RY (2003) Reversing cerebellar long-term depression. Proc Natl Acad Sci U S A 100:15989–15993.

Lev-Ram V, Wong ST, Storm DR, Tsien RY (2002) A new form of cerebellar long-term potentiation is postsynaptic and depends on nitric oxide but not cAMP. Proc Natl Acad Sci U S A 99:8389–8393.

Linden DJ, Connor JA (1991) Participation of postsynaptic PKC in cerebellar long-term depression in culture. Science 254:1656–1659.

Lisberger SG (1988) The neural basis for learning of simple motor skills. Science 242:728–735.

Lister RG (1987) The use of a plus-maze to measure anxiety in the mouse. Psychopharmacology (Berl):0–5.

Llano I, Gerschenfeld HM (1993) Inhibitory synaptic currents in stellate cells of rat cerebellar slices. J Physiol 468:177–200.

Llinás R, Sugimori M (1980) Electrophysiological properties of in vitro Purkinje cell somata in mammalian cerebellar slices. J Physiol 305:171–195.

- M -

Maguire E a. (1998) Knowing Where and Getting There: A Human Navigation Network. Science (80-) 280:921–924.

Mann-Metzer P, Yarom Y (2000) Electrotonic coupling synchronizes interneuron activity in the cerebellar cortex. Prog Brain Res 124:115–122.

Manzoni D, Pompeiano O, Bruschini L, Andre P (1999) Neck input modifies the reference frame for coding labyrinthine signals in the cerebellar vermis: a cellular analysis. Neuroscience 93:1095–1107.

Marr D (1969) A theory of cerebellar cortex. J Physiol.

Mateos JM, Osorio A., Azkue JJ, Benitez R, Elezgarai, I., Bilbao A, Diez J, Puente N, Kuhn R, Knopfel T, Hawkes R, Donate-Oliver F, Grandes P (2001) Parasagittal compartmentalization of the metabotropic glutamate receptor mGluR1b in the cerebellar cortex. Eur J Anat 5:15–21.

Matsushita M, Yaginuma H (1995) Projections from the central cervical nucleus to the cerebellar nuclei in the rat, studied by anterograde axonal tracing. J Comp Neurol 353:234–246.

McCrea RA, Gdowski GT, Boyle R, Belton T (1999) Firing behavior of vestibular neurons during active and passive head movements: vestibulo-spinal and other non-eye-movement related neurons. J Neurophysiol 82:416–428.

Mcnaughton BL, Battaglia FP, Jensen O, Moser EI (2006) Path integration and the neural basis of the " cognitive map ." 7:663–678.

McNaughton BL, Mizumori SJ, Barnes CA, Leonard BJ, Marquis M, Green EJ (1994) Cortical representation of motion during unrestrained spatial navigation in the rat. Cereb Cortex 4:27–39.

Metzger F, Kapfhammer JP (2003) Protein kinase C: its role in activity-dependent Purkinje cell dendritic development and plasticity. Cerebellum 2:206–214.

Miale IL, Sidman RL (1961) An autoradiographic analysis of histogenesis in the mouse cerebellum. Exp Neurol 4:277–296.

Middleton F a, Strick PL (2001) Cerebellar projections to the prefrontal cortex of the primate. J Neurosci 21:700–712.

Mihailoff GA (1993) Cerebellar nuclear projections from the basilar pontine nuclei and nucleus reticularis tegmenti pontis as demonstrated with PHA-L tracing in the rat. J Comp Neurol 330:130–146.

Mittelstaedt, ML ; Mittelstaedt H (1980) Homing by Path Integration in a Mammal. Naturwissenschaften 67.

Miyashita Y, Nagao S (1984) Contribution of cerebellar intracortical inhibition to Purkinje cell response during vestibulo-ocular reflex of alert rabbits. J Physiol 351:251–262.

Mizumori SJ, Williams JD (1993) Directionally selective mnemonic properties of neurons in the lateral dorsal nucleus of the thalamus of rats. J Neurosci 13:4015–4028.

Moita M a P, Rosis S, Zhou Y, LeDoux JE, Blair HT (2003) Hippocampal place cells acquire location-specific responses to the conditioned stimulus during auditory fear conditioning. Neuron 37:485–497.

Molinari M, Petrosini L, Misciagna S, Leggio MG (2004) Visuospatial abilities in cerebellar disorders. J Neurol Neurosurg Psychiatry 75:235–240.

Monaco JD, Abbott LF, Abbott LF (2011) Modular realignment of entorhinal grid cell activity as a basis for hippocampal remapping. J Neurosci 31:9414–9425.

Morissette J, Bower JM (1996) Contribution of somatosensory cortex to responses in the rat cerebellar granule cell layer following peripheral tactile stimulation. Exp brain Res 109:240–250.

Morris R (1984) Developments of a water-maze procedure for studying spatial learning in the rat. J Neurosci Methods 11:47–60.

Morris RG, Garrud P, Rawlins JN, O'Keefe J (1982) Place navigation impaired in rats with hippocampal lesions. Nature 297:681–683.

Morris RGM (1981) Spatial localization does not require the presence of local cues. Learn Motiv 12:239–260.

Moser EI, Moser M-B (2008) A metric for space. Hippocampus 18:1142–1156.

Moussa R, Poucet B, Amalric M, Sargolini F (2011) Contributions of dorsal striatal subregions to spatial alternation behavior. Learn Mem 18:444–451.

Mugnaini E, Sekerková G, Martina M (2011) The unipolar brush cell: a remarkable neuron finally receiving deserved attention. Brain Res Rev 66:220–245.

Muller R, Kubie J, Bostock E, Taube J, Quirk G (1991) Spatial firing correlates of neurons in the hippocampal formation of freely moving rats. Brain Sp (Paillard, J, ed), Oxford Univ Press:pp. 296–333.

Muller RU, Kubie JL (1987) The effects of changes in the environment on the spatial firing of hippocampal complex-spike cells. J Neurosci 7:1951–1968.

Muller RU, Kubie JL (1989) The firing of hippocampal place cells predicts the future position of freely moving rats. J Neurosci 9:4101–4110.

Muller U, Kubie JL, Ranck B (1987) Spatial Firing Patterns Fixed Environment of Hippocampal Complex-Spike Cells in a. J Neurosci 7.

Murase S, Hayashi Y (1996) Expression pattern of integrin beta 1 subunit in Purkinje cells of rat and cerebellar mutant mice. J Comp Neurol 375:225–237.

Muzzio I a, Levita L, Kulkarni J, Monaco J, Kentros C, Stead M, Abbott LF, Kandel ER (2009) Attention enhances the retrieval and stability of visuospatial and olfactory representations in the dorsal hippocampus. PLoS Biol 7:e1000140.

- N -

Nagahara AH, Otto T, Gallagher M (1995) Entorhinal-perirhinal lesions impair performance of rats on two versions of place learning in the Morris water maze. Behav Neurosci 109:3–9.

Nagao S, Ito M (1991) Subdural application of hemoglobin to the cerebellum blocks vestibuloocular reflex adaptation. Neuroreport 2:193–196.

Nagao S, Kitazawa H (2003) Effects of reversible shutdown of the monkey flocculus on the retention of adaptation of the horizontal vestibulo-ocular reflex. Neuroscience 118:563–570.

Napper RM, Harvey RJ (1988) Number of parallel fiber synapses on an individual Purkinje cell in the cerebellum of the rat. J Comp Neurol 274:168–177.

Nieto-Bona MP, Garcia-Segura LM, Torres-Alemán I (1997) Transynaptic modulation by insulin-like growth factor I of dendritic spines in Purkinje cells. Int J Dev Neurosci 15:749–754.

Norman G, Eacott MJ (2005) Dissociable effects of lesions to the perirhinal cortex and the postrhinal cortex on memory for context and objects in rats. Behav Neurosci 119:557–566.

Nunzi MG, Mugnaini E (2000) Unipolar brush cell axons form a large system of intrinsic mossy fibers in the postnatal vestibulocerebellum. J Comp Neurol 422:55–65.

- O -

O'Donoghue DL, King JS, Bishop GA (1989) Physiological and anatomical studies of the interactions between Purkinje cells and basket cells in the cat's cerebellar cortex: evidence for a unitary relationship. J Neurosci 9:2141–2150.

O'Keefe J, Black AH (1977) Single unit and lesion experiments on the sensory inputs to the hippocampal cognitive map. Ciba Found Symp:179–198.

O'Keefe J, Burgess N (1996) Geometric determinants of the place fields of hippocampal neurons. Nature 381:425–428.

O'Keefe J, Dostrovsky J (1971) The hippocampus as a spatial map. Preliminary evidence from unit activity in the freely-moving rat. Brain Res 34:171–175.

O'Keefe J, Speakman A (1987) Single unit activity in the rat hippocampus during a spatial memory task. Exp brain Res 68:1–27.

O'Steen WK, Spencer RL, Bare DJ, McEwen BS (1995) Analysis of severe photoreceptor loss and Morris water-maze performance in aged rats. Behav Brain Res 68:151–158.

Oberdick J, Smeyne RJ, Mann JR, Zackson S, Morgan JI (1990) A promoter that drives transgene expression in cerebellar Purkinje and retinal bipolar neurons. Science 248:223–226.

Oertel WH (1993) Neurotransmitters in the cerebellum. Scientific aspects and clinical relevance. Adv Neurol 61:33–75.

Ohtsuki G, Hirano T (2008) Bidirectional plasticity at developing climbing fiber-Purkinje neuron synapses. Eur J Neurosci 28:2393–2400.

Olton DS, Samuelson RJ (1976) Journal of Experimental Psychology : Animal Behavior Processes Remembrance of Places Passed : Spatial Memory in Rats. 2.

Orduz D, Llano I (2007) Recurrent axon collaterals underlie facilitating synapses between cerebellar Purkinje cells. Proc Natl Acad Sci U S A 104:17831–17836.

Oscarsson O (1979) Functional units of the cerebellum - sagittal zones and microzones. Trends Neurosci 2:143–145.

- P -

Packard MG, McGaugh JL (1996) Inactivation of hippocampus or caudate nucleus with lidocaine differentially affects expression of place and response learning. Neurobiol Learn Mem 65:65–72.

Palay S, Chan-Palay V (1974) Cerebellar cortex: cytology and organization.

Palkovits M, Magyar P, Szentágothai J (1971) Quantitative histological analysis of the cerebellar cortex in the cat. 3. Structural organization of the molecular layer. Brain Res 34:1–18.

Palkovits M, Mezey E, Hámori J, Szentágothai J (1977) Quantitative histological analysis of the cerebellar nuclei in the cat. I. Numerical data on cells and on synapses. Exp brain Res 28:189–209.

Park E, Dvorak D, Fenton A a (2011) Ensemble place codes in hippocampus: CA1, CA3, and dentate gyrus place cells have multiple place fields in large environments. PLoS One 6:e22349.

Parron C, Save E (2004) Evidence for entorhinal and parietal cortices involvement in path integration in the rat. Exp brain Res 159:349–359.

Paylor R, Nguyen M, Crawley JN, Patrick J, Beaudet A, Orr-urtreger A (1998) Alpha 7 Nicotinic Receptor Subunits Are Not Necessary for Hippocampal-Dependent Learning or Sensorimotor Gating : A Behavioral Characterization of Acra7-Deficient Mice. Learn Mem.

Paz-Villagrán V, Save E, Poucet B (2004) Independent coding of connected environments by place cells. Eur J Neurosci 20:1379–1390.

Pellow S, Chopin P, File SE, Briley M (1985) Validation of open:closed arm entries in an elevated plus-maze as a measure of anxiety in the rat. J Neurosci Methods 14:149–167.

Penner MR, Mizumori SJY (2012) Neural systems analysis of decision making during goal-directed navigation. Prog Neurobiol 96:96–135.

Person AL, Raman IM (2012) Synchrony and neural coding in cerebellar circuits. Front Neural Circuits 6:97.

Pichitpornchai C, Rawson JA, Rees S (1994) Morphology of parallel fibres in the cerebellar cortex of the rat: an experimental light and electron microscopic study with biocytin. J Comp Neurol 342:206–220.

Piochon C, Levenes C, Ohtsuki G, Hansel C (2010) Purkinje cell NMDA receptors assume a key role in synaptic gain control in the mature cerebellum. J Neurosci 30:15330–15335.

Poucet B (1993) Spatial cognitive maps in animals: new hypotheses on their structure and neural mechanisms. Psychol Rev 100:163–182.

Poucet B, Benhamou S (1997) The neuropsychology of spatial cognition in the rat. Crit Rev Neurobiol 11:101–120.

Prevosto V, Graf W, Ugolini G (2010) Cerebellar inputs to intraparietal cortex areas LIP and MIP: functional frameworks for adaptive control of eye movements, reaching, and arm/eye/head movement coordination. Cereb Cortex 20:214–228.

- Q -

Qiu D, Knöpfel T (2009) Presynaptically expressed long-term depression at cerebellar parallel fiber synapses. Pflugers Arch 457:865–875.

Quirk QJ, Muller U, Kubie JL (1990) The Firing of Hippocampal Rat ' s Recent Experience Place Cells in the Dark Depends on the. 7:2008–2017.

Quy PN, Fujita H, Sakamoto Y, Na J, Sugihara I (2011) Projection patterns of single mossy fiber axons originating from the dorsal column nuclei mapped on the aldolase C compartments in the rat cerebellar cortex. J Comp Neurol 519:874–899.

- R -

Racine RJ, Wilson DA, Gingell R, Sunderland D (1986) Long-term potentiation in the interpositus and vestibular nuclei in the rat. Exp brain Res 63:158–162.

Ragozzino ME, Adams S, Kesner RP (1998) Differential involvement of the dorsal anterior cingulate and prelimbic-infralimbic areas of the rodent prefrontal cortex in spatial working memory. Behav Neurosci 112:293–303.

Rahmati N, Owens CB, Bosman LWJ, Spanke JK, Lindeman S, Gong W, Potters J-W, Romano V, Voges K, Moscato L, Koekkoek SKE, Negrello M, De Zeeuw CI (2014) Cerebellar potentiation and learning a whisker-based object localization task with a time response window. J Neurosci 34:1949–1962.

Raman IM, Bean BP (1999) Ionic currents underlying spontaneous action potentials in isolated cerebellar Purkinje neurons. J Neurosci 19:1663–1674.

Ramnani N (2006) The primate cortico-cerebellar system: anatomy and function. Nat Rev Neurosci 7:511–522.

Ramon Y Cajal S (1911) Histologie du systeme nerveux de l'homme et des vertebres. Maloine, Paris.

Rancillac A, Crépel F (2004) Synapses between parallel fibres and stellate cells express long-term changes in synaptic efficacy in rat cerebellum. J Physiol 554:707–720.

Ravassard P, Kees A, Willers B, Ho D, Aharoni D, Cushman J, Aghajan ZM, Mehta MR (2013) Multisensory control of hippocampal spatiotemporal selectivity. Science 340:1342–1346.

Reep RL, Chandler HC, King V, Corwin J V (1994) Rat posterior parietal cortex: topography of corticocortical and thalamic connections. Exp brain Res 100:67–84.

Reisel D, Bannerman DM, Schmitt WB, Deacon RMJ, Flint J, Borchardt T, Seeburg PH, Rawlins JNP (2002) Spatial memory dissociations in mice lacking GluR1. Nat Neurosci 5:868–873.

Renaudineau S, Poucet B, Laroche S, Davis S, Save E (2009) Impaired long-term stability of CA1 place cell representation in mice lacking the transcription factor zif268/egr1. Proc Natl Acad Sci U S A 106:11771–11775.

Renaudineau S, Poucet B, Save E (2007) Flexible use of proximal objects and distal cues by hippocampal place cells. Hippocampus 17:381–395.

Resnik E, McFarland JM, Sprengel R, Sakmann B, Mehta MR (2012) The effects of GluA1 deletion on the hippocampal population code for position. J Neurosci 32:8952–8968.

Rivard B, Li Y, Lenck-Santini P-P, Poucet B, Muller RU (2004) Representation of objects in space by two classes of hippocampal pyramidal cells. J Gen Physiol 124:9–25.

Rochefort C, Arabo a., Andre M, Poucet B, Save E, Rondi-Reig L (2011) Cerebellum Shapes Hippocampal Spatial Code. Science (80-) 334:385–389.

Rogers DC, Fisher EM, Brown SD, Peters J, Hunter AJ, Martin JE (1997) Behavioral and functional analysis of mouse phenotype: SHIRPA, a proposed protocol for comprehensive phenotype assessment. Mamm Genome 8:711–713.

Rokni D, Llinas R, Yarom Y (2008) The Morpho/Functional Discrepancy in the Cerebellar Cortex: Looks Alone are Deceptive. Front Neurosci 2:192–198.

Rondi-Reig L, Burguière E (2005) Is the cerebellum ready for navigation? Prog Brain Res.

Rondi-Reig L, Delhaye-Bouchaud N, Mariani J, Caston J (1997) Role of the inferior olivary complex in motor skills and motor learning in the adult rat. Neuroscience 77:955–963.

Rondi-Reig L, Le Marec N, Caston J, Mariani J (2002) The role of climbing and parallel fibers inputs to cerebellar cortex in navigation. Behav Brain Res 132:11–18.

Rondi-Reig L, Lemaigre-Dubreuil Y, Montécot C, Müller D, Martinou JC, Caston J, Mariani J (2001) Transgenic mice with neuronal overexpression of bcl-2 gene present navigation disabilities in a water task. Neuroscience 104:207–215.

Rondi-Reig L, Mariani J (2002) To die or not to die, does it change the function? Behavior of transgenic mice reveals a role for developmental cell death. Brain Res Bull 57:85–91.

Rossier J, Haeberli C, Schenk F (2000) Auditory cues support place navigation in rats when associated with a visual cue. Behav Brain Res 117:209–214.

Rossier J, Schenk F (2003) Olfactory and/or visual cues for spatial navigation through ontogeny: Olfactory cues enable the use of visual cues. Behav Neurosci 117:412–425.

Rotenberg A, Muller RU (1997) Variable place-cell coupling to a continuously viewed stimulus: evidence that the hippocampus acts as a perceptual system. Philos Trans R Soc Lond B Biol Sci 352:1505–1513.

Rousseau C V, Dugué GP, Dumoulin A, Mugnaini E, Dieudonné S, Diana MA (2012) Mixed inhibitory synaptic balance correlates with glutamatergic synaptic phenotype in cerebellar unipolar brush cells. J Neurosci 32:4632–4644.

Roy JE, Cullen KE (2001) Selective processing of vestibular reafference during self-generated head motion. J Neurosci 21:2131–2142.

Roy JE, Cullen KE (2003) Brain stem pursuit pathways: dissociating visual, vestibular, and proprioceptive inputs during combined eye-head gaze tracking. J Neurophysiol 90:271–290.

Roy JE, Cullen KE (2004) Dissociating self-generated from passively applied head motion: neural mechanisms in the vestibular nuclei. J Neurosci 24:2102–2111.

Ruigrok T (1997) Cerebellar nuclei: the olivary connection. Prog Brain Res.

Ruigrok TJH (2004) Precerebellar nuclei and red nucleus. Rat Nerv Syst:1328.

- S -

Sahin M, Hockfield S (1990) Molecular identification of the Lugaro cell in the cat cerebellar cortex. J Comp Neurol 301:575–584.

Salin PA, Malenka RC, Nicoll RA (1996) Cyclic AMP mediates a presynaptic form of LTP at cerebellar parallel fiber synapses. Neuron 16:797–803.

Sargolini F, Fyhn M, Hafting T, McNaughton BL, Witter MP, Moser M-B, Moser EI (2006) Conjunctive representation of position, direction, and velocity in entorhinal cortex. Science 312:758–762.

Sarna JR, Marzban H, Watanabe M, Hawkes R (2006) Complementary stripes of phospholipase Cbeta3 and Cbeta4 expression by Purkinje cell subsets in the mouse cerebellum. J Comp Neurol 496:303–313.

Save E, Guazzelli A, Poucet B (2001) Dissociation of the effects of bilateral lesions of the dorsal hippocampus and parietal cortex on path integration in the rat. Behav Neurosci 115:1212–1223.

Save E, Moghaddam M (1996) Effects of lesions of the associative parietal cortex on the acquisition and use of spatial memory in egocentric and allocentric navigation tasks in the rat. Behav Neurosci 110:74–85.

Save E, Nerad L, Poucet B (2000) Contribution of multiple sensory information to place field stability in hippocampal place cells. Hippocampus 10:64–76.

Save E, Paz-Villagran V, Alexinsky T, Poucet B (2005) Functional interaction between the associative parietal cortex and hippocampal place cell firing in the rat. Eur J Neurosci 21:522–530.

Save E, Poucet B (2000) Involvement of the hippocampus and associative parietal cortex in the use of proximal and distal landmarks for navigation. Behav Brain Res 109:195–206.

Save E, Poucet B (2009) Role of the parietal cortex in long-term representation of spatial information in the rat. Neurobiol Learn Mem 91:172–178.

Save E, Poucet B, Foreman N, Buhot MC (1992) Object exploration and reactions to spatial and nonspatial changes in hooded rats following damage to parietal cortex or hippocampal formation. Behav Neurosci 106:447–456.

Savelli F, Yoganarasimha D, Knierim JJ (2008) Influence of boundary removal on the spatial representations of the medial entorhinal cortex. Hippocampus 18:1270–1282.

Sawtell NB, Bell CC (2008) Adaptive processing in electrosensory systems: links to cerebellar plasticity and learning. J Physiol Paris 102:223–232.

Sawtell NB, Williams A (2008) Transformations of electrosensory encoding associated with an adaptive filter. J Neurosci 28:1598–1612.

Schmahmann JD, Sherman JC (1998) The cerebellar cognitive affective syndrome. Brain 121 (Pt 4:561–579.

Schmidt-Hieber C, Häusser M (2013) Cellular mechanisms of spatial navigation in the medial entorhinal cortex. Nat Neurosci 16:325–331.

Schmolesky MT, Weber JT, De Zeeuw CI, Hansel C (2002) The making of a complex spike: ionic composition and plasticity. Ann N Y Acad Sci 978:359–390.

Schonewille M, Belmeguenai a, Koekkoek SK, Houtman SH, Boele HJ, van Beugen BJ, Gao Z, Badura a, Ohtsuki G, Amerika WE, Hosy E, Hoebeek FE, Elgersma Y, Hansel C, De Zeeuw CI (2010) Purkinje cell-specific knockout of the protein phosphatase PP2B impairs potentiation and cerebellar motor learning. Neuron 67:618–628.

Schonewille M, Gao Z, Boele H-J, Veloz MFV, Amerika WE, Simek A a M, De Jeu MT, Steinberg JP, Takamiya K, Hoebeek FE, Linden DJ, Huganir RL, De Zeeuw CI (2011) Reevaluating the role of LTD in cerebellar motor learning. Neuron 70:43–50.

Seja P, Schonewille M, Spitzmaul G, Badura A, Klein I, Rudhard Y, Wisden W, Hübner C a, De Zeeuw CI, Jentsch TJ (2012) Raising cytosolic Cl- in cerebellar granule cells affects their excitability and vestibulo-ocular learning. EMBO J 31:1217–1230.

Semenov L V, Bures J (1989) Vestibular stimulation disrupts acquisition of place navigation in the Morris water tank task. Behav Neural Biol 51:346–363.

Serapide MF, Pantó MR, Parenti R, Zappalá A, Cicirata F (2001) Multiple zonal projections of the basilar pontine nuclei to the cerebellar cortex of the rat. J Comp Neurol 430:471–484.

Shaikh AG, Meng H, Angelaki DE (2004) Multiple reference frames for motion in the primate cerebellum. J Neurosci 24:4491–4497.

Shambes GM, Gibson JM, Welker W (1978) Fractured somatotopy in granule cell tactile areas of rat cerebellar hemispheres revealed by micromapping. Brain Behav Evol 15:94–140.

Shapiro ML, Tanila H, Eichenbaum H (1997) Cues that hippocampal place cells encode: dynamic and hierarchical representation of local and distal stimuli. Hippocampus 7:624–642.

Shibuki K, Gomi H, Chen L, Bao S, Kim JJ, Wakatsuki H, Fujisaki T, Fujimoto K, Katoh a, Ikeda T, Chen C, Thompson RF, Itohara S (1996) Deficient cerebellar long-term depression, impaired eyeblink conditioning, and normal motor coordination in GFAP mutant mice. Neuron 16:587–599.

Sillitoe R V, Chung S-H, Fritschy J-M, Hoy M, Hawkes R (2008) Golgi cell dendrites are restricted by Purkinje cell stripe boundaries in the adult mouse cerebellar cortex. J Neurosci 28:2820–2826.

Sillitoe R V, Marzban H, Larouche M, Zahedi S, Affanni J, Hawkes R (2005) Conservation of the architecture of the anterior lobe vermis of the cerebellum across mammalian species. Prog Brain Res 148:283–297.

Simat M, Parpan F, Fritschy J-M (2007) Heterogeneity of glycinergic and gabaergic interneurons in the granule cell layer of mouse cerebellum. J Comp Neurol 500:71–83.

Simpson JI, Wylie DR, De Zeeuw CI (1996) On climbing fiber signals and their consequence(s). Behav Brain Sci 19:384–398.

Smeyne RJ, Chu T, Lewin A, Bian F, Sanlioglu S, S-Crisman S, Kunsch C, Lira SA, Oberdick J (1995) Local control of granule cell generation by cerebellar Purkinje cells. Mol Cell Neurosci 6:230–251.

Solstad T, Boccara CN, Kropff E, Moser M-B, Moser EI (2008) Representation of geometric borders in the entorhinal cortex. Science 322:1865–1868.

Solstad T, Moser EI, Einevoll GT (2006) From Grid Cells to Place Cells : A Mathematical Model. 1031:1026–1031.

Song M, Messing RO (2005) Protein kinase C regulation of GABAA receptors. Cell Mol Life Sci 62:119–127.

Sotelo C (1967) Cerebellar neuroglia: morphological and histochemical aspects. Prog Brain Res 25:226–250.

Spiers HJ, Maguire E a (2006) Thoughts, behaviour, and brain dynamics during navigation in the real world. Neuroimage 31:1826–1840.

Stackman RW, Clark AS, Taube JS (2002) Hippocampal spatial representations require vestibular input. Hippocampus 12:291–303.

Stackman RW, Herbert AM (2002) Rats with lesions of the vestibular system require a visual landmark for spatial navigation. Behav Brain Res 128:27–40.

Stackman RW, Taube JS (1997) Firing properties of head direction cells in the rat anterior thalamic nucleus: dependence on vestibular input. J Neurosci 17:4349–4358.

Stackman RW, Taube JS (1998) Firing properties of rat lateral mammillary single units: head direction, head pitch, and angular head velocity. J Neurosci 18:9020–9037.

Stackman RW, Tullman ML, Taube JS (2000) Maintenance of rat head direction cell firing during locomotion in the vertical plane. J Neurophysiol 83:393–405.

Stein JF, Glickstein M (1992) Role of the cerebellum in visual guidance of movement. Physiol Rev 72:967–1017.

Stensola H, Stensola T, Solstad T, Frøland K, Moser M-B, Moser EI (2012) The entorhinal grid map is discretized. Nature 492:72–78.

Strick PL, Dum RP, Fiez J a (2009) Cerebellum and nonmotor function. Annu Rev Neurosci 32:413–434.

Sugihara I, Quy PN (2007) Identification of aldolase C compartments in the mouse cerebellar cortex by olivocerebellar labeling. J Comp Neurol 500:1076–1092.

Sugihara I, Shinoda Y (2004) Molecular, topographic, and functional organization of the cerebellar cortex: a study with combined aldolase C and olivocerebellar labeling. J Neurosci 24:8771–8785.

Sugihara I, Wu H, Shinoda Y (1999) Morphology of single olivocerebellar axons labeled with biotinylated dextran amine in the rat. J Comp Neurol 414:131–148.

Sultan F, Bower JM (1998) Quantitative Golgi study of the rat cerebellar molecular layer interneurons using principal component analysis. J Comp Neurol 393:353–373.

Szapiro G, Barbour B (2007) Multiple climbing fibers signal to molecular layer interneurons exclusively via glutamate spillover. Nat Neurosci 10:735–742.

- T -

Taube JS (1995) Head direction cells recorded in the anterior thalamic nuclei of freely moving rats. J Neurosci 15:70–86.

Taube JS (2007) The head direction signal: origins and sensory-motor integration. Annu Rev Neurosci 30:181–207.

Taube JS, Muller RU, Ranck JB (1990) Head-direction cells recorded from the postsubiculum in freely moving rats. II. Effects of environmental manipulations. J Neurosci 10:436–447.

Thach WT, Goodkin HP, Keating JG (1992) The cerebellum and the adaptive coordination of movement. Annu Rev Neurosci 15:403–442.

Thompson L, Best P (1990) Long-term stability of the place-field activity of single units recorded from the dorsal hippocampus of freely behaving rats. Brain Res.

Tolman EC (1948) Cognitive maps in rats and men. Psychol Rev 55:189–208.

- U -

Uusisaari M, Obata K, Knöpfel T (2007) Morphological and electrophysiological properties of GABAergic and non-GABAergic cells in the deep cerebellar nuclei. J Neurophysiol 97:901–911.

- V -

Valerio S, Taube JS (2012) Path integration: how the head direction signal maintains and corrects spatial orientation. Nat Neurosci 15:1445–1453.

Van Cauter T, Camon J, Alvernhe A, Elduayen C, Sargolini F, Save E (2013) Distinct roles of medial and lateral entorhinal cortex in spatial cognition. Cereb Cortex 23:451–459.

Van den Burg EH, Engelmann J, Bacelo J, Gómez L, Grant K (2007) Etomidate reduces initiation of backpropagating dendritic action potentials: implications for sensory processing and synaptic plasticity during anesthesia. J Neurophysiol 97:2373–2384.

Van der Meer M a a, Richmond Z, Braga RM, Wood ER, Dudchenko P a (2010) Evidence for the use of an internal sense of direction in homing. Behav Neurosci 124:164–169.

Van Ham JJ, Yeo CH (1992) Somatosensory Trigeminal Projections to the Inferior Olive, Cerebellum and other Precerebellar Nuclei in Rabbits. Eur J Neurosci 4:302–317.

Verbitsky M, Yonan AL, Malleret G, Kandel ER, Gilliam TC, Pavlidis P (2004) Altered hippocampal transcript profile accompanies an age-related spatial memory deficit in mice. Learn Mem 11:253–260.

Von Holst E, Mittelstaedt H (1950) Das reafferenzprinzip. Naturwissenschaften.

Voogd J (2004) Cerebellum. Rat Nerv Syst.

Voogd J, Gerrits NM, Ruigrok TJ (1996) Organization of the vestibulocerebellum. Ann N Y Acad Sci 781:553–579.

Voogd J, Pardoe J, Ruigrok TJH, Apps R (2003) The distribution of climbing and mossy fiber collateral branches from the copula pyramidis and the paramedian lobule: congruence of climbing fiber cortical zones and the pattern of zebrin banding within the rat cerebellum. J Neurosci 23:4645–4656.

Vorhees C V, Williams MT (2006) Morris water maze: procedures for assessing spatial and related forms of learning and memory. Nat Protoc 1:848–858.

Vos BP, Maex R, Volny-Luraghi A, De Schutter E (1999) Parallel fibers synchronize spontaneous activity in cerebellar Golgi cells. J Neurosci 19:RC6.

- W -

Wada N, Kishimoto Y, Watanabe D, Kano M, Hirano T, Funabiki K, Nakanishi S (2007) Conditioned eyeblink learning is formed and stored without cerebellar granule cell transmission. Proc Natl Acad Sci U S A 104:16690–16695.

Wallace DG, Hines DJ, Pellis SM, Whishaw IQ (2002) Vestibular information is required for dead reckoning in the rat. J Neurosci 22:10009–10017.

Walter H, Vetter SC, Grothe J, Wunderlich a P, Hahn S, Spitzer M (2001) The neural correlates of driving. Neuroreport 12:1763–1767.

Wang D-J, Su L-D, Wang Y-N, Yang D, Sun C-L, Zhou L, Wang X-X, Shen Y (2014) Long-term potentiation at cerebellar parallel fiber-Purkinje cell synapses requires presynaptic and postsynaptic signaling cascades. J Neurosci 34:2355–2364.

Wang X, Chen G, Gao W, Ebner T (2009) Long-term potentiation of the responses to parallel fiber stimulation in mouse cerebellar cortex in vivo. Neuroscience 162:713–722.

Wang YT, Linden DJ (2000) Expression of cerebellar long-term depression requires postsynaptic clathrin-mediated endocytosis. Neuron 25:635–647.

Watanabe M, Kano M (2011) Climbing fiber synapse elimination in cerebellar Purkinje cells. Eur J Neurosci 34:1697–1710.

Weiskrantz L, Elliott J, Darlington C (1971) Preliminary observations on tickling oneself. Nature.

Welsh JP, Harvey JA (1998) Acute inactivation of the inferior olive blocks associative learning. Eur J Neurosci 10:3321–3332.

Welsh JP, Yamaguchi H, Zeng X-H, Kojo M, Nakada Y, Takagi A, Sugimori M, Llinás RR (2005) Normal motor learning during pharmacological prevention of Purkinje cell long-term depression. Proc Natl Acad Sci U S A 102:17166–17171.

Whishaw IQ, Gorny B (1999) Path integration absent in scent-tracking fimbria-fornix rats: evidence for hippocampal involvement in “sense of direction” and “sense of distance” using self-movement cues. J Neurosci 19:4662–4673.

Whitlock JR, Derdikman D (2012) Head direction maps remain stable despite grid map fragmentation. Front Neural Circuits 6:9.

Whitlock JR, Pfuhl G, Dagslott N, Moser M-B, Moser EI (2012) Functional split between parietal and entorhinal cortices in the rat. Neuron 73:789–802.

Wilber A, Clark BJ, Forster TC, Tatsuno M, McNaughton BL (2014) Interaction of egocentric and world-centered reference frames in the rat posterior parietal cortex. J Neurosci 34:5431–5446.

Wiener SI (1993) Spatial and behavioral correlates of striatal neurons in rats performing a self-initiated navigation task. J Neurosci 13:3802–3817.

Wills TJ, Cacucci F, Burgess N, O’Keefe J (2010) Development of the hippocampal cognitive map in preweanling rats. Science 328:1573–1576.

Wilson M a, McNaughton BL (1993) Dynamics of the hippocampal ensemble code for space. Science 261:1055–1058.

Witter MP, Moser EI (2006) Spatial representation and the architecture of the entorhinal cortex. Trends Neurosci 29:671–678.

Witter MP, Wouterlood FG, Naber P a, Van Haeften T (2000) Anatomical organization of the parahippocampal-hippocampal network. Ann N Y Acad Sci 911:1–24.

Woolston DC, La Londe JR, Gibson JM (1982) Comparison of response properties of cerebellar- and thalamic-projecting interpolaris neurons. J Neurophysiol 48:160–173.

Wu HS, Sugihara I, Shinoda Y (1999) Projection patterns of single mossy fibers originating from the lateral reticular nucleus in the rat cerebellar cortex and nuclei. J Comp Neurol 411:97–118.

- X -

Xu W, Edgley SA (2008) Climbing fibre-dependent changes in Golgi cell responses to peripheral stimulation. J Physiol 586:4951–4959.

- Y -

Yaginuma H, Matsushita M (1986) Spinocerebellar projection fields in the horizontal plane of lobules of the cerebellar anterior lobe in the cat: an anterograde wheat germ agglutinin-horseradish peroxidase study. Brain Res 365:345–349.

Yakusheva T a, Blazquez PM, Chen A, Angelaki DE (2013) Spatiotemporal properties of optic flow and vestibular tuning in the cerebellar nodulus and uvula. J Neurosci 33:15145–15160.

Yakusheva TA, Shaikh AG, Green AM, Blazquez PM, Dickman JD, Angelaki DE (2007) Purkinje cells in posterior cerebellar vermis encode motion in an inertial reference frame. Neuron 54:973–985.

Yoder RM, Clark BJ, Brown JE, Lamia M V, Valerio S, Shinder ME, Taube JS (2011) Both visual and idiothetic cues contribute to head direction cell stability during navigation along complex routes. J Neurophysiol 105:2989–3001.

Yoder RM, Taube JS (2014) The vestibular contribution to the head direction signal and navigation. Front Integr Neurosci 8:32.

Yoganarasimha D, Knierim JJ (2005) Coupling between place cells and head direction cells during relative translations and rotations of distal landmarks. Exp brain Res 160:344–359.

Yoganarasimha D, Yu X, Knierim JJ (2006) Head direction cell representations maintain internal coherence during conflicting proximal and distal cue rotations: comparison with hippocampal place cells. J Neurosci 26:622–631.

- Z -

Zamanillo D, Sprengel R, Hvalby O, Jensen V, Burnashev N, Rozov A, Kaiser KM, Köster HJ, Borchardt T, Worley P, Lübke J, Frotscher M, Kelly PH, Sommer B, Andersen P, Seeburg PH, Sakmann B (1999) Importance of AMPA receptors for hippocampal synaptic plasticity but not for spatial learning. Science 284:1805–1811.

Zeng H, Chattarji S, Barbarosie M, Rondi-Reig L, Philpot BD, Miyakawa T, Bear MF, Tonegawa S (2001) Forebrain-specific calcineurin knockout selectively impairs bidirectional synaptic plasticity and working/episodic-like memory. Cell 107:617–629.

Zhang S, Manahan-Vaughan D (2013) Spatial Olfactory Learning Contributes to Place Field Formation in the Hippocampus. Cereb Cortex:1–10.

Zhang S-J, Ye J, Miao C, Tsao A, Cerniauskas I, Ledergerber D, Moser M-B, Moser EI (2013) Optogenetic dissection of entorhinal-hippocampal functional connectivity. Science 340:1232627.

Zhou H, Lin Z, Voges K, Ju C, Gao Z, Bosman LW, Ruigrok TJ, Hoebeek FE, De Zeeuw CI, Schonewille M (2014) Cerebellar modules operate at different frequencies. Elife:e02536.

Zoladek L, Roberts W a. (1978) The sensory basis of spatial memory in the rat. Anim Learn Behav 6:77–81.

Zugaro MB, Berthoz A, Wiener SI (2001) Background, but not foreground, spatial cues are taken as references for head direction responses by rat anterodorsal thalamus neurons. J Neurosci 21:RC154.

Journal of Neuroscience Methods 215 (2013) 196–209

Contents lists available at SciVerse ScienceDirect

Journal of Neuroscience Methods

journal homepage: www.elsevier.com/locate/jneumeth

Basic Neuroscience

A Navigation Analysis Tool (NAT) to assess spatial behavior in open-field and structured mazes

Frédéric Jarlier[1], Angelo Arleo[1], Géraldine H. Petit, Julie M. Lefort, Céline Fouquet, Eric Burguière, Laure Rondi-Reig*

CNRS – University Pierre and Marie Curie-P6, Unit of Neurobiology of Adaptive Processes, UMR 7102, F-75005 Paris, France

HIGHLIGHTS

- Novel analysis tool probing spatial behavior in open-field and structured mazes.
- Multi-parametric analysis of goal-oriented navigation and decision making policy.
- Wide range of protocols and data managed within the same relational database.
- Unified view through observations from multiple spatial navigation paradigms.
- Results on the ability of mice to learn the Morris watermaze and the starmaze tasks.

ARTICLE INFO

Article history:
Received 19 November 2012
Received in revised form 26 February 2013
Accepted 27 February 2013

Keywords:
Spatial behavior
Navigation strategies
Goal-oriented behavior
Decision point analysis
Automated statistical analysis
MATLAB analysis toolbox
MySQL relational database
JAVA graphical user interface
Open source software

ABSTRACT

Spatial navigation calls upon mnemonic capabilities (e.g. remembering the location of a rewarding site) as well as adaptive motor control (e.g. fine tuning of the trajectory according to the ongoing sensory context). To study this complex process by means of behavioral measurements it is necessary to quantify a large set of meaningful parameters on multiple time scales (from milliseconds to several minutes), and to compare them across different paradigms. Moreover, the issue of automating the behavioral analysis is critical to cope with the consequent computational load and the sophistication of the measurements. We developed a general purpose Navigation Analysis Tool (NAT) that provides an integrated architecture consisting of a data management system (implemented in MySQL), a core analysis toolbox (in MATLAB), and a graphical user interface (in JAVA). Its extensive characterization of trajectories over time, from exploratory behavior to goal-oriented navigation with decision points using a wide range of parameters, makes NAT a powerful analysis tool. In particular, NAT supplies a new set of specific measurements assessing performances in multiple intersection mazes and allowing navigation strategies to be discriminated (e.g. in the starmaze). Its user interface enables easy use while its modular organization provides many opportunities of extension and customization. Importantly, the portability of NAT to any type of maze and environment extends its exploitation far beyond the field of spatial navigation.

1. Introduction

Spatial navigation is a manifold process whose dynamics depend on a wide range of competitive and/or cooperative mechanisms (see Arleo and Rondi-Reig, 2007, for a review). Dissecting spatial behavior into its elementary components is instrumental, for instance, to correlate single neuron activity to specific behavioral patterns (e.g. Whitlock et al., 2012), and then to infer novel anatomo-functional properties based on causal animal–environment interactions. Analyzing spatial behavior can also help to elucidate the link between specific neuronal adaptation deficits (e.g. lack of synaptic plasticity in transgenic animals) and subtle goal-oriented navigation impairments (e.g. Rondi-Reig et al., 2001; Burguière et al., 2005; Rochefort et al., 2011).

Meaningful accounts of spatial behavior require multi-parameter analysis of large experimental datasets. Also, the ability to bind observations across multiple spatial learning tasks (which produce heterogeneous data in terms of performance indicators, protocols, maze shapes, and task complexity) is a necessary condition toward a unified view of the mechanisms underpinning spatial cognition. During the last decades, these considerations have given rise to a substantial effort to conceive automated analysis tools

* Corresponding author at: ENMVI Lab, UMR 7102, Case 01, UPMC, 9 quai Saint Bernard, 75005 Paris, France. Tel.: +33 144 272 044.
E-mail address: laure.rondi@snv.jussieu.fr (L. Rondi-Reig).
[1] These authors contributed equally to this work.

0165-0270/$ – see front matter © 2013 Elsevier B.V. All rights reserved.
http://dx.doi.org/10.1016/j.jneumeth.2013.02.018

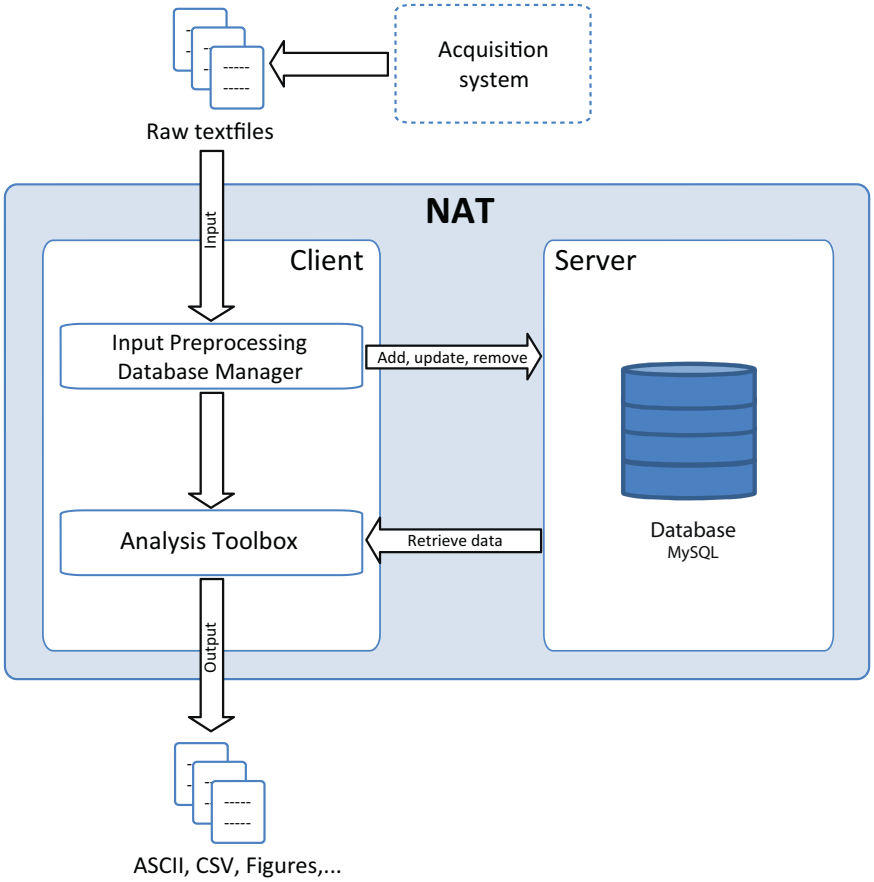

Fig. 1. NAT overview. NAT consists of a client/server architecture. On the client side, a first module allows the experimenter to preprocess and import recorded data, whereas a second module (in MATLAB) implements the behavioral parametric analysis. On the server side, a MySQL relational database allows large sets of behavioral recordings to be stored and managed. A graphical user interface (in JAVA) assists the experimenter throughout the entire database managing and analysis process.

and data management systems (e.g. Bradley et al., 2005; Drai and Golani, 2001; Wolfer and Lipp, 1992; see Section 4 for a Discussion on existing solutions).

This paper presents a Navigation Analysis Tool (NAT) that was explicitly designed to cope with large behavioral datasets, and to draw coherent interpretations across multiple spatial learning tasks (e.g. involving both open-field and structured mazes). NAT provides an extended parameter space to characterize spatial behavior quantitatively, with a focus on goal-directed navigation and decision point analysis. It offers a flexible and easy-to-use tool aimed at benchmarking the analysis of spatial navigation data. The rationale behind the development of NAT is indeed to provide a standardized analysis framework to study learning and memory in the case of spatial navigation. NAT is released as open source software under the CeCILL license (compatible with GNU GPL), and it can be downloaded from the Plume web site www.projet-plume.org/en (see also the Supplementary User Guide).

In the following, we first describe the main features of NAT, which include information processing and management, and statistical behavioral analysis. We then provide a series of results obtained by applying NAT to quantify the spatial behavior of mice in two navigation tasks, namely the watermaze (Morris et al., 1982; Morris, 1981) and the starmaze (Rondi-Reig et al., 2006).

2. Materials and methods

NAT has a modular environment based on a client/server architecture (Fig. 1). On the client side, a graphical user interface (implemented in JAVA) helps the experimenter throughout the entire analysis process, which is mediated by two primary modules. First, the 'Input preprocessing and database manager' module allows behavioral recordings from an acquisition system to be preprocessed and imported into NAT (Section 2.1). Second, the 'Statistical analysis toolbox' (implemented in MATLAB) allows the experimenter to execute a set of parametric measurements to characterize spatial navigation performance (Section 2.2). The results of these parametric measures form the output of NAT (Fig. 1), which can be used for additional analyses (e.g. statistical significance). On the server side, a relational database (implemented in MySQL) provides an information management solution for storing large ensembles of behavioral data. It also allows specialized analysis software (e.g. MATLAB) to easily connect to and interact with the NAT base of knowledge.

2.1. Input preprocessing and database manager

For each experimental trial, NAT expects a text file containing (i) a time series of the positions visited by the animal $\{t, x(t), y(t)\}$ (where $x(t), y(t)$ denote the Cartesian coordinates of the barycenter of the body), and (ii) a numerical identifier for the subject. The format of the input data stream processed by NAT is described in the Supplementary User Guide, Sec. 2b.

2.1.1. Preprocessing and artifact correction

Video tracking systems can occasionally produce spurious data that lead to incongruent measures of the spatial coordinates of the animal over time. These artifacts can ultimately bias the evaluation

of some behavioral parameters. Prior to the feeding of data into the SQL server database, NAT preprocesses the time series $\{t, x(t), y(t)\}$ recorded by the acquisition system, and corrects possible artifacts automatically. It employs two artifact correction procedures. The first denoising algorithm relies on an iterative low-pass filter using a speed threshold to identify artifactual points and correct them based on a linear interpolation algorithm. The second procedure (optional) implements a Kalman filter on the speed domain to produce smooth navigation speed profiles. See Appendix A and Figs. A.1 and A.2 for further details on the two artifact correction algorithms.

2.1.2. Database manager

The graphical interface provided by NAT allows the experimenter to feed the database with the preprocessed data. At a lower level, a database manager module (installed on the client side) handles all user commands by communicating with the SQL server through a standard TCP/IP network protocol. The experimenter can either create a new project in the database or update (and eventually remove) an existing one. The creation of a new project involves a setup procedure allowing the experimenter to inform NAT about the type of maze (e.g. open-field, multi-intersection), the specific navigation task (e.g. Morris watermaze, Y-maze, starmaze), and the protocol details (e.g. number of training days, trials per day, starting locations, target(s) location(s), and so on). NAT provides a series of setup templates that can be used to speed up this configuration procedure. After the creation of project, the experimenter can feed the database with recorded data. Based on the setup information, NAT will store data according to rules that are specific to the type of maze and navigation protocol, which aims at producing and maintaining consistent data structures in the database. The experimenter can also update an existing project at any time, for instance by inserting a new experimental protocol to the project or by adding a new set of behavioral data.

2.2. Statistical analysis toolbox

At the core of NAT is an analysis toolbox that (i) measures a series of behavioral parameters to characterize goal-oriented navigation and locomotor activity (Section 2.2.1), (ii) performs decision-point analyses in multi-intersection navigation tasks (Section 2.2.2), and (iii) computes 3D representations of the spatial distribution of some measured parameters suitable for qualitative behavioral assessment (Section 2.2.3). Table 1 provides a summary of the analysis spectrum performed by NAT.

The NAT graphical interface allows the experimenter to select a project from the server database. Then, NAT runs the analysis in batch mode, which allows all the trials of the project to be processed (e.g. an experiment with 2 groups of 10 animals each, 4 trials per day per animal, and 10 training days would result in 800 trials processed by NAT). The system measures all desired parameters for each trial, then it averages the observed values over all training days, all animals of the same group, and all groups (e.g. control and mutant mice). All the numerical results (e.g. means, standard deviations, and mean standard errors) are saved as both ASCII and CSV files, whereas all graphics (e.g. the profile of the progression speed over a trial) are saved as both postscript and MATLAB figures. These results are then suited to carry out statistical significance analyses (e.g. *t*- and ANOVA tests) at any intermediate level (e.g. comparing the performance time course of the same animal over multiple trials, or comparing the learning capabilities across training of different groups of animals). In order to facilitate additional post hoc factor analysis (Boguszewski and Zagrodzka, 2002; Graziano et al., 2003), NAT provides a graphical interface to gather and organize sets of measured parameters from processed experiments/sessions/trials into tables (e.g. with rows indexing different subjects and columns indexing different parameters).

Table 1
Summary of the behavioral parameters analyzed by the current version of NAT.

Parameters	Maze type	
	Multi-intersection	Open-field
Goal-oriented navigation and locomotor activity analysis		
Escape latency	•	•
Traveled distance	•	•
Navigation speed	•	•
Resting/rearing/stop events	•	•
Distance to the target	•	•
Body rotation	•	•
Heading-to-goal	•	•
Curvature radius	•	•
Parallelism index	•	•
Path sinuosity	•	•
Path tortuosity		•
Spatial preference	•	•
Mean trajectory	•	
Distance to walls and/or objects	•	•
Number of alleys visited before reaching the target	•	
Decision point analysis		
Sequence of visited alleys	•	
Localization score	•	
Direct path scores	•	
3D-maps for qualitative behavioral analysis		
Spatial occupancy	•	•
Instantaneous speed	•	•
Instantaneous heading variability	•	•
Curvature radius	•	•

2.2.1. Goal-oriented navigation and locomotor activity analysis

NAT computes a set of performance indicators to assess both goal-directed navigation and more general (e.g. geometry-related) characteristics of locomotor activity (e.g. exploratory patterns). See Appendix B for formal definitions of some parameters presented below.

Escape latency. This parameter quantifies the time (expressed in s) needed, on average, by an animal to navigate to the goal from any starting location in the environment. The smaller the escape latency is (i.e. the shorter the mean time-to-goal value is), the more efficient is the navigation behavior adopted by the animal.

Traveled distance. It represents the mean distance (cm) that is either swum or run by an animal before reaching the target position. Similar to the escape latency, this parameter measures the navigation performance across training.

Navigation speed. It is the mean progression speed (expressed in cm/s) of the animal (e.g. while navigating to the goal) across a trial. This parameter allows the escape latencies across multiple trials/subjects to be compared. It is also suited to characterize different learning phases during training (e.g. Verbitsky et al., 2004). For instance, a low mean speed may correspond to a 'mental reorganization' phase, most likely to occur during the acquisition of a navigation task, whereas a high locomotion speed may correlate to automated execution of an acquired navigation procedure. NAT also estimates the instantaneous traveling speed of the animal, which is useful to characterize sequential micro-behavioral phases within the same navigation path. For instance, based on this kinematics analysis Hamilton et al. (2004) found that mice solving the Morris watermaze tend to swim slowly when using distal cues, whereas they tend to accelerate when being guided by a proximal cue identifying the escape platform.

Resting/rearing/stop events. NAT employs the instantaneous progression speed to compute parameters as the percentage of resting time (with respect to the total duration of a trial), the number of stops, and their spatial distribution. For instance, stops that

are both location specific and repeated in time may indicate the establishment of a home base, whereas a sparse even distribution of stops may correspond to rearing and/or grooming events (Benjamini et al., 2011; Eilam and Golani, 1989). NAT allows the experiment to set the lower-bound speed threshold used by the system to classify progression versus stationary events over a trial. Importantly, this lower-bound speed threshold allows navigation parameters to be computed on the running segments of the path only. This is a crucial point for analysis of trajectories in dry mazes since the animals are more likely to stay at a given place than in water mazes. These stop events dramatically affect navigation parameters like speed but also traveled distance and all angle-related parameters (body rotation, curvature radius, path sinuosity; see below). Indeed, when the animal is stationary, its barycenter slightly oscillates leading to an apparent speed above zero, and an apparent traveled distance that grows proportionally with the resting time. Moreover, the path segments between these very close points display aberrant angle-related measures. An iterative low pass filter using the lower-bound speed threshold allows these stationary points to be neglected for the computation of navigation parameters.

Distance to target. NAT computes both the *mean* and the *cumulative* distances (in cm) between the animal and the goal location. The shorter the distance-to-goal over time, the better the target localization capability of the animal (Burguière et al., 2005; Gallagher et al., 1993).

Body rotation. This parameter quantifies the mean and cumulative stepwise angular changes (in degrees) of the locomotion direction of the animal, which correlate to the smoothness of the navigation pathway (Wolfer and Lipp, 1992). NAT also quantifies two akin parameters, namely the percentage of left-and-right turns, and the total number of directional changes per trial.

Heading-to-goal. It estimates the mean stepwise egocentric angle (in degrees) between the actual direction of the animal and the ideal (straight) direction toward the target (Wolfer and Lipp, 1992). This parameter estimates to which extent the navigation behavior is optimized with respect of a direct goal-reaching pathway.

Curvature radius. NAT computes the curvature radius (in cm) function of the navigation trajectory (see Fig. A.3A). The values of this geometrical parameter enable to distinguish different searching strategies (Fig. A.3B). For example, the circling strategy, consisting of finding the platform based on its distance relative to the pool wall, will display high values of curvature radius. By contrast, a scanning strategy will have a curvature radius of lower absolute values. The lowest curvature radius values will correspond to trajectories generated by a focused goal search behavior, with frequent and small turns, as it can be observed when the animal persistently searches around the platform. Note that, although the signed curvature radius can capture locomotion directional changes, this parameter can be orthogonal with respect to the body rotation measure. For instance, two concentric circular pathways will have the same mean body rotation, whereas they will have different curvature radii.

Parallelism index. This parameter reflects the general tendency of the animal to change its egocentric direction between two successive movements (Brudzynski and Krol, 1997). Its dimensionless value ranges between −1 and 1. An average value close to −1 reflects a tendency for back and forth oscillatory patterns. Conversely, an average value close to 1 means that the animal tended to follow straight trajectories. A mean value close to 0 reflects a majority of 90° turns. The parallelism index is independent from the total traveled distance.

Path sinuosity. This parameter (expressed in radians/cm$^{1/2}$) represents the relative amount of angular variation with respect to the distance covered by the animal (Brudzynski and Krol, 1997).

Path tortuosity. It quantifies how well a trajectory approximates the optimal (i.e. most direct) pathway to the target. Its dimensionless value is computed as the ratio between the length of the actual pathway and the shortest (linear) distance from the starting location to the target. Path tortuosity allows the optimality of individual trials starting from different departure points to be compared. The current version of NAT computes this parameter for open-field navigation tasks only, although it can be further extended to account for piecewise linear trajectories in structured environments.

Spatial preference. NAT provides a graphical editor to partition the environment into custom virtual zones (e.g. regions of interest). Then, it computes both the number of entries to each zone and the percentage of time spent by an animal (or group of animals) in each zone, i.e. spatial occupancy distribution (Graziano et al., 2003). These parameters are suited to assess target localization performance (e.g. by measuring the time spent in the platform quadrant of the Morris watermaze or the number of crossings of an annulus corresponding to the platform area), as well as to evaluate emotional states as, for instance, anxiety (Kulikov et al., 2008; Ramos et al., 1997). For instance, they are appropriate to characterize thigmotaxis behavior (e.g. by quantifying the number of entries and/or time spent along the peripheral wall of the arena, Lipkind et al., 2004).

Mean trajectory. NAT also estimates the mean trajectory performed by an animal (group of animals) within custom regions of interest. To do so, it re-samples all trajectories and computes the center of mass of the sampled points. Two re-sampling methods can be employed, according to the binning strategy (either temporal or spatial, see Fig. A.4). NAT measures the mean dispersion (standard deviation) of points around the estimated barycenter. The mean trajectory parameter is suited, for instance, to quantitatively compare actual paths against optimal goal-directed trajectories (e.g. against minimum jerk trajectories, Flash and Hogan, 1985). The intra-subject dispersion evaluates the animal ability to reproduce its own path. Because the mean trajectory parameter is only meaningful in the case of similar paths, this measure is recommended for structured maze (e.g. Y-maze).

Distance to walls and/or objects. In circular open-field environments, stereotyped behaviors (e.g. thigmotaxis) are automatically identifiable by monitoring the ongoing distance between the animal and one or few points in the maze (e.g. the central location). However, complex mazes require more elaborated distance-to-wall estimations. For each sampled position of the animal's trajectory, NAT computes the minimal distance (in cm) with respect to the walls of the maze and/or to every object (either polygonal or ellipsoid) inside the maze.

2.2.2. Decision point analysis

Spatial behavior in structured mazes is primarily determined by decision-taking events that occur at intersection (e.g. bifurcation) points. NAT allows a decision point analysis to be performed for structured environments such as the plus maze (O'Keefe and Speakman, 1987), the Y-maze (Conrad et al., 1996), and the starmaze (Rondi-Reig et al., 2006). For sake of clarity, we henceforth use the starmaze as a case study to introduce the decision point analysis implemented by NAT.

The starmaze consists of five alleys forming a pentagonal ring and five alleys radiating from the ring (Fig. 2A). These ten alleys join themselves in five intersections. In order to solve the task, animals have to reach an escape platform hidden below the surface of the water. Hence, given a departure point, the optimal trajectory leading to the goal corresponds to a unique specific sequence of alleys (e.g. pathway *I–II–III* in Fig. 2A). In order to analyze the sequence of visited alleys automatically, the user can use the graphical editor provided by NAT to define, for instance, three distinct types of zone for the starmaze: the 'alley zone', the 'intermediate zone', and

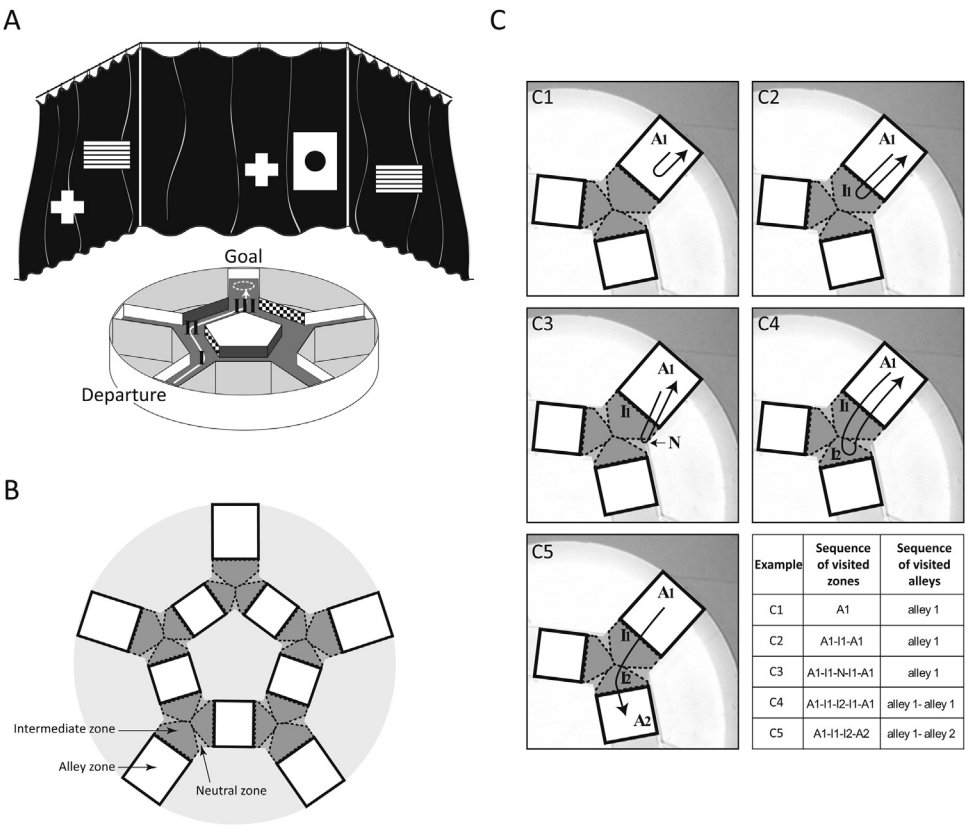

Example	Sequence of visited zones	Sequence of visited alleys
C1	A1	alley 1
C2	A1-I1-A1	alley 1
C3	A1-I1-N-I1-A1	alley 1
C4	A1-I1-I2-I1-A1	alley 1- alley 1
C5	A1-I1-I2-A2	alley 1- alley 2

Fig. 2. The starmaze task and an example of partitioning of the environment into virtual zones carried out by NAT to support decision point analysis. (A) The multiple-strategy version of the starmaze protocol (Rondi-Reig et al., 2006). The alleys forming the central pentagonal ring have either black or chessboard-like walls, whereas the radial alleys have white walls. The maze is placed inside a black square curtain with distal visual cues attached on the curtains (crosses, circle, black and white stripes). Animals must find the submerged platform ('goal'; dashed white circle) to solve the navigation task. In this example, the optimal goal-directed trajectory (white arrow) involves the sequence of intersections I, II, and III. (B) Top view of the starmaze with a typical partitioning of the environment into virtual zones. Three types of zones are used in this example: 'alley zone', 'intermediate zone', and 'neutral zone'. (C) Examples illustrating some rules used by NAT to determine the sequence of visited alleys. (C1 and C2) Moving from 'alley zone 1', A1, to its adjacent 'intermediate zone', I1, and then coming back to A1 is interpreted as remaining within alley 1. (C3) Similarly, moving from A1 to a 'neutral zone', N, and coming back to A1 is considered equivalent to remain within alley 1. (C4) If the animal goes from A1 to the 'intermediate zone' I2 adjacent to 'alley zone 2' and comes back to A1, NAT counts two visits to alley 1. (C5) Moving subsequently from A1, to I1, then to I2, and finally to 'alley zone 2', A2, is interpreted as visiting alley 1 and then alley 2. The bottom-right table summarizes the correspondence between the sequence of visited virtual zones and the interpreted sequence of visited alleys in figures C1–5.

the 'neutral zone' (Fig. 2B). NAT associates each 'intermediate zone' to the adjacent 'alley zone', and it employs a simple set of rules to determine the sequence of visited alleys (Fig. 2C). Based on these rules, NAT computes automatically the following parameters.

Number of visited alleys. This performance indicator is inversely proportional to the efficiency of the goal-directed navigation trajectory.

Localization scores. This analysis segments the trajectory into local decision events, and measures the ability of animals to select and follow the best direction to the goal at each intersection of the maze. It can be carried out at different levels:

- At the first level, NAT considers all the intersection points *i* visited by the animal as independent from each other (both spatially and temporally). Let *t* be the time at which the animal encounters a choice point *i*. NAT assigns *i* either a positive value depending on the choice made by the animal (i.e. $s_i(t) = +100$ if it is a pertinent choice with respect to the goal; $s_i(t) = 0$ otherwise). Then, NAT computes the mean score $S = \langle s_i(t)\rangle_{i,0\le t\le T}$ by averaging over all the intersection points *i* and over the entire trial duration *T*. Hence, the parameter *S* provides a global measure of the efficiency of the decision policy adopted by the animal at all choice points of the maze.
- At the second level, NAT focuses on the subset of intersections belonging to a specific sequence of alleys (e.g. the optimal goal-directed sequence *I–II–III* in Fig. 2A) and scores them independently from each other at each visit of the animal (e.g. $s_I(t) = +100$ means that the animal encountered intersection *I* at time *t* and made the right choice relative to the target). Then, NAT computes the mean score $S_I = \langle s_I(t)\rangle_{0\le t\le T}$ by averaging over all the times *t* the animal passed through the intersection point *I* during a trial of duration *T*. Similarly, NAT computes the mean values $S_{II} = \langle s_{II}(t)\rangle_{0\le t\le T}$ and $S_{III} = \langle s_{III}(t)\rangle_{0\le t\le T}$ for intersections *II* and *III*, respectively. The scores $S_{I,II,III}$ inform about the ability of an animal (group of animals) to take, on average, the right decisions at specific (spatially relevant) intersection points.

Direct path score. This parameter evaluates the ability of animals to reach the target through the most direct path within a multi-intersection maze. To compute the direct path score, NAT focuses again on the subset of intersections belonging to a specific alley sequence (e.g. *I–II–III* in Fig. 2A), but it accounts for their spatiotemporal relations (in contrast to the localization scores for which it considers them as independent events). Each time the animal encounters an intersection and makes a choice, a score is computed as above. Then, this score is normalized with respect to the number of alleys visited before reaching this intersection. For instance, in the starmaze the direct path score per trial is equal to $[s_I(t) + s_{II}(t)/n1 + s_{III}(t)/n2]/N$, with $n1$ denoting the number of alleys visited between the first and the second alley, $n2$ is the

number of alleys visited between the second and the third alley, and N is the total number of intersections (in our case $N = 3$). Thus, the most direct path is scored 100. Finally, the score is averaged over the total number of trials of each session. The larger the average score, the better the animal has learned the relations between the intersections forming the optimal sequence to the goal. Rather than evaluating the number of correct trials, the direct path score assigns a score to each trajectory taking into account errors, and is thus well suited to evaluate the progressive learning of a sequence.

Sequence of alleys visited. This parameter is essential when analyzing the probe test. During the latter, the departure point is changed in order to reveal the strategy adopted by the mice, as each learning strategy will lead to a different path to reach the goal (e.g. sequential egocentric vs. allocentric strategies, Rondi-Reig et al., 2006.

2.2.3. 3D-maps for qualitative behavioral analysis

NAT computes and displays three-dimensional maps of the spatial distribution (across the environment) of some behavioral parameters. The first two dimensions correspond to the Cartesian plane where movement occurs, whereas the third dimension provides the amplitude of the measured parameter. NAT samples spatial locations by means of a uniform square grid, whose spacing can be set by the user (with a maximum resolution of 1 cm × 1 cm). The value assigned to each pixel of the grid corresponds to the parameter function evaluated in the corresponding location.

The current version of NAT provides 3D-readouts for the following subset of parameters: (i) *mean spatial occupancy*, i.e. the average fraction of time spent by an animal within each square of the grid (normalized with respect to the duration of a trial); (ii) *mean instantaneous speed*, i.e. the average progression speed of the animal within each square; (iii) *mean instantaneous heading variability*, i.e. the angular changes of the trajectory of the animal within each pixel; (iv) *mean curvature radius*, which characterizes the circular-like component of the animal movement per each cell of the map.

These grid-based functions are averaged over all trials carried out by an animal, and eventually over all the trials of the animals of a same group. Hence, these 3D functions provide qualitative accounts of the spatial behavior of an animal (or group of animals) as a function of its position in the environment. They are suited, for instance, to differentiate local vs. global behavioral patterns, as well as to characterize the evolution of spatial behavior across learning stages (see Results). NAT allows the user to perform statistical analyses (e.g. ANOVA and t-test) to evaluate the significance of the intergroup differences across spatial locations.

3. Results

Two different apparatus were employed for the navigation tasks, namely the watermaze and the starmaze (Figs. 3 and 4), illustrating goal-oriented navigation in an open-field (Burguière et al., 2005) and in a multi-intersection environment (Fouquet et al., 2011), respectively.

3.1. The watermaze: an example of open-field navigation task

Mice were trained in a circular water tank (150 cm in diameter, 40 cm high) to find an escape platform (10 cm of diameter) hidden 1 cm below the surface of the water at a fixed location (Fig. 3A – upper left). The pool contained water (21 °C) made opaque by the addition of an inert and nontoxic product. Both the pool and the surrounding distal cues were kept fixed during all experiments. Each mouse underwent one training session per day consisting of four trials. The starting position (North, East, West, or South) was randomly selected with each quadrant sampled once a day. At the beginning of each trial, the mouse was released at the starting point ($S_{1,\ldots,4}$ in Fig. 3A – upper left) and made facing the inner wall. Then, it was given a maximum of 90 s to locate and climb onto the escape platform. If the mouse was unable to find the platform within the 90 s period, it was taken to the platform by the experimenter. In either case, the mouse was allowed to remain on the platform for 30 s. Animals ($n = 8$ adult mice) received 40 training trials over 10 days (4 trials/day).

As illustrated in Fig. 3A, escape latency and traveled distance are two parameters suited to quantify the learning improvement over training sessions. Their values significantly decreased across sessions (ANOVA $F(9,190) = 16.1$, $p < 10^{-4}$; $F(9,190) = 17.4$, $p < 10^{-4}$; respectively), revealing that mice successfully learned to locate and reach the target location. Distance to target, heading, and path tortuosity are complementary parameters that reflect the ability of mice to optimize their trajectories toward the goal. Both distance to target and heading significantly decreased over training (ANOVA $F(9,190) = 23.5$, $p < 10^{-4}$; $F(9,190) = 6.9$, $p < 10^{-4}$; respectively). The value of path tortuosity decreased significantly with learning (ANOVA $F(9, 190) = 5.0$, $p < 10^{-4}$), the theoretical lower limit being 1 in the presence of a straight trajectory to the goal.

Fig. 3B shows two parameters that provide insight about the evolution of the exploratory behavior over training, i.e. the distance to wall and the curvature radius. Our results in the watermaze suggest that mice significantly increased their average distance from the circular wall (ANOVA $F(9,190) = 15.4$, $p < 10^{-4}$), from a predominant circling behavior on day 1 to a truly open-field exploration on day 10. Consistently, the curvature radius was reduced dramatically after the first training day (ANOVA $F(9,190) = 5.8$, $p < 10^{-4}$).

NAT allows 3D-diagrams of the mean time spent by a group of mice at each spatial location to be represented at different learning phases (the occupancy maps corresponding to days 1 and 10 are presented in Fig. 3C). These representations show qualitatively the behavioral adaptation of mice solving the Morris watermaze, in terms of searching patterns and goal-oriented navigation.

3.2. The starmaze: an example of multi-intersection navigation task

A second series of experimental results was obtained with the aquatic hidden platform version of the starmaze (Fig. 4A – upper left), with all alleys filled with water made opaque with an inert nontoxic product. Both the pool and the surrounding distal cues were kept fixed during all experiments (Fig. 2A). The departure point and arrival were fixed (S_4 and goal in Fig. 4A – upper left, respectively). Similar to the watermaze experiments, each trial lasted a maximum of 90 s. If the mouse was unable to find the platform, it was taken to the platform by the experimenter. In either case, the mouse was allowed to remain on the platform for 30 s. A group of $n = 22$ adult mice underwent a training consisting of 50 trials over 10 days.

We assessed the ability of mice to learn the starmaze task by measuring the mean escape latency and the mean distance swum before reaching the platform (Fig. 4A). Both values decreased significantly over training (ANOVA $F(9,210) = 56.3$, $p < 10^{-4}$; $F(9,210) = 38.4$, $p < 10^{-4}$; respectively). In addition, due to the presence of intersections in the starmaze, we quantified the mean number of visited alleys per trial and found a significant decrease over learning (ANOVA $F(9,210) = 17.8$, $p < 10^{-4}$).

The mean distance to target decreased significantly across sessions (ANOVA $F(9,210) = 36.4$; $p < 10^{-4}$), indicating a progressive improvement of the global optimality of navigation trajectories (Fig. 4A). Complementarily, we assessed mice's ability to adapt their trajectories with training by measuring the mean body rotation parameter. Its value also decreased significantly over time (ANOVA

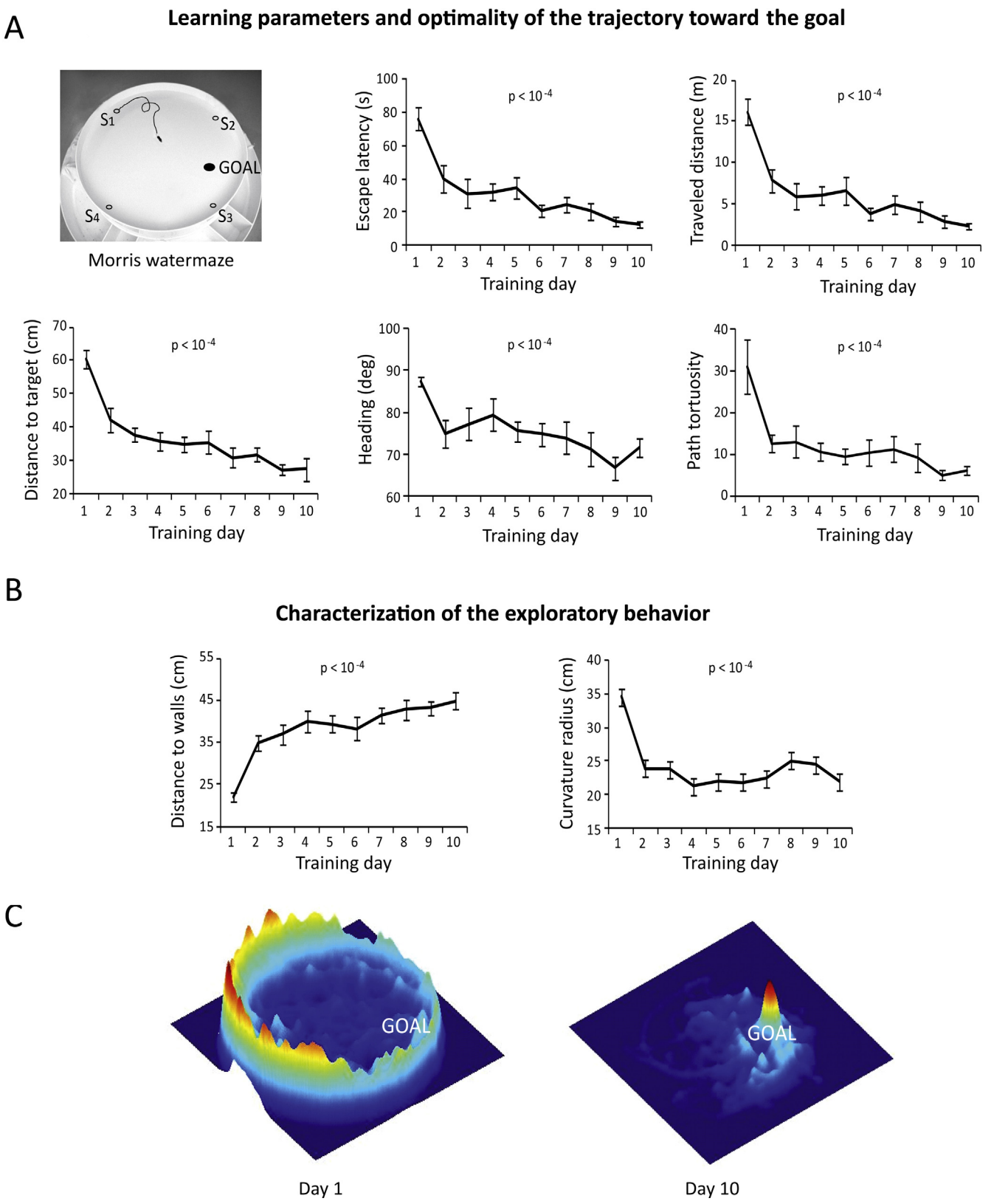

Fig. 3. Experimental results. Spatial navigation in the watermaze, an example of open-field navigation task. (A) Mice had to learn to swim to a hidden escape platform (black filled circle, upper-left figure) from any of four starting locations (black empty circles). We investigated the time course of learning across training sessions through multiple parametric measures, e.g. the mean escape latency; the mean traveled distance; the mean distance to target; the heading; and the path tortuosity. All these complementary observations suggest a significant improvement in goal-oriented navigation performance throughout training. (B) Two parameters provided by NAT to characterize the evolution of the exploratory behavior across sessions, namely the distance to wall and the curvature radius, indicate a significant progressive improvement of mice's goal searching behavior. (C) Two examples of 3D occupancy maps representing the mean time spent by mice at each location of the maze at the beginning (day 1) and the end (day 10) of training. They show qualitatively how mice adapted from circling behavior to more effective goal-oriented navigation. Colormap: red denotes high occupancy values, whereas dark blue corresponds to very low occupancy values.

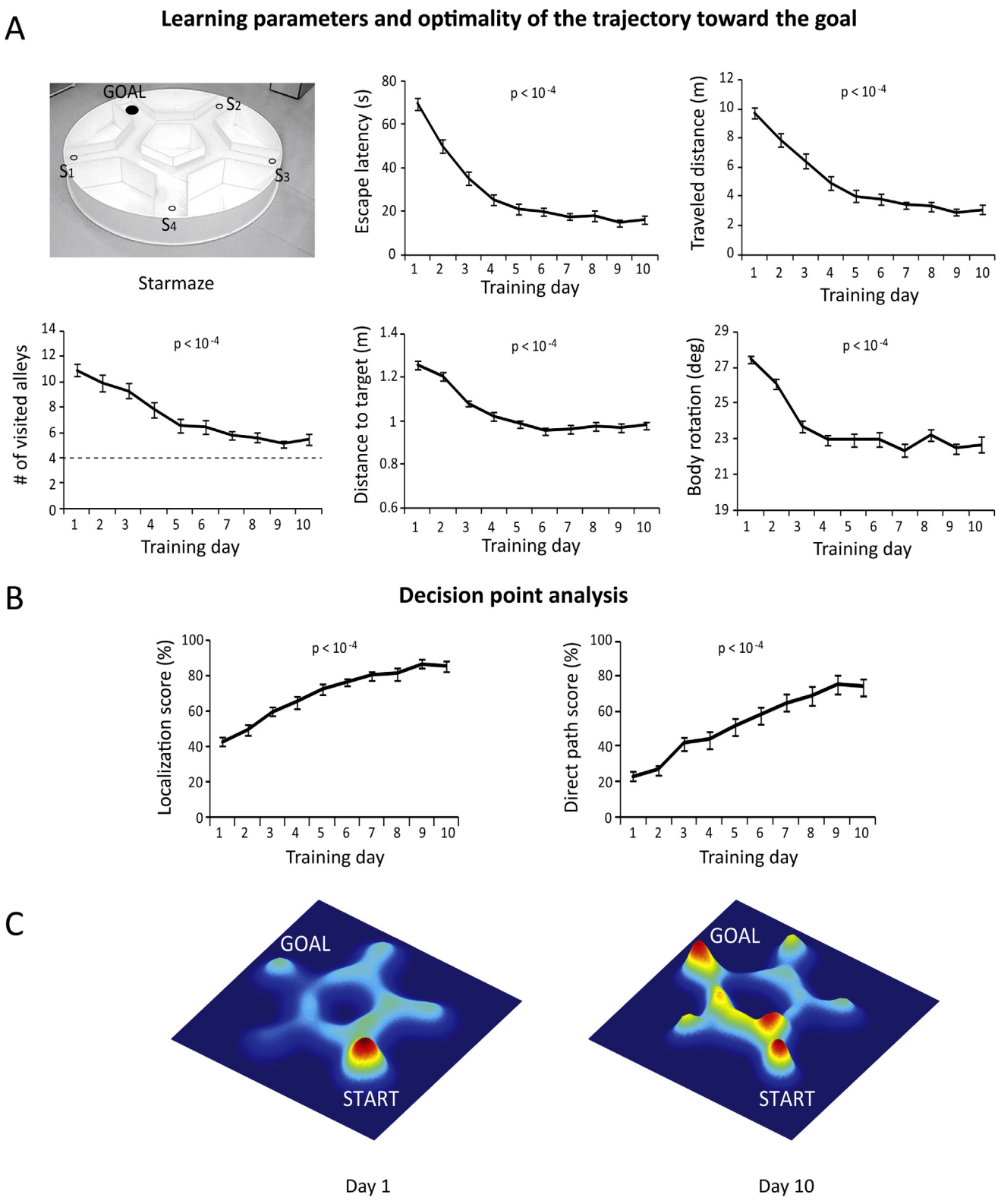

Fig. 4. Experimental results. Spatial navigation in the starmaze, an example of multi-intersection navigation task. (A) The ability of mice to solve the starmaze task (upper-left figure) was probed by quantifying the mean escape latency, the mean traveled distance, the mean number of visited alleys, the mean distance to target, and the body rotation. All these measures showed a significant improvement of performance over training. (B) We carried out a decision point analysis by measuring the time course of the localization and direct path scores. They both suggested that mice learned to progressively optimize their decision-making policy at each intersection of the maze. (C) The 3D occupancy maps showing the distribution of spatial locations visited by mice on days 1 and 10 corroborated, in a qualitative manner, the significant improvement of goal-directed performance. Colormap: red denotes high occupancy values, whereas dark blue corresponds to very low occupancy values.

$F(9,210) = 27.3$, $p < 10^{-4}$) indicating that animals improved the optimality of their local spatial behavior.

A decision point analysis showed a significant improvement of the ability of mice to locate themselves and the target platform, as indicated by the significant increase in the localization score through training (Fig. 4B – left; ANOVA $F(9,210) = 29.2$, $p < 10^{-4}$). Also, the increase of the direct path score reflected an optimization of the decision-making policy at each intersection over learning (Fig. 4B – right; ANOVA $F(9,210) = 16.2$, $p < 10^{-4}$).

Finally, Fig. 4C shows 3D occupancy distributions at the beginning (day 1) and at the end (day 10) of training. For sake of clarity, we only considered for this example the subset of trials involving departures from location S_4. On day 1, mice explored the different alleys of the starmaze, though predominantly returning to the starting alley. Nearly no direct trajectory from the departure point to the platform was observed on day 1. By contrast, after 10 days of training, mice learned to swim directly to the platform and exploited this optimal navigation strategy most frequently.

4. Discussion

Unfolding spatial behavior requires the assessment of a large spectrum of parameters. Automated tools are therefore suited to improve the efficacy and reliability of spatial behavior analysis. They also foster the interpretation of large data sets gathered across multiple experimental protocols, ultimately providing a unified picture. This paper describes an automated Navigation Analysis Tool (NAT) that quantifies a wide range of meaningful parameters to characterize spatial learning and goal-oriented navigation in both open-field and structured environments. We present two series of behavioral experiments probing the ability of mice to learn the hidden platform versions of the Morris watermaze (open-field) task and the starmaze (multi-intersection) task. The results, presented through the multiple vantage points offered by the parametric analysis of NAT, show significant improvements in mice's performances over training in both navigation tasks.

NAT provides an integrated architecture consisting of a data management system (implemented in MySQL), a core analysis toolbox (in MATLAB), and a graphical user interface (in JAVA). The latter enables the user to flexibly set up and control the entire process, which includes importing raw data (from the acquisition system) into the relational database, selecting and executing the appropriate analyses, and exporting the results into suitable readout formats. For instance, the graphical interface allows the user to re-sample the acquisition data, draw custom virtual zones (e.g. regions of interest), and set critical computation parameters (e.g. the lower-bound speed threshold used to classify motion vs. stop events). NAT allows large sets of behavioral data to be processed on a small time-scale basis (ms), which provides parametric analysis capabilities that would otherwise be either unfeasible or extremely time-consuming. The flexibility of NAT also stems from the modularity of its components. The object-oriented structure of the analysis toolbox can be either customized or extended by the addition of novel parametric measures. Also, ad hoc analysis (software) tools can be plugged-in as long as they are compatible with the MySQL database. Importantly, the NAT information system can be made accessible through the internet to provide online access to the data (Bradley et al., 2005), e.g. a remote user could send a query and retrieve data from the NAT database by means of PHP-based web pages.

NAT is independent from the actual acquisition system that provides the behavioral data to be fed into the relational database. The output of NAT is usable by any statistical tool to quantify the significance of the results of the parametric behavioral analysis. To improve the readability and transparency of the results, NAT keeps track of all intermediate computation steps in a structured file system (e.g. to enable the user to access the values and time course profile of every parameter for each trial/session/day).

The portability across multiple spatial navigation paradigms is one of the major aspects of NAT. So far, NAT has been used to analyze navigation in the Morris watermaze (Burguière et al., 2005), the starmaze (Rondi-Reig et al., 2006), and the Y-maze (Burguière et al., 2010), as well as to evaluate basic locomotor activity in a squared open-field, a circular arena, and the holeboard test. Moreover, NAT is also suited for large open fields like the Barnes maze (Barnes, 1979), for alley mazes like the plus maze (O'Keefe and Speakman, 1987), the radial maze (Olton and Samuelson, 1976) or

Table A.1
Comparison of NAT against existing navigation analysis software (either commercial or open source).

	Purpose	GUI	Language	Main advantages	Deltas	Reference
Commercial						
Ethovision (NOLDUS)	Tracking and path analysis	Yes	C++	Multi-tracking; zone partitionning	No code customization	Spink et al. (2001)
SMART (Bioseb)	Tracking and path analysis	Yes	C++	Multi-tracking; zone partitionning	No code customization	
Plexon (CinePlex)	Tracking and path analysis	Yes	C++	3 methods of tracking; zone partitionning	No code customization; needs a complete suit of plexon tools	
Open source						
SEE	Exploratory behavior analysis	Yes	C++	Robust smoothing and segmentation (description of behavior in terms of modes of movement)	Off-line analysis; open field oriented	Drai and Golani (2001) and Fonio et al. (2009)
Wintrack	Path analysis, navigation strategy	Yes	C++	70 parameters for automated strategy classification; zone partitionning	Off-line analysis; open field oriented	Wolfer and Lipp (1992) and Graziano et al. (2003)
Flytrack	Tracking and path analysis	No	MATLAB	Easy to use and adapt	Off-line analysis; open field oriented	Fry et al. (2008)
EthoStudio	Spatial preference analysis (pixel-based)	No	Unspecified	Transmitted light technology	Off-line analysis; open field oriented	Kulikov et al. (2008)
NAT	Path analysis, navigation strategy	Yes	MATLAB, MySQL, JAVA	Classic and extended parameters; zone partitioning; map analysis; open field and multi-intersection mazes	Off-line analysis	

the multiple T-maze (Stone, 1929), structured environments like in the conditioned place preference test (Beach, 1957), or any specific design. This portability property can further be enhanced by the addition of novel experimental protocols, which can either share or re-specify some critical configuration settings. For example, setting the maximum speed threshold is relevant to the preliminary artifact correction procedure that NAT carries out prior to the feeding of the relational database (see Section 2). Another example concerns the user-defined criterion to determine the sequence of visited alleys in structured environments. In the case of the starmaze, NAT partitions the environment into discrete two-dimensional virtual zones ('alley zone', 'intermediate zone', and 'neutral zone'; see Section 2). Then, it detects the entries to each alley based on the animal's displacements across adjacent zones. Due to the discrete boundary problem, this procedure is vulnerable to false positives (e.g. when a mouse swims across the edge separating two virtual zones), and it needs to be set properly. The user can employ the configuration tool to customize the environment partitioning procedure in order to mitigate the false positive risk based on the specific knowledge on the morphology of the added structured maze.

NAT is an open source software that offers an alternative to the existing solutions to perform automated parametric analyses of spatial behavior (Drai and Golani, 2001; Fry et al., 2008; Graziano et al., 2003; Kulikov et al., 2008; Spink et al., 2001; Wolfer and Lipp, 1992). Table A.1 compares the properties of NAT against existing systems. The Wintrack system (Wolfer and Lipp, 1992) allows up to 71 parameters to be measured in order to analyze spatial behavior in open-field mazes. However, it does not handle decision point analysis. Wintrack offers a script-based programming environment to customize parameters as well as zone definition. The SEE software tool (Drai and Golani, 2001; Fonio et al., 2009) describes the spatial behavior of rodents in terms of segmentation of motion modes (e.g. stops, progressions), and of classification of home-centered exploratory trajectories (e.g. inbound and outbound velocities, spatial spread, diversity, space occupancy). SEE primarily accounts for open-field spatial exploration analysis. The Ethovision system (Spink et al., 2001) provides a complete framework (from acquisition to analysis) to assess behavior-related quantities such as distance, velocity, heading, rotation angle, meander, motion, and rearing. Ethovision, which is commercialized by Noldus Information Technology, does not allow the user to

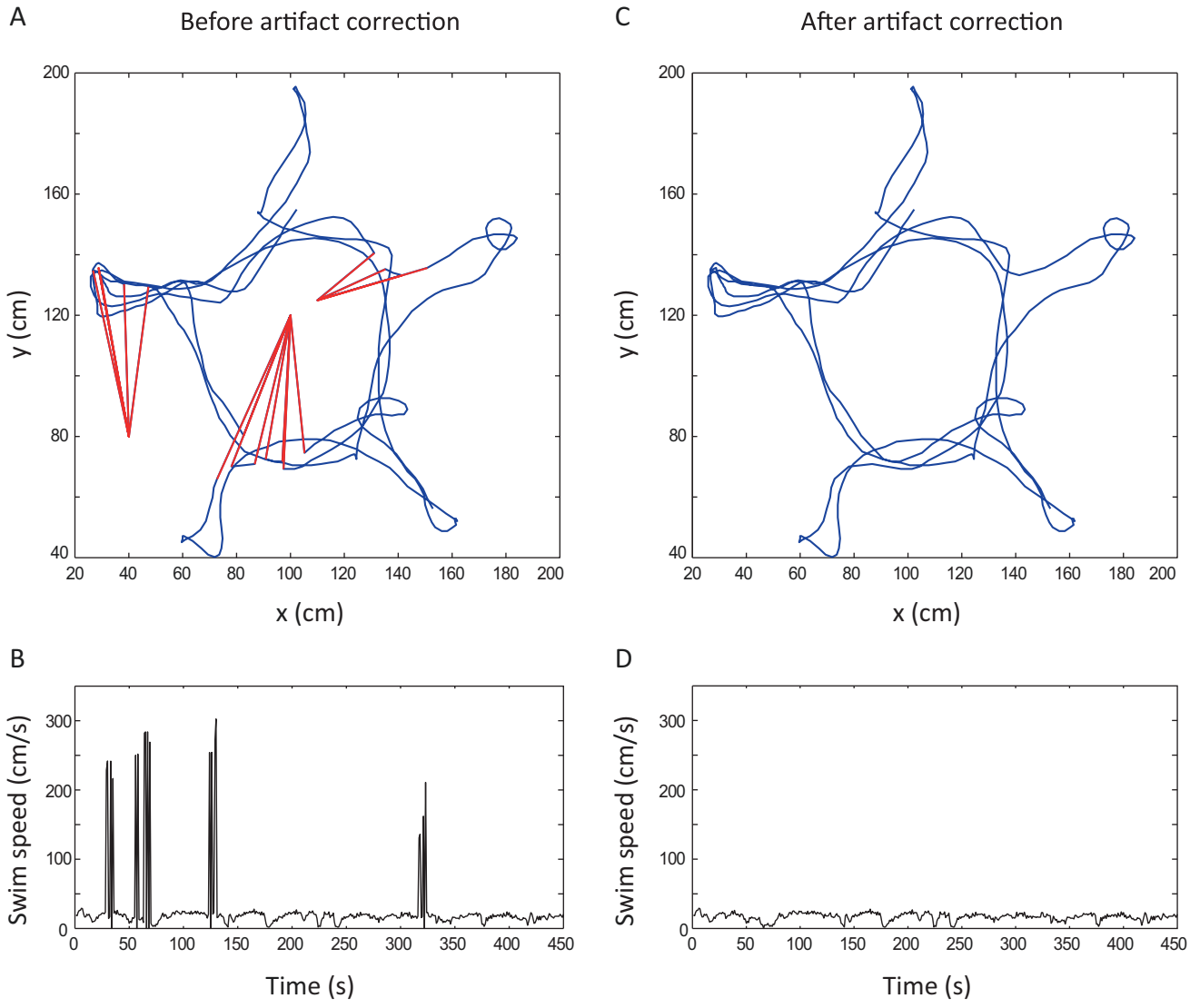

Fig. A.1. Artifact correction procedure implemented by NAT. The algorithm relies on a speed low-pass filter (for artifact recognition) and on a linear interpolation of spatial coordinates (for artifact correction). (A) Sample trajectory of a mouse solving the starmaze as recorded by the video-tracking system. (B) Corresponding (swim) speed profile prior to the execution of the artifact correction algorithm. (C and D) Trajectory and speed profile, respectively, after the application of the artifact recognition and correction procedure on the raw acquired data. In this example, the cutoff speed was set to 40 cm/s.

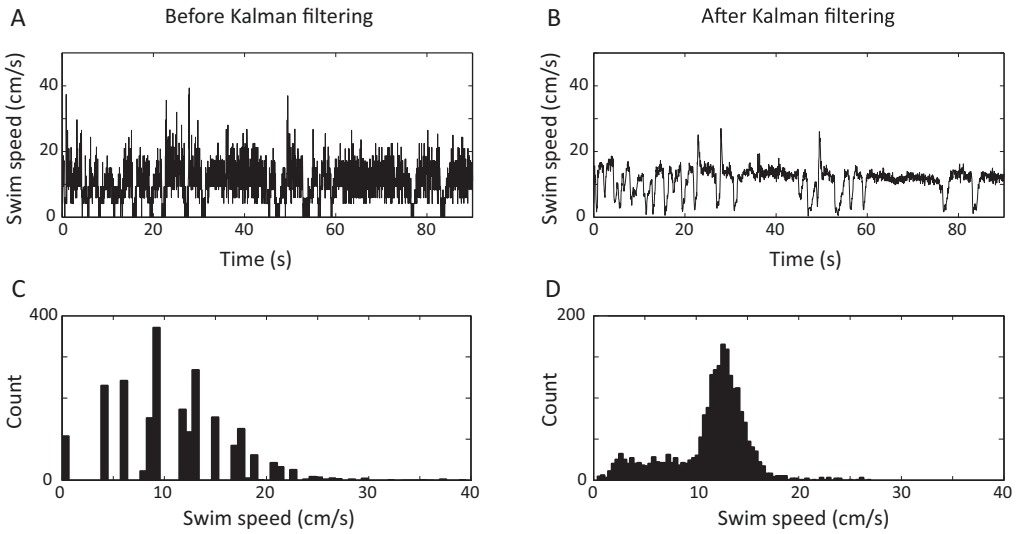

Fig. A.2. Trajectory smoothing based on Kalman filtering. (A and B) Swim speed profile of a mouse solving the Morris watermaze task before and after (respectively) the application of the Kalman filter. (C and D) Distribution of swim speeds before and after the smoothing procedure.

customize the parameters to be assessed. Flytrack (Fry et al., 2008) is an open-field oriented behavioral analysis system. It provides a set of functions to denoise and smooth the recorded trajectories. It computes path curvatures, reorientation angles, as well as speed and space segmentation, and it has mainly be used for fly track analysis (Valente et al., 2007). Finally, the EthoStudio software (Kulikov et al., 2008) computes spatial preference in open-field environments in terms of map density (pixel resolution) and probability distribution.

NAT extends the capabilities of these systems in several aspects. The aforementioned portability across multiple paradigms (from open-field to multi-intersection environments) makes NAT a general-purpose analysis tool. The opportunity to manage a wide range of projects, protocols, and data within the same relational database is suitable for linking and comparing observations gathered through different spatial navigation experiments. The analysis toolbox of NAT covers the classical measures that are extensively used in behavioral navigation studies. Moreover, it provides a set of measures to characterize the geometrical properties of goal-directed and exploratory trajectories in deeper detail and accuracy. It also contains a subset of parameters useful to evaluate decision-making processes in structured mazes, such as in multi-intersection navigation tasks (Rondi-Reig et al., 2006).

Acknowledgements

This work was granted by the ANR Project EvoNeuro, ANR-09-EMER-005-01. It was previously supported by the GIS Program 'Longevity' (grant nos. SRI20001117030, L0201), and by the ACI Program 'Integrative and Computational Neuroscience' (NIC 0083). The authors thank S. Thierry and C. Poussineau for their help in developing NAT, and F. Maloumian for her help for the figures.

Appendix A. Artifact recognition-correction algorithms

NAT preprocesses the input time series $\{t, x(t), y(t)\}$ recorded by the acquisition system prior to their insertion into the relational database. It employs two artifact correction algorithms.

The first consists of a simple low-pass filtering procedure that relies on an empirical (user-defined) estimation of the upper limit $v_{\max}$ of the progression speed of the animal (which depends, among other contextual factors, on the particular type of maze and navigation task). NAT uses this speed threshold to recognize all artifactual points (for which $v > v_{\max}$) throughout the entire dataset. Then, NAT goes sequentially through all data points, and for each pair of valid coordinates $x(t), y(t)$ and $x(t+n), y(t+n)$ defining an interval containing $n-1$ artifacts $x(t+i), y(t+i)$, with $1 \le i \le n-1$, NAT employs a linear interpolation algorithm to correct these artifactual points by distributing them uniformly between $x(t), y(t)$ and $x(t+n), y(t+n)$. The corrected coordinates of an artifact point $x(t+i), y(t+i)$ are $x(t+i) = x(t) + (x(t+n) - x(t)) \cdot n^{-1} \cdot i$ and $y(t+i) = y(t) + (y(t+n) - y(t)) \cdot n^{-1} \cdot i$, respectively. The example in Fig. A.1 shows both the trajectory and the speed profile, of an animal solving the starmaze task, before and after the application of this simple artifact correction algorithm.

The second (optional) procedure relies on a Kalman filter that minimizes, at each time step, the quadratic error between the measured variable (e.g. speed, acceleration) and a probabilistic estimate of the value of that variable (Kalman, 1960). The Kalman smoothing procedure assumes that measurements are drawn from multivariate Gaussian distributions. The example in Fig. A.2 shows both the swim speed profile and the speed histogram of an animal solving the watermaze task, before and after the application of the Kalman smoothing algorithm.

Appendix B. Formal definition of some measured parameters

Distance to target. The mean and cumulative distances (expressed in cm) between the animal and the goal (e.g. the hidden platform in the Morris watermaze) are simply calculated as:

$$\bar{d}_g = \langle d_g(t) \rangle_{t \in [0,T]}$$

$$D_g = \sum_{t \in [0,T]} d_g(t)$$

respectively, where T is the trial duration, and $d_g(t)$ is the Euclidian distance at time t between the animal position $x(t), y(t)$ and the goal coordinates $x_g(t), y_g(t)$, i.e. $d_g(t) = \sqrt{(x_g - x(t))^2 + (y_g - y(t))^2}$.

Body rotation. The mean and cumulative stepwise angular changes (in degrees,°) of the motion direction of the animal over a trial duration T are computed as:

$$\overline{\Delta\vartheta} = \langle \Delta\vartheta(t) \rangle_{t\in(0,T]}$$

$$\Delta\Theta = \sum_{t\in(0,T]} \Delta\vartheta(t)$$

respectively, where $\Delta\vartheta(t)$, mapped into the range $[0^\circ, 180^\circ]$, is the difference between the direction of trajectory at two consecutive timesteps:

$$\Delta\vartheta(t) = \min\{|\vartheta(t) - \vartheta(t-1)|, \min\{|\vartheta(t) - \vartheta(t-1) + 360|, |\vartheta(t) - \vartheta(t-1) - 360|\}\}$$

where

$$\vartheta(t) = a\tan2[(y(t+1) - y(t)), (x(t+1) - x(t))]$$

with $x(t), y(t)$ denoting the animal position at time t, and $\vartheta(t) \in (-180^\circ, 180^\circ]$. Positive angles are assumed to be generated by counterclockwise rotations. NAT also computes the total number of directional changes per trial:

$$n = \sum_{t\in(0,T]} H(\Delta\vartheta(t))$$

where H is the Heaviside step function, defined as: $H(z) = 1$ for $z > 0$, and $H(z) = 0$ otherwise. Finally, the percentage of left-and-right turns is simply taken as:

$$L = \frac{1}{n} \cdot \sum_{t\in(0,T]} H(\vartheta(t) - \vartheta(t-1))$$

$$R = 1 - L.$$

Heading-to-goal. This parameter is the mean stepwise egocentric angle between the motion direction of the animal and the straight path to the target. It is computed as:

$$\bar{\phi} = \langle \phi(t) \rangle_{t\in[0,T]}$$

where

$$\phi(t) = |\vartheta(t) - \vartheta_g(t)| \quad \text{mapped into} \quad [0^\circ, 180^\circ]$$

with

$$\vartheta(t) = a\tan2[(y(t+1) - y(t)), (x(t+1) - x(t))]$$

$$\vartheta_g(t) = a\tan2[(y_g - y(t)), (x_g - x(t))]$$

with $x(t), y(t)$ denoting the animal position at time t, and x_g, y_g indicating the position of the target. Both $\vartheta(t)$ and $\vartheta_g(t)$ are mapped into the range $[0^\circ, 360^\circ]$.

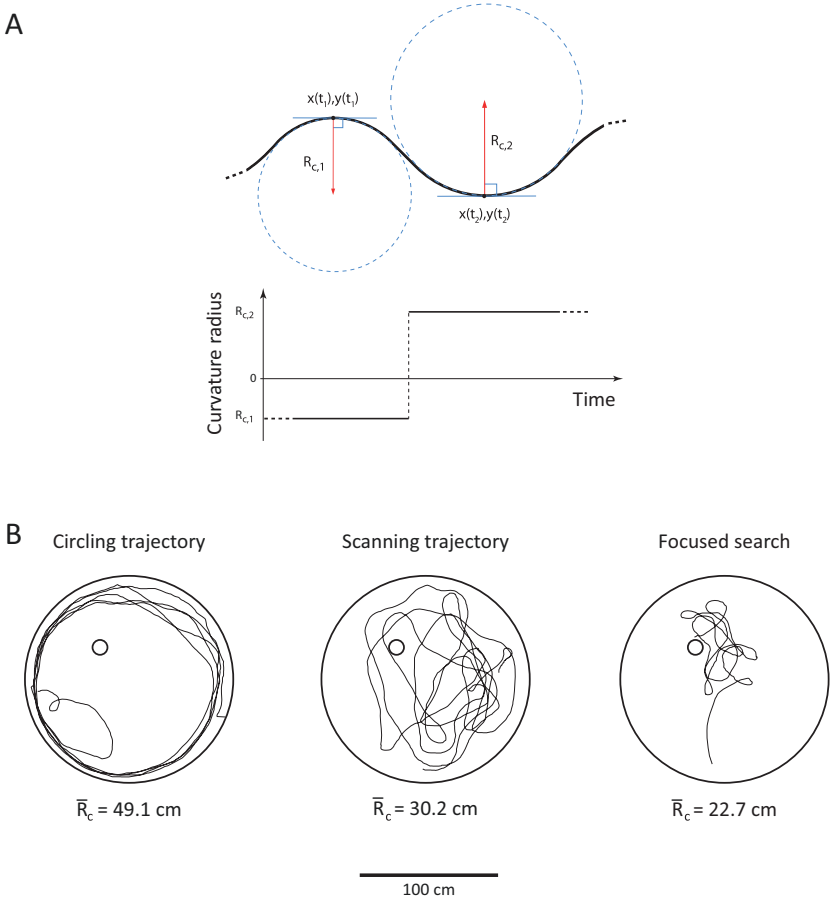

Fig. A.3. About the curvature radius parameter. (A) Example of curvature radius over time for a toy navigation trajectory (black curve). The change of sign of the curvature radius corresponds to a zigzag behavior. (B) Examples of mean curvature radii corresponding to a circling strategy (left), a scanning strategy (center), and a focused search strategy (right).

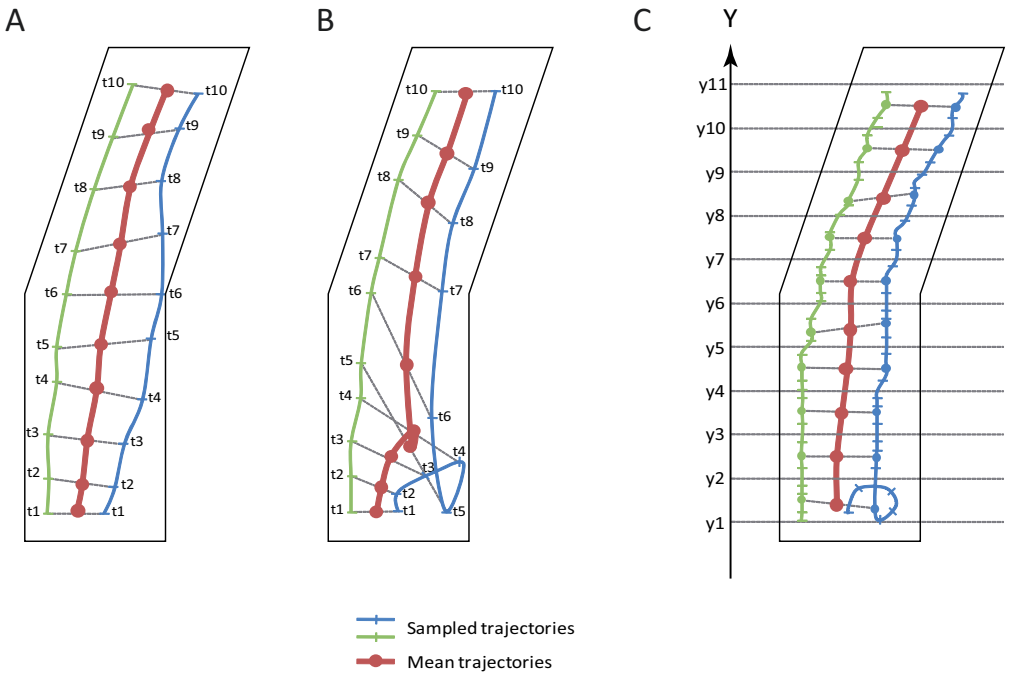

Fig. A.4. About the mean trajectory parameter. (A) Example illustrating the calculation of the mean trajectory using temporal re-sampling along one alley of a structured environment (e.g. Y-maze). (B) Example illustrating the sensitivity of temporal re-sampling to differences in the time course of maze crossing. For the blue trajectory the animal made a small loop, which has a strong influence on the considered points in the mean trajectory. (C) Example illustrating the calculation of the mean trajectory using spatial re-sampling. (For interpretation of the references to color in this figure legend, the reader is referred to the web version of the article.)

Curvature radius. For each data point $x(t), y(t)$, NAT computes the radius of the osculating circle as:

$$R_c(t) = \begin{cases} \sqrt[3]{\dot{x}^2 + \dot{y}^2}/\dot{x}\ddot{y} - \dot{y}\ddot{x} & \dot{x}\ddot{y} \neq \dot{y}\ddot{x} \\ 0 & \text{otherwise} \end{cases}$$

where the translational speeds and accelerations $\dot{x}, \dot{y}, \ddot{x}, \ddot{y}$ are estimated based on the Kalman smoothing procedure (see Appendix A). As shown in the example in Fig. A.3A, a shift in the sign of the curvature radius can be used to detect zigzag-like behavioral patterns.

Parallelism index, correlation coefficient, and path sinuosity. Similar to Brudzynski and Krol (1997), NAT computes the following parameters:

$$\bar{P} = \langle P(t) \rangle_{t \in [0,T]} = \langle \cos \Delta\vartheta(t) \rangle_{t \in [0,T]}$$

$$\bar{Q} = \langle Q(t) \rangle_{t \in [0,T]} = \langle \sin \Delta\vartheta(t) \rangle_{t \in [0,T]}$$

where $\Delta\vartheta(t)$ is the angular difference between the direction of two successive movements of the animal (see also the heading variability parameter). $\bar{P} \in [-1, 1]$ is the parallelism index. $\bar{P} \approx 1$ shows a tendency of the animal to perform straight paths, whereas $\bar{P} \approx -1$ indicates an oscillatory-like behavior (i.e. successive back and forth movements). $\bar{Q}$ estimates the mean tendency to turn to the left or to the right at each movement. As proposed by Brudzynski and Krol (1997), these two measures can then be used to compute the average angle of moment $\bar{\alpha}$:

$$\bar{\alpha} = \arctan\left(\frac{\bar{P}}{\bar{Q}}\right),$$

as well as the correlation coefficient r:

$$r = \sqrt{\bar{P}^2 + \bar{Q}^2},$$

and the angular dispersion σ (in radians) around the average angle:

$$\sigma = \sqrt{2(1-r)}.$$

Finally, NAT computes the path sinuosity index S (expressed in radians/cm$^{1/2}$):

$$S = \frac{\sigma}{\sqrt{\langle d(t) \rangle_{t \in [0,T]}}}$$

where T is the trial duration, and $d(t)$ is the Euclidian distance traveled by the animal at a given timestep t.

Path tortuosity. In open-field navigation tasks only, this parameter is computed as:

$$Z = \frac{1}{d_g(t_0)} \sum_{t \in (0,T]} d(t)$$

where T is the trial duration, $\sum_{t \in (0,T]} d(t)$ is the length of the actual trajectory followed by the animal to reach the target, and $d_g(t_0)$ is the distance from the position of the animal at time $t = 0$ (i.e. starting location) to the target (i.e. $d_g(t_0)$ is the length of the direct path to the goal).

Mean trajectory. NAT first re-samples all trajectories in a given zone and then computes the center of mass of the sampled points within each bin. Two methods are employed for the re-sampling step. First, the temporal procedure re-samples all trajectories according to the same temporal binning (Fig. A.4A). After computation, the mean trajectory consists of the set of consecutive points $\{\langle x_i(t) \rangle_i, \langle y_i(t) \rangle_i\}$, where $t \in [t_0, t_n]$, and $i \in [1, N]$ where N is the number of trajectories. The experimenter sets the resolution of the temporal binning procedure. However, this sampling method is sensitive to artifacts due to differences in the time course of maze crossing between different subjects (Fig. A.4B). For example, a mouse staying a few seconds at the departure point before performing the task will dramatically displace the barycenter of the considered time points. For this reason, NAT also implements

a spatial sampling procedure that consists in dividing the maze in small bins along one axis (the y-axis in the example of Fig. A.4C). For each y-bin, the barycenter of all points in the bin is estimated. Again, the experimenter sets the resolution of the spatial binning procedure (i.e. the bin width, in cm).

Appendix C. Supplementary User Guide

Supplementary data associated with this article can be found, in the online version, at http://dx.doi.org/10.1016/j.jneumeth.2013.02.018.

References

Arleo A, Rondi-Reig L. Multimodal sensory integration and concurrent navigation strategies for spatial cognition in real and artificial organisms. J Integr Neurosci 2007;6:327–66.

Barnes CA. Memory deficits associated with senescence: a neurophysiological and behavioral study in the rat. J Comp Physiol Psychol 1979;93:74–104.

Beach HD. Morphine addiction in rats. Can J Psychol 1957;11:104–12.

Benjamini Y, Fonio E, Galili T, Havkin GZ, Golani I. Quantifying the buildup in extent and complexity of free exploration in mice. Proc Natl Acad Sci U S A 2011;108(Suppl. 3):15580–7.

Boguszewski P, Zagrodzka J. Emotional changes related to age in rats—a behavioral analysis. Behav Brain Res 2002;133:323–32.

Bradley DC, Mascaro M, Santhakumar S. A relational database for trial-based behavioral experiments. J Neurosci Methods 2005;141:75–82.

Brudzynski SM, Krol S. Analysis of locomotor activity in the rat: parallelism index, a new measure of locomotor exploratory pattern. Physiol Behav 1997;62:635–42.

Burguière E, Arleo A, Hojjati M, Elgersma Y, De Zeeuw CI, Berthoz A, et al. Spatial navigation impairment in mice lacking cerebellar LTD: a motor adaptation deficit. Nat Neurosci 2005;8:1292–4.

Burguière E, Arabo A, Jarlier F, De Zeeuw CI, Rondi-Reig L. Role of the cerebellar cortex in conditioned goal-directed behavior. J Neurosci 2010;30(40):13265–71.

Conrad CD, Galea LA, Kuroda Y, McEwen BS. Chronic stress impairs rat spatial memory on the Y maze, and this effect is blocked by tianeptine pretreatment. Behav Neurosci 1996;110:1321–34.

Drai D, Golani I. SEE: a tool for the visualization and analysis of rodent exploratory behavior. Neurosci Biobehav Rev 2001;25:409–26.

Eilam D, Golani I. Home base behavior of rats (*Rattus norvegicus*) exploring a novel environment. Behav Brain Res 1989;34:199–211.

Flash T, Hogan N. The coordination of arm movements: an experimentally confirmed mathematical model. J Neurosci 1985;5:1688–703.

Fonio E, Benjamini Y, Golani I. Freedom of movement and the stability of its unfolding in free exploration of mice. Proc Natl Acad Sci U S A 2009;106:21335–40.

Fouquet C, Petit GH, Auffret A, Gaillard E, Rovira C, Mariani J, et al. Early detection of age-related memory deficits in individual mice. Neurobiol Aging 2011;32:1881–95.

Fry SN, Rohrseitz N, Straw AD, Dickinson MH. TrackFly: virtual reality for a behavioral system analysis in free-flying fruit flies. J Neurosci Methods 2008;171:110–7.

Gallagher M, Burwell R, Burchinal M. Severity of spatial learning impairment in aging: development of a learning index for performance in the Morris water maze. Behav Neurosci 1993;107:618–26.

Graziano A, Petrosini L, Bartoletti A. Automatic recognition of explorative strategies in the Morris water maze. J Neurosci Methods 2003;130:33–44.

Hamilton DA, Rosenfelt CS, Whishaw IQ. Sequential control of navigation by locale and taxon cues in the Morris water task. Behav Brain Res 2004;154:385–97.

Kalman RE. A new approach to linear filtering and prediction problems. J Basic Eng 1960;82D:35–45.

Kulikov AV, Tikhonova MA, Kulikov VA. Automated measurement of spatial preference in the open field test with transmitted lighting. J Neurosci Methods 2008;170:345–51.

Lipkind D, Sakov A, Kafkafi N, Elmer GI, Benjamini Y, Golani I. New replicable anxiety-related measures of wall vs center behavior of mice in the open field. J Appl Physiol 2004;97:347–59.

Morris RG, Garrud P, Rawlins JN, O'Keefe J. Place navigation impaired in rats with hippocampal lesions. Nature 1982;297:681–3.

Morris RGM. Spatial localization does not require the presence of local cues. Learn Motiv 1981;12:239–60.

O'Keefe J, Speakman A. Single unit activity in the rat hippocampus during a spatial memory task. Exp Brain Res 1987;68:1–27.

Olton DS, Samuelson RJ. Remembrance of places passed: spatial memory in rats. J Exp Psychol: Anim Behav Process 1976;2:97–116.

Ramos A, Berton O, Mormede P, Chaouloff F. A multiple-test study of anxiety-related behaviours in six inbred rat strains. Behav Brain Res 1997;85:57–69.

Rochefort C, Arabo A, Andre M, Poucet B, Save E, Rondi-Reig L. Cerebellum shapes hippocampal spatial code. Science 2011;334:385–9.

Rondi-Reig L, Lemaigre-Dubreuil Y, Montécot C, Müller D, Martinou JC, Caston J, et al. Transgenic mice with neuronal overexpression of bcl-2 gene present navigation disabilities in a water task. Neuroscience 2001;104(1):207–15.

Rondi-Reig L, Petit GH, Tobin C, Tonegawa S, Mariani J, Berthoz A. Impaired sequential egocentric and allocentric memories in forebrain-specific-NMDA receptor knock-out mice during a new task dissociating strategies of navigation. J Neurosci 2006;26:4071–81.

Spink AJ, Tegelenbosch RA, Buma MO, Noldus LP. The EthoVision video tracking system—a tool for behavioral phenotyping of transgenic mice. Physiol Behav 2001;73:731–44.

Stone C. The age factor in animal learning: I. Rats in the problem box and maze. Genet Psychol Monogr 1929;5:1–130.

Valente D, Golani I, Mitra PP. Analysis of the trajectory of *Drosophila melanogaster* in a circular open field arena. PLoS ONE 2007;2:e1083.

Verbitsky M, Yonan AL, Malleret G, Kandel ER, Gilliam TC, Pavlidis P. Altered hippocampal transcript profile accompanies an age-related spatial memory deficit in mice. Learn Mem 2004;11:253–60.

Whitlock JR, Pfuhl G, Dagslott N, Moser MB, Moser EI. Functional split between parietal and entorhinal cortices in the rat. Neuron 2012;73:789–802.

Wolfer DP, Lipp HP. A new computer program for detailed off-line analysis of swimming navigation in the Morris water maze. J Neurosci Methods 1992;41:65–74.

frontiers in
NEURAL CIRCUITS

REVIEW ARTICLE
published: 13 March 2013
doi: 10.3389/fncir.2013.00035

The cerebellum: a new key structure in the navigation system

***Christelle Rochefort*[1,2†], *Julie M. Lefort*[1,2†] *and Laure Rondi-Reig*[1,2*]**

[1] *UPMC Univ Paris 06, UMR 7102, Paris, France*
[2] *CNRS, UMR 7102, Paris, France*

Edited by:
Chris I. De Zeeuw, ErasmusMC, Netherlands; Netherlands Institute for Neuroscience, Netherlands

Reviewed by:
Piergiorgio Strata, University of Turin, Italy
Mitchell Goldfarb, Hunter College of City University, USA
Dagmar Timmann, University Clinic Essen, Germany

****Correspondence:***
Laure Rondi-Reig, Laboratory of Neurobiology of Adaptive Processes, Navigation, Memory, and Aging Team, CNRS UMR7102, Université Pierre et Marie Curie, Bâtiment B-5ème étage, 9 Quai Saint-Bernard, 75005 Paris, France.
e-mail: laure.rondi@snv.jussieu.fr
† These authors have contributed equally to this work.

Early investigations of cerebellar function focused on motor learning, in particular on eyeblink conditioning and adaptation of the vestibulo-ocular reflex, and led to the general view that cerebellar long-term depression (LTD) at parallel fiber (PF)–Purkinje cell (PC) synapses is the neural correlate of cerebellar motor learning. Thereafter, while the full complexity of cerebellar plasticities was being unraveled, cerebellar involvement in more cognitive tasks—including spatial navigation—was further investigated. However, cerebellar implication in spatial navigation remains a matter of debate because motor deficits frequently associated with cerebellar damage often prevent the dissociation between its role in spatial cognition from its implication in motor function. Here, we review recent findings from behavioral and electrophysiological analyses of cerebellar mutant mouse models, which show that the cerebellum might participate in the construction of hippocampal spatial representation map (i.e., place cells) and thereby in goal-directed navigation. These recent advances in cerebellar research point toward a model in which computation from the cerebellum could be required for spatial representation and would involve the integration of multi-source self-motion information to: (1) transform the reference frame of vestibular signals and (2) distinguish between self- and externally-generated vestibular signals. We eventually present herein anatomical and functional connectivity data supporting a cerebello-hippocampal interaction. Whilst a direct cerebello-hippocampal projection has been suggested, recent investigations rather favor a multi-synaptic pathway involving posterior parietal and retrosplenial cortices, two regions critically involved in spatial navigation.

Keywords: cerebellum, hippocampus, navigation, LTD, self-motion, path integration, place cells, spatial representation

INTRODUCTION

Whilst the cerebellum has long been exclusively associated with motor function, its role in cognitive processes has, in the last decades, progressively become apparent. This review will first focus on the original work leading to the major hypothesis that long-term depression (LTD) at parallel fiber (PF)–Purkinje cell (PC) synapses underlies cerebellar motor learning. We then provide an overview of the arguments suggesting that cerebellar processing is also required in cognitive function such as spatial navigation and that it contributes to both hippocampal spatial map formation and optimal goal-directed navigation. The potential computation undertaken by the cerebellum for building hippocampal spatial representation is also discussed. Finally, the possible anatomical pathways involved in this cerebello-hippocampal association are explored.

CEREBELLAR LTD AND MOTOR LEARNING

LTD refers to an activity-dependent long lasting decrease in synaptic efficacy. This anti-hebbian form of synaptic plasticity was initially discovered in and thought to be unique to the cerebellum (Ito and Kano, 1982; but see Ito, 1989) until it was also described in many other brain areas [e.g., hippocampus (Stanton and Sejnowski, 1989) and cortex (Artola et al., 1990)]. Although Brindley was the first to propose plastic synaptic features to PC (Brindley, 1964), the Marr–Albus theory, which emerged after the fine description of the cerebellar circuitry (Eccles, 1965, 1967), was the one that historically inspired future research. According to this model, the cerebellum acts as a pattern classification device that can form an appropriate output in response to an arbitrary input (Boyden et al., 2004). This implies that the cerebellar circuitry allows adjustments of PF–PC synaptic efficacy, which would enable the storage of stimulus-response associations by linking inputs converging to the cerebellar cortex with appropriate motor outputs. Marr first developed this model by predicting the existence of long-term potentiation (LTP) at PF–PC synapses (Marr, 1969) and Albus modified it two years later by proposing LTD rather than LTP as the learning underlying cellular mechanism (Albus, 1971).

The experimental correlate of the Marr–Albus theory was discovered a few years later by Ito and Kano in 1982. The authors focused on a simple motor learning task and well-defined plastic system: the adaptation of the vestibulo-ocular reflex (VOR). The VOR enables the stabilization of images on the retina during head turns by eliciting eye movements in the opposite direction. Experimental adaptation of this reflex can be obtained by repeatedly displacing the visual stimulus during the head rotation.

By studying the VOR circuitry in the rabbit flocculus cerebellar region, Ito and Kano experimentally demonstrated the existence of LTD on PCs after conjunctive stimulation of parallel and climbing fibers (Ito and Kano, 1982; Ito, 1989). Since cerebellar architecture is composed of several uniform modules, it was then suggested that such signal processing may be similar along the entire cerebellum.

Following this work, the implication of LTD in motor learning has been suggested by the observed correlation between altered LTD and impaired motor learning. A series of mouse models lacking LTD has been studied in two main behavioral paradigms, the VOR adaptation and the eyeblink conditioning tasks. In the latter, for which the cerebellum has been shown to be essential (Clark et al., 1984; McCormick and Thompson, 1984a,b), the animal learns to associate a tone (conditioning stimulus) with a corneal air puff (unconditioned stimulus) leading to the eyelid closure. The analysis of mutant mouse models targeting signaling pathways involved in LTD such as the metabotropic glutamate receptor mGluR1 (Aiba et al., 1994), the protein kinase C (PKC) (De Zeeuw et al., 1998; Koekkoek et al., 2003) or the αCaMKII enzyme (Hansel et al., 2006) provided a strong support in favor of the hypothesis that cerebellar LTD is indeed related to cerebellar-dependent motor learning. Nevertheless, a further step to sustain this assertion would be to demonstrate that LTD is effectively induced after cerebellar motor learning.

The current view that cerebellar LTD underlies motor learning was recently challenged as the pharmacological inactivation of cerebellar LTD was not accompanied by a deficit in eyeblink conditioning and in the rotarod test (Welsh et al., 2005). Moreover using a fine behavioral approach designed to selectively eliminate the instructive signal from the climbing fiber (and thus the induction of heterosynaptic LTD) during a VOR adaptation task, it was shown that cerebellar motor learning was completely normal (Ke et al., 2009). In accordance with these findings, the use of three different mutant mouse models targeting specifically late events in the LTD signaling cascade confirmed the dissociation between LTD and simple motor learning tasks (Schonewille et al., 2011).

Interestingly, Burguiere et al. (2010) investigated the role of LTD in an aversive operant conditioning, using a Y-watermaze task in which mice had to learn to associate the correct turn with a stimulus presented before the turn. Inhibition of the PKC crucial for LTD induction did not prevent the animals from learning the stimulus-response "cue–direction" association. In the light of these recent findings, it thus appears that whereas some cerebellar synaptic transmission mechanisms are involved in motor learning, the LTD occurring at PF–PC synapses is not essential. In addition, another form of plasticity, the PF–PC LTP has been proposed to be important for motor learning (Schonewille et al., 2010). Taking into account the different plasticities of the cerebellar cortex including granule cells and PCs network, Gao et al. (2012a) proposed a new conceptual framework called "distributed synergistic plasticity." They suggest that many forms of synaptic and intrinsic plasticity at different sites combine synergistically to produce optimal output for behavior. This theoretical debate is still ongoing. These mutant mouse models were also an opportunity to extend the study of cerebellar plasticities in other forms of learning abilities, notably in relation to spatial navigation.

CEREBELLUM AND SPATIAL NAVIGATION

Spatial navigation is a cognitive function that can be defined as a dual process. Indeed it requires the integration of both self-motion (vestibular, proprioceptive, optic flow, or motor command efferent copy)[1] and external (visual, olfactory, auditory, or tactile) sensori-motor information to form an internal cognitive representation of the context in which the navigation takes place. This cognitive representation can then be used in order to elaborate an optimal goal-directed path adapted to the context (**Figure 1**).

Contribution of the cerebellum to cognitive functions such as navigation remains a controversial subject. Indeed, whilst an extensive range of cerebellar functions has been pointed out as early as 1950 (Snider, 1950) and since been completed and corroborated by more recent research, the current understanding of cerebellar functions in cognition suffers from great criticism. For instance, some findings providing important evidence in human that the cerebellum is involved in cognitive function has been refuted based on the general comments that reports of cerebellar activation during cognitive demands are not always replicated and might therefore "be related to actual or planned movements of the eyes, vocal apparatus, or finger" (Glickstein, 2007).

It can however be acknowledged that the view of the cerebellum in cognitive function has evolved with reports describing dysfunction of non-motor processes in patients with cerebellar pathology as well as findings from neuroimaging studies in normal adults (Schmahmann, 1991; Schmahmann and Sherman, 1998; Stoodley and Schmahmann, 2009). For instance, the role of the cerebellum in emotion has been suggested by the difference in the pattern of cerebellar activation induced by distinct types of emotion (Damasio et al., 2000; Baumann and Mattingley, 2012). Implication of the cerebellum in such function has also

[1] See Glossary.

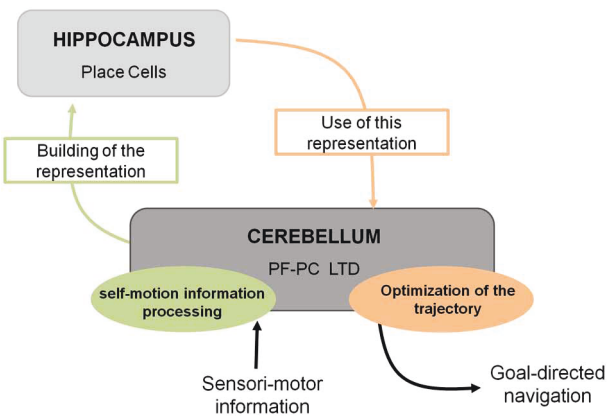

FIGURE 1 | Cerebello-hippocampal interaction for goal-directed navigation. The cerebellum contributes to spatial navigation at two levels, first in processing self-motion information to build spatial representation in the hippocampus at the level of place cells, and second in using this spatial representation to perform an optimal trajectory toward a goal. Studying L7-PKCI mice lacking LTD at PF–Purkinje cell synapses, this plasticity has been shown to be involved in both processes.

emerged from a series of investigations using associative fear learning paradigms in patient with cerebellar lesion (see for review Timmann et al., 2010). These results are further supported by studies in rodents, which clearly demonstrated that PF–PC LTP underlies associative memory processes related to fear behavior (for reviews see Sacchetti et al., 2009; Strata et al., 2011). Importantly it has been evidenced that cerebellar LTP was indeed induced by associative fear learning (Sacchetti et al., 2004; Zhu et al., 2007).

The earliest studies combining mental or virtual navigation tasks with brain imaging and focusing on hippocampal and cortical networks reported that cerebellum was also activated during these tasks (Maguire et al., 1998; Ino et al., 2002; Moffat et al., 2006). A few neuroimaging studies using driving simulators showed that a network of brain structures including the cerebellum was specifically activated during driving (Walter et al., 2001; Calhoun et al., 2002; Uchiyama et al., 2003; Horikawa et al., 2005). Findings emerging from patients with cerebellar damage led to diverging conclusions. A series of investigation in children who underwent a resection of cerebellar tumors points toward a role of the cerebellum in visuo-spatial skills (Levisohn et al., 2000; Riva and Giorgi, 2000; Steinlin et al., 2003), although discrepancies exist regarding the part of the cerebellum associated to it. Whereas impaired spatial abilities have been specifically associated to lesions of the left cerebellum in the study of Riva and Giorgi, others works did not find any lateralization (Levisohn et al., 2000). Several studies assessing visuo-spatial abilities in adult cerebellar patient reported that cerebellar lesion leads to an alteration in spatial function (Wallesch and Horn, 1990; Malm et al., 1998; Schmahmann and Sherman, 1998; Molinari et al., 2004), with for some reports a specific involvement of the posterior part of the cerebellum (Schmahmann and Sherman, 1998). However, other reports attribute the observed visuo-spatial deficits of cerebellar patient to unspecific attention impairment rather than spatial neglect (Frank et al., 2007, 2008, 2010). Moreover, in a study assessing the ability of adult subject to navigate without any visual input, patient with cerebellar ataxia displayed trajectories that were even more accurate than control (Paquette et al., 2011), although their angular motion was impaired (Goodworth et al., 2012). Based on the results emerging from both fMRI and cerebellar lesion studies, it has been recently suggested that the cerebellum is part of at least two distinct functional loops, one involved in motor processing and the other involved in cognitive processes (Strick et al., 2009; Ramnani, 2012). Whereas accumulating evidence support the idea that cerebellum participate in both motor and non-motor function, its specific involvement in human spatial navigation remains to be established.

In non-human primates, one of the first reports on the contribution of the cerebellum to spatial learning abilities emerged in the 80's. This study carried out on adult monkeys with experimental lesions of the deep cerebellar dentate nucleus revealed an impaired performance in the spatial parameter of a visuo-motor task involving a goal-directed movement of the arm (Trouche et al., 1979). These results represented a first step toward an enlarged view of cerebellar functions, encompassing more complex spatial learning task. The role of the cerebellum in spatial learning has also been investigated using water maze tasks in rodents given the reduced impact cerebellar lesions exert on swimming movements (see review in Lalonde and Strazielle, 2003). However, whilst several authors emphasized the navigation deficit in cerebellar mutant models, a recurrent problem has been to dissociate between the navigation process deficit *per se* and motor-related problems. Therefore, rodents were tested in cued or spatial learning paradigms of a water maze in order to evaluate their visuo-motor abilities or their spatial navigation abilities respectively (see **Figure 2** for more details about the paradigms). Several cerebellar mutant mice such as Grid2^{Lc}, Rorα^{sg}, reeler and weaver presented deficits in both cued and spatial learning (see review in Rondi-Reig and Burguiere, 2005). However, these natural mutations were relatively large and affected the whole cerebellar organization. Nevertheless, another cerebellar mutant mouse (Nna1^{pcd}) which displays a postnatal specific degeneration of virtually all cerebellar PCs (Mullen et al., 1976) was able to perform the cued but not the spatial version of the task indicating that the severe spatial navigation deficit of this mutant was not simply due to motor dysfunction (Goodlett et al., 1992). Similarly, hemicerebellar lesions led to deficits in both spatial and cue version of the MWM (Petrosini et al., 1996), whereas more restricted lesions to the lateral cerebellar cortex, the dentate nucleus (Joyal et al., 2001; Colombel et al., 2004) or the Purkine cell layer (Gandhi et al., 2000) reveals a specific impairment in the spatial version of this task. Altogether, based on the specificity of the behavioral and neurobiological alterations, these data clearly supported the hypothesis that the cerebellum is involved in spatial learning (see reviews in Petrosini et al., 1998; Molinari and Leggio, 2007).

The accumulation of evidence supporting a role of the cerebellum in navigation raised the question of the potential roles of the two major cerebellar inputs, the olivo-cerebellar input (climbing fiber) and the mossy fiber–granule cells–PF input. Rondi-Reig et al. (2002) tested rats with lesion of climbing (CF) and/or PF inputs of the cerebellum in either the cued or the place protocol of the water maze. Rats with a lesion of CF associated with partial or total lesion of PF presented a deficit in the latency to find the platform in the spatial version of the task but not in the cued one. Interestingly a difference appeared between the CF and PF lesion in the initial body orientation relative to the platform. Animals presenting a lesion of the PF were unable to learn how to orient their body toward the non-visible platform and opted instead for a circling behavior, whereas animals with lesion of the CF were still able to reach control level. These results indicated a substantial role of the PF cerebellar inputs in navigation (Rondi-Reig et al., 2002) and pointed toward an underlying mechanism occurring at the PC synapse.

Recent use of the L7-PKCI transgenic model, in which the PKC dependent LTD that occurs at PF–PC synapses is altered, brought new insight regarding the process performed by the cerebellum (Burguiere et al., 2005, 2010; Rochefort et al., 2011) (**Figure 1**). Using this L7-PKCI model in an operant conditioning task, our team highlighted the idea that cerebellar LTD is not required for the learning of a stimulus-response association but is rather involved in the optimization of a motor response during a goal-directed navigation conditioning task (Burguiere et al., 2005, 2010). Using a behavioral protocol assessing specifically

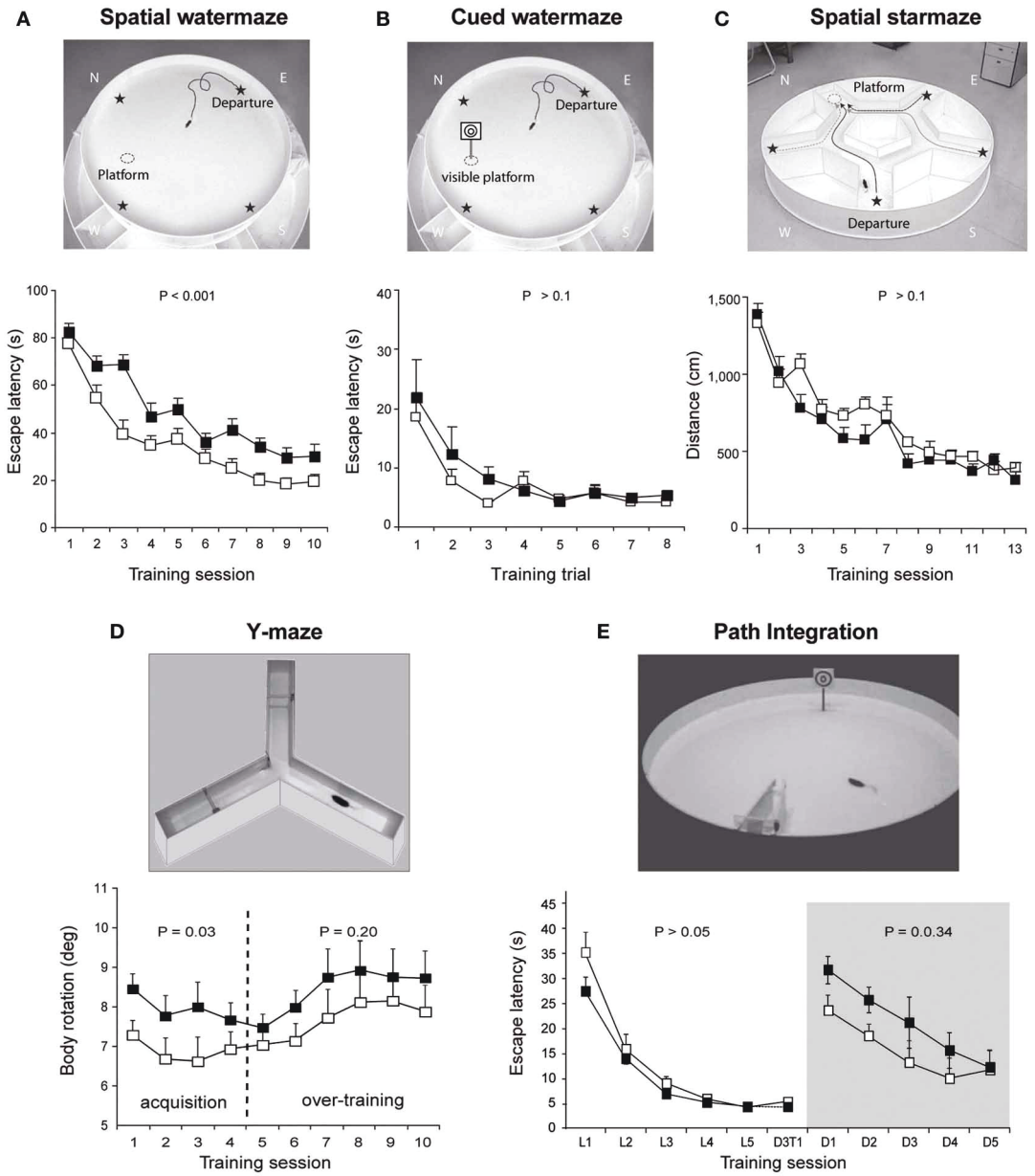

FIGURE 2 | Overview of the different paradigms used in L7-PKCI mice to assess their spatial navigation performances. (A) The spatial version of the Morris watermaze, in which a hidden platform can be found using the configuration of distal visual cues around the maze revealed spatial learning deficits in L7-PKCI mice. **(B)** These lower performances are not due to a deficit in visual guidance abilities, as revealed by subsequent training in the cued version of this maze. In this task, L7-PKCI mice correctly found the platform location indicated by a proximal visual cue. **(C)** The absence of deficit in the starmaze, in which alleys help to execute efficient trajectories toward an invisible platform, suggests that while L7-PKCI can learn to locate a goal using distal visual cues, they are unable to execute a direct trajectory toward it. **(D)** The use of a single intersection maze called the Y-maze enables analysis of trajectory quality. Trajectories optimization was quantified by the body rotation parameter which measures the angle between 3 successive points of the trajectory and is averaged over the whole path. Body rotation was specifically impaired in L7-PKCI mice during the acquisition of the task. **(E)** The inability of L7-PKCI mice to navigate in the dark (i.e., using self-motion information) was revealed in a path integration task, in which mice have to find a platform in a constant location and from a fixed departure point with an alley guiding the initial orientation of the body. In this task, mice first learn the path in the light and then reproduce it in the dark. **(A,B,C)** Data from Burguiere et al. (2005); **(D)** data from Burguiere et al. (2010); **(E)** data from Rochefort et al. (2011). N, W, E, S: North, West, East, and South, respectively. Stars on the pictures in **(A,B,C)** indicate each possible departure point.

path integration of the L7-PKCI mice (i.e., the ability to navigate using self-motion information only), we revealed an implication of cerebellar LTD in the formation of the self-motion based internal spatial map encoded in the hippocampus. Indeed, mice lacking this form of cerebellar plasticity presented impaired hippocampal place cell firing properties. Interestingly, the deficit in the hippocampal place code was observed only when mice had to rely on self-motion information. Subsequently, mice were

tested in a path integration task, in which they had to find a platform in a constant location and from a fixed departure point with an alley guiding the initial orientation of the body (**Figure 2**). Mice first learned the path in the light and then had to reproduce it in the dark. Consistently with their hippocampal place cell alteration, L7-PKCI mice were unable to navigate efficiently toward a goal in the absence of external information (**Figure 2**). Princeps studies on navigation in rats suggested that the cerebellum is not required for the retention of a learned path in a maze habit task with guiding alleys, even in the absence of vision (Lashley and McCarthy, 1926). It is possible that the fact that mice are overtrained and the presence of alleys guiding the animal movement had hidden a potential deficit. Likewise, L7-PKCI mice were also not deficient in the starmaze, a navigation task in which mice swim only within alleys (Burguiere et al., 2005).

The deficit in the spatial map observed in L7-PKCI mouse model brought the first evidence of a functional interaction between the cerebellum and the hippocampus in the acquisition of a spatial representation required to perform path integration (Rochefort et al., 2011). According to these findings, cerebellar LTD might participate in the mental construction of the representation of space whose seat is in the hippocampus, suggesting that the cerebellum takes part in the representation of the body in space. The next section is focused on describing the mechanisms by which the cerebellum might participate in navigation by processing and combining multimodal self-motion information and give pertinent information about body location in space.

CEREBELLAR CONTRIBUTION TO NAVIGATION INFORMATION PROCESSING

As previously explained, spatial navigation is an active process that requires the accurate and dynamic representation of our location, which is given by the combination of both external and self-motion cues. Vestibular information has been shown to be crucial for spatial representation (Stackman et al., 2002), spatial navigation (Stackman and Herbert, 2002; Smith et al., 2005), and specifically path integration (Wallace et al., 2002). However, vestibular information by itself does not provide sufficient information to properly locate in an environment. Coherent body motion information is indeed given by the combination of multiple sources of idiothetic information including vestibular, proprioceptive, optic flow, and motor command efferent copy signals. **Figure 3** suggests the role of the cerebellum in such integration.

Vestibular information is first detected in the inner ear by the otoliths organs for the linear component and by the semi-circular canals for the rotational component. As receptor cells are fixed to

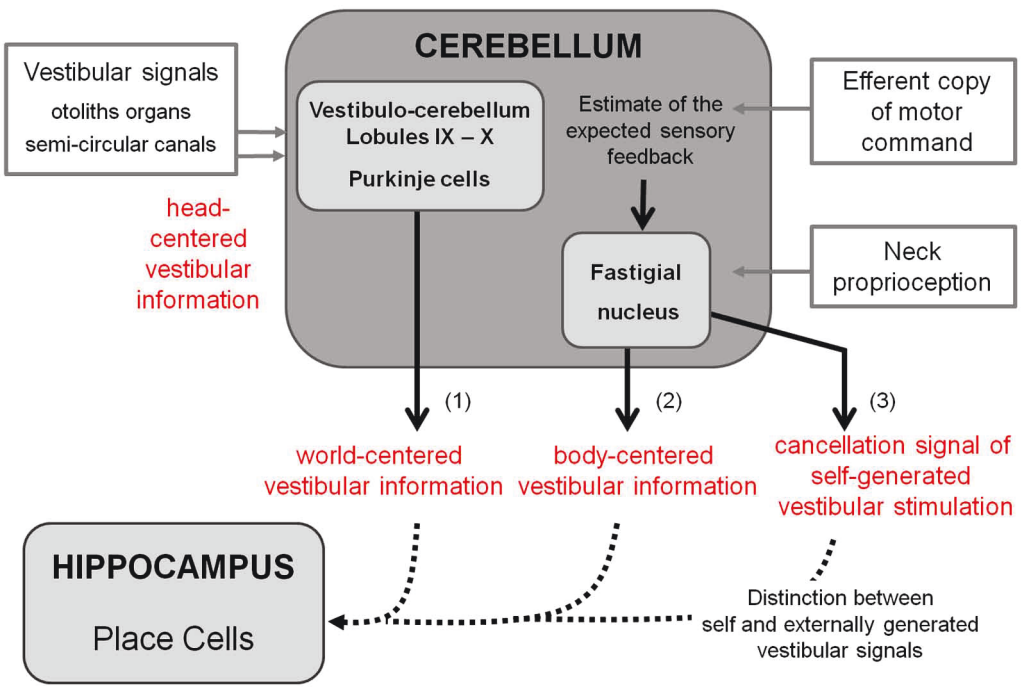

FIGURE 3 | Detailed cerebellar processing of self-motion information that can be used for building spatial representation. This figure represents the ascendant branch of **Figure 1** and highlights the cerebellar contribution to building spatial representation. Based on the existing literature, cerebellar processing of self-motion information could involve three different computations: **(1)** The combination of otolith and semi-circular signals to convert head centered vestibular information into world centered vestibular information. **(2)** The integration of neck proprioceptive information with head motion vestibular information to compute an estimate of body motion in space. **(3)** The hypothesis proposed by Cullen et al. (2011) of a possible production of a cancellation signal to suppress self-generated vestibular stimulation due to active movements. This computation implies using the efferent copy of motor command to predict expected sensory feedback and to compare it to the effective proprioceptive signal (Roy and Cullen, 2004). Such a cancellation allows distinguishing between self-and externally-generated vestibular signals. These transformations are required to provide the hippocampus with the appropriate self-motion information (dotted lines).

the head bone, vestibular signals are detected in a head reference frame (**Figure 4**). This means for example that based on semicircular signals only, a rotation of the head upright relative to the vertical axis cannot be distinguished from a rotation of the head horizontal relative to the horizontal axis. In other words, semicircular canal information alone does not discriminate vertical or horizontal body position. To compute the movement of the body in space, vestibular information needs to be integrated relative both to the body (taking into account the relative position of the head and the body, given by the neck curvature) and to the world, converting the signal initially in head-fixed coordinates into a signal in world-frame coordinates (taking into account gravity). These computations are not necessarily successive and result from the integration of different types of signals. Several recent studies showed that these two reference frame transformations occur in different cerebellar subregions. An elegant report recently pointed out that the cerebellar cortex computes the head-to-world reference frame conversion by combining semicircular and otolith organs inputs (Yakusheva et al., 2007). This computation takes place in the lobules 9 and 10 of the cerebellum and involves GABA transmission (Angelaki et al., 2010).

Head-to-body frame transformation seems to occur in the cerebellar fastigial nucleus. This region contains indeed a subpopulation of neurons (50%)—one synapse downstream the PCs—that has been shown to encode motion in body coordinates (Kleine et al., 2004; Shaikh et al., 2004). More recently, this idea has been further supported by the demonstration that fastigial neurons respond to both vestibular and neck proprioception, and specifically encode body movement in space (Brooks and Cullen, 2009). However, since head to body position has also been shown to modulate PC activity in the cerebellar anterior vermis in decerebrate cats (Manzoni et al., 1999), meaning that PCs also receive neck proprioceptive information, one cannot exclude that the head to body frame transformation might also take place in the cerebellar cortex.

Another implication of the cerebellum in the sensory processing involved in spatial navigation has been highlighted by studies on the cancellation of self-generated vestibular signals. During spatial navigation, displacement of the body in the environment undoubtedly generates stimulations of vestibular receptors. This includes translational stimulations corresponding to the displacement vector as well as rotational stimulations due to head and body reorientation. However, vestibular stimulations are not perceived, meaning that these self-generated signals have been canceled out, enabling reliable detection of stimuli from external sources. Crucial to navigation, the ability to distinguish self-generated vestibular signals coming from an active movement allows proper integration with other

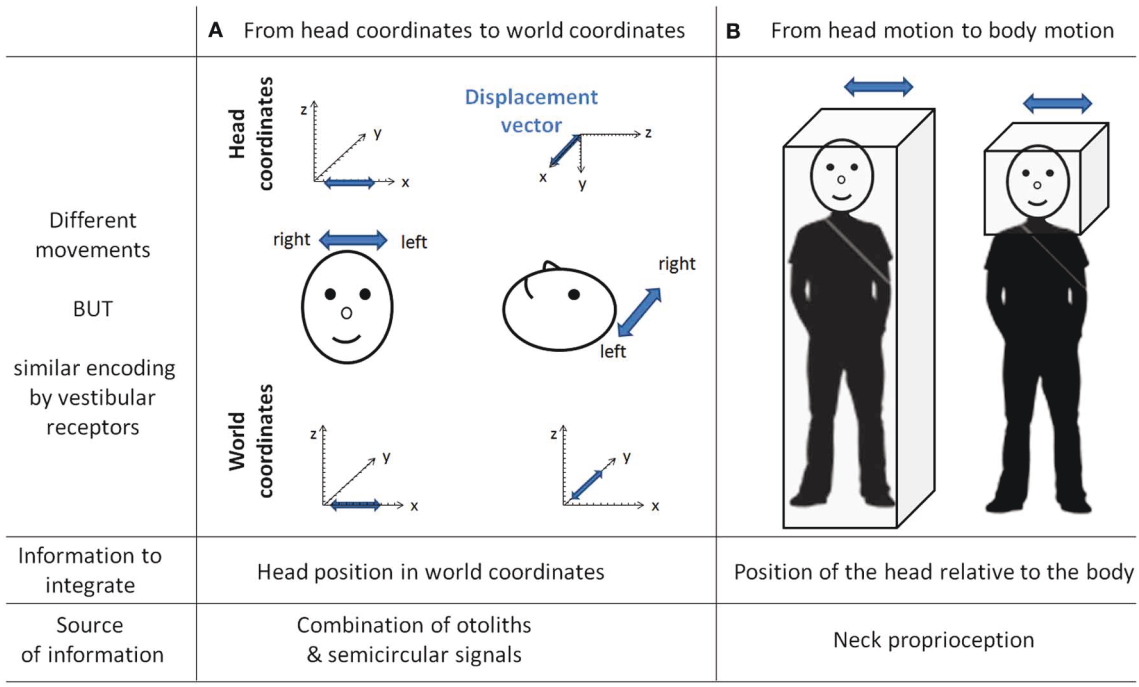

FIGURE 4 | The need for transformation of the vestibular signals. As the vestibular organs are located in the head, vestibular signal is detected in head coordinates. This implies several transformations of the vestibular signal to correctly compute body motion in space. This figure gives two examples of different movements similarly encoded by vestibular receptors. In column **(A)** is a linear displacement from left to right, with the head either vertical or horizontal. Indeed both movements are identical in the head reference frame [displacement vectors (in blue) project onto the x-axis] whereas they are different in the world coordinates (displacement vectors project either onto the x-axis or onto the y-axis). These two movements can be distinguished by taking into account the head position in space, which can be extracted from the combination of semicircular and otolith organs signals (Yakusheva et al., 2007). Column **(B)** illustrates two movements corresponding to the same head motion in space, but different body motions in space (i.e., on the right the body is stationary). These two movements can be distinguished by integrating information about the position of the head relative to the body (that is, the neck curvature, given by neck proprioceptors).

types of idiothetic signals to produce an accurate estimate of body movement, which forms the basic computation for path integration.

A particular population of neurons within vestibular nuclei termed Vestibular Only (VO) are selectively active during passively applied movements (McCrea et al., 1999; Roy and Cullen, 2001). The lack of response during active movements implies that self-generated vestibular signals are indeed canceled. Such cancellation requires knowledge about the currently performed movement provided by the combination of the different self-motion signals, and in particular the efferent copy of the motor command and proprioception. Because the VO neurons are modulated by neither proprioceptive inputs nor efferent copy of motor command when presented in isolation to alert animals, some authors suggested that a cancellation signal arrives from higher structures in the case of active movements (Roy and Cullen, 2003, 2004). Moreover, Roy and Cullen (2004) showed that during active movements, this cancellation signal occurs only if the actual movement matches the intended one. These authors proposed that, using the efferent copy of motor command, an internal model of proprioception is computed and compared to the actual proprioceptive signal. If it matches, a cancellation signal is generated and sent to the vestibular nuclei. The exact location of the cancellation signal generation remains to be determined. Such a region should receive proprioceptive signals, efferent copies of the motor commands or an estimate of the expected sensory consequences of actions, and vestibular signals. For these reasons Cullen et al. (2011) proposed that the cerebellar rostral fastigial nucleus would be a good candidate. Indeed it does receive inputs from the cerebellar cortex—whose function is thought to be (among others) the generation of sensory prediction—neck proprioception from the central cervical nucleus and the external cuneate nucleus and vestibular inputs from the vestibular nucleus (Voogd et al., 1996). Additionally, recordings in fastigial nucleus (Brooks and Cullen, 2009) strongly suggested that the integration of proprioceptive and vestibular information takes place in the rostral fastigial nuclei during passive movement. Whether this integration occurs during active movement and is used to generate a cancellation signal remains to be demonstrated.

Thus, the cerebellum is likely to act in a heterogeneous manner, involving several subregions in the cerebellar cortex and deep nuclei for the transformation of the reference frame adapted to navigation in space and for the cancellation of self-generated vestibular signals, enabling a focus on pertinent external stimulation for optimal path. The information, adequately transformed, is subsequently conveyed to the hippocampus (**Figure 3**).

The exact network and plasticities involved in this computation during navigation remains to be elucidated. Deficits observed in the L7-PKCI mice suggest that cerebellar PF–PCs LTD is involved in such computation and plays an important role in self-motion based hippocampal space representation.

ANATOMICAL AND FUNCTIONAL RELATION BETWEEN CEREBELLUM AND FOREBRAIN NAVIGATION AREAS

Demonstration that the cerebellum assists navigation at least in part by participating in the building of the hippocampal spatial map (Rochefort et al., 2011) implies that these structures are interconnected. Therefore, the cerebellum communicates either directly with the hippocampal system or with the forebrain navigation areas connected to it. Interestingly, a functional interaction between the hippocampus and the cerebellum has recently been supported by two studies conducted in rabbits using the hippocampal-dependent *trace* version of the eyeblink conditioning task (Hoffmann and Berry, 2009; Wikgren et al., 2010). Both investigations clearly demonstrate that during trace eyeblink conditioning, theta oscillation (3–7 Hz) occurs in the lobule HVI and the interpositus nucleus of the cerebellum and is synchronized with hippocampal theta oscillation. The cerebellar theta oscillations appeared to depend on the hippocampal theta rhythm. These data demonstrate that the hippocampus and the hemispheric lobule HVI of the cerebellum, which is involved in the stimulus-response association of the trace eyeblink conditioning, can synchronize their activity during specific cognitive demands. Whilst the data from Hoffmann and Berry (2009) suggest that this coordination enhances the associative learning abilities, Wikgren et al. (2010) did not observe a link between hippocampo-cerebellar synchronization and learning performances. Regardless, the latter investigations invite speculation on the possibility of multiple synchronization areas between the hippocampus and the cerebellum, which may be required for spatial navigation.

One important question raised by these findings is the anatomical circuitry underlying such functional interaction. Some evidence suggests a direct anatomical link between the hippocampus and the cerebellum. In cat and monkey, fastigial nucleus stimulation consistently evoked responses bilaterally in the rostro-caudal region of the hippocampus at delays indicating a monosynaptic connection (Heath and Harper, 1974; Snider and Maiti, 1976; Heath et al., 1978; Newman and Reza, 1979). Heath and Harper (1974) also found degenerated fibers in the hippocampus following lesion of the fastigial nucleus, meaning that these fibers could directly originate from the deep cerebellar nucleus. Hippocampal responses following posterior vermis stimulation were also reported (Heath et al., 1978; Newman and Reza, 1979) but not after stimulation of other cerebellar subregions. However, these observations have not, so far, been confirmed by anatomical investigations, possibly because of the potentially low number of implicated fibers.

Nevertheless, a recent study combining retrograde tracing and degeneration analysis after hippocampal lesion demonstrated a direct projection from the hippocampal formation to the cerebellum in chicken (folia VI–VIII) (Liu et al., 2012). The existence of a hippocampo-cerebellar projection does not imply a backward projection from the cerebellum to the hippocampus, which could explain the influence of cerebellar plasticity in shaping hippocampal place cell properties (Rochefort et al., 2011). However, tracing studies performed in the monkey in the last decade suggest a general organizational principle of the cerebello-cortical system where different areas of the neocortex are reciprocally connected to the cerebellum in closed loops (Clower et al., 2001; Middleton and Strick, 2001; Kelly and Strick,

2003; Prevosto et al., 2010). A direct cerebello-hippocampal projection remains to be discovered.

Alternatively, the cerebellum could interact with the hippocampus through multi-synaptic connections via the forebrain navigation circuit. Evidence from rat studies suggests that this interaction may take place via multiple pathways. The cerebellum reaches the forebrain mainly through the projection from the deep cerebellar nuclei toward the thalamus. Interestingly, substantial cerebellar inputs are found in the central-lateral thalamic nucleus (Haroian et al., 1981; Angaut et al., 1985; Aumann et al., 1994). The central lateral nucleus projects to both the posterior parietal and the retrosplenial cortices (Van der Werf et al., 2002), two cortical areas particularly involved in spatial navigation.

The posterior parietal cortex (PPC) is a multi-modal cortical area integrating self-motion and visuo-spatial information (Snyder et al., 1998; Save and Poucet, 2009). Its role in spatial navigation has been recently enlightened by the discovery of rat PPC cells the activity of which is tuned to self-motion and acceleration irrespective to the animal location or heading (Whitlock et al., 2012). The presence of cells encoding movement in an egocentric reference frame thus makes the PCC a primary candidate for the reception of cerebellar information and its transmission to other navigation areas. Such hypothesis is further supported by the close interaction between PPC and cerebellar lobule VIIa and Crus I and II showed in a human resting state functional connectivity study (O'Reilly et al., 2010). Moreover, combining anterograde and retrograde tracing, studies in both rat and primate confirmed that the PPC receives cerebellar input from the interposed and lateral nuclei via a thalamic relay in the central-lateral and ventro-lateral nuclei (Amino et al., 2001; Clower et al., 2001; Giannetti and Molinari, 2002; Prevosto et al., 2010). The existence of reciprocal connections from the parietal cortex to the cerebellum has not been documented so far in the rodent but cerebello-parietal interaction could follow the closed-loop architecture of cerebro-cerebellar interactions. Moreover in monkey, the homologous area to the rat PPC (the area 7) has indeed been shown to project to the cerebellar hemispheres via the pontine nucleus (Glickstein et al., 1985; Dum et al., 2002). Such projection could contribute substantially to multisensory integration (Glickstein, 2003).

The retrosplenial cortex is also thought to be involved in the allocentric-to-egocentric transformation process (Vann et al., 2009). Indeed, retrosplenial inactivation has been shown to impair allocentric navigation and path integration as well as field location of hippocampal place cells (Cooper et al., 2001; Cooper and Mizumori, 2001; Whishaw et al., 2001). This cortical area also contains head direction cells which are found in a network of structures (Taube, 2007) and were recently shown to underlie a rodent's sense of direction during path integration (Valerio and Taube, 2012). Head direction signal is prominently dependent on vestibular information (Stackman et al., 2002) and is believed to be generated subcortically and then processed by higher structures such as the retrospenial cortex (Taube, 2007).

Therefore, the cerebellum may contribute to two major circuits crucial for the representation of space in the hippocampal system (**Figure 5**): one comprising the retrospenial cortex more closely associated to the vestibulo-cerebellum, and the other involving the PPC receiving inputs from deep cerebellar nuclei and possibly involved in planning and execution of navigation behavior. Nevertheless the precise anatomical pathways between cerebellum and hippocampus activated during spatial navigation remain to be elucidated.

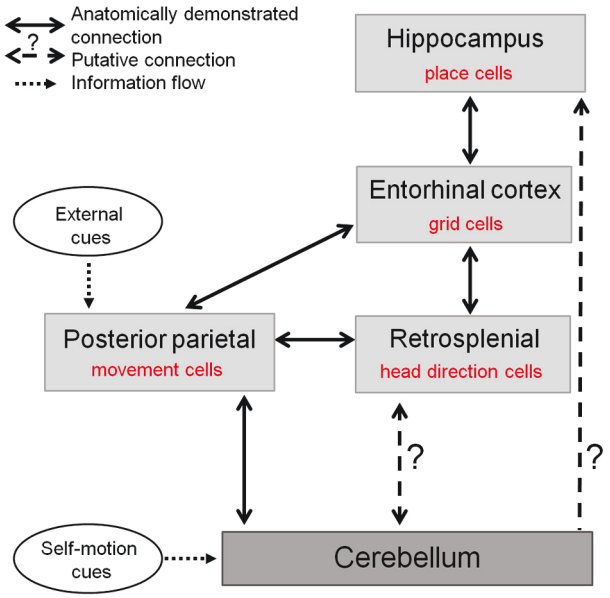

FIGURE 5 | The cerebellum in the anatomo-functional circuit underlying spatial navigation. Navigation system comprises a whole network of structures: (1) the hippocampus containing ≪place cells≫, which correlate with animal's location in space and underlie animal's spatial representation (O'Keefe and Dostrovsky, 1971), (2) the medial enthorinal cortex, containing ≪grid cells≫ which fire according to a grid-like pattern and are thought to constitute the metric system of the brain (Hafting et al., 2005), (3) a network of structures—among which the retrospenial cortex—containing ≪head direction cells≫, specific for a given direction of the head in space (Taube et al., 1990), and (4) posterior parietal cortex containing ≪movement cells≫, encoding self-motion and acceleration (Whitlock et al., 2012). The cerebellum takes part in this navigation system as it shapes hippocampal place cells properties (Rochefort et al., 2011). This contribution could occur either through a direct projection to the hippocampus or via a multi-synaptic connection involving a thalamic relay, to the posterior parietal cortex or the retrosplenial cortex.

CONCLUDING REMARKS

Recent converging evidence demonstrates the importance of the cerebellum in spatial navigation. Such implication in the navigation system at the hippocampal level or in forebrain navigation areas has been elucidated using electrophysiological, anatomical, and behavioral analyses in both human and animal models. Although the cerebellar network does not encode a spatial map of the environment, it does participate in map formation in the forebrain navigation areas by specifically encoding and computing self-motion information from different sources required to build the representation of the body in space. PF–PC LTD is implicated in this process, and other as yet to be determined modes of cerebellar plasticity may participate as well. The recent development of tetrodes multi-unit recordings in rat's cerebellum (de Solages et al., 2008; Gao et al., 2012b) opens new perspectives

to unravel the cerebellar computation occurring during goal-directed navigation. In order to unravel the precise contributions of the cerebellum to the processing of information during navigation, such technique will have to be combined with the use of mutant animals bearing specific cerebellar plasticity deficits.

ACKNOWLEDGMENTS

This is supported by the Fondation pour la Recherche Médicale DEQ20120323730, France, and National Agency for Research ANR-REG-071220-01-01, France. We are grateful to Glenn Dallérac and Pauline Obiang for helpful comments on the manuscript.

REFERENCES

Aiba, A., Kano, M., Chen, C., Stanton, M. E., Fox, G. D., Herrup, K., et al. (1994). Deficient cerebellar long-term depression and impaired motor learning in mGluR1 mutant mice. *Cell* 79, 377–388.

Albus, J. S. (1971). A theory of cerebellar function. *Math. Biosci.* 10, 25–61.

Amino, Y., Kyuhou, S., Matsuzaki, R., and Gemba, H. (2001). Cerebello-thalamo-cortical projections to the posterior parietal cortex in the macaque monkey. *Neurosci. Lett.* 309, 29–32.

Angaut, P., Cicirata, F., and Serapide, F. (1985). Topographic organization of the cerebellothalamic projections in the rat. An autoradiographic study. *Neuroscience* 15, 389–401.

Angelaki, D. E., Yakusheva, T. A., Green, A. M., Dickman, J. D., and Blazquez, P. M. (2010). Computation of egomotion in the macaque cerebellar vermis. *Cerebellum* 9, 174–182.

Artola, A., Brocher, S., and Singer, W. (1990). Different voltage-dependent thresholds for inducing long-term depression and long-term potentiation in slices of rat visual cortex. *Nature* 347, 69–72.

Aumann, T. D., Rawson, J. A., Finkelstein, D. I., and Horne, M. K. (1994). Projections from the lateral and interposed cerebellar nuclei to the thalamus of the rat: a light and electron microscopic study using single and double anterograde labelling. *J. Comp. Neurol.* 349, 165–181.

Baumann, O., and Mattingley, J. B. (2012). Functional topography of primary emotion processing in the human cerebellum. *Neuroimage* 61, 805–811.

Boyden, E. S., Katoh, A., and Raymond, J. L. (2004). Cerebellum-dependent learning: the role of multiple plasticity mechanisms. *Annu. Rev. Neurosci.* 27, 581–609.

Brindley, G. (1964). The use made by the cerebellum of the information that it receives from sense organs. *IBRO Bull.* 3:80.

Brooks, J. X., and Cullen, K. E. (2009). Multimodal integration in rostral fastigial nucleus provides an estimate of body movement. *J. Neurosci.* 29, 10499–10511.

Burguiere, E., Arabo, A., Jarlier, F., De Zeeuw, C. I., and Rondi-Reig, L. (2010). Role of the cerebellar cortex in conditioned goal-directed behavior. *J. Neurosci.* 30, 13265–13271.

Burguiere, E., Arleo, A., Hojjati, M., Elgersma, Y., De Zeeuw, C. I., Berthoz, A., et al. (2005). Spatial navigation impairment in mice lacking cerebellar LTD: a motor adaptation deficit? *Nat. Neurosci.* 8, 1292–1294.

Calhoun, V. D., Pekar, J. J., McGinty, V. B., Adali, T., Watson, T. D., and Pearlson, G. D. (2002). Different activation dynamics in multiple neural systems during simulated driving. *Hum. Brain Mapp.* 16, 158–167.

Clark, G. A., McCormick, D. A., Lavond, D. G., and Thompson, R. F. (1984). Effects of lesions of cerebellar nuclei on conditioned behavioral and hippocampal neuronal responses. *Brain Res.* 291, 125–136.

Clower, D. M., West, R. A., Lynch, J. C., and Strick, P. L. (2001). The inferior parietal lobule is the target of output from the superior colliculus, hippocampus, and cerebellum. *J. Neurosci.* 21, 6283–6291.

Cooper, B. G., Manka, T. F., and Mizumori, S. J. (2001). Finding your way in the dark: the retrosplenial cortex contributes to spatial memory and navigation without visual cues. *Behav. Neurosci.* 115, 1012–1028.

Cooper, B. G., and Mizumori, S. J. (2001). Temporary inactivation of the retrosplenial cortex causes a transient reorganization of spatial coding in the hippocampus. *J. Neurosci.* 21, 3986–4001.

Colombel, C., Lalonde, R., and Caston, J. (2004). The effects of unilateral removal of the cerebellar hemispheres on spatial learning and memory in rats. *Brain Res.* 1004, 108–115.

Cullen, K. E., Brooks, J. X., Jamali, M., Carriot, J., and Massot, C. (2011). Internal models of self-motion: computations that suppress vestibular reafference in early vestibular processing. *Exp. Brain Res.* 210, 377–388.

Damasio, A. R., Grabowski, T. J., Bechara, A., Damasio, H., Ponto, L. L., Parvizi, J., et al. (2000). Subcortical and cortical brain activity during the feeling of self-generated emotions. *Nat. Neurosci.* 3, 1049–1056.

de Solages, C., Szapiro, G., Brunel, N., Hakim, V., Isope, P., Buisseret, P., et al. (2008). High-frequency organization and synchrony of activity in the purkinje cell layer of the cerebellum. *Neuron* 58, 775–788.

De Zeeuw, C. I., Hansel, C., Bian, F., Koekkoek, S. K., van Alphen, A. M., Linden, D. J., et al. (1998). Expression of a protein kinase C inhibitor in Purkinje cells blocks cerebellar LTD and adaptation of the vestibulo-ocular reflex. *Neuron* 20, 495–508.

Dum, R. P., Li, C., and Strick, P. L. (2002). Motor and nonmotor domains in the monkey dentate. *Ann. N.Y. Acad. Sci.* 978, 289–301.

Eccles, J. (1965). Functional meaning of the patterns of synaptic connections in the cerebellum. *Perspect. Biol. Med.* 8, 289–310.

Eccles, J. C. (1967). Circuits in the cerebellar control of movement. *Proc. Natl. Acad. Sci. U.S.A.* 58, 336–343.

Frank, B., Maschke, M., Groetschel, H., Berner, M., Schoch, B., Hein-Kropp, C., et al. (2010). Aphasia and neglect are uncommon in cerebellar disease: negative findings in a prospective study in acute cerebellar stroke. *Cerebellum* 9, 556–566.

Frank, B., Schoch, B., Hein-Kropp, C., Hovel, M., Gizewski, E. R., Karnath, H. O., et al. (2008). Aphasia, neglect and extinction are no prominent clinical signs in children and adolescents with acute surgical cerebellar lesions. *Exp. Brain Res.* 184, 511–519.

Frank, B., Schoch, B., Richter, S., Frings, M., Karnath, H. O., and Timmann, D. (2007). Cerebellar lesion studies of cognitive function in children and adolescents - limitations and negative findings. *Cerebellum* 6, 242–253.

Gandhi, C. C., Kelly, R. M., Wiley, R. G., and Walsh, T. J. (2000). Impaired acquisition of a Morris water maze task following selective destruction of cerebellar purkinje cells with OX7-saporin. *Behav. Brain Res.* 109, 37–47.

Gao, Z., van Beugen, B. J., and De Zeeuw, C. I. (2012a). Distributed synergistic plasticity and cerebellar learning. *Nat. Rev. Neurosci.* 13, 619–635.

Gao, H., Solages, Cd., and Lena, C. (2012b). Tetrode recordings in the cerebellar cortex. *J. Physiol. Paris* 106, 128–136.

Giannetti, S., and Molinari, M. (2002). Cerebellar input to the posterior parietal cortex in the rat. *Brain Res. Bull.* 58, 481–489.

Glickstein, M. (2003). Subcortical projections of the parietal lobes. *Adv. Neurol.* 93, 43–55.

Glickstein, M. (2007). What does the cerebellum really do? *Curr. Biol.* 17, R824–R827.

Glickstein, M., May, J. G. 3rd., and Mercier, B. E. (1985). Corticopontine projection in the macaque: the distribution of labelled cortical cells after large injections of horseradish peroxidase in the pontine nuclei. *J. Comp. Neurol.* 235, 343–359.

Goodlett, C. R., Hamre, K. M., and West, J. R. (1992). Dissociation of spatial navigation and visual guidance performance in Purkinje cell degeneration (pcd) mutant mice. *Behav. Brain Res.* 47, 129–141.

Goodworth, A. D., Paquette, C., Jones, G. M., Block, E. W., Fletcher, W. A., Hu, B., et al. (2012). Linear and angular control of circular walking in healthy older adults and subjects with cerebellar ataxia. *Exp. Brain Res.* 219, 151–161.

Hafting, T., Fyhn, M., Molden, S., Moser, M. B., and Moser, E. I. (2005). Microstructure of a spatial map in the entorhinal cortex. *Nature* 436, 801–806.

Hansel, C., de Jeu, M., Belmeguenai, A., Houtman, S. H., Buitendijk, G. H., Andreev, D., et al. (2006). alpha-CaMKII Is essential for cerebellar LTD and motor learning. *Neuron* 51, 835–843.

Haroian, A. J., Massopust, L. C., and Young, P. A. (1981). Cerebellothalamic projections in the rat: an autoradiographic and

degeneration study. *J. Comp. Neurol.* 197, 217–236.

Heath, R. G., Dempesy, C. W., Fontana, C. J., and Myers, W. A. (1978). Cerebellar stimulation: effects on septal region, hippocampus, and amygdala of cats and rats. *Biol. Psychiatry* 13, 501–529.

Heath, R. G., and Harper, J. W. (1974). Ascending projections of the cerebellar fastigial nucleus to the hippocampus, amygdala, and other temporal lobe sites: evoked potential and histological studies in monkeys and cats. *Exp. Neurol.* 45, 268–287.

Hoffmann, L. C., and Berry, S. D. (2009). Cerebellar theta oscillations are synchronized during hippocampal theta-contingent trace conditioning. *Proc. Natl. Acad. Sci. U.S.A.* 106, 21371–21376.

Horikawa, E., Okamura, N., Tashiro, M., Sakurada, Y., Maruyama, M., Arai, H., et al. (2005). The neural correlates of driving performance identified using positron emission tomography. *Brain Cogn.* 58, 166–171.

Ino, T., Inoue, Y., Kage, M., Hirose, S., Kimura, T., and Fukuyama, H. (2002). Mental navigation in humans is processed in the anterior bank of the parieto-occipital sulcus. *Neurosci. Lett.* 322, 182–186.

Ito, M. (1989). Long-term depression. *Annu. Rev. Neurosci.* 12, 85–102.

Ito, M., and Kano, M. (1982). Long-lasting depression of parallel fiber-Purkinje cell transmission induced by conjunctive stimulation of parallel fibers and climbing fibers in the cerebellar cortex. *Neurosci. Lett.* 33, 253–258.

Joyal, C. C., Strazielle, C., and Lalonde, R. (2001). Effects of dentate nucleus lesions on spatial and postural sensorimotor learning in rats. *Behav. Brain Res.* 122, 131–137.

Ke, M. C., Guo, C. C., and Raymond, J. L. (2009). Elimination of climbing fiber instructive signals during motor learning. *Nat. Neurosci.* 12, 1171–1179.

Kelly, R. M., and Strick, P. L. (2003). Cerebellar loops with motor cortex and prefrontal cortex of a nonhuman primate. *J. Neurosci.* 23, 8432–8444.

Kleine, J. F., Guan, Y., Kipiani, E., Glonti, L., Hoshi, M., and Buttner, U. (2004). Trunk position influences vestibular responses of fastigial nucleus neurons in the alert monkey. *J. Neurophysiol.* 91, 2090–2100.

Koekkoek, S. K., Hulscher, H. C., Dortland, B. R., Hensbroek, R. A., Elgersma, Y., Ruigrok, T. J., et al. (2003). Cerebellar LTD and learning-dependent timing of conditioned eyelid responses. *Science* 301, 1736–1739.

Lalonde, R., and Strazielle, C. (2003). The effects of cerebellar damage on maze learning in animals. *Cerebellum* 2, 300–309.

Lashley, K. S., and McCarthy, D. (1926). The survival of the maze habit after cerebellar injuries. *J. Comp. Physiol. Psychol.* 6, 423–433.

Levisohn, L., Cronin-Golomb, A., and Schmahmann, J. D. (2000). Neuropsychological consequences of cerebellar tumour resection in children: cerebellar cognitive affective syndrome in a paediatric population. *Brain* 123(Pt 5), 1041–1050.

Liu, W., Zhang, Y., Yuan, W., Wang, J., and Li, S. (2012). A direct hippocampo-cerebellar projection in chicken. *Anat. Rec. (Hoboken)* 295, 1311–1320.

Maguire, E. A., Burgess, N., Donnett, J. G., Frackowiak, R. S., Frith, C. D., and O'Keefe, J. (1998). Knowing where and getting there: a human navigation network. *Science* 280, 921–924.

Malm, J., Kristensen, B., Karlsson, T., Carlberg, B., Fagerlund, M., and Olsson, T. (1998). Cognitive impairment in young adults with infratentorial infarcts. *Neurology* 51, 433–440.

Manzoni, D., Pompeiano, O., Bruschini, L., and Andre, P. (1999). Neck input modifies the reference frame for coding labyrinthine signals in the cerebellar vermis: a cellular analysis. *Neuroscience* 93, 1095–1107.

Marr, D. (1969). A theory of cerebellar cortex. *J. Physiol. (London)* 202, 437–470.1.

McCormick, D. A., and Thompson, R. F. (1984a). Cerebellum: essential involvement in the classically conditioned eyelid response. *Science* 223, 296–299.

McCormick, D. A., and Thompson, R. F. (1984b). Neuronal responses of the rabbit cerebellum during acquisition and performance of a classically conditioned nictitating membrane-eyelid response. *J. Neurosci.* 4, 2811–2822.

McCrea, R. A., Gdowski, G. T., Boyle, R., and Belton, T. (1999). Firing behavior of vestibular neurons during active and passive head movements: vestibulo-spinal and other non-eye-movement related neurons. *J. Neurophysiol.* 82, 416–428.

Middleton, F. A., and Strick, P. L. (2001). Cerebellar projections to the prefrontal cortex of the primate. *J. Neurosci.* 21, 700–712.

Moffat, S. D., Elkins, W., and Resnick, S. M. (2006). Age differences in the neural systems supporting human allocentric spatial navigation. *Neurobiol. Aging* 27, 965–972.

Molinari, M., and Leggio, M. G. (2007). Cerebellar information processing and visuospatial functions. *Cerebellum* 6, 214–220.

Molinari, M., Petrosini, L., Misciagna, S., and Leggio, M. G. (2004). Visuospatial abilities in cerebellar disorders. *J. Neurol. Neurosurg. Psychiatry* 75, 235–240.

Mullen, R. J., Eicher, E. M., and Sidman, R. L. (1976). Purkinje cell degeneration, a new neurological mutation in the mouse. *Proc. Natl. Acad. Sci. U.S.A.* 73, 208–212.

Newman, P. P., and Reza, H. (1979). Functional relationships between the hippocampus and the cerebellum: an electrophysiological study of the cat. *J. Physiol.* 287, 405–426.

O'Keefe, J., and Dostrovsky, J. (1971). The hippocampus as a spatial map. Preliminary evidence from unit activity in the freely-moving rat. *Brain Res.* 34, 171–175.

O'Reilly, J. X., Beckmann, C. F., Tomassini, V., Ramnani, N., and Johansen-Berg, H. (2010). Distinct and overlapping functional zones in the cerebellum defined by resting state functional connectivity. *Cereb. Cortex* 20, 953–965.

Paquette, C., Franzen, E., Jones, G. M., and Horak, F. B. (2011). Walking in circles: navigation deficits from Parkinson's disease but not from cerebellar ataxia. *Neuroscience* 190, 177–183.

Petrosini, L., Leggio, M. G., and Molinari, M. (1998). The cerebellum in the spatial problem solving: a co-star or a guest star? *Prog. Neurobiol.* 56, 191–210.

Petrosini, L., Molinari, M., and Dell'Anna, M. E. (1996). Cerebellar contribution to spatial event processing: Morris water maze and T-maze. *Eur. J. Neurosci.* 8, 1882–1896.

Prevosto, V., Graf, W., and Ugolini, G. (2010). Cerebellar inputs to intraparietal cortex areas LIP and MIP: functional frameworks for adaptive control of eye movements, reaching, and arm/eye/head movement coordination. *Cereb. Cortex* 20, 214–228.

Ramnani, N. (2012). Frontal lobe and posterior parietal contributions to the cortico-cerebellar system. *Cerebellum* 11, 366–383.

Riva, D., and Giorgi, C. (2000). The cerebellum contributes to higher functions during development: evidence from a series of children surgically treated for posterior fossa tumours. *Brain* 123(Pt 5), 1051–1061.

Rochefort, C., Arabo, A., André, M., Poucet, B., Save, E., and Rondi-Reig, L. (2011). Cerebellum shapes hippocampal spatial code. *Science* 334, 385–389.

Rondi-Reig, L., and Burguiere, E. (2005). Is the cerebellum ready for navigation? *Prog. Brain Res.* 148, 199–212.

Rondi-Reig, L., Le Marec, N., Caston, J., and Mariani, J. (2002). The role of climbing and parallel fibers inputs to cerebellar cortex in navigation. *Behav. Brain Res.* 132, 11–18.

Roy, J. E., and Cullen, K. E. (2001). Selective processing of vestibular reafference during self-generated head motion. *J. Neurosci.* 21, 2131–2142.

Roy, J. E., and Cullen, K. E. (2003). Brain stem pursuit pathways: dissociating visual, vestibular, and proprioceptive inputs during combined eye-head gaze tracking. *J. Neurophysiol.* 90, 271–290.

Roy, J. E., and Cullen, K. E. (2004). Dissociating self-generated from passively applied head motion: neural mechanisms in the vestibular nuclei. *J. Neurosci.* 24, 2102–2111.

Sacchetti, B., Scelfo, B., and Strata, P. (2009). Cerebellum and emotional behavior. *Neuroscience* 162, 756–762.

Sacchetti, B., Scelfo, B., Tempia, F., and Strata, P. (2004). Long-term synaptic changes induced in the cerebellar cortex by fear conditioning. *Neuron* 42, 973–982.

Save, E., and Poucet, B. (2009). Role of the parietal cortex in long-term representation of spatial information in the rat. *Neurobiol. Learn. Mem.* 91, 172–178.

Schmahmann, J. D. (1991). An emerging concept. The cerebellar contribution to higher function. *Arch. Neurol.* 48, 1178–1187.

Schmahmann, J. D., and Sherman, J. C. (1998). The cerebellar cognitive affective syndrome. *Brain* 121(Pt 4), 561–579.

Schonewille, M., Belmeguenai, A., Koekkoek, S. K., Houtman, S. H., Boele, H. J., van Beugen, B. J., et al. (2010). Purkinje cell-specific knockout of the protein phosphatase PP2B impairs potentiation and cerebellar motor learning. *Neuron* 67, 618–628.

Schonewille, M., Gao, Z., Boele, H. J., Veloz, M. F., Amerika, W. E., Simek, A. A., et al. (2011). Reevaluating the role of LTD in cerebellar motor learning. *Neuron* 70, 43–50.

Shaikh, A. G., Meng, H., and Angelaki, D. E. (2004). Multiple reference frames for motion in the primate cerebellum. *J. Neurosci.* 24, 4491–4497.

Smith, P. F., Horii, A., Russell, N., Bilkey, D. K., Zheng, Y., Liu, P., et al. (2005). The effects of vestibular lesions on hippocampal function in rats. *Prog. Neurobiol.* 75, 391–405.

Snider, R. S. (1950). Recent contributions to the anatomy and physiology of the cerebellum. *Arch. Neurol. Psychiatry* 64, 196–219.

Snider, R. S., and Maiti, A. (1976). Cerebellar contributions to the Papez circuit. *J. Neurosci. Res.* 2, 133–146.

Snyder, L. H., Grieve, K. L., Brotchie, P., and Andersen, R. A. (1998). Separate body- and world-referenced representations of visual space in parietal cortex. *Nature* 394, 887–891.

Stackman, R. W., Clark, A. S., and Taube, J. S. (2002). Hippocampal spatial representations require vestibular input. *Hippocampus* 12, 291–303.

Stackman, R. W., and Herbert, A. M. (2002). Rats with lesions of the vestibular system require a visual landmark for spatial navigation. *Behav. Brain Res.* 128, 27–40.

Stanton, P. K., and Sejnowski, T. J. (1989). Associative long-term depression in the hippocampus induced by hebbian covariance. *Nature* 339, 215–218.

Steinlin, M., Imfeld, S., Zulauf, P., Boltshauser, E., Lovblad, K. O., Ridolfi Luthy, A., et al. (2003). Neuropsychological long-term sequelae after posterior fossa tumour resection during childhood. *Brain* 126, 1998–2008.

Stoodley, C. J., and Schmahmann, J. D. (2009). Functional topography in the human cerebellum: a meta-analysis of neuroimaging studies. *Neuroimage* 44, 489–501.

Strata, P., Scelfo, B., and Sacchetti, B. (2011). Involvement of cerebellum in emotional behavior. *Physiol. Res.* 60(Suppl. 1), S39–S48.

Strick, P. L., Dum, R. P., and Fiez, J. A. (2009). Cerebellum and nonmotor function. *Annu. Rev. Neurosci.* 32, 413–434.

Taube, J. S. (2007). The head direction signal: origins and sensory-motor integration. *Annu. Rev. Neurosci.* 30, 181–207.

Taube, J. S., Muller, R. U., and Ranck, J. B. Jr. (1990). Head-direction cells recorded from the postsubiculum in freely moving rats. I. Description and quantitative analysis. *J. Neurosci.* 10, 420–435.

Timmann, D., Drepper, J., Frings, M., Maschke, M., Richter, S., Gerwig, M., et al. (2010). The human cerebellum contributes to motor, emotional and cognitive associative learning. A review. *Cortex* 46, 845–857.

Trouche, E., Beaubaton, D., Amato, G., and Grangetto, A. (1979). Impairments and recovery of the spatial and temporal components of a visuomotor pointing movement after unilateral destruction of the dentate nucleus in the baboon. *Appl. Neurophysiol.* 42, 248–254.

Uchiyama, Y., Ebe, K., Kozato, A., Okada, T., and Sadato, N. (2003). The neural substrates of driving at a safe distance: a functional MRI study. *Neurosci. Lett.* 352, 199–202.

Valerio, S., and Taube, J. S. (2012). Path integration: how the head direction signal maintains and corrects spatial orientation. *Nat. Neurosci.* 15, 1445–1453.

Van der Werf, Y. D., Witter, M. P., and Groenewegen, H. J. (2002). The intralaminar and midline nuclei of the thalamus. Anatomical and functional evidence for participation in processes of arousal and awareness. *Brain Res. Brain Res. Rev.* 39, 107–140.

Vann, S. D., Aggleton, J. P., and Maguire, E. A. (2009). What does the retrosplenial cortex do? *Nat. Rev. Neurosci.* 10, 792–802.

Voogd, J., Gerrits, N. M., and Ruigrok, T. J. (1996). Organization of the vestibulocerebellum. *Ann. N.Y. Acad. Sci.* 781, 553–579.

Wallace, D. G., Hines, D. J., Pellis, S. M., and Whishaw, I. Q. (2002). Vestibular information is required for dead reckoning in the rat. *J. Neurosci.* 22, 10009–10017.

Wallesch, C. W., and Horn, A. (1990). Long-term effects of cerebellar pathology on cognitive functions. *Brain Cogn.* 14, 19–25.

Walter, H., Vetter, S. C., Grothe, J., Wunderlich, A. P., Hahn, S., and Spitzer, M. (2001). The neural correlates of driving. *Neuroreport* 12, 1763–1767.

Welsh, J. P., Yamaguchi, H., Zeng, X. H., Kojo, M., Nakada, Y., Takagi, A., et al. (2005). Normal motor learning during pharmacological prevention of Purkinje cell long-term depression. *Proc. Natl. Acad. Sci. U.S.A.* 102, 17166–17171.

Whishaw, I. Q., Hines, D. J., and Wallace, D. G. (2001). Dead reckoning (path integration) requires the hippocampal formation: evidence from spontaneous exploration and spatial learning tasks in light (allothetic) and dark (idiothetic) tests. *Behav. Brain Res.* 127, 49–69.

Whitlock, J. R., Pfuhl, G., Dagslott, N., Moser, M. B., and Moser, E. I. (2012). Functional split between parietal and entorhinal cortices in the rat. *Neuron* 73, 789–802.

Wikgren, J., Nokia, M. S., and Penttonen, M. (2010). Hippocampo-cerebellar theta band phase synchrony in rabbits. *Neuroscience* 165, 1538–1545.

Yakusheva, T. A., Shaikh, A. G., Green, A. M., Blazquez, P. M., Dickman, J. D., and Angelaki, D. E. (2007). Purkinje cells in posterior cerebellar vermis encode motion in an inertial reference frame. *Neuron* 54, 973–985.

Zhu, L., Scelfo, B., Hartell, N. A., Strata, P., and Sacchetti, B. (2007). The effects of fear conditioning on cerebellar LTP and LTD. *Eur. J. Neurosci.* 26, 219–227.

Conflict of Interest Statement: The authors declare that the research was conducted in the absence of any commercial or financial relationships that could be construed as a potential conflict of interest.

Received: 07 October 2012; accepted: 22 February 2013; published online: 13 March 2013.

Citation: Rochefort C, Lefort JM and Rondi-Reig L (2013) The cerebellum: a new key structure in the navigation system. Front. Neural Circuits ***7****:35. doi: 10.3389/fncir.2013.00035*

GLOSSARY

Vestibular organs: Semicircular canals and otolith organs. The latter detect linear acceleration whereas the former are sensitive to angular acceleration.

Proprioception: Perception of the relative position of the different parts of one's body using information from proprioceptors (i.e., stretch receptors located in the muscles, tendons, and joints).

Efferent copy of motor command: It has been suggested that during an active movement, while the motor cortex sends a command to the periphery, a copy of the motor command is also generated and could be used to generate a prediction of the sensory consequences of the intended movement.

Optic flow: The displacement of images on the retina due to the relative motion between the observer and the scene. The displacement speed can be used to estimate one's proper acceleration.